DISSERTATION

submitted to the

COMBINED FACULTIES FOR THE NATURAL SCIENCES AND FOR MATHEMATICS

OF THE RUPERTO-CAROLA UNIVERSITY OF HEIDELBERG, GERMANY

for the degree of

DOCTOR OF NATURAL SCIENCES

Put forward by

Dipl.-Phys. Joschka Johannes Beyer

born in Göttingen, Germany

Oral examination: 29.10.2014

ASPECTS OF COSMIC STRUCTURE FORMATION IN COUPLED SCALAR FIELD DARK MATTER MODELS

Referees: Prof. Dr. Christof Wetterich

Prof. Dr. Björn Malte Schäfer

ASPEKTE KOSMOLOGISCHER STRUKTURBILDUNG IN MODELLEN MIT GEKOPPELTER SKALARER DUNKLER MATERIE

In dieser Arbeit stellen wir ein durch höherdimensionale dilatationssymmetrische Gravitationstheorien motiviertes kosmologisches Modell vor, in dem dunkle Materie und dunkle Energie aus zwei gekoppelten Skalarfeldern bestehen. Die Analyse dieses Modells besteht aus vier Teilen. In einem ersten Abschnitt untersuchen wir die homogene und isotrope Hintergrundkosmologie und finden eine Dynamik ähnlich wie in Quintessenz-Kosmologien im frühen Universum sowie ein Szenario von gekoppelter dunkle Materie und Quintessenz für späte Zeiten. In der linearen Störungstheorie entwickeln wir zunächst eine effektive Fluid-Beschreibung des Modell, welches wir in einen Boltzmann-Code implementieren um das lineare Power-Spektrum numerisch zu berechnen. Dieses zeigt eine Unterdrückung der kosmologischen Strukturbildung bei einer charakteristischen Jeans Skala. Weiterhin analysieren wir Störungsmoden außerhalb des Horizonts im frühen Universum, mit besonderem Augenmerk auf die Stabilität der adiabatischen Mode. Zuletzt analysieren wir die nicht-lineare Strukturbildung in diesem Modell mit Hilfe des Press-Schechter Formalismus und benutzen die Resultate um Grenzen für die Modellparameter anzugeben.

ASPECTS OF COSMIC STRUCTURE FORMATION IN COUPLED SCALAR FIELD DARK MATTER MODELS

In this thesis we introduce a novel coupled two scalar field model of the dark sector motivated by higher dimensional dilatation symmetric theories of gravity, which could potentially provide a solution to the cosmological constant problem. This work is split up into four parts. First, we motivate the model and discuss its evolution at the background level. We find a quintessence-type scaling solution in the early universe and a coupled cold dark matter scenario for later times. At the level of linear perturbations we introduce an effective fluid description of this model and implement it into a Boltzmann-code to recover the linear power spectrum, which exhibits a characteristic suppression of power at a Jeans scale. In a third step we analyze superhorizon perturbations in the early universe in some detail, with particular focus on the issue of the stability of the adiabatic perturbation mode. Finally we apply the extended Press-Schechter formalism to predict substructure abundances within a typical galaxy like the Milky Way and use the results to obtain parameter bounds for our model.

PREFACE

This thesis contains the results of my work at the Institute for Theoretical Physics of the Ruperto Carola University of Heidelberg carried out over a little more than three years between 2011 and 2014. And while the work presented here, unless marked otherwise, is my own, there are many people who have contributed to it in many small (or not so small) ways, and their contributions should not be forgotten.

First and foremost, thanks are due Christof Wetterich, who provided me with the opportunity to work in his research group and proofed to be an inexhaustible source of ideas, optimism and support. His guidance has certainly contributed a great deal to this work. Furthermore I would like to thank Björn Malte Schäfer, who kindly agreed to act as the second referee for this work on rather short notice, as well as Matthias Bartelmann and Ulrich Uwer, who agreed to serve as examiners during my defense of this thesis. Finally I am grateful to Jan Pawlowski and Luca Amendola for agreeing to serve as my second and third project advisors.

Special thanks go out to Valery Rubakov, who, after giving a set of excellent lectures in Heidelberg during the spring of 2012, discussed with me some of the problems I was facing at the time and could point me towards his textbook on cosmology, which contained crucial information very helpful for understanding the evolution of late time linear perturbations in the cosmon-bolon model.

Like many other graduate students, I am indebted to Eduard Thommes for his excellent administrative work and to Elmar Bittner and Adrian Vollmer for reliable and patient technical support. Furthermore thanks go out to the always kind and helpful secretarial staff of the ITP, in particular to Jeanette Bloch-Ditzinger and Tina Birke.

During my time at the ITP, multiple discussions with the large number of bachelor, master and PhD students have provided both improved physical understanding and much needed distractions. In this context I particularly want to mention the changing cast of the Dachzimmer crowd, in particular Maik, Youness, Igor, Nic, Fabian, Nasseemudin and Conrad, who shared this journey with me for most of the time, and those of my fellow students who have taken a similar path towards a PhD at other institutes.

Outside the world of physics I have found welcome distractions, I would in particular like to thank all the people who were conducting various musical activities with me on a regular basis, the St. Illgen people and the Ultimate Frisbee groups for both saturdays and sundays. Thanks also go out to my astonishingly persevering group of old friends from Göttingen, which I still enjoy seeing very much at our twice-a-year meetings.

I could always count on support from my family, for which I will be ever grateful.

Last but not least, I want to thank Yen-Hsi for all her love and support, and for her endurance during the last six weeks, when I was constantly preoccupied with writing this thesis.

CONTENTS

1 INTRODUCTION 1

1.1 Our universe . . . 1
1.2 Outline . . . 5
1.3 Conventions . . . 6

2 THE HOMOGENEOUS UNIVERSE 7

2.1 The spatial symmetry assumptions . . . 7
2.2 General relativity . . . 9
2.2.1 Einstein gravity . . . 9
2.2.2 Alternative theories of gravity . . . 12
2.3 Dynamics of an expanding universe . . . 19
2.3.1 FLRW-solutions . . . 19
2.3.2 The cosmic inventory . . . 22
2.3.3 A short history of our universe . . . 26
2.3.4 The ΛCDM model . . . 32

3 THE DARK SECTOR AND DILATATION SYMMETRY 35

3.1 The cosmological constant problem . . . 35
3.1.1 The nature of Λ . . . 36
3.1.2 The anthropic argument . . . 41
3.2 Quintessence . . . 46
3.2.1 Minimally coupled quintessence . . . 47
3.2.2 Coupled quintessence . . . 52
3.2.3 Alternative models . . . 53
3.3 Dilatation symmetry and Λ . . . 56
3.3.1 Dilatations . . . 56
3.3.2 Higher dimensional gravity . . . 57
3.4 The Cosmon-Bolon model . . . 62
3.4.1 Cosmic scenario: Asymptotic dilatation symmetry . . . 62
3.4.2 Cosmon & bolon . . . 64
3.4.3 Cosmological Evolution . . . 66

4 THE INHOMOGENEOUS UNIVERSE 1: LINEAR PERTURBATIONS 77

4.1 Basics . . . 78
4.1.1 Perturbing Einstein-gravity . . . 80
4.1.2 Scalar field perturbations . . . 85
4.1.3 Alternative perturbation variables . . . 86
4.1.4 Entropy and curvature perturbations . . . 88
4.1.5 Statistics . . . 90
4.2 Baryons, photons and neutrinos . . . 93
4.2.1 Full equations . . . 93
4.2.2 Tight coupling approximation . . . 96
4.2.3 Relativistic fluid approximation . . . 98
4.2.4 Radiation streaming approximation . . . 98
4.3 Cosmon and bolon . . . 99
4.3.1 Effective theory near the minimum . . . 100
4.3.2 RSA for the cosmon . . . 111
4.4 Numerical evolution . . . 112
4.4.1 The Boltzmann code . . . 112
4.4.2 The bolon power spectrum . . . 116

5 PERTURBATIONS ALONG MULTIPLE-FIELD SCALING SOLUTIONS 125

5.1 Generic multi-field scaling solutions . . . 127
5.1.1 Shape of the common potential . . . 127
5.1.2 Exact scaling solutions . . . 129
5.2 Perturbations along scaling solutions . . . 137
5.2.1 Basic formalism . . . 137
5.2.2 Eigenvalues and Eigenmodes . . . 142

6 THE INHOMOGENEOUS UNIVERSE 2: STRUCTURE FORMATION 149

6.1 Structure formation on small scales . . . 150
6.1.1 Small scale issues . . . 150
6.1.2 Modifying dark matter . . . 151
6.2 Extended Press-Schechter formalism . . . 154
6.2.1 Structure formation as a random walk . . . 154
6.2.2 Filter choices and mass assignments . . . 155
6.2.3 Barriers . . . 156
6.2.4 Random walks . . . 157
6.3 Total number counts . . . 157
6.3.1 Problems with spherical collapse . . . 158
6.3.2 The barriers we employ . . . 160
6.3.3 Calculation of the first crossing rate . . . 161
6.3.4 Total number counts . . . 163
6.4 Progenitors and substructures . . . 166
6.4.1 Progenitor mass functions . . . 167

6.4.2 Milky Way subhalos 168
6.5 Observing the oscillations? 173

7 CONCLUSION 175

LIST OF FIGURES 178

LIST OF TABLES 181

ABBREVIATIONS 183

A PARTICLES OF THE STANDARD MODEL 185

B FITTING THE POWER SPECTRUM CUTOFF 187

BIBLIOGRAPHY 191

1 INTRODUCTION

1.1 OUR UNIVERSE

Just before the turn of the millennium, a paradigm-shifting discovery altered our understanding of the universe dramatically. Two research groups, lead by Saul Perlmutter, Brian P. Schmidt and Adam G. Riess, independently found that distant supernova appear systematically dimmer than they should be in a universe dominated by ordinary matter [Perlmutter et al., 1999, Riess et al., 1998]. In fact, the data could only be explained by an expanding universe that is accelerating. In 2012, the nobel prize in physics was awarded for these observations.

At first glance, this finding seems to contradict our basic understanding of gravitational interactions, at least from a Newtonian viewpoint. Is not all matter supposed to source an attractive gravitational force? Even in a big bang scenario, where one imagines the universe starting off as a hot primordial fireball driven apart rapidly by radiation pressure, one would expect gravity to slow down the cosmic expansion, not accelerate it. Still, by today the notion of an accelerating universe has become widely accepted in the scientific community and has been verified to be compatible with a vast number of cosmological observations.

The reason why this notion may be surprising or unintuitive, but not truly problematic, is the following: Our understanding of the evolution of the universe as a whole is based to a large part on the theory of general relativity, invented by Albert Einstein [Einstein, 1915c,a], a theory which provides plenty of room for an explanation of the observed accelerated cosmic expansion. There are basically two ways account for such a phenomenon within general relativity. One can either introduce a cosmological constant into the theory, or postulate the existence of some form of exotic matter which violates the strong energy condition. Both types of models are commonly referred to as *dark energy* models, a wonderfully mysterious term to indicate our ignorance about what actually causes the accelerated expansion of the universe. As an alternative, one can try to explain the observations by going beyond the theory of general relativity. Such models are referred to as *modified gravity* theories.

The most commonly used description of dark energy is the cosmological constant, which has a rich history in its own right. It was originally introduced by Einstein in order to account for the possibility of a static universe within the framework of general relativity, and famously abandoned later, after Edwin Hubble discovered the expansion of the universe [Hubble, 1929]. Currently the cosmological constant appears to be consistent with virtually all cosmological observations and it has become

the standard paradigm for dark energy. Despite its undeniable successes, this mathematically simple model is far from uncontested as an explanation for dark energy. The main reason why many researchers are not satisfied with this assertion is the so called *cosmological constant problem*. The complaint is, essentially, that the value of the cosmological constant necessary to explain current cosmological observations, roughly $\sqrt{\Lambda} \sim 10^{-33}$ eV, is too small to be compatible with expectations arising from quantum field theory considerations. The discrepancy asserted here is huge. Typically authors cite the famous 122 orders of magnitude difference between theoretical predictions and observed value, and while this may be an overstatement arising from an overly simplified calculation of the theoretical value, even under rather realistic assumptions a discrepancy of more than 50 orders of magnitude appears to be persistent [Martin, 2012].

There have been many attempts to find solutions to the cosmological constant problem, none of which have been entirely satisfactory. A very common assumption is that the cosmological constant is set to zero by some unknown mechanism, on the grounds that it seems more likely to find such a mechanism than one which tunes the value expected from theory very close, but not equal to zero to an accuracy of more than 50 orders of magnitude. In this case the observed accelerated expansion of the universe needs a new explanation, and dark energy is typically attributed to some exotic form of matter. Among the most popular models for this type of matter are *quintessence* models, where a cosmological scalar field, or *cosmon*, is introduced [Wetterich, 1988a,b, Ratra and Peebles, 1988], which is then assumed to be the driving component behind the cosmic acceleration. The dynamics of the cosmon field φ are then generally determined by a scalar self-interaction potential $V(\varphi)$. Depending on the form of the potential, these quintessence models can exhibit very appealing features, in particular so called *attractive scaling solutions*, for which the evolution of the cosmological scalar field tracks that of the dominant background fluid, i.e. matter or radiation, and adjusts to this evolution largely irrespective of the initial conditions. In such models the quintessence field typically makes up a fraction of the order of a few percent of the energy budget of the universe throughout its evolution, which is why they are known as *early dark energy* models. In the late universe this scaling behavior has to be stopped in some way, since dark energy needs to become the dominant component of the cosmic fluid and cause cosmic acceleration. The question why this happened only recently in the cosmic history and not much earlier is known as the *why now* or *coincidence problem*, and poses one of the major challenges to quintessence models.

Long before the discovery of dark energy, another mysterious substance called *dark matter* entered the cosmological stage. It was first discovered by Fritz Zwicky [1933, 1937], who found that the velocities of galaxies in the outer region of the Coma cluster are too high to be compatible with the observed amount of luminous matter within that cluster. By today many findings have confirmed the existence of dark matter, notably by a set of cosmological observations spanning an enormous period of time in the cosmic evolution. Measurements testing this paradigm within the current matter distribution of the universe range from observations of rotation curves of stars in galaxies and galaxies in clusters, much in the spirit of Zwicky's original findings, to gravitational lensing surveys, which provide what is probably the most direct evidence of gravitationally bound dark matter structures in the universe today. Furthermore the amplitude of temperature anisotropies in the cosmic microwave background require a dark matter component to be present already when the CMB was released, roughly 14 billion years ago [Peebles, 1982]. So far (almost) all observational findings point towards

dark matter being a substance which consists of non-relativistic particles which are collisionless (at least to good approximation) and do not interact with light, called *cold dark matter*.

Naturally the search for dark matter is an important field of research within the particle physics community, and many experiments have been set up trying to find evidence of dark matter directly through weak interactions with ordinary matter. The situation is currently both exciting and confusing, with two experiments claiming a detection signal [Bernabei et al., 2008, Angloher et al., 2012] in a parameter range other experiments claim to have excluded (e.g. [Aprile et al., 2012]). This area of research will be very exciting in for the next decade or so, since the increasing precision of these experiments may well yield the final verdict on weakly interacting dark matter soon. From the theory side a large number of extensions of the standard model have been constructed accounting for various forms of the mysterious particle [Steigman and Turner, 1985, Bertone et al., 2005, Peccei and Quinn, 1977b,a, Duffy and van Bibber, 2009, Steffen, 2009, Drewes, 2013]. These include both models yielding dark matter which is detectable by laboratory experiments, and also models where it is not. So far no clear favorite has emerged.

Despite the unresolved issues concerning the particle physics origin of both dark energy and dark matter, within the science of cosmology a standard model has been established a number of years ago, which has managed to stand its ground against the ever increasing precision of observations until today. In this model dark energy is described by a cosmological constant and dark matter as a cold non-relativistic relic of the early universe. Together these two components make up the majority of todays energy budget of the universe, dark energy roughly 70 %, dark matter about 25 %. Only the remaining 5% consist of known particles, mostly atoms, with a tiny fraction of photons and neutrinos. The successes of this relatively simple model have been quite impressive. We can use it to construct the history of the universe backwards in time from today, when the universe is about 13.7 billion years old, back to the first few seconds and possibly even further. The range of phenomena taking place within this enormous timespan which can explained within this model is remarkable. It includes the production of elements in the early universe during *big bang nucleosynthesis*, the abundance of which can be predicted and measured [Alpher et al., 1948], the emission of the almost isotropic Planck-spectrum of cosmic microwave background radiation [Penzias and Wilson, 1965a], the anisotropies of which can be measured an fitted to excellent accuracy [Hinshaw et al., 2013, Ade et al., 2013a], and the formation of virialized structures in the cosmos, which can be observed through a number of different methods. In fact, very recent observations of B-mode polarization in the cosmic microwave background may have opened up a window into an even earlier period of the cosmic evolution, called inflation, which probably took place within the first fractions of a second in the cosmic evolution [Ade et al., 2014].

Despite all its successes, the cosmological standard model, also known as ΛCDM model, may not be a perfect fit. There has been, for about 20 years by now, a persistent problem with the formation of structures on small scales. Originally this problem was identified as an issue between simulations of structure formation in pure cold dark matter scenarios and observations [Navarro et al., 1997], but even more and more sophisticated simulations including baryonic physics of galaxy formation are so far unable to completely dissolve these discrepancies [Genel et al., 2014]. The debate about how severe these problems are and if a better understanding of baryonic physics will ultimately lead to a

resolution is ongoing [Weinberg et al., 2013a], but these discrepancies might well point us towards a new paradigm going beyond the simple model of cold dark matter and a cosmological constant.

In this work we investigate an alternative unified model of the dark sector, in which both dark energy and dark matter consist of cosmological scalar fields. This scenario is motivated by a recent investigation of higher dimensional dilatation symmetric theories of gravity, which may provide a solution to the cosmological constant problem [Wetterich, 2009, 2010a,b]. Imposing dilatation or scale symmetry on a theory effectively removes all fundamental mass scales. In a cosmological setting such a theory can be realized as a fixed point of the quantum effective action, reached asymptotically by the cosmic evolution. At the fixed point, the dilaton, the Goldstone boson of dilatation symmetry, is massless, but for finite times, couplings in the action which break dilatation symmetry give it a small mass. This makes the pseudo-Goldstone boson of dilatation symmetry a prime candidate to act as a cosmological cosmon field in quintessence scenarios.

Within a higher dimensional setting dimensional reduction typically leads to a number of effective degrees of freedom in the four-dimensional theory. We consider a simple model where only a second scalar field is present and we investigate scenarios where it can act as a dark matter field. We name this second field *bolon* (i.e. 'lump'), since it is ultimately responsible for the formation of structures in the universe. Considerations of the asymptotic dilatation symmetric state then lead is to the important conclusion that the two scalar fields are necessarily coupled in such a model.

The resulting coupled cosmon-bolon model of dark energy and dark matter has several interesting features. First, we obtain a cosmology which is largely independent of the initial conditions chosen for the scalar fields, as both will follow a scaling evolution in the early universe. Second, for the late universe we will recover a coupled model of dark matter to dark energy. Interestingly, such a coupled model could be slightly favored by current best parameter fits of cosmic microwave background data [Pettorino, 2013], if not on a significant level. Third, similar to other models of scalar dark matter, the coupled cosmon-bolon model exhibits a cutoff in linear matter power spectrum. This cutoff can be chosen to sit at a scale where it can have significant effects on small scale structure formation, where the cosmological standard model might run into problems. Finally, the scalar nature of dark matter yields predictions for the structure of dark matter halos which are significantly different from standard cold dark matter predictions. While a calculation of halo number counts leads to results very similar to warm dark matter models, the inner structure of halos is expected to look very different. We check if these differences could be detectable in the forseeable future, if the parameters of the model are chosen in a range consistent with current cosmological constraints.

This work is based on three preprints, which include major parts of the content presented in this thesis. These works are:

- "Small scale structures in coupled scalar field dark matter" [Beyer and Wetterich, 2014]
- "Adiabatic initial conditions in coupled scalar field cosmologies" [Beyer, 2014a]
- "Linear Perturbations in a coupled cosmon-bolon cosmology" [Beyer, 2014b]

All three of them are currently under consideration for publication by peer-review journals and we expect them to be published by the time of the defense of this thesis. We have taken figures from

the all three publications and excerpts only from the last two, which were written exclusively by the author. These excerpts had to be partly adapted or extended to fit into the framework of this thesis. We have not marked all these changes explicitly, but have denoted which sections of these papers we follow in our presentation at the beginning of each chapter. At the time of writing this thesis, copyright for this material resides with the author, however, it will be transferred to the respective publisher upon acceptance of these papers.

1.2 Outline

We will proceed as follows.

In chapter 2 we will introduce the basics of cosmology. After a short discussion of the symmetry assumptions of spatial homogeneity and isotropy underlying most of modern cosmological research, we then move on to discuss Einstein's theory of gravity and some generalizations of it in section 2.2. The generalizations will be important in chapter 3. We then go on to discuss the class of solutions to Einstein's equations which have become known as Friedmann-solutions [Friedmann, 1922], which form the basis of modern cosmology, and discuss the cosmological standard model.

In chapter 3 we move on to discuss the cosmological constant problem in section 3.1, quintessence cosmologies in section 3.2 and their connection to dilatation symmetry in section 3.3. Finally, we introduce the comson-bolon model and discuss its features at the level of the background cosmology in section 3.4.

Chapter 4 deals with the evolution of linear perturbations in our model. After we introduce our conventions concerning cosmological linear perturbation theory, we derive the linear perturbation equations which govern the evolution of linear perturbations in a coupled scalar field cosmology in section 4.1. A numerical evolution of these equations requires a Boltzmann code, which we wrote ourselves in a completely gauge-invariant manner. This required a recalculation of several approximation schemes commonly used for baryons, photons and neutrinos in such codes in order to adapt them to our variables, which is what we present in section 4.2. The implementation of the scalar field perturbations into the Boltzmann code is also not straight forward, and we have to resort to an effective fluid description for the bolon field for late times. This is derived in section 4.3. Finally, in section 4.4, we describe how our code works and present the evolution of linear perturbations in the cosmon-bolon model.

Chapter 5 takes a step back and looks at the perturbations in the very early universe. First, we derive the generic shape of the scalar potential allowed in scenarios involving scaling solutions for multiple scalar fields in section 5.1 and classify all such possible solutions. In the next section 5.2 we discuss perturbations around such scaling solutions, with particular focus on the stability of the adiabatic perturbation mode.

Chapter 6 deals with the formation of structures in our model, with particular focus on small scale structures. After a short review of the issues of small scale structure formation within the cold dark matter paradigm in section 6.1 and a short introduction to the extended Press-Schechter excursion set formalism in section 6.2, we go on to apply this formalism to our model to predict total number

counts in section 6.3 and the abundance of substructure within a Milky Way-like galaxy in section 6.4. Finally we check, based on parameter bounds derived in the previous section, whether the distinctive structure of dark matter halos present in scalar field dark matter models such as ours can be observed in the near future in section 6.5.

We present our conclusions in chapter 7.

1.3 CONVENTIONS

We will make all our conventions clear when they are introduced in this thesis for the first time, but it might nonetheless be helpful to give a short overview over the most important ones at this point.

- We work in units with $\hbar = k_B = c = 1$.
- The metric signature we employ is $(-1, 1, \ldots, 1)$.
- A dot (like $\dot{a}$) denotes a derivative with respect to cosmic time t, whereas a prime (like a') denotes a derivative with respect to conformal time τ.
- Greek indices run over all spacetime coordinates (e.g. $\alpha = 0, \ldots, n$), whereas latin indices run only over the spatial coordinates (e.g. $i = 1, \ldots, n$).
- A subscript 0 denotes a quantity evaluated for the present time t_0. The scale factor is always normalized to $a_0 = 1$.

2 THE HOMOGENEOUS UNIVERSE

The science of cosmology saw its foundations laid in the early 20$^{\text{th}}$ century with the groundbreaking formulation of the theory of general relativity (GR) by Albert Einstein [Einstein, 1915c,a]. Since then, physicists from both theory and observation have developed an extensive set of fundamental concepts and calculational techniques which are used to predict and/or explain a vast multitude of physical observations. Many of these concepts and techniques are nowadays widely used and have become standard repertoire for every aspiring cosmologist to master. In this chapter we want to introduce the most fundamental cornerstone of this language, the ingredients necessary to proceed with investigations of the so called *background cosmology*, which describes the evolution of our universe under the assumption of spatial homogeneity and isotropy.

The contents of this chapter are standard material and can be found in many textbooks, review articles and lecture notes, we mainly rely on [Weinberg, 1972, Carroll, 2004, Weinberg, 2008, Amendola and Tsujikawa, 2010, Gorbunov and Rubakov, 2011b]. Our presentation will therefore be very compact, skipping many details and calculations which are readily available in the literature. Our purpose is not to give an exhaustive overview of the subject matter, but to provide the reader with the necessary information to understand the more advanced work presented in the following chapters and to set up our notational conventions. The experienced reader may safely skip this part and move on directly to chapter 3.

2.1 THE SPATIAL SYMMETRY ASSUMPTIONS

Before we continue, we want to pause for a moment to discuss one fairly obvious objection: The universe is clearly not homogeneous. Nor is it isotropic. The planets in our solar system move around the sun on a preferred spatial hyperplane and so do the stars in our galaxy. Furthermore, even within these hyperplanes, the distribution of matter is clearly not homogeneous, and one could provide many additional examples. So why is the science of cosmology based on a set assumptions that seems to be, plainly spoken, wrong?

First, as we will see below in more detail, Einstein's equation describing gravity are quite intricate, and trying to find a solution corresponding to a matter distribution as complicated as we find in our universe does not appear feasible. Without any simplifying symmetry assumptions, which are necessarily approximations, we can not hope to make substantial progress. Second, these symmetry assumptions are not as bad as they appear at first sight. If we average the matter content of the

universe over sufficiently large scales of roughly 100 Mpc (approximately 3×10^8 lightyears), the resulting distribution appears to be homogeneous [Sarkar et al., 2009]. Furthermore, observations of the cosmic microwave background (CMB) indicate that the universe must have been homogenous and isotropic to very high accuracy in its early days [Dicke et al., 1965, Penzias and Wilson, 1965a, Fixsen et al., 1996, Ade et al., 2013a]. It therefore seems that the symmetry assumptions of spatial homogeneity and isotropy hold on sufficiently large scales.

Before moving on to a mathematical description of such a universe we want to mention some caveats. First, the observations supporting large-scale homogeneity and isotropy are still under scrutiny, and a differing scenario may ultimately emerge. This holds for both the distribution of galaxies [Labini et al., 2009b,a] and the temperature anisotropies of the CMB at large scales [Copi et al., 2009, Hansen et al., 2009, Hoftuft et al., 2009]. Second, all observations are naturally limited to the observable universe and can not tell us anything about space outside this region. In fact, some theoretical models of the very early universe, so called *eternal inflation* models, suggest that the universe may look drastically different outside of our own observable 'bubble' [Linde, 1982, Steinhardt, 1982, Vilenkin, 1983]. This scenario, however, does not have any consequences for the mathematical description of our observable universe and may be considered a less serious problem in that respect. Third, there is the longstanding issue of averaging Einstein's equations, which are non-linear. In the context of cosmology the problem can be described as follows: An averaging of the matter content over some large scale R corresponds to washing out all inhomogeneities at smaller scales by applying a window function $W_R(\vec{x})$. We then want to integrate the resulting equations in time starting from some initial configuration, but immediately find that, due to the non-linearity of Einstein's equations, application of the window function and time-evolution do not commute. Evolving the equations first with the full complicated matter distribution and then averaging the result gives a different outcome than averaging the matter content first and then evolving the equations. This issue of course does not arise if all fluctuations are small and we can linearize Einstein's equations. Current gravitationally bound structures are however roughly 200 times denser than the average cosmic matter density, and therefore highly non-linear. Any effect they might have on the overall cosmic expansion which deviates from the results of the homogenous and isotropic calculation is called *backreaction*. Such effects have been invoked to try and explain the observed accelerated cosmic expansion without a dark energy component, but so far these attempts have been unsuccessful. It appears that backreaction merely provides precision corrections to standard results, at least for the cosmological standard model [Schwarz, 2010]. For more exotic (strongly coupled) models, however, this effect can be much bigger and in fact alter the expansion history of the universe considerably [Ayaita et al., 2012b].

Bearing these caveats in mind, the bottom line remains that the description of the universe on very large scales as homogeneous and isotropic has been tremendously successful in explaining a vast number of observations and therefore seems to be justified. We can of course not explain the emergence of cosmic structure within this framework, we will describe how that is done in the later chapters of this thesis. For now we restrict ourselves to a scenario in which all dynamical quantities describing the matter content of the universe and spacetime itself can only depend on time, not on spatial coordinates.

2.2 General relativity

Probably the most striking feature of general relativity when compared to Newtonian gravity is that time and space are no longer considered to be a fixed background in which physical events take place, instead they become dynamical quantities themselves. Together they form a differentiable manifold called *spacetime*, and the dynamical variable describing its evolution is the metric $g_{\mu\nu}$, formally defined as a (non-degenerate) $(0,2)$-tensorfield on spacetime. It is often given in terms of a line element

$$ds^2 = g_{\mu\nu}dx^\mu dx^\nu . \tag{2.1}$$

In this context gravity is no longer given by an additional force which can be described as a force-field (vector-field) or gravitational potential (function) on spacetime, but is instead realized through the curvature of spacetime itself. The number of models one can write down within this basic framework is infinite. The theory named general relativity by Einstein is only one version, one could argue the simplest one available. Many extensions of it exist, and we will discuss some of them below and in chapter 3. Since a large class of such generalizations are frequently referred to as generally relativistic as well, we will call Einstein's specific theory as derived from the Einstein-Hilbert action below *Einstein gravity* (and not GR), in order to avoid confusion.

2.2.1 Einstein gravity

Amazingly, with the basic idea of curved spacetime as the manifestation of gravity in mind, Einstein was able to develop his theory of gravity (largely) without guidance from observations, as conflicts between the prevailing theory of Newtonian gravity and observations were (almost) non-existent at that time. Instead he used physical intuition and a few additional principles. As a starting point, the theory obviously had to recover Newtonian mechanics in some suitable limit, which is the limit of weak gravitational fields, meaning small curvature of spacetime, and of small velocities, if we want to avoid special relativity. From this principle it is already obvious that the spacetime-manifold needs to be Lorentzian, i.e. the signature of the metric is necessarily $(-1,1,1,1)$, since we want to be able to recover Minkowski-spacetime at least locally. (Sometimes the sign-convention is chosen in precisely the opposite manner, i.e. $(1,-1,-1,-1)$. We will work with a minus-sign in the time coordinate, which is far more common in cosmology.) Furthermore Einstein invoked a generalized version of the weak equivalence principle of equality of gravitational and inertial mass already present in Newtonian mechanics, known as the *Einstein equivalence principle* (EEP). Carroll [2004] formulates it as follows:

> "In small enough regions of spacetime, the laws of physics reduce to those of special relativity; it is impossible to detect the presence of a gravitational field by local experiments."

After some consideration one can convince oneself that the essential implication of the EEP is the following: All forms of matter, even all forms of energy-momentum, should couple to gravity in the same fashion. This concept of *universality* is at the heart of GR, but does not uniquely determine the

theory. In fact, it is hard to state precisely what its mathematical implications are, as we will discuss further below. But first, we want to introduce Einstein gravity. As a generalization of Newtonian mechanics, it should sensibly also consist of two kinds of equations: One determining the motion of particles in a gravitational field (like Newtons law of motion) and one describing how matter (or rather energy-momentum) sources the gravitational potential, which in GR is curvature (like the Poisson equation of Newtonian mechanics). A necessary preface to writing down these equations is a quantification of curvature. On any manifold this requires a connection (or *covariant derivative*) $\mathcal{D}_\mu$ with corresponding connection-coefficients $\Gamma^\alpha_{\beta\gamma}$, which tell us how to move tensors from one point of the manifold to another one along a given path. With such a connection the Riemann-curvature-tensor is defined as

$$R^\rho_{\sigma\mu\nu} = \partial_\mu \Gamma^\rho_{\nu\sigma} - \partial_\nu \Gamma^\rho_{\mu\sigma} + \Gamma^\rho_{\mu\lambda}\Gamma^\lambda_{\nu\sigma} - \Gamma^\rho_{\nu\lambda}\Gamma^\lambda_{\mu\sigma}\,, \tag{2.2}$$

where $\partial_\mu \equiv \partial/\partial x^\mu$ is a partial derivative and x^μ are some local coordinates.

While the choices of connections on a manifold are plentiful, given a metric, there is a canonical choice known as the *Levi-Civita connection*, which is defined uniquely by the demands that is should be torsion-free and preserve the metric, i.e.

$$\mathcal{T}^\lambda_{\mu\nu} \equiv \Gamma^\lambda_{\mu\nu} - \Gamma^\lambda_{\nu\mu} = 2\Gamma^\lambda_{[\mu\nu]} = 0\,, \quad \mathcal{D}_\mu g_{\mu\nu} = 0\,. \tag{2.3}$$

For this connection the coefficients (also known as *Levi-Civita symbols* in this case) can be calculated directly from the metric as follows:

$$\Gamma^\alpha_{\mu\nu} = \frac{1}{2} g^{\alpha\rho}\left(\partial_\mu g_{\rho\nu} + \partial_\nu g_{\rho\mu} - \partial_\rho g_{\mu\nu}\right)\,. \tag{2.4}$$

One of the nice features of the Levi-Civita connection is that, due to the absence of torsion, one can easily convince oneself that the Riemann tensor indeed measures curvature. If we parallel transport a vector v^μ along an infinitesimal closed loop spanned by two vector fields A^μ and B^μ, it will change according to

$$\delta v^\mu = \mathcal{F} A^\sigma B^\tau \left[\mathcal{D}_\sigma, \mathcal{D}_\tau\right] v^\mu = \mathcal{F} R^\mu_{\rho\sigma\tau} v^\rho A^\sigma B^\tau\,, \tag{2.5}$$

where we have assumed that v^μ is first transported along A^μ and then along B^μ, and $\mathcal{F}$ denotes the area enclosed by the loop.

Having quantified curvature (we will only consider the Levi-Civita connection from now on), we can finally write down Einstein's equations, which read:

$$R_{\mu\nu} - \frac{1}{2} R g_{\mu\nu} = \frac{1}{M_p^2} T_{\mu\nu}\,. \tag{2.6}$$

Here $R_{\mu\nu}$ is the Ricci tensor, which, due to the symmetry constraints arising from the first Bianchi identity, is the only non-trivial independent contraction of the Riemann tensor with the (inverse) metric, and R is its trace, known as the Ricci scalar:

$$R_{\mu\nu} \equiv R^\lambda_{\mu\lambda\nu}\,, \quad R \equiv R^\mu_\mu\,. \tag{2.7}$$

Furthermore we have introduced the reduced Planck mass $M_p = \sqrt{\hbar c/8\pi G} \approx 2.435 \times 10^{18}$ GeV/c^2. Throughout this thesis, we will work with units of $\hbar = c = 1$, i.e. express everything in terms of energy scales. Finally, $T_{\mu\nu}$ is the energy-momentum tensor of matter, which we will define more rigorously below. The principle of universality is directly visible in this equation, as the curvature is simply determined by the overall energy-momentum.

Having written down the generalization of the Poisson-equation in Newtonian gravity, we still have to do the second part, explain how particles react to the presence of curvature. The way this is done in Einstein gravity is to generalize Newtons first law to curved spaces, which can be formulated as follows:

> "In the absence of external forces, particles move on geodesics."

This is of course only true as long as there are no additional fields present which can change this behaviour, like the electromagnetic field for charged particles. The geodesic equation reads

$$\frac{\mathrm{d}^2 x^\mu}{\mathrm{d}\eta^2} + \Gamma^\mu_{\rho\sigma} \frac{\mathrm{d}x^\rho}{\mathrm{d}\eta} \frac{\mathrm{d}x^\sigma}{\mathrm{d}\eta} = 0\,, \tag{2.8}$$

where η is the proper time of the particle.

Both sets of relevant equations (2.6) and (2.8) can be derived from an action principle, which we consider to be the most adequate approach for a field theory such as Einstein gravity. For GR, this concept goes back to Hilbert [1915], who first wrote down the gravitational part of the following action:

$$S = \underbrace{\frac{M_p^2}{2} \int \sqrt{-g} R \,\mathrm{d}^4 x}_{S_G} + \underbrace{\int \sqrt{-g}\, \mathcal{L}_m \,\mathrm{d}^4 x}_{S_m}\,. \tag{2.9}$$

Here S_G denotes the gravitational part of the action, also known as *Einstein-Hilbert action*, and S_m is the matter part of the action, with $\mathcal{L}_m$ containing all matter fields present in the theory. The measure factor in the integrals contains the determinant of the metric $g = |g_{\mu\nu}|$. Now we can define the energy-momentum tensor rigorously:

$$T_{\mu\nu} = \frac{-2}{\sqrt{-g}} \frac{\delta S_m}{\delta g^{\mu\nu}}\,, \tag{2.10}$$

and Einstein's equations follow from variation of this action with respect to the metric. The influence of curvature on the matter fields can be obtained from varying the action with respect to the matter fields present. For a single particle of mass m without any external forces the action reads

$$S_m = -m \int \mathrm{d}\eta\,, \quad \text{i.e.} \quad \mathcal{L}_m = -\frac{m}{\sqrt{-g}} \sqrt{g_{\mu\nu} \frac{\mathrm{d}x^\mu}{\mathrm{d}\lambda} \frac{\mathrm{d}x^\nu}{\mathrm{d}\lambda}} \frac{\mathrm{d}\lambda}{\mathrm{d}x^0} \delta^3\left(\vec{x} - \vec{x}(\lambda)\right)\,, \tag{2.11}$$

where we chose λ to parameterize the path of the particle. Variation (this time with respect to the trajectory, as we have a point particle) directly recovers the geodesic equation (2.8).

At this point the description or Einstein gravity can be considered complete, Einstein's equations plus the equations of motion arising from the variation of the action with respect to the matter fields

are all we need. There are no additional equations required on a fundamental level. It is nonetheless very useful in many instances to employ the equations of energy- and momentum conservation as they arise in Einstein gravity. The most direct approach is to employ the second Bianchi identity in connection with Einstein's equations, which directly leads to

$$\mathcal{D}_\mu T^{\mu\nu} = 0\,. \tag{2.12}$$

This set of equations is usually referred to as energy conservation for the time-component ($\nu = 0$) and momentum conservation for the spatial ones ($\nu = 1,2,3$). We do want to point out that there need not necessarily be a conserved charge associated with this equation, this is a major distinction between a dynamical global geometry when compared to a fixed background.

If the matter part of the action contains several components, i.e.

$$S_m = \sum_i S_{m,i}\,, \tag{2.13}$$

generically only the total energy-momentum tensor is conserved. However, if the matter fields appearing in $S_{m,i}$ do not appear in $S_{m,j}$ for $i \neq j$ we think of these different fields as uncoupled (even though they do of course couple gravitationally), and in fact their individual energy-momentum tensors are conserved separately:

$$T_{i\mu\nu} = \frac{-2}{\sqrt{-g}}\frac{\delta S_{m,i}}{\delta g^{\mu\nu}}\,, \quad \mathcal{D}_\mu T_i^{\mu\nu} = 0\,. \tag{2.14}$$

This can be (heuristically) understood from the fact that variations of the total action include cases where only the metric and one single uncoupled matter field are varied, everything else is kept fixed. It is these variations which give rise to the conservation of the energy-momentum tensors separately.

Before we move on to describe some alternative theories of gravity, we want to come back to one interesting point. As we already mentioned above, when first developing GR, Einstein was guided by the EEP, which lead him to the concept of universality. What this means mathematically is not very clear, however, probably the most useful definition is that all matter fields ψ_i appearing in the matter Lagrangian $\mathcal{L}_m$ should be *minimally coupled* to gravity. By this we means that $\mathcal{L}_m$ neccessariy contains the matter fields ψ_i and the metric $g_{\mu\nu}$, but no direct coupling to the curvature tensors should be present. In accordance with common usage, we will refer to fields satisfying this constraint as minimally coupled (in contrast to *non-minimally coupled*), whereas the expression *uncoupled* refers to the absence of explicit couplings between different matter fields ψ_i. As will soon see, there are still many different theories one can write down which satisfy the constraint of universality (e.g. $f(R)$-theories of gravity) and even some theories which seem to violate it at first sight, but can be transformed into a form where they do (like scalar-tensor theories of gravity).

2.2.2 ALTERNATIVE THEORIES OF GRAVITY

One can deviate from Einstein's theory and come up with alternatives in many ways, even when one sticks to the very basic notion of gravity being realized as the curvature of spacetime. Since this will

become relevant in chapter 3, we want to shorty discuss some possibilities, but are not claiming to be comprehensive here. In this section we particularly follow [Carroll, 2004].

On the most fundamental level, one could use a connection different from the Levi-Civita one. However, as long as one leaves oneself enough freedom in the matter part of the action, this does not really create anything new. To see this one needs to know one important fact, which we state here without proof:

> Any connection which does not preserve the metric (i.e. $\mathcal{D}_\mu g_{\mu\nu} \neq 0$) can be written as a metric compatible part plus a tensorial correction.

One should remember here that the connection coefficients are not tensors, they follow a different, non-tensorial transformation rule under coordinate change. However, the difference of two connection coefficients is tensorial. Therefore any theory based on a non-Levi-Civita connection can be recast as a theory based on a Levi-Civita connection with additional tensor fields in the matter sector of the action, which represent either torsion or departure from metric-compatibility or both. In most cases such a matter Lagrangian would contain derivative couplings, i.e. non-minimally coupled fields, as for example the torsion-tensor typically couples directly to the Ricci scalar (see e.g. [Sotiriou and Faraoni, 2010]), which violates the principle of universality. These theories are sometimes referred to as non-metric theories. In this sense these theories can be seen as a true extension of Einstein-gravity, but we will not consider them further in this thesis.

A second possibility we want to discuss is an extension of Einstein gravity to higher dimensions. Obviously we only observe four-dimensional spacetime, the extra dimensions need to be hidden from us in some way. There are essentially two popular possibilities to do this: The first one is to assume that somehow all fundamental interactions other than gravity are spatially restricted to a three-dimensional subspace, called a brane, within the higher-dimensional space, called the bulk. If the extra dimensions are macroscopic, such a *braneworld* approach could potentially explain the weakness of the gravitational interaction [Rubakov and Shaposhnikov, 1983, Gogberashvili, 1999]. As an alternative, one could assert that the extra dimensions are very small. This obviously implies that their volume is finite and the usual suspects are therefore compact spaces, but this is not mandatory. There are non-compact finite volume spaces. In such a scenario the additional spatial directions would be hidden from us because all experiments take place at energy scales below the typical inverse length scale of the extra dimensions, making them insensitive for their detection. These models fall into the class of *Kaluza-Klein theories*, named after the first researchers who investigated them [Kaluza, 1921, Klein, 1926].

Let us examine these models a little further. To do this we need to introduce the concept of dimensional reduction, which shows how to derive effective four-dimensional equations of motion for these theories. As a toy example, we consider Einstein gravity in $d = D+4$ dimensions and a simple ansatz for the metric which reads

$$\mathrm{d}s^2 = \hat{g}_{\hat{\mu}\hat{\nu}}\,\mathrm{d}\hat{x}^{\hat{\mu}}\,\mathrm{d}\hat{x}^{\hat{\nu}} = \tilde{g}_{\mu\nu}(x)\,\mathrm{d}x^\mu\,\mathrm{d}x^\nu + l^2(x)\,\gamma_{\alpha\beta}(y)\,\mathrm{d}y^\alpha\,\mathrm{d}y^\beta\,. \tag{2.15}$$

In this ansatz x^μ are the coordinates in four-dimensional space with μ,ν running from 0 to 3 and y^α are the coordinates on the extra-dimensional space, with α,β running from 4 to $d-1$. The four-dimensional metric is denoted by $\tilde{g}_{\mu\nu}$ (the reason for the use of the tilde will become apparent below), the metric on the *internal space* by $\gamma_{\alpha\beta}$ and $l(x)$ is a so called warping factor. The coordinates $\hat{x}^{\hat{\mu}}$ describe the entire higher dimensional spacetime, with $\hat{\mu},\hat{\nu}$ running from 0 to $d-1$ and $\hat{g}_{\hat{\mu}\hat{\nu}}$ is the corresponding metric. In the following formulas we will extend this nomenclature to the curvature quantities, in particular $\tilde{R}$ will denote the four-dimensional Ricci scalar, $R^{(D)}$ the one corresponding to the internal metric $\gamma_{\alpha\beta}$ and $\hat{R}$ will be the complete higher-dimensional one. Similarly $\tilde{\mathcal{D}}_\mu$ will be covariant derivatives with the connection derived from the four-dimensional metric, M_p will be the effective four-dimensional reduced Planck mass and $\hat{M}_p$ will be the higher-dimensional equivalent.

Einstein gravity in higher dimensions is of course determined by the action

$$S = \int \mathrm{d}^d\hat{x}\,\sqrt{-\hat{g}}\left(\frac{\hat{M}_p^2}{2}\hat{R} + \hat{\mathcal{L}}_m\right), \tag{2.16}$$

where $\hat{\mathcal{L}}_m$ denotes the higher-dimensional matter Lagrangian. We now want to integrate over the internal space, i.e. perform the integral over the y-coordinates in the action (2.16) explicitly, thereby reducing the dimensionality of the theory to four. To do this we need to rewrite the higher-dimensional Ricci scalar as

$$\hat{R} = \tilde{R} + l^{-2}R^{(D)} - 2Dl^{-1}\tilde{g}^{\mu\nu}\tilde{\mathcal{D}}_\mu\tilde{\mathcal{D}}_\nu l - D(D-1)l^{-2}\tilde{g}^{\mu\nu}(\tilde{\mathcal{D}}_\mu l)(\tilde{\mathcal{D}}_\nu l)\,. \tag{2.17}$$

The integration over the y-coordinates gives rise to new quantities in the effective four-dimensional theory, which we label as follows:

$$\mathcal{V} \equiv \int \mathrm{d}^D y\,\sqrt{\gamma}, \quad \kappa \equiv \int \mathrm{d}^D y\,\sqrt{\gamma}R^{(D)}, \quad \mathcal{L}_m \equiv \int \mathrm{d}^D y\,\sqrt{\gamma}\hat{\mathcal{L}}_m\,. \tag{2.18}$$

Note that with our ansatz for the metric, only the matter Lagrangian $\mathcal{L}_m$ still contains degrees of freedom depending on the coordiates x^μ, $\mathcal{V}$ and κ are constants which can be interpreted as volume (for $l(x)=1$) and curvature of the internal space. With these quantities defined we can perform the dimensional reduction using that

$$\sqrt{-\hat{g}} = l^D\sqrt{-\tilde{g}}\sqrt{\gamma} \tag{2.19}$$

and obtain:

$$S = \int \mathrm{d}^4x\,\sqrt{-\tilde{g}}\,l^D\left\{\frac{\hat{M}_p^2\mathcal{V}}{2}\left[\tilde{R} + l^{-2}\kappa + D(D-1)l^{-2}\tilde{g}^{\mu\nu}(\tilde{\mathcal{D}}_\mu l)(\tilde{\mathcal{D}}_\nu l)\right] + \mathcal{L}_m\right\}, \tag{2.20}$$

where we integrated once by parts. The theory we have recovered is gravity coupled the scalar field l in four dimensions. Such a *scalar-tensor theory* is the third possibility of modifying Einstein gravity we want to discuss here, and it arises naturally from a higher-dimensional setting.

Before we investigate this further, let us look a bit closer at what we have done. We have assumed a specific form of the metric and also the matter fields, in particular a specific shape of the internal geometry and a matter field configuration in the higher dimensions, which allows us to define the

integrals in equation (2.18). Strictly speaking this is quite a leap. We have taken for granted that the following procedure is in principle possible for a given matter Lagrangian $\hat{\mathcal{L}}_m$:

1. Find a solution of the higher-dimensional field equations.
2. Expand all dynamical quantities $(\zeta_1, ..., \zeta_n)$ in this solution (both metric an matter fields) in a complete set of functions $f_i(y)$, $i \in \mathbb{N}$ (like a Fourier-series) on the internal coordinates: $\zeta_i(x,y) = \zeta_{ij}(x) f_j(y)$.[1]
3. Integrate the action over the internal y-coordinates to arrive at an effective four-dimensional theory.

While steps 1 and 2 can be very difficult to calculate explicitly, the crucial part is really step three, as there is no guarantee that all the necessary integrals do exist, they may well be infinite if the internal geometry and/or the internal matter field configuration is not suitable. It is therefore clear that the *reducability* of a higher-dimensional solution is an additional requirement, it goes beyond the higher-dimensional field equations. We will come back to this crucial point in chapter 3.

If dimensional reduction is possible, it is only appropriate as long as the excitations we integrate out correspond to high energy excitations. This means that the resulting four-dimensional theory is valid in the limit of energies which are small compared to the internal excitations. In such a situation dimensional reduction will in general give rise to a huge number of effective four-dimensional degrees of freedom, one for each coefficient ζ_{ij}. These degrees of freedom can be manifested as scalar fields (as we have seen above), but also vector fields or tensor fields can arise from higher-dimensional Einstein gravity alone, even without a matter Lagrangian. If the original matter Lagrangian contains spinors, spinor degrees of freedom can show up in the effective four-dimensional theory as well. From these considerations it should be clear that the ansatz (2.15) and the resulting theory (2.20) is a prticularly simple example, the existence of which is far from obvious for a given matter Lagrangian. (It can however be rigorously derived with a specific choice of gauge fields in $\mathcal{L}_m$, as was shown in [Carroll et al., 2002]).

Let us now go back and investigate the resulting scalar-tensor theory given by equation (2.20). For convenience, we introduce the four-dimensional Planck mass $M_p^2 = \hat{M}_p^2 \mathcal{V}$ and a redefined scalar field

$$\phi \equiv \sqrt{\frac{D(D+2)}{2}} M_p \ln(l)\,. \tag{2.21}$$

Now the dimensionally reduced action reads

$$S = \int \mathrm{d}^4x \sqrt{-\tilde{g}} \left[\frac{M_p^2}{2} \mathrm{e}^{\alpha\phi/M_p} \tilde{R} + \kappa \frac{M_p^2}{2} \mathrm{e}^{\frac{(D-2)}{D}\alpha\phi/M_p} + \frac{D-1}{D-2} \mathrm{e}^{\alpha\phi/M_p} \tilde{g}^{\mu\nu} (\tilde{\mathcal{D}}_\mu \phi)(\tilde{\mathcal{D}}_\nu \phi) + \mathrm{e}^{\alpha\phi/M_p} \mathcal{L}_m \right], \tag{2.22}$$

[1] We only consider a discrete set of functions here. The generalization to a continuous set is straightforward.

where $\alpha = \sqrt{2D/(D+2)}$. This seems to be quite a complicated theory. The coupling in front of the Ricci-scalar is now ϕ-dependent, which can be interpreted as a time-dependent Planck-mass. Furthermore the scalar field ϕ has a non-canonical kinetic term, an exponential potential and a coupling to the matter sector. We can however simplify things considerably by a simple redefinition of the metric by means of a so called Weyl-transformation:

$$g_{\mu\nu} \equiv \tau^2 \tilde{g}_{\mu\nu} \,. \tag{2.23}$$

The transformation of the curvature tensors under such a scaling is straightforward (if a little tedious) to calculate, the results can be found e.g. in [Carroll, 2004]. What we need here is the result for the Ricci scalar, which reads in n dimensions:

$$\tilde{R} = \tau^2 R + 2(n-1) g^{\mu\nu} \tau^2 \mathcal{D}_\mu \mathcal{D}_\nu \ln\tau - (n-2)(n-1)\tau^2 g^{\mu\nu} (\mathcal{D}_\mu \ln\tau)(\mathcal{D}_\nu \ln\tau) \,. \tag{2.24}$$

Note that the backtransformation can not be directory obtained from rearranging this equation, as the covariant derivatives need to be adjusted to the respective metric as well. With the choice

$$\tau = \mathrm{e}^{\alpha\phi/2M_p} \tag{2.25}$$

the action (2.22) can be rewritten in terms of the new metric $g_{\mu\nu}$ as

$$S = \int \mathrm{d}^4x \sqrt{-g} \left[\frac{M_p^2}{2} R - \frac{1}{2} g^{\mu\nu} (\mathcal{D}_\mu \phi)(\mathcal{D}_\nu \phi) + \kappa \frac{M_p^2}{2} \mathrm{e}^{\frac{D+2}{D} \frac{\alpha\phi}{M_p}} + \mathrm{e}^{-\alpha\phi/M_p} \mathcal{L}_m \right] . \tag{2.26}$$

This looks a lot more familiar. The curvature term is now the same as in the Einstein-Hilbert action (2.9), and if we interpret the scalar kinetic and potential terms as part of the matter action, Einstein's equations remain unchanged. For this reason the action in this form (with a constant Planck mass) is known as valid in the *Einstein frame*, whereas the form (2.22) with a time-dependent Planck mass is called the *Jordan frame* action.

In a more general context, scalar-tensor theories in four dimensions can be written as follows:

$$S = \int \mathrm{d}^4x \sqrt{-\tilde{g}} \left[F(\phi)\tilde{R} - \frac{1}{2} G(\phi) \tilde{g}^{\mu\nu} (\tilde{\mathcal{D}}_\mu \phi)(\tilde{\mathcal{D}}_\nu \phi) - \tilde{V}(\phi) + \mathcal{L}_m \right] , \tag{2.27}$$

with a scalar potential $\tilde{V}(\phi)$ and a possibly non-canonical kinetic term in the Jordan frame. One can of course still make a Weyl-transformation to the Einstein frame, this time choosing

$$\tau^2 = 2M_p^{-2} F(\phi) \tag{2.28}$$

and obtain the following action:

$$S = \int \mathrm{d}^4x \sqrt{-g} \left[\frac{M_p^2}{2} R - \frac{1}{2} K(\phi) g^{\mu\nu} (\mathcal{D}_\mu \phi)(\mathcal{D}_\nu \phi) - V(\phi) + \frac{M_p^4}{4F^2(\phi)} \mathcal{L}_m \right] , \tag{2.29}$$

where

$$K(\phi) = \frac{M_p^2}{2F^2(\phi)}\left(3F'(\phi)^2 + G(\phi)F(\phi)\right) \quad \text{and} \quad V(\phi) = \frac{M_p^4}{4F^2(\phi)}\tilde{V}(\phi)\,. \tag{2.30}$$

One can now redefine the scalar field and make it canonical by introducing

$$\varphi \equiv \int \sqrt{K(\phi)}\mathrm{d}\phi\,, \tag{2.31}$$

which change the functional shape of the scalar potential and the coupling to the matter sector to

$$V(\phi(\varphi)) \quad \text{and} \quad \frac{M_p^4}{4F^2(\phi(\varphi))} \quad \text{respectively.} \tag{2.32}$$

The corresponding field equations from variation of φ then read

$$\mathcal{D}_\mu\mathcal{D}^\mu\varphi - \frac{\partial V(\phi)}{\partial\phi}|_{\phi(\varphi)}\frac{\partial\phi(\varphi)}{\partial\varphi} - \frac{M_p^4}{2F^3(\phi(\varphi))}\frac{\partial F(\phi)}{\partial\phi}|_{\phi(\varphi)}\frac{\partial\phi(\varphi)}{\partial\varphi}\mathcal{L}_m = 0\,. \tag{2.33}$$

Again, a possibly non-canoncial scalar-tensor theory in the Jordan frame can be rewritten as a canonical scalar field in Einstein-gravity in the Einstein frame, if we interpret the scalar field as part of the matter action. In contrast to the non-metric theories discussed above, scalar-tensor theories remain minimally coupled in the Einstein frame, as can be seen from the action (2.29). It is therefore justified to say that this possibility has already been incorporated in Einstein-gravity, if one allows for sufficient freedom in the matter part of the action. One need not even give up universality. This statement should not be misunderstood! Once we fix the matter Lagrangian $\mathcal{L}_m$, the physical predictions of using either a scalar-tensor type theory or Einstein gravity can of course be very different. However, we can, by a suitable extension of the matter Lagrangian in Einstein gravity including a scalar field and a suitable coupling, come up with a theory which is related to the scalar-tensor scenario by a simple Weyl-scaling and therefore equivalent.

As a last generalization of Einstein-gravity we want to discuss a modification of the Einstein-Hilbert action through higher order curvature terms, making extensive use of the review [Sotiriou and Faraoni, 2010]. The motivation for considering this can be twofold: First of all, we expect Einstein-gravity to be an effective theory of gravity, valid at sufficiently low energy scales. At higher energies (around the Planck scale) we expect quantum effects to become relevant, and, in accordance with what we know from other quantum field theories, all terms allowed by the basic symmetries of the theory should in principle be present. In fact, these terms are necessary in order to render the theory renormalizable. Second, the presence of dark matter and dark energy in cosmology could potentially be explained not by so far unknown particles, but by a modification of the laws of gravity (though these effects can be difficult to disentangle, as we will soon see). However, some higher order curvature-terms have severe disadvantages, so let us take a closer look. A possible generalized gravity-action could look like this:

$$S = \underbrace{\int \mathrm{d}^4x\sqrt{-g}\,\frac{M_p^2}{2}f(R)}_{S_{fR}} + \underbrace{\int \mathrm{d}^4x\sqrt{-g}\,\alpha_1 R_{\mu\nu}R^{\mu\nu}}_{S_d} + S_m\,. \tag{2.34}$$

One of the major issues with higher order curvature terms can be seen from the variation of the action S_d. The field equations resulting from the $R_{\mu\nu}R^{\mu\nu}$-term will give rise to field equations which are higher than second order. This is a very fundamental change to the nature of theory! It no longer suffices to provide initial conditions for the dynamical fields and their first derivatives, one needs higher derivatives as well. This is generally considered very undesirable and might be difficult to reconcile with the limit of Newtonian gravity, which is based on second order equations. But there are even more serious objections. For the action S_d, if one transforms the variables to a Hamiltonian formulation, one finds that the resulting Hamiltonian is not bound from below, resulting in a linear instability sometimes referred to as *Ostrogradsky instability*. This is clearly unacceptable. It can in some instances be fixed by imposing constraints through the insertion of additional fields in the action [Chen et al., 2013], but let us keep in mind that the example given in S_d is only one example of many possible higher order contractions of the curvature tensor, the inclusion of which will typically give rise to the same issue. We will stay away from these kind of theories.

The first part of the action, named S_{fR}, is free of such issues, which is one of the major reasons it has been a popular modification of gravity known as $f(R)$-gravity. The modified Einstein equations arising from this action (and the matter action S_m) simply read [Sotiriou and Faraoni, 2010]

$$f'(R)R_{\mu\nu} - \frac{1}{2}f(R)g_{\mu\nu} - \left[\mathcal{D}_\mu\mathcal{D}_\nu - g_{\mu\nu}\mathcal{D}^\lambda\mathcal{D}_\lambda\right]f'(R) = \frac{1}{M_p^2}T_{\mu\nu}\,, \tag{2.35}$$

which is still a second order equation. This seems like a perfectly valid true alternative to Einstein-gravity at first sight, since it allows for the correct Newtonian limit (e.g. for $f(R) = R + O(R^2)$) and a minimally coupled matter sector. It is however possible to show that this class of theories again only has one additional scalar degree of freedom when compared to Einstein gravity, and in fact, can be rewritten as a particular class of scalar-tensor theory, known as *Brans-Dicke models* [Brans and Dicke, 1961]. These models are a subclass of the generic scalar-tensor theory given above, with the specific choice

$$F(\phi) = \phi \quad \text{and} \quad G(\phi) = \frac{2\omega}{\phi}\,, \tag{2.36}$$

where ω is known as the Brans-Dicke parameter. As long as $f''(R) \neq 0$ everywhere, $f(R)$-theories are equivalent to Brans-Dicke theories with $\omega = 0$, i.e. to a theory without a kinetic term for the scalar field.

As we have seen, many modifications of Einstein-gravity are often problematic due to very fundamental reasons (such as instabilities of the Hamiltonian) or can be re-expressed as Einstein-gravity with some form of exotic matter, typically scalar fields, in the matter part of the action. In the latter case of equivalent theories both viewpoints are perfectly valid and correct. Whether one tries to explain effects typically attributed to dark matter or dark energy one way or the other, is then merely a matter of choice. In this thesis we will not be much concerned with the viewpoint of modified gravity, but will extensively focus on the second possibility, exotic forms of matter, in particular scalar fields, instead. The only exception is chapter 3, where we will combine higher dimensions, scalar tensor theories and higher order curvature terms to discuss one particularly interesting class of gravity-theories, which serves as motivation for the work presented in the later chapters. But for

now, let us move on to the description of our universe in the approximation of spatial homogeneity and isotropy within the framework of Einstein gravity.

2.3 Dynamics of an expanding universe

2.3.1 FLRW-solutions

Not long after the invention of general relativity, the first investigations of so called *world models*, meaning mathematical descriptions of our universe in its totality based on the field equations of GR, were carried out by Einstein himself [Einstein, 1917] and others. Most mentionable amongst those researchers are probably Alexander Friedmann, who was the first to reduce Einstein's field equations to a much smaller set of equations now known as Friedmann's equations and find simple solutions [Friedmann, 1922, 1924], George Lemaître, who arrived at similar results somewhat later, but independently of Friedmann [Lemaître, 1927, 1931], and Howard Percy Robertson and Arthur Geoffrey Walker, who proved conclusively that the geometries of the Friedmann-universes are the only possible solutions for a spacetime which is spatially homogeneous and isotropic. These solutions, commonly called *Friedmann-Lemaître-Robertson-Walker* (FLRW)-universes, form the basis of modern cosmology up to today.

The symmetry assumptions of spatial homogeneity and isotropy are of course dependent on the reference frame. An observer for which the universe appears in this way on large scales is called a *comoving observer*, the corresponding coordinate system *comoving coordinates*. In such a reference frame the most generic metric consistent with our symmetry assumptions is known as the FLRW-metric. It describes spacetime with a maximally symmetric spatial hyperplane, the line-element of which reads

$$ds^2 = -\mathrm{d}t^2 + a(t)^2\left[\mathrm{d}r^2 + f_K^2(r)\left(\mathrm{d}\theta^2 + \sin^2\theta \mathrm{d}\varphi^2\right)\right], \tag{2.37}$$

with the radial function

$$f_K(r) = \begin{cases} K^{-\frac{1}{2}}\sin(K^{\frac{1}{2}}r) & \text{for } K > 0 \\ r & \text{for } K = 0 \\ |K|^{-\frac{1}{2}}\sinh(|K|^{\frac{1}{2}}r) & \text{for } K < 0 \end{cases}. \tag{2.38}$$

Here the comoving coordinates are (t, r, θ, φ), where t is the *cosmic time* and (r, θ, φ) are the usual spatial spherical coordinates, $a(t)$ is known as the *scale factor*. The constant K can be interpreted as the spatial curvature, it is related to the three-dimensional Ricci scalar via $R^{(3)} = 6K$. An object which has no *peculiar motion*, i.e. which only changes its spatial position due to the cosmic expansion, remains at fixed comoving coordinates $\vec{x}$. The corresponding physical coordinate is given by $\vec{r}_{ph} = a(t)\vec{x}$.

It is also common to recast this metric in a slightly different form for $K \neq 0$ by introducing a new dimensionless radial coordinate $\omega \equiv |K|^{\frac{1}{2}} r$ and a corresponding scale factor $b(t) \equiv |K|^{-\frac{1}{2}} a(t)$, which has the units of a length. In this case the resulting metric depends only on the sign of the curvature

$k \equiv \mathrm{sgn}(K)$ and looks slightly simpler. However, we prefer to use a dimensionless scale factor here and normalize it to

$$a_0 \equiv a(t_0) = 1\,, \tag{2.39}$$

where t_0 is the current cosmic time, as is common in cosmology. For most of this thesis we will be working with a flat spatial geometry, i.e. with $K = 0$, which is supported by the current best fits to cosmological data sets and also predicted by inflationary scenarios [Ade et al., 2013a,c, Guth, 1981, Guth and Weinberg, 1981, Linde, 1982].

Similar to the metric, the energy momentum tensor is also restricted by our symmetry assumptions. It has to obey the perfect fluid form

$$T_{\mu\nu} = (\rho + p)u_\mu u_\nu + p g_{\mu\nu}\,, \quad u^\mu = (1,0,0,0)\,. \tag{2.40}$$

Here ρ can be interpreted as the energy density and p as the pressure. The form of the four-velocity reflects the fact that the cosmic fluid has no peculiar velocity in its rest frame.

Evaluating Einstein's equations for this metric and energy momentum tensor yields two equations, which are famously known as Friedmann's equations:

$$H^2 \equiv \left(\frac{\dot{a}}{a}\right)^2 = \frac{\rho}{3M_p^2} - \frac{K}{a^2}\,, \tag{2.41}$$

$$\frac{\ddot{a}}{a} = -\frac{1}{6M_p^2}(\rho + 3p)\,. \tag{2.42}$$

Here a dot (like $\dot{a}$) refers to a derivative with respect to cosmic time. The expansion rate $\dot{a}/a$ is called the Hubble rate $H(t)$, and its current value is often parameterized as

$$H_0 \equiv H(t_0) = 100\,h\,\frac{\mathrm{km}}{\mathrm{s\,Mpc}}\,, \tag{2.43}$$

with $h \approx 0.7$. The universe is expanding if $H > 0$ and contracting if $H < 0$, the expansion is accelerating if $\ddot{a} > 0$ and decelerating if $\ddot{a} < 0$. By virtue of equation (2.42) an accelerated expansion as we observe today requires the existence of a matter component with $p < \rho/3$, which violates the strong energy condition.

In the course of this work we will sometimes switch between the usage of cosmic time and other time-like quantities which change as the universe evolves. We will need the quantities $N = \ln(a)$, the redshift $z = 1/a - 1$ and the *conformal time* τ, defined by $\mathrm{d}t = a(t)\mathrm{d}\tau$. The corresponding conformal Hubble rate is then given by

$$\mathcal{H}^2 \equiv \left(\frac{a'}{a}\right)^2 = \frac{a^2\rho}{3M_p^2} - K\,, \tag{2.44}$$

where a prime denotes a derivative with respect to conformal time. Similarly the second Friedmann equation now reads

$$\frac{a''}{a} = \frac{a^2}{6M_p^2}(\rho - 3p) - K\,. \tag{2.45}$$

The equation of energy-momentum conservation $\mathcal{D}_\mu T^{\mu\nu} = 0$ reduces to one single equation for the FLRW-cosmology, which reads

$$\rho' + 3\mathcal{H}(\rho + p) = 0\,. \tag{2.46}$$

From this point onward, we will always work with a flat spatial geometry, i.e. $K = 0$, unless explicitly stated otherwise.

Horizons

Before we move on, we quickly want to discuss a topic central to modern cosmology: horizons. In a FLRW universe, photons travel on lightlike geodesics, which are defined by $\mathrm{d}s = 0$. We can assume that the photon in question travels in the radial direction, and we thus obtain for a flat spatial geometry

$$\mathrm{d}t = a(t)\,\mathrm{d}r\,. \tag{2.47}$$

In a big bang cosmology the matter content of the early universe is dominated by highly relativistic matter ($p = \rho/3$, see below), and thus satisfies $a(t) \propto t^{1/2}$. Extrapolating this evolution to $a(t) = 0$ would result in a finite age of the universe, which starts in a singularity at $t = 0$. In fact, current parameter fits estimate the age of the universe to be roughly 13.8×10^9 years [Ade et al., 2013a,c]. This is indeed the standard picture, but we want to point out that this is not the only possibility. One can construct models where the age of the universe is in infinite [Wetterich, 2014a]. We will however remain in the standard picture for now and discuss horizons.

The number of definitions for different horizons is quite large, we will follow the basic classification of Rindler [1956]. First, we can calculate the maximal radial comoving distance which light can have travelled at time t in a big bang scenario, which is known as the *particle horizon*

$$r_{ph}(t) = \int_0^t \frac{\mathrm{d}t'}{a(t')}\,. \tag{2.48}$$

It coincides precisely with the definition of the conformal time τ. Two points which are separated by a physical distance $d > a(t)\,r_{ph}(t)$ at time t were never in causal contact with each other for $t' < t$. For some simple universes, this quantity is closely related to the *comoving hubble radius*

$$r_{ch}(t) = \frac{1}{a(t)H(t)}\,. \tag{2.49}$$

If an objects physical distance to an observer is bigger than $a(t)\,r_{ch}(t)$, the recession velocity due to the cosmic expansion is bigger than the speed of light. A scenario where the comoving hubble radius is very different from the particle horizon is inflationary cosmology, where the difference between these two quantities is crucial for the solution of the *horizon problem*.

Rindler then goes on to define the *event horizon* as the maximal comoving distance light can ever travel when emitted at time t:

$$r_{eh}(t) = \int_t^{t_{\mathrm{end}}} \frac{\mathrm{d}t'}{a(t')}\,. \tag{2.50}$$

Here $t_{\rm end}$ denotes the (possibly infinite) time at which the universe ends. One should note that this need not be a well defined quantity, the integral can be divergent if $t_{\rm end} = \infty$ or the scale factor recollapses quickly to zero within some finite time. In fact, one can easily show that the physical distance $a(t)\, r_{eh}(t)$ is necessarily infinite if the universe never recollapses. Nonetheless, if dark energy is indeed a cosmological constant, the comoving event horizon $r_{eh}(t_0)$ is finite.

2.3.2 THE COSMIC INVENTORY

The energy content of our universe clearly consists of more than just one single component. From particle physics we expect stable particles, in particular photons, neutrinos and atoms to contribute. (We will frequently refer to atoms as baryons in this thesis, which is of course slightly inaccurate but common in cosmology.) Furthermore there are the - today still mysterious - substances referred to as dark matter and dark energy. Each of these components comes with its own energy-momentum tensor and we can write

$$T^{\mu\nu} = \sum_\alpha T^{\mu\nu}_\alpha \,. \tag{2.51}$$

In general, these tensors are not separately conserved, but can couple to each other through non-gravitational interactions. The generic equations of energy-momentum conservation for a single component (denoted by α) therefore read

$$\mathcal{D}_\mu T^{\mu\nu}_\alpha = Q^\nu_\alpha \,, \quad \text{with} \quad \sum_\alpha Q^\nu_\alpha = 0 \,. \tag{2.52}$$

In a FLRW-universe the couplings are constrained by maximal spatial symmetry and have to be of the particularly simple shape

$$Q^\nu_\alpha = (-aQ_\alpha, 0, 0, 0) \,. \tag{2.53}$$

This allows us to rewrite the corresponding equations of energy-(non-)conservation for each component separately as follows:

$$\rho'_\alpha + 3\mathcal{H}(\rho_\alpha + p_\alpha)(1 - q_\alpha) = 0 \,, \quad \text{with} \quad q_\alpha = \frac{aQ_\alpha}{3\mathcal{H}(\rho_\alpha + p_\alpha)} \,. \tag{2.54}$$

It is often very useful to integrate this equation in order to find out how the energy density of a given matter component evolves as a function of the scale factor. However, generically both the dimensionless couplings q_α and the *equations of state* $\omega_\alpha \equiv p_\alpha/\rho_\alpha$ can be time-dependent, and an explicit solution is only possible if this dependence (or rather the dependence on $a(t)$) is known. A particularly simple case arises if both quantities are constant, then we directly obtain

$$\rho_\alpha \propto a^{-3(1+\omega_\alpha)(1-q_\alpha)} \,. \tag{2.55}$$

From this relation it is reasonable to expect that the energy density of the universe is dominated by different matter components at different times. A very convenient way to quantify these changes is

through the *density parameters* and the *effective equation of state*

$$\Omega_\alpha \equiv \frac{\rho_\alpha}{\rho}\,, \quad \omega_{\text{eff}} = \frac{p}{\rho}\,, \quad \text{where} \quad \rho = \sum_\alpha \rho_\alpha\,, \quad p = \sum_\alpha p_\alpha\,. \tag{2.56}$$

Equilibrium thermodynamics and decoupling

In the big bang scenario, all matter was created at some very early stage in the evolution of the universe known as *reheating*, probably following an inflationary era. Immediately after this event, the universe was very hot and dense, full of highly relativistic particles. Scattering processes involving leptons and gauge bosons were very frequent, keeping the the cosmic plasma in thermal equilibrium and particle-anti-particle pairs abundant. As the universe expanded and the temperature of the cosmic plasma decreased, more and more of the particle-anti-article pairs annihilated, charged particles combined into stable neutral ones and eventually interaction rates became very low and one by one different particles dropped out of thermal equilibrium with the rest of the cosmic plasma. As a first approximation one can assume that this happened when the interaction rate Γ_α relevant for keeping the particle species α in equilibrium dropped below the expansion rate H.

In thermal equilibrium the phase-space distribution of particles is simply given by either a Bose-Einstein distribution (for bosons) or a Fermi-Dirac distribution (for fermions). The parameters of these distributions are the temperature T_α and the chemical potential μ_α, both of which can be dependent on time, but not on spatial coordinates in a FLRW geometry. We therefore get

$$f_\alpha(\vec{x},\vec{p}) = f_\alpha(|\vec{p}|) = \left(\mathrm{e}^{\frac{E_\alpha-\mu_\alpha}{T_\alpha}} \pm 1\right)^{-1}\,, \tag{2.57}$$

with $E_\alpha = \sqrt{m_\alpha^2 + \vec{p}^{\,2}}$, where m_α is the particle rest-mass and $\vec{p}$ is the physical momentum. We have also set $k_B = 1$ and $+$ and $-$ are valid for fermions and bosons respectively. From this distribution we can directly calculate the energy-momentum tensor for any particle species as follows:

$$T_\alpha^{\mu\nu} = g_\alpha \int \frac{\mathrm{d}^3 P}{(2\pi)^3} \frac{1}{\sqrt{-g}} \frac{P^\mu P^\nu}{|P_0|} f_\alpha(\vec{x},\vec{p})\,, \tag{2.58}$$

where g_α are the internal degrees of freedom[2] and $P^\mu = m_0\,\mathrm{d}x^\mu/\mathrm{d}\lambda$ (with $x^\mu(\lambda)$ some parameterization of the world lines) is the comoving four-momentum. It is related to the physical momentum via $\vec{p}^{\,2} = g_{ij}P^iP^j$.

In the limiting cases of highly-relativistic and non-relativistic matter the integrals can be solved analytically. In the non-relativistic Maxwell-Boltzmann limit $T_\alpha \ll m_\alpha$, $T_\alpha \ll m_\alpha - \mu_\alpha$ we have $E_\alpha \approx m_\alpha + \vec{p}^{\,2}/2m_\alpha$ and therefore obtain for both fermions and bosons (to first order in T_α/m_α)

$$\rho_\alpha = T_\alpha^{00} = g_\alpha \left(\frac{m_\alpha T_\alpha}{2\pi}\right)^{\frac{3}{2}} \mathrm{e}^{-\frac{m_\alpha-\mu_\alpha}{T_\alpha}} m_\alpha\,, \quad p_\alpha = \frac{1}{3} g_{ij} T_\alpha^{ij} = \rho_\alpha \frac{T_\alpha}{m_\alpha}\,. \tag{2.59}$$

[2]Do not confuse g_α with the metric $g_{\mu\nu}$. These two objects should, however, be easy to distinguish by the index structure.

Clearly we have $p_\alpha \ll \rho_\alpha$ and we can set as a first approximation $\omega_\alpha \approx 0$. We thus obtain in the case of no couplings (i.e. $q_\alpha = 0$) $\rho_\alpha \propto a^{-3}$ from equation (2.54) and if the universe is dominated by a non-relativistic component $a(t) \propto t^{2/3}$ and thus $H \propto a^{-3/2}$. The number density for non-relativistic particles is simply given by $n_\alpha = \frac{\rho_\alpha}{m_\alpha}$. For highly relativistic particles we can work in the limit $T_\alpha \gg \mu_\alpha, m_\alpha$. In this case the approximation $\mu_\alpha = m_\alpha = 0$ is justified and we get

$$\rho_\alpha = \begin{cases} g_\alpha \frac{\pi^2}{30} T_\alpha^4 & \text{for bosons} \\ g_\alpha \frac{7}{8} \frac{\pi^2}{30} T_\alpha^4 & \text{for fermions} \end{cases}, \qquad p_\alpha = \frac{\rho_\alpha}{3}. \tag{2.60}$$

Therefore $\omega_\alpha = 1/3$ for relativistic species and, as long as there is no energy transfer at the background level, $\rho_\alpha \propto a^{-4}$, which directly implies $T_\alpha \propto a^{-1}$. If the energy density of the universe is dominated by such a component we have $a(t) \propto t^{\frac{1}{2}}$ and $H \propto a^{-2}$. The number density of relativistic particles requires an independent calculation and leads to

$$n_\alpha = \frac{g_\alpha}{(2\pi)^3} \int \mathrm{d}^3 p f_\alpha(|\vec{p}|) = g_\alpha \frac{\zeta(3)}{\pi^2} T_\alpha^3 \begin{cases} 1 & \text{for bosons} \\ 3/4 & \text{for fermions} \end{cases}. \tag{2.61}$$

Clearly, in thermal equilibrium, the abundance of non-relativistic particles is Boltzmann-suppressed by the factor $\mathrm{e}^{-(m_\alpha - \mu_\alpha)/T_\alpha}$ compared to relativistic ones. This sharp drop in the number density of a particle at $T_\alpha \approx m_\alpha$ can be interpreted as particles and antiparticles annihilating, when the temperature is no longer high enough for particle-antiparticle pair-production to occur frequently and make up for the losses. If thermal equilibrium continued forever, eventually all massive particles would eventually have become non-relativistic and the universe would consist of (mostly) photons by now. This is clearly not the case, as interaction rates eventually became lower than the expansion rate, leading to various decoupling processes and the freeze-out of non-relativistic matter.

Particles dropping out of equilibrium with the photons will travel freely through the universe from this point on, i.e. keep their distribution function but with physical momenta redshifted by the cosmic expansion

$$f_\alpha(p; t > t_{\mathrm{dec}}) = f_\alpha\left(\frac{a(t)}{a(t_{\mathrm{dec}})} p; t_{\mathrm{dec}}\right). \tag{2.62}$$

From this one can directly deduce that the temperature of particles which decouple while relativistic continues to fall like $T_\alpha \propto a^{-1}$, wheres particles decoupling while non-relativistic cool faster, namely like $T_\alpha \propto a^{-2}$. For non-relativistic matter one can quickly calculate the effect of such a decoupling on the number-density. As a toy model, let us consider two kinds of particles with number densities n_1 and n_2, both with equal mass m and chemical potential μ but with different interaction rates, so that the first one (denoted by subscript 1) decoupled at some time t_{dec} (corresponding to a scale factor a_{dec} and temperature $T_\gamma(t_{\mathrm{dec}}) = T_{\mathrm{dec}}$) and the second one stayed in thermal equilibrium. Assuming a sudden complete decoupling at a_{dec} we obtain for $a > a_{\mathrm{dec}}$

$$n_1 \propto a^{-3} \propto T_\gamma^3 \propto n_\gamma \quad \text{and} \quad \frac{n_2}{n_1} = \mathrm{e}^{-\frac{m-\mu}{T_{\mathrm{dec}}}\left(\frac{a}{a_{\mathrm{dec}}} - 1\right)} \left(\frac{a}{a_{\mathrm{dec}}}\right)^{3/2} \ll 1, \tag{2.63}$$

where T_γ is the photon temperature, which is usually taken to be the 'temperature of the universe'. This is what is called *freeze out* of non-relativistic particles and is responsible for the matter we observe in the universe today. Realistic freeze-out processes are of course much more complicated than the simple sudden decoupling approximation used here, a thorough calculation requires knowledge about the specific interactions relevant to the decoupling scenario and use of the Boltzmann equation. As this is not the topic of this thesis we will not go into it much further and cite only the results of the relevant calculations below.

In a universe consisting of a mixture of different particles (in or out of thermal equilibrium with photons), a useful quantity to describe the energy content of the cosmic fluid is the effective number of degrees of freedom g_*, defined via

$$\rho = \frac{\pi^2}{30} g_*(T_\gamma) T_\gamma^4 . \tag{2.64}$$

The cosmological constant

As both relativistic and non-relativistic matter lead to a decelerated expansion of the universe with $\ddot{a} < 0$, an accelerated cosmic expansion requires the existence of a more exotic substance with $p_\alpha < -\rho_\alpha/3$ (we are ignoring possible solutions involving backreaction). Since high redshift supernovae were observed to be dimmer than expected in a matter-dominated universe slightly before the turn of the millennium [Riess et al., 1998, Perlmutter et al., 1999], we do indeed know that such a substance is present in the universe. There are a number of theories what this might be, but probably the simplest scenario, at least mathematically, is that of a cosmological constant. This concept was first introduced by Einstein himself with the intent to construct a static universe, but famously abandoned after Hubble discovered the cosmic expansion [Hubble, 1929].

On a fundamental level the cosmological constant is just a term which can be introduced in the Einstein-Hilbert action, which then reads

$$S_G = \frac{M_p^2}{2} \int \sqrt{-g} \, (R - 2\Lambda) \, \mathrm{d}^4 x . \tag{2.65}$$

Einstein's field equations then read (after inclusion of a matter part)

$$R_{\mu\nu} - \frac{1}{2} R g_{\mu\nu} + \Lambda g_{\mu\nu} = \frac{1}{M_p^2} T_{\mu\nu} . \tag{2.66}$$

Clearly one could also consider the cosmological constant to be part of the matter action, with energy momentum tensor

$$T_\Lambda^{\mu\nu} = -\Lambda M_p^2 g^{\mu\nu} . \tag{2.67}$$

In this picture Λ would correspond to a perfect fluid with $p_\Lambda = -\rho_\Lambda = -\Lambda M_p^2$, i.e. $\omega_\Lambda = -1$. Thus the corresponding energy density remains constant ($\rho_\Lambda \propto a^0$) and a universe dominated by Λ will perform an exponential expansion $a(t) \propto \mathrm{e}^{Ht}$, where $H = \sqrt{\Lambda/3}$, which is accelerated.

The cosmological constant is currently the standard model for dark energy, but it comes with its own theoretical problems, which we will discuss in some detail in chapter 3.

Cosmological scalar fields

One of the most popular alternatives to a cosmological constant is to model dark energy with a cosmological scalar field, called a *cosmon*. In the simplest of these so called *quintessence* scenarios, one employs a single minimally coupled canonical scalar field φ with potential $V(\varphi)$, corresponding to an action

$$S_\varphi = \int \mathrm{d}^4x\sqrt{-g}\left[-\frac{1}{2}\left(\mathcal{D}_\mu\varphi\right)\left(\mathcal{D}^\mu\varphi\right) - V(\varphi)\right]. \tag{2.68}$$

The energy momentum tensor for such a field reads

$$T^{\mu\nu}_\varphi = \left(\mathcal{D}^\mu\varphi\right)\left(\mathcal{D}^\nu\varphi\right) + g^{\mu\nu}\mathcal{L}_\varphi\,, \tag{2.69}$$

and in a FLRW-background, where φ is necessarily homogenous and only depends on time, this can be identified with a perfect fluid with

$$\rho_\varphi = \frac{1}{2}\dot{\varphi}^2 + V(\varphi)\,, \quad p_\varphi = \frac{1}{2}\dot{\varphi}^2 - V(\varphi)\,. \tag{2.70}$$

Clearly the equation of state ω_φ can vary between -1 (for $\dot{\varphi}=0$) and $+1$ (for $V(\varphi)=0$), and such a scalar field is therefore a possible candidate for causing an accelerated expansion. The equations governing the field dynamics can be deduced from equation (2.33) without a coupling to matter and read (in conformal time):

$$\varphi'' + 2\mathcal{H}\varphi' + a^2V_{,\varphi} = 0\,. \tag{2.71}$$

We will discuss such scalar fields in much more detail in the later chapters of this thesis.

2.3.3 A SHORT HISTORY OF OUR UNIVERSE

At this point we can finally give an overview over the most relevant cosmological events as they can be deduced from the standard model of particle physics and cosmological observations as well as some theoretical speculation for very high energies.

Planck epoch

At energy densities close to the Planck mass, i.e. of about 10^{19} GeV, the theory of general relativity is expected to become invalid. Interpolating backwards from the radiation dominated era using Einstein gravity would put the Planck epoch at a time close to the Planck time of about 5×10^{-44} s. An understanding of this era would require knowledge about a full quantum theory of gravity.

Electroweak and GUT epoch

At lower energies, roughly from 10^2 GeV to 10^{16} GeV, we can expect Einstein gravity to work well. At these energies, still above the scale of electroweak symmetry breaking, the universe is filled with

	T_γ	redshift	t	g_*
electroweak symmetry breaking	~ 100 GeV	10^{15}	20 ps	106.75
Top annihilation	< 173 GeV	$< 1.7 \times 10^{15}$	> 7 ps	96.25
$W^\pm$, Z^0, H^0 annihilation	< 80 GeV	$< 8 \times 10^{14}$	> 31 ps	86.25
Bottom annihilation	< 4 GeV	$< 4 \times 10^{13}$	> 12 ns	75.75
Charm, τ annihilation	< 1 GeV	$< 10^{13}$	$> 0.2\ \mu$s	61.75

TABLE 2.1: Annihilation events in the quark epoch.

massless fermions, gauge bosons and the Higgs, and it makes sense to talk about the temperature of the cosmic plasma T_γ. The hypothesized unification of strong and electroweak interactions lies in this era, at the GUT scale of roughly 10^{16} GeV.

The predicted era of inflation (which we will explain in more detail below) lies within this time as well. It describes an epoch of the cosmic evolution in which the expansion is accelerated at high energies, typically driven by one (or more) scalar fields. The precise energy scale of inflation has been a subject of debate, but the recent discovery of B-mode polarization patterns caused by primordial gravitational waves in the CMB by the BICEP2-experiment suggest a large ratio of primordial tensor-to scalar perturbations of roughly 0.2 [Ade et al., 2014]. If these results hold, they would point towards a high energy scale of inflation close to 10^{16} GeV. (These results and alternative explanations are obviously still being debated and confirmation from the Planck mission data is, at the time of writing this, still missing, but this is the basic picture.) If this inflationary era did exist, its end would have been the era of reheating, during which the inflaton field decayed, creating massless fermions and gauge bosons.

Finally, the electroweak epoch ended with the electroweak phase transition, during which the Higgs field acquired its vacuum expectation value, breaking the $SU(2)_Y \times U(1)$ symmetry to the $SU(2) \times U(1)$ of the weak and electromagnetic interactions, giving both fermions and the weak gauge bosons masses in the process. This happened at a temperature corresponding to the Higgs mass, so roughly at $T_\gamma \approx 100$ GeV.

The quark epoch

After the electroweak phase transition, there were a number of annihilation events, the temperature of which can be approximated by the masses of the standard model particles given in appendix A in Tables A.1 and A.2. We have summarized these events and the resulting effective degrees of freedom (which are only valid for temperatures far enough away from the transitions) in Table 2.1. The decimal points come from the fact that $g_* = g_b + \frac{7}{8} g_f$ (where subscript b stands for bosons and f for fermions). Note that due to $m_t > m_{H^0}$, massive top quarks were never abundant. The quark epoch ended with the QCD phase transition, when quarks and gluons were confined into hadrons, i.e. baryons and mesons. This happened at a temperature of roughly $T_\gamma \approx 150$ MeV.

The hadron epoch

During the hadron epoch, several annihilation events of baryons and mesons took place. The last mesons to annihilate were the lightest ones, i.e. the pions. The last remaining stable baryons are the

	T_γ	redshift	t	g_*
QCD phase transition	~ 150 MeV	10^{12}	20 μs	17.25
π, μ annihilation	< 100 MeV	$< 7\times 10^{11}$	> 45 μs	10.75
neutrino decoupling	~ 1 MeV	6×10^9	1 s	10.75
e^--e^+-annihilation	~ 500 keV	2×10^9	6 s	3.38

TABLE 2.2: Annihilation and decoupling events in the hadron epoch.

stable protons and the long lived neutrinos (long compared to the timescales of the hadron epoch). The remaining leptons also annihilated during this era, as can be seen in Table 2.2. The end of the hadron era is the event of primordial nucleosynthesis (BBN), when protons and neutrons formed light nuclei.

During this era the weakly interacting neutrinos decoupled from the cosmic plasma. As the universe cools down, the weak interactions become much weaker than the electromagnetic ones, and the last particles keeping the neutrinos in equilibrium are free electron-positron pairs. The interaction rate of the neutrinos with these pairs can be approximated by

$$\Gamma_\nu = n_e\langle\sigma v\rangle \approx G_F^2 T_\nu^5 \propto a^{-5}\,, \tag{2.72}$$

where $G_F \simeq 1.16\times 10^{-5}\,\mathrm{GeV}^{-2}$ is Fermi's constant. Once this interaction rate becomes much lower than the Hubble expansion, $\Gamma_\nu \ll H$, the neutrinos will decouple from the cosmic plasma and free stream. This happens at a temperature of about 1 MeV.

The effective degrees of freedom after electron-positron annihilation are a little more complex to calculate. The energy set free by this event heats the baryon-photon plasma, but not the neutrinos, as they have decoupled earlier. Therefore the temperature of the neutrinos drops below that of the photons. The precise difference can be calculated from entropy conservation and we obtain

$$T_\nu = \left(\frac{4}{11}\right)^{1/3} T_\gamma, \tag{2.73}$$

and therefore $g_* = 2 + 6\times\frac{7}{8}\times\left(\frac{4}{11}\right)^{4/3} \approx 3.36$.[3]

Big bang nucleosynthesis

Big bang nucleosynthesis ended the hadron epoch. The abundance of the lightest elements we observe in the universe today can be compared with theoretical predictions for this process, they agree to high accuracy [O'Meara et al., 2001, Bania et al., 2002, Olive and Skillman, 2004, Charbonnel and Primas, 2005, Steigman, 2007]. As we will use constraint from BBN on early dark energy models later, we want to quickly mention the two major cosmological parameters determining the abundance of light elements. The first is the baryon-to-photon ratio, which we can infer from measurements of

[3] The correction to 3.38 originates in QED corrections.

	T_γ	redshift	t
BBN	~ 100 keV	4×10^8	3 min
Matter-radiation equality	~ 0.75 keV	3400	60 kyr
Recombination	~ 0.3 eV	1100	380 kyr
Reionization	2.6 - 7 meV	11-30	100-400 Myr
Dark energy - dark matter equality	~ 0.33 meV	0.4	9 Gyr
Today	~ 0.24 meV	0	13.7 Gyr

TABLE 2.3: Cosmological events after big bang nucleosynthesis.

the CMB and the current baryon density to be tiny:

$$\eta = \frac{n_b}{n_\gamma} \approx 5 \times 10^{-10}\,. \tag{2.74}$$

This ratio determines the temperature at which BBN takes place. The second parameter is the time between neutrino decoupling and BBN. This enters because neutrinos decay via

$$n \to p + e^- + \bar{\nu}_e \tag{2.75}$$

with a lifetime of roughly $\tau_n \approx 887$s. Neutrons and protons were kept in thermal equilibrium by the weak interaction until neutrinos decoupled at $t \approx 1$s, after that time neutrons decayed into protons. As the neutron-to-proton ratio is clearly relevant to the outcome of BBN, the time of BBN is important for its predictions. It is this time that is changed in models with early dark energy. Note that due to the tiny baryon-to-photon ratio η, BBN took place at temperatures considerably below the typical binding energy per nucleus in light elements, which is of the order of a few MeV.

After big bang nucleosynthesis there is a long period where the energy density of the universe is still dominated by relativistic photons and neutrinos. Atoms and dark matter eventually catch up with radiation, the time when the energy densities of relativistic and non-relativistic particles are equal is called *matter radiation equality*, but it takes about 5 ten-foldings of the scale factor. This time is very important, because the smallest perturbation modes relevant for cosmological observations enter the horizon during the later stages of this era. The early stages therefore present a phase in the cosmic evolution which is long (in terms of order of magnitude changes of the scale factor), nothing happens, and relevant perturbations are outside the horizon. This makes it a period uniquely suited to calculate the initial conditions for cosmological perturbations. We will come back to this in the later chapters of this thesis

Recombination

The last particles left to interact with the photons are ionized atoms, mostly hydrogen. The electrons keep the photons in thermal equilibrium with the baryons through Compton-scattering:

$$\gamma + H \longleftrightarrow p + \mathrm{e}^-\,. \tag{2.76}$$

This works efficiently until the universe has cooled down so far that these processes also become very rare. After that time, the photons are set free and travel throughout the universe essentially as freely streaming particles. Naively one could expect that this takes place at temperatures of roughly 13.6 eV, the ionization-temperature of hydrogen. However, the huge photon-to-baryon ratio η^{-1} kept the photons in thermal equilibrium down to much lower temperatures, and in fact recombination happened at $T_\gamma \approx 0.3$ eV.

The CMB was first measured by Penzias and Wilson [1965a], and much later the COBE-satellite confirmed that its spectral shape is indeed a black-body spectrum to excellent accuracy [Mather et al., 1994, Fixsen et al., 1996]. Its temperature today is $T_\gamma = (2.7260 \pm 0.0013)$ K [Fixsen, 2009], which corresponds to a density paramter

$$\Omega_{\gamma,0} \approx 5 \times 10^{-5}\,. \tag{2.77}$$

From these numbers we can calculate the temperature of the neutrino background using equation (2.73) to be roughly 1.95 K. When calculating the corresponding energy density we have to take into account the degeneracy and the Fermi-factor of $7/8$ in (2.60) to obtain

$$\Omega_{\nu,0} = 3 \times \frac{7}{8} \times \left(\frac{4}{11}\right)^{4/3} \times \Omega_{\gamma,0} \approx 3.4 \times 10^{-5}\,. \tag{2.78}$$

One should note one caveat here: These results are only valid as long as neutrinos are relativistic. Neutrinos do, however, have a small mass, as we know from neutrino-oscillation experiments [Maki et al., 1962, Pontecorvo, 1968, Davis et al., 1968, Gribov and Pontecorvo, 1969, Ahmad et al., 2001]. Current upper bounds on the neutrino-masses are in the eV-regime (see appendix A), so that it is conceivable that cosmic neutrinos have become non-relativistic recently. This possibility has an interesting connection to the *why now* problem of dark energy, which we will discuss in chapter 3. It might have an elegant solution if the neutrino mass depends on a cosmological cosmon field. In that case, neutrinos becoming non-relativistic could trigger the start of an accelerated cosmological expansion. The details of this scenario are not the contents of this thesis, but can be found in a series of papers on this model, known as *growing neutrino quintessence* [Wetterich, 2007, Amendola et al., 2008, Mota et al., 2008, Ayaita et al., 2012b, 2013].

These (largely) homogeneous energy densities are by far the largest fraction of the total energy density of relativistic matter in the universe today, much bigger than the one attributed to photons and neutrinos produced in stars and other astronomical sources (like Gamma-ray bursts). The neutrino background, however, remains undetected until today.

Structure formation

At the time of the CMB release, deviations from the FLRW-universe were present, but small (of the order 10^{-5}). They can be seen as temperature anisotropies in the CMB today. During the epoch of matter-domination, these small fluctuation grew into larger and larger structures, which eventually formed the galaxies and galaxy clusters we observe today. An important event during this era was *reionization*, when the radiation from first stars reionized the cosmic baryonic gas in clusters (see

Table 2.3). This has the effect of decreasing the fluctuation amplitude in the CMB through Thomson-scattering by $e^{-\tau_{reio}}$, where τ_{reio} is called the *reionization optical depth*.

Cosmic acceleration

Finally, at very low redshifts, the universe started an accelerated expansion. This is usually attributed to some form of dark energy, which we will discuss in more detail later in this thesis.

Baryons and dark matter

As we already mentioned above, what we refer to as *baryons* in this thesis could also simply be called visible matter or atoms. Most of the atoms in our universe are hydrogen, with smaller fractions of heavier elements. Today most baryonic matter is concentrated in galaxy clusters and groups of galaxies, but not primarily in stars or other very dense objects. The biggest fraction resides in hot intergalactic gas, which can be detected via X-ray Bremsstrahlung, emitted by the free electrons [Meekins et al., 1971, Cavaliere et al., 1971, Gursky et al., 1971, Forman et al., 1972]. Within this thesis we will always consider baryons in a FLRW cosmology to be non-relativistic, i.e. consider their velocities to be negligible. This is well justified, as we have seen that the QCD phase transition happened at temperature of roughly 150 MeV, whereas the proton mass is roughly 938 MeV.

Still, by far the biggest fraction of the mass of a galaxy or galaxy cluster is not in baryons, but in *dark matter*. The existence of such a substance has been predicted as early as in the 30's by Fritz Zwicky [1933, 1937], who observed that the rotation curves of galaxies could not be explained by the amount of luminous matter visible in the COMA cluster, and Sinclair Smith, who found similar results in the Virgo cluster [Smith, 1936]. Today, a huge number of direct and indirect probes have confirmed this idea. Probably the most direct evidence comes from gravitational lensing [Mellier, 1999, Bartelmann and Schneider, 2001, Refregier, 2003] and the rotation curves of galaxies [Sofue and Rubin, 2001, Kregel et al., 2004], but equally impressive results come from the observation of small anisotropies in the CMB, which would be expected to be two orders of magnitude larger if dark matter interacted (considerably) with light [Peebles, 1982, Hinshaw et al., 2013, Ade et al., 2013a,c].
We know a lot less about dark matter particles than we do about baryons, in fact, they have not even been detected yet in the laboratory. Let us collect a few facts we do know:

- Dark matter cannot interact electromagnetically.
- Dark matter cannot consist of baryons. For a while massive compact halo objects (MaCHOs) have been popular candidates for baryonic dark matter, but they are difficult to reconcile with observational facts. Probably the most relevant issues come from the amplitude of temperature fluctuations in the CMB [Penzias and Wilson, 1965a, Ade et al., 2013a,c, Hinshaw et al., 2013], which tell us that such objects must have formed before the era of recombination, and abundances of deuterium and helium from primordial nucleosynthesis, which are dependent on the baryon-to-photon ratio and push the required formation time of such objects to even higher temperatures. The formation of dense baryonic objects at such early times is difficult to realize, as all existing gravitational wells were very shallow. One way out of this could be primordial black holes [Hawkins, 2011].

- The free streaming length of the dark matter particles cannot be too large. This length sets the scale at which the small fluctuations from the FLRW-geometry - which form the seeds of current structures in the universe - are effectively erased, and if it is too large cosmic structure formation can not produce the structures we see today.

This still leaves a large number of candidates. The most popular particle physics model is probably dark matter consisting of WIMPs (weakly interacting massive particles) [Steigman and Turner, 1985, Bertone et al., 2005]. The reason for this lies in the so called *WIMP miracle*, which is related to the freeze-out of dark matter. A relatively simple calculation shows that the abundance of dark matter observed today is compatible with a cross section characteristic for the weak interaction and a mass close to the weak scale ($m \sim 100$ GeV), i.e. a freeze-out relatively quickly after electroweak symmetry breaking.
There are many other possibilities, like axions [Peccei and Quinn, 1977b,a, Duffy and van Bibber, 2009], gravitinos [Steffen, 2009] or sterile neutrinos [Drewes, 2013]. In the later chapters of this thesis we will consider a very different form of dark matter, an ultralight scalar field. At the background level, such a field will have very similar properties to the cold dark matter fluid we just described.

2.3.4 THE ΛCDM MODEL

For some years by now, cosmology has a standard model. Within this model, dark matter is modeled by *cold dark matter* (CDM), which could be a WIMP, whereas dark energy is simply modeled by a cosmological constant. Therefore this model is known as the ΛCDM model. In its simplest form (and for a flat universe), is is completely determined by 7 parameters, which can be taken to be the current CMB temperature T_{CMB}, the current Hubble rate, the baryon and CDM density parameters, the reionization optical depth τ_{reio} and two quantities determining the initial amplitude and wavenumber dependence of the perturbations, which we will discuss in more detail in chapter 4: the scalar spectral index n_s and the amplitude of fluctuations enclosed within an 8 h^{-1} Mpc sphere, σ_8. In practice a different set of fundamental parameters is often used for fitting reasons, and the ones named here are then derived from those. From a theoretical viewpoint, however, this set can well be taken as fundamental. Furthermore T_{CMB} is usually not included in this list and people only cite 6 free parameters in the minimal ΛCDM model.

In Table 2.4 we sum up the current best fits for the free and some derived parameters of the ΛCDM model. The data is taken from Hinshaw et al. [2013], other groups (like the Planck mission) report slightly different values for some parameters, but there are no major contradictions. We give here the set of parameters mentioned above as one possible fundamental set, not the one used for the fitting procedure in [Hinshaw et al., 2013].

The evolution of the energy densities and the effective equation of state in the ΛCDM model can be seen in Figure 2.1.

	Symbol	Value
Free parameters		
Temperature of the CMB [K]	T_{CMB}	2.726
Current Hubble rate [km s^{-1} Mpc^{-1}]	H_0	69.7
baryon density parameter	Ω_b	0.046
CDM density parameter	Ω_c	0.236
Reionization optical depth	τ_{reio}	0.08
scalar spectral index	n_s	0.965
Density fluctuations at 8 h^{-1} Mpc	σ_8	0.817
Derived parameters		
Cosmological constant density parameter	Ω_Λ	0.718
Age of the universe [Gyr]	t_0	13.75
Redshift of matter-radiation equality	z_{eq}	3280
Redshift of reionization	z_{reio}	9.97

TABLE 2.4: Parameters of the ΛCDM model.

FIGURE 2.1: **Energy densities in the ΛCDM model**

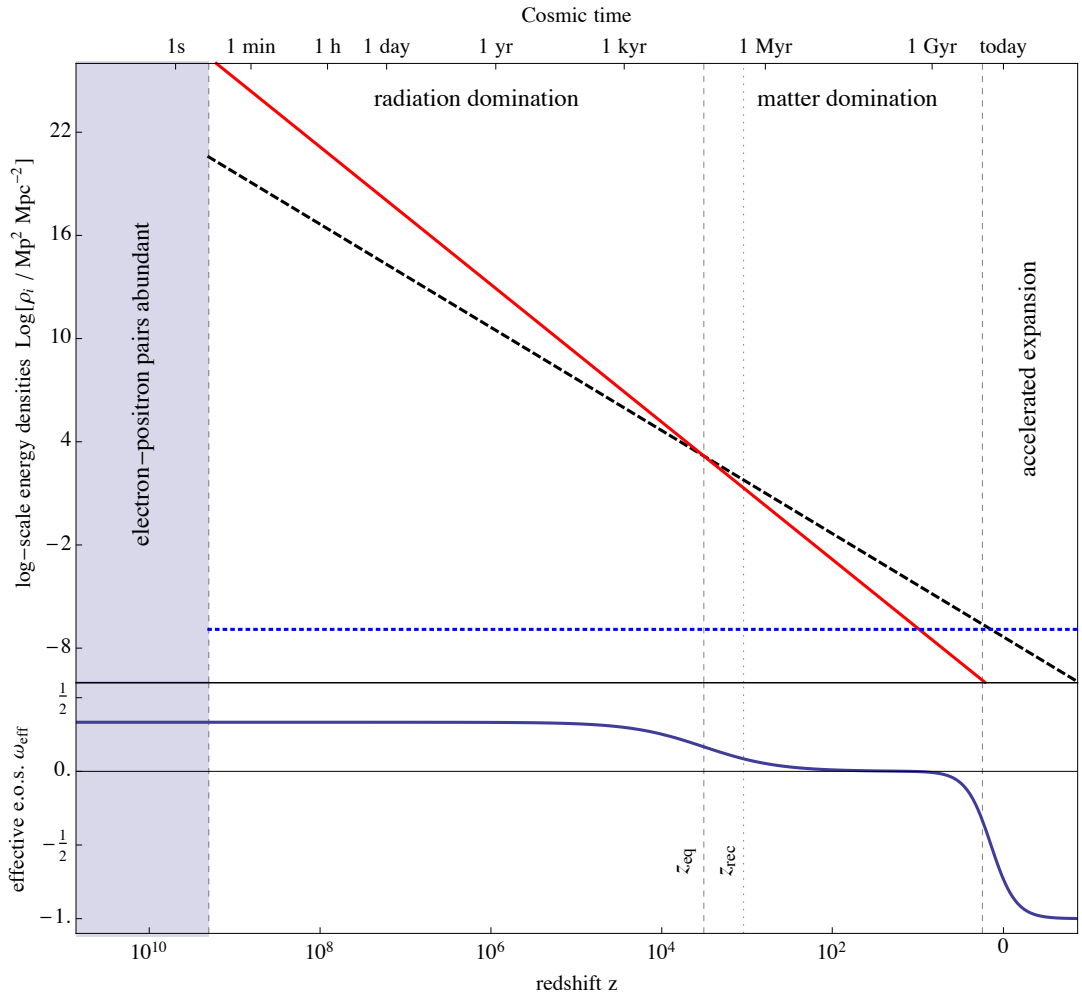

The upper panel shows the energy density for relativistic matter (both neutrinos and photons) in red (solid line), the one for matter (both baryonic matter and cold dark matter) in black (dashed line) and the energy density associated with the cosmological constant in blue (dotted line). The lower panel shows the effective equation of state.

3 THE DARK SECTOR AND DILATATION SYMMETRY

According to the cosmological standard model, a large portion of todays energy content of the universe, roughly 95%, consists of dark matter and dark energy. In this chapter we will discuss this dark sector of cosmology, focussing mainly on dark energy and including dark matter only in the last section. We will not be concerned with the observational evidence for an accelerated cosmic expansion and thus the existence of dark energy, discussions of this subject matter can be found e.g. in [Weinberg et al., 2013b]. Instead, we are interested in the most common models of dark energy, in particular the cosmological constant and quintessence models.

In the first section of this chapter we will review why many researchers are unhappy with the simple model of cosmological constant, despite the fact that it it appears to be consistent with virtually all observational findings. After a quick review of the *cosmological constant problem* and the *anthropic argument*, we will then move on to discuss one important class of alternative models of dark energy, quintessence models. Finally, we go on to review a topic which has been connected to quintessence models since they were first thought up and could potentially provide a solution to the cosmological constant problem: dilatation symmetric theories of gravity. In the last section we will then introduce the cosmon-bolon model of coupled dark energy and dark matter, with which much of the work in the following chapters is concerned.

For our discussion of the cosmological constant problem we mainly rely on [Martin, 2012], in our short treatment of inflation we use [Weinberg, 2008, Baumann, 2009], the material covered in the section on quintessence models can be found in many textbooks and review articles, e.g. [Copeland et al., 2006, Amendola and Tsujikawa, 2010], our review of dilatation symmetric theories of gravity is based on [Wetterich, 2009, 2010a,b] and finally the cosmon-bolon model in its basics as presented here has been published in [Beyer et al., 2011] and [Beyer, 2014b].

3.1 THE COSMOLOGICAL CONSTANT PROBLEM

In chapter 2 we introduced the cosmological constant as a parameter which can be introduced into Einstein-gravity. As a free parameter of the theory, it can in principle take any value, much like the couplings and charges in the standard model (which determine the particle masses through the Higgs mechanism). Its value needs to be determined by observations or experiments, there is a priory no reason to prefer a specific one. Nonetheless, cosmologists often complain that the value of Λ necessary to explain current observations, which is roughly $\sqrt{\Lambda} \approx 10^{-33}$ eV ($\rho_\Lambda \approx 10^{-47}\text{GeV}^4$),

is unnaturally small. It is indeed tiny when compared to other fundamental mass scales present in physics, like the Planck scale M_p, the electroweak scale $M_{\rm EW}$ or the QCD scale $M_{\rm QCD}$, but that fact by itself need not necessarily be reason for concern. In this section we want to explain why it is indeed justified to consider this value unnatural, and take a short look at one possible way out, the so called anthropic principle.

3.1.1 THE NATURE OF Λ

In addition to the cosmological constant as a free parameter of Einstein gravity, there is also a part of the energy-momentum tensor which has the same gravitational effect: the vacuum. Its energy-momentum tensor is necessarily of the form

$$< 0|T_{\mu\nu}|0 >= -\rho_{\rm vac}\, g_{\mu\nu}\,, \tag{3.1}$$

where $\rho_{\rm vac}$ denotes the vacuum energy and $|0>$ the vacuum state. We can thus absorb this contribution into a single effective cosmological constant

$$\Lambda_{\rm eff} = \Lambda_G + \frac{\rho_{\rm vac}}{M_p^2}\,, \tag{3.2}$$

where Λ_G denotes the gravitational cosmological constant introduced in chapter 2. Cosmological observations constrain the effective cosmological constant, i.e. the sum of Λ_G and $\Lambda_{\rm vac} \equiv \rho_{\rm vac}/M_p^2$, and therein lies the problem.

The contributions to the vacuum energy $\rho_{\rm vac}$ can be split up into two parts: Classical contributions and quantum fluctuations. We will discuss these two parts separately.

Classical contributions: Phase transitions

Classical contributions to the vacuum energy originate from field configurations minimizing the energy. In the case of a single canonical scalar field ϕ, the energy is smallest when the kinetic energy vanishes and the field sits at a fixed value $\phi_{\rm min}$ minimizing the the potential energy. The total size of such a contribution is not the concern here, it could indeed be absorbed by the gravitational constant Λ_G, the issue is that this contribution changes during phase transitions, and the amounts by which it changes during the electroweak and QCD phase transitions (which we can be quite certain happened in the early universe) are huge compared to its observational value. Let us discuss this is a little more detail.

The Higgs field is a doublet of complex scalars Σ which is charged under the group $U(1)_Y \times SU(2)$. Its Lagrangian density (in flat Minkowski spacetime) is given by

$$\mathcal{L}_{\rm Higgs} = -(\nabla_\mu \Sigma)^\dagger (\nabla^\mu \Sigma) - V(\Sigma, \Sigma^\dagger)\,, \tag{3.3}$$

where the covariant derivative reads

$$\nabla_\mu \Sigma = \partial_\mu \Sigma + i\frac{g_c'}{2} Y_H B_\mu \Sigma + i g_c T_a W_\mu^a \Sigma, \tag{3.4}$$

and g_c', g_c are the gauge couplings under $U(1)_Y$ and SU(2) respectively, Y_H is the Higgs-Hypercharge, $T_a = \sigma_a/2$ ($a = 1,...,3$, σ_a being the Pauli matrices) are the generators of SU(2) and B_μ and W_μ^a are the gauge bosons. The Higgs potential is given by

$$V(\Sigma, \Sigma^\dagger) = \frac{m^2}{2}\Sigma^\dagger\Sigma + \frac{\lambda}{4}(\Sigma^\dagger\Sigma)^2, \tag{3.5}$$

where $m^2 < 0$ and $\lambda > 0$. In addition to this, the Higgs field also appears in the fermionic mass terms of the standard model Lagrangian where it is responsible for the masses of both quarks and leptons after electroweak symmetry breaking. Using the gauge freedom one can fix the Higgs-field to be of the shape

$$\Sigma = \begin{pmatrix} 0 \\ \chi \end{pmatrix}, \tag{3.6}$$

where χ is real. The potential now simply reads

$$V(\chi) = \frac{m^2}{2}\chi^2 + \frac{\lambda}{4}\chi^4. \tag{3.7}$$

Since $m^2 < 0$, the minimum of the potential is at $\chi = \pm v = \pm\sqrt{-m^2/\lambda}$ and one defines the scalar Higgs field ϕ as the deviation from the vacuum expectation value, i.e. $\chi = v + \phi$.

Before electroweak symmetry breaking, the interactions with the massless fermions stabilize the Higgs field around the local maximum at $\phi = -v$. If one interprets the fermion interactions to contribute to an effective Higgs potential, which is justified at sufficiently high temperatures, this is of the same form as eq. (3.7), but with a positive mass squared. This leads to a minimum of the effective potential at $\phi = -v$ for sufficiently high temperatures.

After electroweak symmetry breaking, however, the Higgs field adjusts to its true vacuum at $\phi = 0$. This causes a shift in potential energy evaluated at the vacuum expectation value of the scalar Higgs field of

$$V(v) - V(0) = -\frac{m^4}{4\lambda}. \tag{3.8}$$

As this potential energy contributes to the vacuum energy ρ_{vac}, it is shifted by $-m^4/4\lambda$ during the electroweak phase transition. How big is this shift? This can be answered by determining the Higgs mass and Fermi's constant. The Higgs mass is given by the second derivative of the potential at the vacuum expectation value v, which gives

$$m_H^2 = -m^2 > 0. \tag{3.9}$$

It has recently been measured to be at around 125 GeV [Aad et al., 2012, Chatrchyan et al., 2012]. In order to find v (or equivalently λ) one can resort to measurements of the weak gauge boson masses

and the effective Fermi theory of weak interactions, in which the following identification is made:

$$\frac{g_c^2}{8m_W^2} = \frac{G_F}{\sqrt{2}}, \quad \text{where} \quad m_W^2 = \frac{g_c^2 v^2}{2}. \tag{3.10}$$

From this we obtain

$$\lambda = \frac{m_H^2}{v^2} = \frac{4m_H^2 G_F}{\sqrt{2}} \approx \frac{1}{2}. \tag{3.11}$$

Now we can calculate the shift in the vacuum energy induced by the electroweak phase transition, which is

$$\Delta\rho_{\text{vac}}^{\text{EW}} = -\frac{m_H^4}{4\lambda} \approx -1.2 \times 10^8 \text{GeV}^4 \approx -10^{55}\rho_0\,, \tag{3.12}$$

where ρ_0 is the current energy density of the universe (which is roughly $\rho_{\Lambda_{\text{eff}}}$). A similar calculation for the QCD phase transition yields [Martin, 2012]

$$\Delta\rho_{\text{vac}}^{\text{QCD}} \approx 10^{45}\rho_0\,. \tag{3.13}$$

Let us quickly discuss what this means. Clearly we could adjust the gravitational cosmological constant Λ_G in such a way that the current effective cosmological constant Λ_{eff} is as small as observations suggest. This would already be cause for some concern, as it seems somewhat unnatural for two independent quantities to cancel almost precisely, but leave a tiny remnant of the order 10^{-55} which makes up dark energy today. Furthermore this would imply that the vacuum energy before the QCD phase transition was huge by absolute value and negative, and even earlier, before the electroweak phase transition, it was huge and positive. This is clearly unsatisfactory.

One point might be worth mentioning here. We do not know from observations if these phase transitions really took place. The earliest era in the universe which is observationally accessible to us is big bang nucleosynthesis (other than possibly inflation through CMB polarization patterns). But even if this 'classical' cosmological constant problem is ignored, we will now see how quantum fluctuations pose a possibly even more severe challenge.

Quantum fluctuations

In addition to the classical configurations, the vacuum energy also receives contributions from the zero point fluctuations of all fields present in the universe. In this subsection we quickly review the estimate for these contributions presented in [Martin, 2012]. We start by considering the simple case of a free canonical complex scalar field ϕ of mass m in Minkowski spacetime. In the process of canonical quantization the field is expressed as

$$\phi(t,\vec{x}) = \frac{1}{(2\pi)^3}\int \frac{\mathrm{d}^3k}{2\omega_{\vec{k}}}\sqrt{2\omega_{\vec{k}}}\left(c_{\vec{k}}\,\mathrm{e}^{ik\cdot x} + c_{\vec{k}}^{\dagger}\,\mathrm{e}^{-ik\cdot x}\right), \tag{3.14}$$

where $c_{\vec{k}}$ and $c^{\dagger}_{\vec{k}}$ are the usual annihilation and creation operators, $\omega_{\vec{k}} = k^0 = \sqrt{\vec{k}^2 + m^2}$ and

$$\frac{\mathrm{d}^3 k}{2\omega_{\vec{k}}} = \mathrm{d}^4 k\, \delta(k^2 + m^2)\, \Theta(k^0) \tag{3.15}$$

is the Lorentz-invariant measure. (The +-sign in the δ-function comes from the fact that we use a metric with the signature $(-,+,+,+)$, in contrast to what is usually employed in particle physics.) The vacuum state $|0>$ by definition fulfills $c_{\vec{k}}|0>=0$ for all $\vec{k}$. We have already seen in chapter 2 how to calculate the energy-momentum tensor for such a scalar field (see eq. (2.69)). After quantization, the vacuum energy momentum tensor can easily be calculated from $<0|T^{\mu\nu}_{\phi}|0>$ using the commutation relations

$$[c_{\vec{k}}, c^{\dagger}_{\vec{k}'}] = (2\pi)^3 \delta^3(\vec{k} - \vec{k}')\,, \tag{3.16}$$

all other commutators vanish. This results in the following expressions for the only non-vanishing parts of the energy-momentum tensor:

$$<\rho^{\phi}_{\mathrm{vac}}> = <0|T^{00}_{\phi}|0> = \frac{1}{(2\pi)^3}\frac{1}{2}\int \mathrm{d}^3 k\, \omega_{\vec{k}}\,, \tag{3.17}$$

$$<p^{\phi}_{\mathrm{vac}}> = <0|\frac{1}{3}T^{i}_{\phi\, i}|0> = \frac{1}{(2\pi)^3}\frac{1}{6}\int \mathrm{d}^3 k \frac{k^2}{\omega_{\vec{k}}}\,. \tag{3.18}$$

Clearly both these quantities are divergent. This divergence is usually ignored in quantum field theory, either with the argument that only differences in energy can be measured or removed by normal ordering of the creation and annihilation operators. There are, however, clear experimental signatures verifying the existence of vacuum fluctuations, such as the Lamb-shift [Lamb and Retherford, 1947, Welton, 1948] or the Casimir effect [Plunien et al., 1986, Milton, 2004, 2011, Lambrecht and Reynaud, 2012]. Furthermore, the vacuum energy can be measured in gravity, and these infinities need to be regularized somehow.

The most commonly encountered method of regularization for this particular problem is the introduction of an ultraviolet cutoff at some energy scale $M \gg m$. This directly gives

$$<\rho^{\phi}_{\mathrm{vac}}> = \frac{1}{4\pi^2}\int_0^M \mathrm{d}k k^2 \sqrt{k^2 + m^2} = \frac{M^4}{16\pi^2}\left(1 + O\left(\frac{m^2}{M^2}\right)\right). \tag{3.19}$$

The vacuum energy in this scenario is determined by the cutoff scale M, which is sometimes chosen to be the Planck scale M_p, and sometimes to be some lower scale like M_{QCD}. Plugging in M_p leads to the famous 122 orders of magnitude difference between $\rho^{\phi}_{\mathrm{vac}}$ and the observed value of ρ_{Λ}. There is, however, a big caveat here. Calculating the pressure with the same cutoff gives (to the leading order in m^2/M^2)

$$\frac{<p^{\phi}_{\mathrm{vac}}>}{<\rho^{\phi}_{\mathrm{vac}}>} = 1/3 \neq -1\,. \tag{3.20}$$

This is clearly wrong. The vacuum energy needs to respect $<p_{\mathrm{vac}}> = -<\rho_{\mathrm{vac}}>$. The reason for this problem lies in the fact that the cutoff chosen above does not respect Lorentz-symmetry. Any useful regularization scheme leading to credible results should clearly do so.

As a better approach, Martin [2012] discusses dimensional regularization. In this scheme one extends the integrals to $d = 4 - \varepsilon$ dimensions and formally evaluates it, leading to an expression with poles at $d/2 \in \mathbb{N}$. For small ε the resulting expressions can be arranged as a Laurent-series and the divergent parts (and some numerical expressions not containing the mass) are then simply subtracted in what is called a *modified minimal subtraction* ($\overline{MS}$) scheme. The results for the vacuum energy and pressure in this approach read

$$< \rho^{\phi}_{\text{vac}} >= \frac{m^4}{64\pi^2} \ln\left(\frac{m^2}{\mu^2}\right), \quad < p^{\phi}_{\text{vac}} >= - < \rho^{\phi}_{\text{vac}} >, \tag{3.21}$$

where μ is an energy scale originally introduced in order to keep the correct dimensionality for the vacuum energy density after extending the integral to $4 - \varepsilon$ dimensions. It is usually called the renormalization scale. This gives a very different prediction for the energy density of vacuum fluctuations when compared the the standard cutoff, which now depends on the renormalization scale μ. The correct setting of μ is a non-trivial issue which we will not go into here.

Whether this approach through dimensional regularization is better than the standard cutoff method is a question we do not want to answer here, though it might well be, as it preserves the correct form of the vacuum energy momentum tensor. Clearly, there are many factors complicating the situation we have not even mentioned so far. First of all, most of the fundamental fields in the standard model are not scalars, but gauge bosons or fermions. Second, they are not free but interact with each other. Third, we should not be working in flat Minkowski spacetime, but with a general metric $g_{\mu\nu}$. Finally one could also consider fields not included in the standard model, such as the ones predicted by supersymmetric theories. We are not going to give deatils on those issues here, but merely want to mention that they do not fundamentally change the nature of the problem at hand. In fact, the dimensional regularization scheme can be extended to include all the above effects, with the results that

$$< \rho_{\text{vac}} >= \sum_i n_i \frac{m_i^4}{64\pi^2} \ln\left(\frac{m_i^2}{\mu^2}\right), \tag{3.22}$$

where the sum runs over all particles of the standard model (we exclude SUSY here), n_i denotes their degeneracies (with a minus sign for fermions) and m_i their masses. Plugging in the masses and choosing $\mu = M_p$ would give us $< \rho_{\text{vac}} > \approx 1.2 \times 10^8$ GeV$^4 \approx 10^{55} \rho_0$. A much smaller value of μ leads to different predictions. In [Koksma and Prokopec, 2011] the authors argue that a good value would be $\mu \simeq 3 \times 10^{-25}$ GeV, which would lead to $< \rho_{\text{vac}} > \approx -2 \times 10^8$ GeV^4. Clearly, these results are much smaller than the predictions from the standard cutoff method, but still much larger than ρ_0 by absolute value. The dependence of $< \rho_{\text{vac}} >$ on the choice of the renormalization scale is shown in Fig. 3.1. Clearly, a value close to ρ_0 would require an extremely precise tuning of μ.

Conclusion

At this point we can sum up the cosmological constant problem as follows: The vacuum energy associated with the effective cosmological constant Λ_{eff} consists of several parts:

$$\rho_{\Lambda_{\text{eff}}} = \Lambda_G M_p^2 + < \rho_{\text{vac}} > + \Delta\rho^{\text{EW}}_{\text{vac}} + \Delta\rho^{\text{QCD}}_{\text{vac}} + \ldots, \tag{3.23}$$

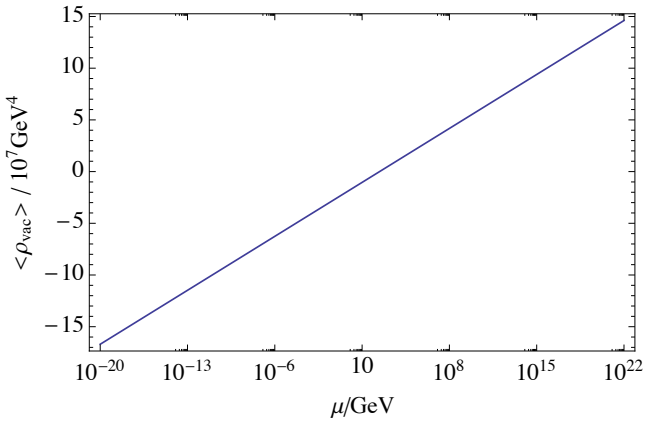

FIGURE 3.1: Dependence of the SM vacuum energy on the renormalization scale

where the dots represent possible additional contributions, like other phase transitions. The issue here is twofold: First, all contributions other than $\Lambda_G M_p^2$ can (in principle) be calculated, or at least approximated, and give a result much bigger than the observed value of $\rho_0 \approx 10^{-47}$ GeV^4. The discrepancy arising from zero point fluctuations gets reduced when choosing dimensional regularization instead of a simple UV cutoff, but it is still huge. One could of course choose Λ_G in such a way that it cancels all other contributions to precisely this accuracy, but this seems very unnatural. And even then, we would still expect the vacuum energy to be huge before the QCD and electroweak phase transitions. This problem persists even if we do assume that quantum fluctuations do not gravitate, as is sometimes done, due to the remaining issue of phase transitions.

What this discussion hopefully made clear is: The cosmological constant problem is hard. In fact, in many cosmological models it is assumed that there is some (unknown) physical mechanism adjusting the effective cosmological constant to zero. The value zero is chosen because it seems much more likely to find such a scenario than one where the value is tuned to 'almost zero'. This would indeed solve the cosmological constant problem, but require a novel explanation for the accelerated expansion of the universe. We will discuss a specific class of such models, so called quintessence models, in the next section. But before that, we want to shortly discuss an alternative, which is sometimes invoked to explain the small value of Λ_{eff}, the anthropic argument.

3.1.2 THE ANTHROPIC ARGUMENT

The problems arising when trying to explain the observed small values of the cosmological constant lead us to one obvious question: What would the universe look like, if Λ were much bigger? The answer is quite simple:
All structures we observe in the universe today have grown out of initially very small fluctuations in the energy density of the universe. As we will discuss in more detail in the coming chapters, the virialized objects we observe have decoupled from the cosmic expansion, and this decoupling happens when the overdensity calculated in linear perturbation theory reaches a value of roughly

1.69. The fact that this value is bigger than one already shows that linear perturbation theory is no longer valid in this regime, and in fact the physical final overdensity of a virialized object is roughly 200 (see chapter 6 for more details).
If the universe is dominated by a cosmological constant, linear perturbations do not grow, they decay. So if the cosmological constant were much bigger than the observed value, an accelerated expansion would have set in earlier and there would not have been enough time for virialized structures to form. As a consequence, we, or any other observer, would not be here to complain about the fact that the cosmological constant is so small. Weinberg [1987] used this argument to derive an upper bound on the cosmological constant consistent with the existence of observers. He arrived at

$$\rho_\Lambda < 10^3 \rho_{\Lambda,\mathrm{obs}}\,. \tag{3.24}$$

This is still a fairly huge margin, but more recent estimates which took into account a much improved understanding of structure formation come up with bounds much closer to the observed value [Tegmark et al., 2006].

How far can we take this argument as an explanation for the cosmological constant problem? At first sight, not very far. If our understanding of the laws of nature dictate that the cosmological constant should be huge, thereby preventing the formation of structure and our existence, the fact that we do exist just means that our understanding of the laws of nature is wrong. Calculating the allowed values for the cosmological constant consistent with the existence of observers and finding that they are in agreement with our observations is merely a tautology, it provides no explanation or understanding for anything and certainly does not resolve the discrepancy between observations and the theoretical understanding of the issue.

Things are different though, if our observable universe is not the only one in existence. In so called *multiverse* scenarios, our universe is just one of many universes which exist, in some sense, parallel to each other, and which can, in principle, differ in the value of the cosmological constant, and possibly other things as well.[1] In such a scenario, some universes would allow for the existence of observers, while others would not. We, as observers, would then necessarily have to be in one of the universes which allow for our existence.

Many scientists are not comfortable with this kind of anthropic reasoning, as it seems to reintroduce the idea that we are in a 'special place', not within our universe, but within the multiverse. If one takes the notion of a multiverse seriously, however, and we will soon see that there are good reasons to do so (beyond it being fun to consider such things), there is no way around the fact that our position is necessarily privileged in precisely the way we just described: It allows for the existence of observers. Within a multiverse scenario this kind of reasoning is perfectly valid. But we have not yet taken it far enough to arrive at a solution of the cosmological constant problem. The question now is: Among the universes allowing for the existence of observers, how common is the value of the cosmological constant we observe? This reintroduces the concept of mediocrity [Vilenkin, 1995]: We should think of ourselves as a civilization randomly picked from the multitude of civilizations in the multiverse. If we could make this prescription precise, i.e. calculate a probability distribution of possible values of

[1] A discussion of the different notions of multiverses introduced in the literature can be found in [Tegmark, 2007]. Here we will only talk about what is referred to as a level 1 multiverse in this reference.

the cosmological constant, one might consider this line of argumentation valid. However, as we will see below, this approach runs into enormous problems due to the very fundamental *measure problem*.

Before we explain what this is, we quickly want to say a few words on the theory of inflation, which, in many cases, gives rise to a multiverse scenario rather naturally.

Inflation

Inflation describes an epoch of accelerated cosmic expansion in the very early universe. Its existence is still speculative, even though first observational hints of inflation may have been detected in the microwave sky [Ade et al., 2014]. Still, inflation has been widely accepted as part of the cosmological standard model, mostly because it provides answers to (among, possibly, other issues) the following questions:

1. Why is the universe flat? The fact that $\Omega_K \equiv K/\mathcal{H}^2 < 1$ today implies that this quantity must have been tiny in the early universe. This is not necessarily a problem, after all $\Omega_K = 0$ is a perfectly acceptable solution, if an unstable one. Still, one might prefer a physical mechanism rendering the universe essentially flat 'from the beginning'.

2. Assuming a primordial singularity and extrapolating the radiation dominated expansion backwards, the particle horizon at recombination was quite small, it corresponds to an angular scale of about 1° on the sky. How, then, can the entire primordial plasma have been in thermal equilibrium, as is suggested by the (almost perfect) isotropy of the CMB temperature?

3. Many high energy extensions of the standard model predict a huge abundance of magnetic monopoles and other exotic relics. Why do we not observe them?

4. What is the origin of cosmic perturbations, and why is the primordial scalar power spectrum of nearly scale-invariant shape?

The first models carrying the name inflation were thought up to solve the monopole problem [Guth and Weinberg, 1981, Sato, 1981], even though an early de-Sitter like early expansion of the universe was proposed slightly earlier [Starobinskiĭ, 1979]. Not long afterwards is is was realized that the horizon- and flatness problems could be addressed in such scenarios well [Guth, 1981]. These first models were based on phase transitions in the early universe, motivated by GUT theories. The simplest inflationary models, so called *new inflation* models, were thought up slightly later [Linde, 1982, Albrecht and Steinhardt, 1982]. In these models the accelerated expansion is driven by a single canonical scalar field.

As we have already seen in chapter 2, a canonical scalar field ϕ can have an equations of state in the regime $\omega_\phi \in [-1,1]$. For a de-Sitter like expansion, this equations of state needs to be $\omega_\phi \approx -1$, i.e. the field is in 'slow roll', its energy density is dominated by the potential energy. For such a state to continue for a prolonged period of time, the potential $V(\phi)$ has to obey the following *slow roll*

conditions for a suitable range of field values:

$$\varepsilon = \frac{1}{2}\left(\frac{M_p V_{,\phi}}{V}\right)^2 \ll 1 \quad \text{and} \quad \eta = \frac{M_p^2 V_{,\phi\phi}}{V} \ll 1\,. \tag{3.25}$$

These conditions ensure that the Hubble damping term $2\mathcal{H}\phi'$ in the field equations slows down the field sufficiently, which is only possible if the potential remains 'flat'. Of course, the era of inflation cannot go on forever, its end is heralded by the scalar field reaching a steeper part of the potential where the slow roll conditions are no longer satisfied, typically eventually stabilizing in a minimum and decaying into the particles of the standard model in a process known as reheating. In order to solve the horizon, flatness and monopole problem, the de-Sitter like expansion must proceed for at least $\mathcal{N}$ =50-60 *e-foldings*, meaning that the scale factor has increased by a factor of $e^{\mathcal{N}}$ during inflation.

Let us now move to what is probably the most interesting aspect of inflation: Quantum fluctuations during inflation as the source for cosmic structure. In this (very short) treatment we will use some terminology from linear perturbation theory in FLRW universes, which we will introduce thoroughly chapter 4. If some notions are unclear, the interested reader may skip ahead and investigate section I of this chapter first.

In the simplest new inflation models, all scalar perturbations are sourced by the scalar field perturbations, and it is therefore sufficient to consider a single perturbative quantity. We will however not use the (gauge invariant) scalar field perturbation $\delta\phi$ here, instead we will use the gauge invariant curvature perturbation

$$\mathcal{R} = \Psi + \frac{\mathcal{H}}{\phi'}\delta\phi\,, \tag{3.26}$$

where Ψ is the usual Bardeen potential. (In a cosmology containing only a scalar field in the matter sector there is no anisotropic stress, hence the two Bardeen potentials coincide.) One can then expand the scalar field action given in eq. (2.68) around the FLRW solution in terms of the curvature perturbation and obtain to second order in $\mathcal{R}$

$$S_{(2)} = \frac{M_p^2}{2}\int \mathrm{d}^4x\, a\frac{\phi'^2}{\mathcal{H}^2}\left[\mathcal{R}'^2 - (\partial_i\mathcal{R}^2)\right]\,. \tag{3.27}$$

Variation of this action then results in a second order partial differential equation for $\mathcal{R}$, which can be rewritten as a set of independent second order ordinary differential equations for each Fourier mode $\mathcal{R}_k(\tau)$ (corresponding to wavenumber k) after a Fourier-decomposition. (We only use $k = |\vec{k}|$ here, as the resulting equations are isotropic.) The equations correspond to to a set of harmonic oscillators with time-dependent frequencies:

$$(zR_k)'' + \left(k^2 - \frac{z''}{z}\right)zR_k = 0\,, \tag{3.28}$$

with $z^2 = a^2\phi'^2/\mathcal{H}^2M_p^2 \approx 2a^2\varepsilon$.

The initial conditions specifying the solutions to these equations can be obtained through canonical quantization of $\mathcal{R}$ and a suitable choice of vacuum. Canonical quantization gives the following

normalization constraint for the mode functions:

$$\mathcal{R}_k^* \mathcal{R}_k' - \mathcal{R}_k^{*\prime} \mathcal{R}_k = (-i) \frac{\mathcal{H}^2 M_p^2}{a^2 \phi'^2} \,. \tag{3.29}$$

Choosing the Bunch-Davis vacuum then yields for subhorizon scales (corresponding to very early times)

$$\lim_{\tau \to -\infty} \mathcal{R}_k(\tau) = \frac{\mathcal{H}}{a\phi'} \frac{\mathrm{e}^{-ik\tau}}{\sqrt{2k}} \,. \tag{3.30}$$

In an exact de-Sitter expansion ($\varepsilon \to 0$), one can find the generic solution to equation (3.28) and match the integration constants to the constraints (3.29) and (3.30). (Strictly speaking, $z = 0$ in de-Sitter space, but one can simply set $z = 1$ and ignore the z''-term to obtain the correct equation.) From the resulting solution one can deduce that $\mathcal{R}$ remains constant on superhorizon scales ($k \ll \mathcal{H}$). This result directly translates to the quasi-de-Sitter regime of slow roll inflation, if we evaluate the solution at horizon crossing. Since all relevant perturbation modes exit the horizon during a sufficiently long era of inflation, one can calculate the the dimensionless primordial power spectrum of the curvature perturbation and obtain

$$\mathcal{P}_{\mathcal{R}}(k) = \left. \frac{\mathcal{H}^4}{(2\pi)^2 a^2 \phi'^2} \right|_{k=\mathcal{H}} \,. \tag{3.31}$$

The scalar spectral index n_s can now be calculated to first order in the slow roll parameters ε and η:

$$n_s - 1 = \frac{\mathrm{d}\,\mathcal{P}_{\mathcal{R}}(k)}{\mathrm{d}\ln(k)} \approx 2\eta - 6\varepsilon \,. \tag{3.32}$$

In principle this result has to be evaluated at horizon crossing for each wavenumber separately, but the slow roll parameters are typically (almost) constant during a long stage of inflation. Already in very simple single field inflation models, one can get a constant $n_s \approx 0.96$, as is currently preferred by observations.

In this calculation we have seen a mixture of classical and quantum mechanical calculations. In partiular, we have treated the classical two point correlators $< ... >$ as equal to vacuum expectation value of the corresponding operators $< 0|...|0 >$. This is by no means a trivial step. In fact, this quantum-to-classical transition presents a whole research area by itself, a detailed investigation of which is far beyond the scope of this thesis. An early review can be found e.g. in [Polarski and Starobinsky, 1996]. Still, the results presented here are standard, and the treatment appears to be justified.

Quantum fluctuations can have effects going beyond what we have presented above. In fact, the quantum fluctuations can contain 'jumps', during which the field suddenly changes its field value by a rather large amount. This effect becomes important precisely if the change in the field value due to the jumps becomes bigger than the change due to slow roll, in this case one speaks of the *fluctuation dominated regime*. As is discussed in [Winitzki, 2008], this evolution can be described by the standard slow roll evolution superimposed by a random walk with stepsize

$$\Delta\phi \sim \mathcal{H}/(2\pi a) \tag{3.33}$$

within a time interval $\Delta t \sim a/\mathcal{H}$. The region with different 'jump histories' are separated by many Hubble distances. The quantum fluctuations are a local effect, but any local jump is quickly blown up to become its own independent patch of the universe through the rapid expansion. This gives rise to many patches of spacetime reaching the end of inflation at different times, each of these patches can be considered an independent universe, the whole collection a multiverse. Interestingly, as the regions which reach reheating later continue to inflate longer, they can split into several distinct patches or universes. This is what is known as 'self-reproduction' of inflating regions. Despite the fact that each single patch will eventually reach the end of inflation within a finite time, the continuous generation of new universes during inflation will make this process continue forever, hence the name *eternal inflation*. As many inflationary models exhibit a fluctuation dominated regime, such a scenario arises rather generically.

The measure problem

Despite the fact that we have just presented a mechanism giving rise to a multiverse scenario, the anthropic argument still runs into problems. As we have argued above, with respect to the anthropic argument, we would basically like to figure out which fraction of universes in the multiverse allowing for the existence of observers has a cosmological constant close to the one measured. So we simply have to count, right? Count the number of universes which have a cosmological constant in the required range and divide by the number of universes allowing for the existence of observers. There is only one problem: Both of these quantities are countably infinite, and the result depends heavily on reordering. To put this more precisely: We want to calculate

$$P = \lim_{N\to\infty} \frac{1}{N} \sum_j B(j)\,, \tag{3.34}$$

where $B(j)$ is either 1 or 0. This is not a well defined limit, as it is not stable under permutations $\sigma \in S_{\mathbb{N}}$. If one could define a canonical measure of finite mass on the group $S_{\mathbb{N}}$, this limit could be defined as well and one could proceed. This is, however, not possible. Nonetheless, many theorists have tackled this problem and proposed different measures in order to make progress. The results are, however, ambiguous, and we will not discuss them here. More information can be found e.g. in [Winitzki, 2008].

3.2 QUINTESSENCE

In this section we will introduce dynamical models of dark energy, focussing on so called *quintessence* models. The underlying assumption for all the scenarios presented here is that the cosmological constant problem is solved by some mechanism setting the effective cosmological constant to zero. In these models dark energy consists of a cosmological scalar field φ with some potential $V(\varphi)$, called a *cosmon* or quintessence field. We will only consider scenarios where the potential has a minimum at $\varphi_{\min}$ with $V(\varphi_{\min}) = 0$, otherwise any remaining potential energy can always be included in a suitable redefinition of the effective cosmological constant. This also includes the case where $\varphi_{\min} = \pm\infty$, the

mathematically correct statement would be that we only consider potentials with $\mathrm{Inf}[V(\varphi)] = 0$. We will first focus on the simplest models of a minimally coupled canonical scalar field and move on to more exotic scenarios later.

3.2.1 Minimally coupled quintessence

As we have already seen in chapter 2, a canonical scalar field φ with a potential $V(\varphi)$ can have an equation of state anywhere in the interval $[-1,1]$, and therefore can drive an accelerated cosmic expansion. The conditions for this are essentially the same as we discussed in the context of inflation in the previous section, just at lower energy scales: The field has to be slow rolling, i.e. the energy density ρ_φ in eq. (2.70) has to be dominated by the potential energy $V(\varphi)$. Current constraints on the equations of state for minimally coupled scalar field dark energy can be obtained e.g. from the nine year WMAP data [Hinshaw et al., 2013] and read[2]

$$\omega_{\varphi,0} = -1.17^{+0.13}_{-0.12}. \tag{3.35}$$

Interestingly, the 1σ bound lies slightly below -1. This is consistent with other results which also find a best fit value less than -1, but cite larger uncertainties [Ade et al., 2013b, Said et al., 2013]. While the signal is not significant by any means, it might be a hint towards interesting physics, as we will discuss below.

If we want the cosmon to constitute dark energy, its dynamics necessarily need to evolve in a way which gives an equation of state close to -1 for small redshifts. For larger redshifts many scenarios are possible, the dynamics can be very complex in general. This brings us to the issue of initial conditions: For a given model, how precisely do we need to tune our initial conditions (i.e. $\varphi(\tau_{\mathrm{in}})$ and $\varphi'(\tau_{\mathrm{in}})$ at some initial conformal time τ_{in}) in order to get a realistic cosmology with late time acceleration? And if we do need to tune them precisely, how natural are the initial conditions that work? In particular we want to avoid *fine tuning problems*, which are present in some quintessence scenarios that give a realistic cosmology only for very precisely tuned initial conditions. This issue is closely related to the *why now* or *coincidence problem*, which asks the question why dark energy became relevant only recently, and not much earlier or much later in the cosmic history.

Tracker solutions

There is one specific class of solutions of the scalar field equations, called *tracker solutions*, which address this issue. These are solutions which act as attractors, meaning that the field dynamics will be driven towards one of these solutions largely independent of the initial conditions.[3] This is clearly a very desirable feature, as the cosmological evolution is determined by the parameters of the potential

[2] These are fitting results for models with a specific non-constant equation of state $\omega_\varphi = \omega_{\varphi,0} + \omega_a z/(1+z)$. This is still a strong restriction considering the very variable dynamics of a cosmon field, but one can expect similar results in general.

[3] It is of course possible to choose initial conditions so far away from the attractor, that even after a very long evolution, say as long as the universe is old, the scalar field dynamics have not yet adjusted to the tracker. Such initial conditions are usually very unnatural and we will not consider them further here.

alone, and not by initial conditions. However, in this case one still has to explain why the parameters appearing in the potential have the values required for the existence of a valid tracker.

Amongst the possible tracker solutions (which we will discuss a little further below), there is a specific subclass, called *attractive scaling solutions*. The nomenclature in this field is not perfectly consistent throughout the literature, in this work we consider the term *scaling solution* to mean a solution for which the energy density scales like the scale factor to some constant power, i.e.

$$\rho_\varphi \propto a^n\,, \quad n = 3(1+\omega_\varphi)\,. \tag{3.36}$$

Clearly n is limited to the range $n \in [0,6]$ for a minimally coupled canonical scalar field and a scaling solution requires $\omega_\varphi = constant$. The term 'attractive' means that, in addition to being a scaling solution, it should also act like a tracker, which is not guaranteed. In fact, sometimes the range of initial conditions for which a solution acts as an attractor is considered. We will be satisfied if the scaling solution is stable, i.e. small perturbations around the solution decay, which is often sufficient to find an attractor for a rather large range of initial conditions.

In the presence of a background fluid with a constant equation of state ω_b, e.g. radiation or matter, we consider an *exact scaling solution* to be a scaling solution for which the scalar density parameter Ω_φ remains constant, i.e. $\omega_\varphi = \omega_b$ or $\rho_b = 0$. This is clearly a stronger constraint than merely demanding a constant equation of state. For a minimally coupled canonical scalar field, the only potential allowing for an exact scaling solution with non-vanishing density parameters for both the scalar field and the background fluid can be shown to be the exponential potential [Liddle and Scherrer, 1999]

$$V(\varphi) = M^4 \mathrm{e}^{-\alpha\varphi/M}\,, \tag{3.37}$$

where the choice of mass M is arbitrary, as it can be redefined to any value through a shift in φ. The exact scaling solutions existing for this potential are universal attractors and given by

$$\Omega_\varphi = \frac{3(1+\omega_b)}{\alpha^2}\,, \tag{3.38}$$

they exist for $\alpha^2 > 3(1+\omega_b)$. For $\alpha^2 < 3(1+\omega_b)$ the universal attractor is a scalar field dominated solution for which

$$\omega_\varphi = \frac{\alpha^2 - 3}{3} < 0\,. \tag{3.39}$$

Clearly, the parameter range allowing for an exact scaling scenario are at odds with the parameter range allowing for an accelerated expansion in this case.

Still, the exponential potential can be of great help for understanding generic properties of tracker solutions leading to late-time cosmic acceleration. It is useful to introduce a 'steepness parameter'

$$\lambda_{\mathrm{eff}}(\varphi) = \left| \frac{M_p V_{,\varphi}}{V} \right|\,, \tag{3.40}$$

which is clearly related to the slow roll parameter ε introduced in the previous section. This quantity measures the local 'steepness' of the scalar potential. To some extent, one can understand the

behavior of generic quintessence potentials with knowledge from the exponential potential and this parameter. We will only quickly review the results here, an exhaustive discussion is given in [Joyce, 2001].

As one would expect, late time acceleration requires that $\lambda_{\text{eff}} \lesssim 1$ for suitable range of field values, which should correspond to energy densities of the order of ρ_0. In contrast, the existence of a tracker solution requires $\lambda_{\text{eff}} \gg 1$ for field values corresponding to higher energy densities, comparable to the early universe. Why is this necessary? In short, there is a dynamical adjustment mechanism which forces the scalar field to adjust to a tracker solution for steep potentials. It can be simply understood as follows: If the initial scalar field energy density is large, the scalar field will quickly roll down its steep potential, leading to dominance of kinetic energy over potential energy within a short period of time. The scalar energy density will therefore (after some short adjustment time) scale away like a^{-6} and quickly become subdominant compared to radiation (and non-relativistic matter). Once the kinetic energy has scaled away sufficiently to catch up with the potential energy, the by now subdominant scalar field will essentially sit at a fixed value (with $\omega_\varphi \approx -1$), as long as [Joyce, 2001]

$$\frac{a^2 V_{,\varphi}}{3\mathcal{H}\varphi'} \approx \frac{M_p V_{,\varphi} V}{3\sqrt{\rho_{\text{tot}}/V}} \left(\frac{a_1}{a}\right)^3 \ll 1\,, \tag{3.41}$$

where a_1 is the scale factor when the freezing sets in. This condition remains valid as long as the potential gradients are sufficiently small, but ultimately the left hand side quantity of eq. (3.41) is increasing in time and so eventually the field will unfreeze. From this point on, a mechanism balancing the two extremes overdamping and fast roll sets in, which leads to a predetermined scalar field evolution, the tracker. This can be thought of as the field adjusting to the exponential exact scaling solution with a slowly varying exponent $\alpha = \lambda_{\text{eff}}$, but this analogy has its limits. If it were exact, we would expect a constant equation of state during radiation domination (and also matter domination) for all tracker scenarios. This is not the case, the equation of state is slowly varying in time for many tracker solutions.

This is what all quintessence potentials allowing for tracker solutions have in common: A steep part with $\lambda_{\text{eff}} \gg 1$ corresponding to field values with high energies, which are responsible for the tracker, and a flat part with $\lambda_{\text{eff}} \lesssim 1$ which is responsible for the current cosmic acceleration. The transition from 'steep' to 'flat' has to happen at an energy scale slightly higher than ρ_0. So instead of adjusting the initial conditions, we have to adjust the potential shape to allow for such a tracker solution. The fine tuning problem then becomes a matter of motivation: We need a credible particle physics model in order to explain the shape of the potential. The number of quintessence potentials with such a behaviour suggested in the literature is quite big, an overview can be found e.g. in [Joyce, 2001]. An example of a tracker quintessence scenario can be seen in Fig. 3.2.

Constraints on early dark energy

In exact scaling or tracker scenarios, the energy density of the cosmon in the early universe is typically small, but not completely negligible. Thus observations can be used to constrain such scenarios. To our knowledge the most stringent observational bounds come from big bang nucleosynthesis [Ferreira

and Joyce, 1997, 1998, Bean et al., 2001] and cosmic microwave background observations [Calabrese et al., 2011, Reichardt et al., 2012, Xia et al., 2013, Pettorino et al., 2013, Ade et al., 2013b].

Let us start with the BBN bounds. Adding a tracking quintessence field to the early radiation dominated era modifies expansion of the universe and thus standard big bang nucleosynthesis, as we have described in chapter 2. Observations of the abundances of the lightest elements in the cosmos can therefore put an upper bound on the quintessence density parameter in an exact scaling scenario. The tightest constraint known to us is given in Bean et al. [2001], where the derived bound is $\Omega_\varphi < 0.045$.

Constraints from the CMB on a scaling scalar quintessence component are strong whenever the scalar field makes up a non-negligible fraction of the energy density of the universe at decoupling [Pettorino et al., 2013], which is the case in most scaling scenarios. Recently bounds from this era have been improved by the Planck mission to give an upper limit of about 0.01 [Ade et al., 2013b] for Ω_φ at 95% confidence level.

Finding scaling solutions - The dynamical system approach

We have already highlighted the importance of tracker solutions for scalar field cosmologies. The question remains how to find them. In the case of exact scaling scenarios, there is indeed an analytical

FIGURE 3.2: **Cosmon field adjusting to a scaling solution**

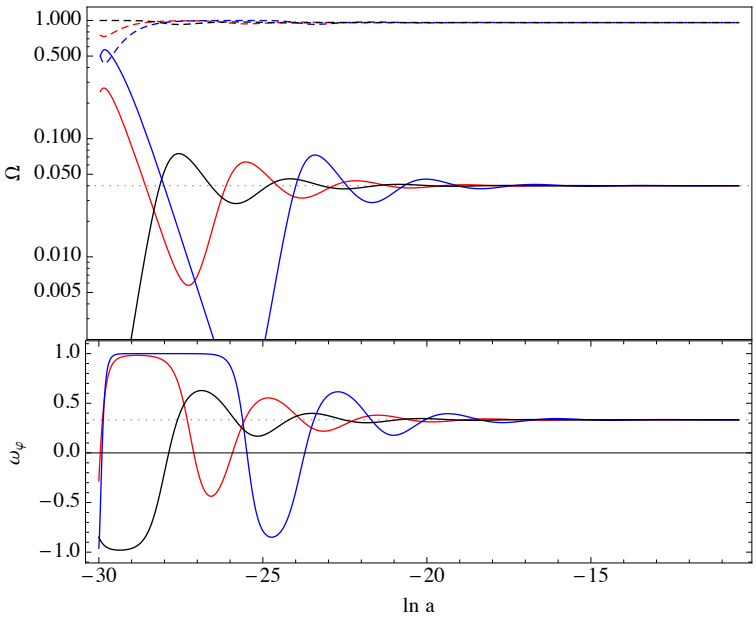

A cosmon field adjusting to its scaling solution in the presence of a radiation fluid. The upper panel shows the density parameters for radiation (dashed) and the cosmon (solid), the lower panel shows the scalar equation of state. The different colors show different initial conditions. The potential used was an exponential potential with $\alpha = 10$, the dashed gridlines represent the attractive scaling solution.

method, called *dynamical systems approach*, which we will now introduce and employ in chapter 5.

Let us consider a system of dynamical variables $x_i(t)\,,\ i = 1,...,n$ whose evolution is governed by a set of differential equations

$$\dot{x}_i(t) = f_i(x_1,...,x_n). \tag{3.42}$$

Here the functions f_i have no explicit t-dependence, rendering the system autonomous. A point $(x_1^c,...,x_n^c)$ is called a critical point of the system if $(f_1,...,f_n)|_{(x_1^c,...,x_n^c)} = 0$.

The behavior of the dynamics around a critical point can be easily understood through first oder perturbation theory. Expanding x_i around the critical point $(x_1^c,...,x_n^c)$, i.e.

$$x_i = x_i^c + \delta x_i\,, \tag{3.43}$$

gives the following equations for the δx_i in linear approximation:

$$\frac{d}{dt}\begin{pmatrix}\delta x_1\\ \vdots\\ \delta x_n\end{pmatrix} = \mathcal{M}\begin{pmatrix}\delta x_1\\ \vdots\\ \delta x_n\end{pmatrix} \quad \text{with} \quad \mathcal{M} = \begin{pmatrix}\frac{\partial f_1}{\partial x_1} & \cdots & \frac{\partial f_1}{\partial x_n}\\ \vdots & \ddots & \vdots\\ \frac{\partial f_n}{\partial x_1} & \cdots & \frac{\partial f_n}{\partial x_n}\end{pmatrix}_{(x_1^c,...,x_n^c)}. \tag{3.44}$$

The matrix $\mathcal{M}$ has n eigenvalues $\mu_1,\ldots,\mu_n$. Once these are determined, the general solution for δx_i reads

$$\delta x_i(t) = C_i^1 e^{\mu_1 t} + \ldots + C_i^n e^{\mu_n t} \tag{3.45}$$

with integration constants $C_i^1,\ldots,C_i^n$. Thus the stability of the fixed point is determined entirely by the eigenvalues of $\mathcal{M}$. Denoting the determinant of $\mathcal{M}$ by $\mathbf{d}$, we can make the following commonly used classification for the fixed points [Copeland et al., 1998, Gumjudpai et al., 2005]: A fixed point is stable if the real parts of all eigenvalues are negative, unstable if they are all positive and a saddle point if some are negative and some are positive. It is called a node if all eigenvalues are real, and a spiral if all eigenvalues have non-vanishing imaginary parts. If $\mathbf{d} = 0$ one of the eigenvalues is zero indicating a flat direction in phase space (in linear order). In this case the stability needs to be established by going to higher orders in the perturbations. A stable fixed point is called an attractor, if it is the only stable fixed point for a given set of parameters it is the universal attractor.

Application to cosmology

In cosmology the dynamical systems approach is applied to the field equations, which can sometimes be translated into an algebraic autonomous dynamical system of finite dimensionality. We start by choosing to be the square roots of the density parameters as variables, which in the case of a universe containing non-relativistic matter, radiation and a scalar field φ means

$$x = \frac{\varphi'}{\sqrt{6}M_p\mathcal{H}}, \quad y = \frac{a\sqrt{V}}{\sqrt{3}M_p\mathcal{H}}, \quad z = \sqrt{\Omega_r}. \tag{3.46}$$

The field equations can the be translated to a set of first order differential equations for x, y and z, where usually $N = \ln(a)$ is used as a time variable. Scaling solutions with constant equations of state and density parameters then precisely correspond to solutions satisfying $x' = y' = z' = 0$. Note that

there is no fourth degree of freedom for non-relativistic matter since $\Omega_{tot} = 1$ by assumption (K=0). Whether or not this set of variables is complete depends on the potential shape, in particular whether or not the potential derivative $V_{,\varphi}$ appearing in the scalar field equation (2.71) introduces a new degree of freedom. If it does, we need to add another variable with its own evolution equation, which will include the second potential derivative $V_{,\varphi\varphi}$ and so forth. Generally speaking we have to add variables of the shape

$$s_i \equiv \frac{\partial^i V}{\partial \varphi^i}\frac{M_p^i}{V} \quad \text{for } i > 1 \tag{3.47}$$

and corresponding first order differential equations. The question is whether or not the system eventually becomes autonomous, meaning that there is some $n \in \mathbb{N}$ such that

$$\frac{\mathrm{d}s_n}{\mathrm{d}N} = f(x, y, z, s_1, ..., s_n)\,. \tag{3.48}$$

If this is the case, one can find all attractive scaling solutions of the potential by looking at the stable critical points of the autonomous system.

It is important to realize that this approach does not yield the complete information about the system. In particular the trajectories in phase space usually need to be determined numerically. Its great value lies in the fact that one can immediately see if there is a stable scaling solution (typically with some desired property) or not.

3.2.2 COUPLED QUINTESSENCE

We now move on to discuss models of *coupled quintessence*, meaning a canonical scalar field with explicit couplings to other matter fields in the theory. As we have seen in chapter 2, such a coupling arises naturally in scalar-tensor theories of gravity after a transformation to the Einstein frame. We will restrict ourselves to one simple form of a coupling here, for which the cosmon field couples to to the trace of the matter energy momentum tensor. Since this trace vanishes for radiation, it makes no difference if take this to mean only non-relativistic matter or include also radiation. In terms of the couplings defined in eq. (2.52) we have

$$Q^\mu_\varphi = \frac{\beta}{M_p} T_m \mathcal{D}^\mu \varphi\,, \tag{3.49}$$

where T_m denotes the trace of the total matter energy momentum tensor. In a FLRW-universe we then have the following equations of motion for radiation (r), non-relativtistic matter (m) and the cosmon:

$$\varphi'' + 2\mathcal{H}\varphi' + a^2 V_{,\varphi} = \frac{\beta}{M_p} a^2 \rho_m\,, \tag{3.50}$$

$$\rho_m' + 3\mathcal{H}\rho_m = -\frac{\beta}{M_p}\rho_M \varphi'\,, \tag{3.51}$$

$$\rho_r' + 4\mathcal{H}\rho_r = 0\,. \tag{3.52}$$

The scaling solutions of this system for the exponential quintessence potential given in eq. (3.37) have been analyzed in [Amendola, 2000a], using the dynamical system approach described above. Since there is now a coupling between matter and the cosmon, a scaling solution no longer has to satisfy $\omega_\varphi = \omega_{\text{eff}}$, we merely require that the scalar equation of state and density parameter be constant in time. Since the results will be of some relevance for the analysis we present in chapter 4, we quickly summarize them in Tables 3.1 and 3.2. The stable fixed point divide the parameter space of coupled quintessence into disjunct sections.

Interestingly, coupled quintessence can provide a possible explanation, if the observed dark energy equation of state turns out to be less than -1. As was shown in [Das et al., 2006], fitting data resulting from a coupled quintessence model to some uncoupled dark energy parameterization can lead to a best fit value of ω_φ below -1, despite the fact that it is bound below by -1 in the coupled quintessence setting. In other words: Fitting observations in an uncoupled dark energy scenario and obtaining 'superacceleration', i.e. an equation of state less than -1 can be hint towards coupled dark energy.

Furthermore, coupled quintessence models can help to provide solution to the coincidence problem. We want to stress two mechanisms to achieve this. First, one can construct models with a φ-dependent coupling function $\beta(\varphi)$. The precise analysis of such a model is non-trivial, but in a simplified picture one can imagine that the time-evolution of the coupling effectively shifts the parameters of coupled quintessence with constant β from a regime where the attractor is a matter dominated epoch with subdominant cosmon energy density to a regime where the attractor gives an accelerated expansion. Thus one can obtain an accelerated expansion and a realistic expansion history independent of initial conditions, but the problem remains that one has to explain the precise shape of the coupling, which needs to tuned somewhat to fit observations [Tocchini-Valentini and Amendola, 2002].
Second, one can imagine a simple constant coupling to the trace of the energy-momentum tensor of a species which becomes non-relativistic in the late universe. The prime candidate for this species are of course neutrinos. In that case, neutrinos becoming non-relativistic would effectively 'switch on' the coupling which could then trigger cosmic acceleration. In order for this to work and stop the cosmon field sufficiently fast, a rather strong coupling is necessary. This *growing neutrino quintessence* model is a very interesting way to solve the coincidence problem, and has been studied extensively in recent years [Wetterich, 2007, Amendola et al., 2008, Mota et al., 2008, Ayaita et al., 2012b, 2013]. Still, it faces some problems. In particular non-linear structure formation is quite complicated in this model, the strong coupling causes strong backreaction effects. Nonetheless, causing cosmic acceleration through a trigger event like neutrinos becoming non-relativistic might seem more appealing than introducing some feature in the scalar field potential or coupling function designed to achieve the same.

3.2.3 Alternative models

In addition to coupled or minimally coupled canonical quintessence, the are a number of alternative models of dynamical dark energy. They will not play any role for the remainder of this thesis, but we feel we should at least quickly mention the most popular ones among them. More details can be found in [Copeland et al., 2006] and references therein.

TABLE 3.1: **Scaling solutions in Coupled Quintessence**

Point	x	y	z	Ω_φ	p	ω_{eff}	ω_φ
a	$\frac{-\alpha}{\sqrt{6}}$	$\left(1-\frac{\alpha^2}{6}\right)^{1/2}$	0	1	$2/\alpha^2$	$\frac{\alpha^2}{3}-1$	$\frac{\alpha^2}{3}-1$
b_r	$\sqrt{\frac{8}{3}}\frac{1}{\alpha}$	$\frac{2}{\sqrt{3}\alpha}$	$\left(1-\frac{4}{\alpha^2}\right)^{1/2}$	$4/\alpha^2$	1/2	1/3	1/3
b_m	$\sqrt{\frac{3}{2}}\frac{1}{\alpha-\beta}$	$\frac{(g-9)^{1/2}}{\sqrt{6}\lvert\alpha-\beta\rvert}$	0	$\frac{g}{6(\alpha-\beta)^2}$	$\frac{2}{3}\left(1-\frac{\beta}{\alpha}\right)$	$\frac{\beta}{\alpha-\beta}$	$\frac{18}{g}-1$
c_r	0	0	1	0	1/2	1/3	-
c_{rm}	$\frac{1}{\sqrt{6}\beta}$	0	$\left(1-\frac{1}{2\beta^2}\right)^{1/2}$	$\frac{1}{6\beta^2}$	1/2	1/3	1
c_m	$\sqrt{\frac{2}{3}}\beta$	0	0	$\frac{2}{3}\beta^2$	$\frac{1}{\beta^2+3/2}$	$\frac{2}{3}\beta^2$	1
d	-1	0	0	1	1/3	1	1
e	+1	0	0	1	1/3	1	1

Only the fixed points of the autonomous systems obeying $y \geq 0$ and $z \geq 0$ are shown, since the variables (x,y,z) are restricted to the quarter of the unitary 3-sphere defined by positive values of y,z by definition. The system is symmetric under a simultaneous sign change of α and β, we fixed this degeneracy by restricting ourselves to $\alpha > 0$. The quantity g is defined to be $g = 6\beta^2 - 6\alpha\beta + 18$. The quantity p describes the evolution of the scale factor for the corresponding fixed points through $a(t) \propto a^p$. Table taken from [Amendola, 2000a].

TABLE 3.2: **Existence and stability for CQ scaling solutions**

Point	Existence	Stability	Acceleration
a	$\alpha < \sqrt{6}$	$\alpha < \alpha_+,\ \alpha < 2$	$\alpha < \sqrt{2}$
b_r	$\alpha > 2$	$0 < \alpha < \sqrt{\frac{2}{3}}4\beta$	never
b_m	$\lvert\alpha-\beta\rvert > \sqrt{\frac{3}{2}},\ \alpha < \alpha_0$	$\alpha > \alpha_+,\ \alpha > \sqrt{\frac{2}{3}}4\beta$	$\alpha < -2\beta$
c_r	$\forall\alpha, \beta$	unstable $\forall\alpha, \beta$	never
c_{rm}	$\lvert\beta\rvert > 1/\sqrt{2}$	$\alpha > \sqrt{\frac{2}{3}}4\beta$	never
c_m	$\lvert\beta\rvert < \sqrt{\frac{3}{2}}$	$\lvert\beta\rvert < 1/\sqrt{2},\ \alpha > \alpha_0$	never
d	$\forall\alpha, \beta$	unstable $\forall\alpha, \beta$	never
e	$\forall\alpha, \beta$	unstable $\forall\alpha, \beta$	never

Only the fixed points of the autonomous systems obeying $y \geq 0$ and $z \geq 0$ are shown, since the variables (x,y,z) are restricted to the quarter of the unitary 3-sphere defined by positive values of y,z by definition. The system is symmetric under a simultaneous sign change of α and β, we fixed this degeneracy by restricting ourselves to $\alpha > 0$. The quantities $\alpha_+ = \frac{1}{2}\left(\beta + \sqrt{12+\beta^2}\right)$ and $\alpha_0 = \begin{cases} 0 & \text{for } \beta < 0 \\ \left(\beta + \frac{3}{\beta}\right) & \text{for } \beta > 0 \end{cases}$ are used. Table taken from [Amendola, 2000a].

k-essence

In so called k-essence models, the scalar field is no longer assumed to be canonical. Instead, one assumes an action of the form

$$S_\varphi = \int \mathrm{d}^4x\,\sqrt{-g}\,\mathcal{L}_\varphi(\varphi, X) \quad \text{with} \quad X = -\frac{1}{2}(\mathcal{D}_\mu\varphi)(\mathcal{D}^\mu\varphi)\,. \tag{3.53}$$

While originally being invented as models of inflation [Armendariz-Picon et al., 1999], these models soon became popular in dark energy research [Chiba et al., 2000, Armendariz-Picon et al., 2000, 2001]. The reason for their popularity is essentially that they potentially provide an elegant solution to the fine tuning problem. On the one hand, a so called 'leaping kinetic term' can trigger cosmic acceleration [Hebecker and Wetterich, 2001], on the other hand the onset of matter domination can function as a trigger event for a suitable choice of Lagrangian [Armendariz-Picon et al., 2000]. These models are in principle distinguishable from canonical quintessence models through the time evolution of the equation of state, which reads

$$\omega_\varphi = \frac{\mathcal{L}_\varphi}{2\frac{\partial\mathcal{L}_\varphi}{\partial X}X - \mathcal{L}_\varphi}\,, \tag{3.54}$$

and the sound speed at the perturbative level. However, as recent analyses have shown, putting strong constraints on the sound speed of dark energy seems to be difficult even with planned future observations like Euclid [Ayaita et al., 2012a].

Tachyon field

A Tachyon field is a scalar field which has an additional coupling to the metric. The actions investigated in such scenarios are of the type

$$S_\varphi = -\int \mathrm{d}^4x\,V(\varphi)\sqrt{-\det(g_{\mu\nu} + (\mathcal{D}_\mu\varphi)(\mathcal{D}_\nu\varphi))}\,. \tag{3.55}$$

The equation of state in such models lies between -1 and 0, and for a suitable choice of tachyon potential $V(\varphi)$ the scalar field can act as dark energy [Copeland et al., 2006].

Phantom dark energy

As we have seen above, current bounds on the equation of state of dark energy are perfectly consistent with an equations state (slightly) below -1. Models which can realize such a scenario are usually referred to as *phantom dark energy* [Caldwell et al., 2003]. A simple possibility to realize such a model is to simply switch the sign of the kinetic term in the standard quintessence action, i.e.

$$S_\varphi = \int \mathrm{d}^4x\,\sqrt{-g}\left[\frac{1}{2}(\mathcal{D}_\mu\varphi)(\mathcal{D}^\mu\varphi) - V(\varphi)\right]. \tag{3.56}$$

In this case, the equation of state in a FLRW universe reads

$$\omega_\varphi = \frac{\varphi'^2 + 2a^2V(\varphi)}{\varphi'^2 - 2a^2V(\varphi)}, \tag{3.57}$$

which satisfies $\omega_\varphi < 1$ for $\varphi'^2 < 2a^2V(\varphi)$. Note that these models can be considered to be included in the class of k-essence models discussed above. While such scenarios are valid at the classical level, at the quantum level they are subject to severe ultraviolet instabilities [Carroll et al., 2003].

Non scalar field models

All the models discussed above were based on a scalar field. There are also models of dark energy which do not rely on scalar fields. The most popular amongst them are probably the modified gravity models we already discussed in chapter 2. But, as we have seen, an important subclass of $f(R)$-gravity models is in fact equivalent to a certain class of scalar field models, and therefore included in the above description in this sense.

In addition to modified gravity, there are other non-scalar-field models of dark energy, like the Chaplin gas [Kamenshchik et al., 2001], but they can often be shown to be equivalent to a scalar field model included in one of the classes above from a gravitational point of view. Therefore the class of scalar field dark energy models is much more general than it may seem at first sight. It can, due to its huge variability, cover an enormous range of models, albeit as an effective description.

3.3 DILATATION SYMMETRY AND Λ

From the very start, quintessence models were tightly connected to the concept of scale symmetry, or dilatation symmetry [Wetterich, 1988a,b]. In this section we quickly review this concept, focussing in particular on its connection to the cosmological constant problem in higher dimensional theories of gravity, which is discussed in [Wetterich, 2009, 2010a,b].

3.3.1 DILATATIONS

Dilatations are transformations which rescale all dynamical fields of a given theory according to an appropriate scaling dimension. For a theory involving a metric $g_{\mu\nu}$ and a scalar field ξ in d dimensions this means

$$g_{\mu\nu} \to \alpha^2 g_{\mu\nu} \quad \text{and} \quad \xi \to \alpha^{-((d-2)/2)}\xi, \tag{3.58}$$

where $\alpha > 0$. As a consequence a generic action with a Lagrangian density $\mathcal{L}$,

$$S = \int \mathrm{d}^d x \sqrt{-g}\,\mathcal{L}, \tag{3.59}$$

is dilatation invariant if $\mathcal{L}$ transforms as follows under dilatations:

$$\mathcal{L} \to \alpha^{-d}\mathcal{L}\,. \tag{3.60}$$

Terms involving explicit mass scales in the Lagrangian density clearly cannot be dilatation symmetric, and thus any dilatation symmetric theory is by construction scale free. Since we observe mass scales in the universe all the time, clearly, dilatation symmetry must be broken either explicitly or spontaneously by the vacuum.

3.3.2 Higher dimensional gravity

Dilatation symmetric theories of gravity have particularly interesting features in higher dimensions, as we will soon discover. One of the main reasons for this lies in the strong constraints dilatation symmetry puts on the action in such theories. We will be working with higher dimensional scalar-tensor theories of gravity here, a combination we have not discussed in chapter 2, where we only focussed on higher-dimensional Einstein gravity and four dimensional scalar-tensor theories. Following the same nomenclature introduced in section 2.2, we work in $d = D+4$ dimensions and use the same notation for the coordinates, the metric and curvature terms as before, with one exception: Now we have to differentiate between the Einstein- and the Jordan-frame in both the higher-dimensional and the dimensionally reduced four dimensional theory. We will therefore use 'hatted' symbols (like $\hat{g}_{\hat{\mu}\hat{\nu}}$) for Jordan-frame quantities is higher dimensions, and 'unhatted' symbols with a superscript (d) for Einstein-frame quantities. As before, Jordan-frame quantities in the effective four dimensional theory are denoted with a superscript tilde (like $\tilde{R}$), and symbols without any ornaments or superscripts denote quantities in the four dimensional Einstein-frame.

For $d > 6$, the most generic action compatible with dilatation symmetry in a scalar-tensor theory is the following:

$$S^{(d)} = \int \mathrm{d}^d\hat{x}\sqrt{-\hat{g}}\left\{-\frac{1}{2}\xi^2\hat{R} + \frac{\zeta}{2}\partial_{\hat{\mu}}\xi\partial^{\hat{\mu}}\xi + F(\hat{R}_{\hat{\mu}\hat{\nu}\hat{\rho}\hat{\sigma}})\right\} \tag{3.61}$$

where F is some function of the curvature tensor in compliance with dilatation symmetry, i.e.

$$F \to \alpha^{-d}F \tag{3.62}$$

under the dilatations introduced above and ζ is a dimensionless constant. In particular, no scalar potential is allowed and the coupling of the scalar field ξ to the curvature tensor is severely restricted. In contrast, for $d = 4$ and $d = 6$ scalar potentials $\propto \xi^4$ and $\propto \xi^3$ would be allowed respectively (see e.g. appendix A of [Beyer, 2011] for a proof). We restrict ourselves to polynomial potentials here. Non-analytic potentials compatible with dilatation symmetry exist, but we will not discuss those in this thesis (see [Wetterich, 2010a] for more information no this).

As a first glimpse at the connection of a higher dimensional setting to the cosmological constant, let us presume that a scalar potential $V(\xi) = \lambda\xi^4$ is present in the action. This is only allowed by dilatation symmetry for $d = 4$. We can now perform a Weyl-transformation to the Einstein-frame (see eq. (2.23)) with

$$\tau = \hat{M}_p\xi^{-\frac{2}{d-2}}, \tag{3.63}$$

where $\hat{M}_p$ is some suitable mass. It might seem a bit strange to simply introduce the Planck mass in this ad-hoc way, but one should remember that the absolute value of the Planck mass has no physical significance. All that can be measured are dimensionless ratios of masses, and any mass

terms appearing in the matter part of the action would be affected by the Weyl-transformation as well. A different choice of $\hat{M}_p$ would affect all ratios of masses in the same way. In fact, typically constant particle masses appearing in the matter Lagrangian in the Jordan frame can become field-dependent in the Einstein frame. This transformation gives the following action:

$$S^{(d)} = \frac{\hat{M}_p^2}{2} \int \mathrm{d}^d\hat{x} \sqrt{-g^{(d)}} \left\{ -R^{(d)} + \partial_{\hat{\mu}}\delta\partial^{\hat{\mu}}\delta + \hat{M}_p^{-2}\,\tilde{F}(R^{(d)}_{\hat{\mu}\hat{\nu}\hat{\rho}\hat{\sigma}}, \delta) + 2\lambda\hat{M}_p^2 \right\}, \tag{3.64}$$

where

$$\delta = \left(\zeta + \frac{4(d-2)(d-1)}{(d-2)^2}\right)^{1/2} \ln(\xi/\hat{M}_p^{(d-2)/2}), \tag{3.65}$$

$$h_d = \frac{2d}{(d-2)} \left(\zeta + \frac{4(d-2)(d-1)}{(d-2)^2}\right)^{-1/2}, \tag{3.66}$$

and $\tilde{F}$ depends on δ only through derivative terms. This last fact might not be obvious, since a completely unconstrained function F can indeed contain terms which lead to a non-derivative dependence on δ in $\tilde{F}$ after the Weyl-transformation. It is dilatation symmetry which ensures that these terms are not allowed. To see that, one simply has to note that the dilatations (3.58) correspond to the following shift in δ:

$$\delta \to \delta - \frac{d-2}{2} \left(\zeta + \frac{4(d-2)(d-1)}{(d-2)^2}\right)^{1/2} \ln(\alpha). \tag{3.67}$$

Hence, δ is the massless Goldstone boson of dilatation symmetry, the *dilaton*. We will extend this name to the field ξ as well.
It is precisely the ξ^4-potential which gives rise to the (higher dimensional) cosmological constant term in eq. (3.64), which is forbidden by dilatation symmetry in $d > 6$. In absence of this term, the action is symmetric under a shift in δ, which can be absorbed into a redefinition of the Planck mass $\hat{M}_p$.

We are, however, not interested in the higher dimensional cosmological constant, we want to investigate the effective four dimensional theory obtained after dimensional reduction. As we have already seen in section 2.2, the number of effective four dimensional degrees of freedom which can in principle arise from the process of dimensional reduction is infinite. This holds not only for higher dimensional Einstein gravity, as discussed in chapter 2, but also, by the same arguments, for the scalar-tensor theory investigated here. We will restrict ourselves to a specific class of solutions, for which only two effective scalar degrees of freedom remain in the four dimensional theory, one of which is the four dimensional 'version' of the dilaton ξ. One might imagine a scenario where only two scalar degrees of freedom are light enough to be of cosmological interest after some very early time, say reheating. To give a specific model, one can consider solutions for which the scalar field and the metric can be decomposed as follows:

$$\xi(\hat{x}) = \kappa(x) f(y), \tag{3.68}$$

$$\hat{g}_{\hat{\mu}\hat{\nu}} = \begin{pmatrix} \sigma(y)\,\tilde{g}_{\mu\nu}(x) & 0 \\ 0 & l(x)\gamma_{\alpha\beta}(y) \end{pmatrix}. \tag{3.69}$$

Here the factor $\sigma(y)$ accounts for a possible warping, whereas the *radion* $l(x)$ accounts for a possible x-dependence of the size of the internal space. In this case the Ricci scalar can be decomposed as follows:

$$\hat{R} = R^{(D)}/l + \tilde{R}/\sigma\,. \tag{3.70}$$

Furthermore we assume that an expansion of F in the four dimensional Ricci scalar $\tilde{R}$ is valid, i.e.

$$F = F_0 + G\tilde{R}/\sigma + \ldots \tag{3.71}$$

where the expansion factors F_0 and G get evaluated for flat four dimensional space and are functions of y and the radion $l(x)$. Following Wetterich [2010a], we introduce canonically normalized scalar fields φ_ξ and φ_l via

$$\varphi_\xi \equiv \kappa l^{D/4}\left[\int_y \sqrt{\gamma}\sigma^2\right]^{1/2}, \quad \varphi_l \equiv l^{-1/2}\left[\int_y \sqrt{\gamma}\sigma^2\right]^{-1/D}. \tag{3.72}$$

In these variables, the effective four dimensional action reads (to leading order in $\tilde{R}$):

$$S^{(4)} = \int \mathrm{d}^4x\,\sqrt{-\tilde{g}}\left[V - \frac{1}{2}\chi^2\tilde{R} + \mathcal{L}_{\mathrm{kin}}\right], \tag{3.73}$$

where $\mathcal{L}_{\mathrm{kin}}$ contains the kinetic terms for the two scalar fields and

$$V = \tilde{F}\varphi_l^4 + \tilde{Q}\varphi_\xi^2\varphi_l^2\,, \tag{3.74}$$

$$\chi^2 = \varphi_\xi^2 - 2\tilde{G}\varphi_l^2\,, \tag{3.75}$$

with $\tilde{F}$, $\tilde{G}$ and $\tilde{Q}$ being constants arising from the integration over internal space. The kinetic terms are generically of the shape

$$\mathcal{L}_{\mathrm{kin}} = \frac{1}{2}c_\xi\left[\partial_\mu\varphi_\xi\partial^\mu\varphi_\xi + \frac{D^2}{4}\varphi_\xi^2\varphi_l^{-2}\partial_\mu\varphi_l\partial^\mu\varphi_l + D\varphi_\xi\varphi_l^{-1}\partial_\mu\varphi_\xi\partial^\mu\varphi_l\right], \tag{3.76}$$

where c_ξ is a constant. A complete derivation of this action (including the definitions of the constants and the shape of the kinetic terms) can be found in appendix B of [Beyer, 2011]. The shape of $S^{(4)}$ (ignoring for now the kinetic terms), can easily be understood: It is the most generic four dimensional two scalar field action compatible with dilatation symmetry, with one exception: a potential term $\propto \varphi_\xi^4$ is missing. This is a direct result of the higher dimensional setting. Let us recall that we can generically expand ξ as

$$\xi = \kappa_i(x) f_i(y)\,, \tag{3.77}$$

where $f_i, i \in \mathbb{N}$ is some complete set of functions on the internal space. Since the dilaton ξ appears only quadratic in the higher dimensional action, any one of its expansion coefficients κ_i can appear at most to second order in the effective dimensionally reduced action. In the above ansatz (3.68) we have made the assumption that the only remaining degree of freedom is the overall normalization. This line of thought shows that the specific ansatz we made above is not necessary to get the theory

(3.73). It is sufficient to assume that only two effective scalar degrees of freedom survive the process of dimensional reduction, and that at least one of them originates from the dilaton. It is however quite natural for the second degree of freedom to be connected to some feature of the geometry of the internal space, and, as we will see below, the radion is a good candidate.

Stable quasistatic solutions

We are particularly interested in stable quasistatic solutions of the dilatation symmetric field equations with maximal four dimensional symmetry, as these are suitable asymptotic states for cosmology (we will discuss this further below). For these solutions we have

$$\tilde{R} = 4V/\chi^2 = 4\Lambda\,, \tag{3.78}$$

and thus

$$S^{(4)} = \int \mathrm{d}^4x\sqrt{-\tilde{g}}\,W\,, \quad \text{with} \quad W = \tilde{Q}\varphi_\xi^2\varphi_l^2 + \tilde{F}\varphi_l^4 - 2\Lambda\varphi_\xi^2 + 4\tilde{G}\Lambda\varphi_l^2\,. \tag{3.79}$$

We ignore here possible contributions from higher orders in $\tilde{R}$, which can be interpreted as a restriction to the regime where the cosmological constant is much smaller than the effective Planck mass, i.e. $|\Lambda| \ll \chi^2$. We also ignore the kinetic terms, as we are interested in quasistatic solutions. One can now put constraints on the parameters $\tilde{F}, \tilde{Q}, \tilde{G}$ and in particular the cosmological constant Λ appearing in W from the following demands:

1. The (quasistatic) Einstein equation $V - \Lambda\chi^2 = 0$ should be obeyed.
2. The quasistatic scalar field equations should be obeyed, i.e. the the extremum condition for W should be satisfied.
3. The stability of the solutions should be guaranteed, i.e. the matrix $\frac{1}{2}\partial^2 W/\partial\varphi_i\partial\varphi_j$ should have non-negative eigenvalues.
4. Stable four dimensional gravity requires $\chi^2 > 0$. There is one possible exception to this condition, which we will discuss below.

One can put additional constraints on the parameters, if on considers the particle-physics models potentially arising from such higher dimensional theories. A thorough treatment of these issues can be found in the original papers [Cho and Jang, 1975, Cho and Freund, 1975], here we give only a very short summary. For a metric of the form

$$\hat{g}_{\hat{\mu}\hat{\nu}}(x,y) = \begin{pmatrix} \tilde{g}_{\mu\nu}(x,y) & A_{\mu\beta}(x,y) \\ A_{\alpha\nu}(x,y) & \gamma_{\alpha\beta}(x,y) \end{pmatrix}, \tag{3.80}$$

the four dimensional coordinate transformations (acting on x) transform $\tilde{g}_{\mu\nu}$, $A_{\mu\beta}$ and $\gamma_{\alpha\beta}$ as a second rank tensor, vector and scalar respectively, but the D-dimensional transformations acting on y transform them as scalar, vector and rank 2 tensor. If the internal space posseses some symmetries, the corresponding group of transformations can act as a gauge group in the reduced four dimensional

theory.
If the cosmological vacuum solution is of block-diagonal form, as assumed above, the gauge-fields $A_{\mu\beta}$ now arise as excitations above this vacuum and the gauge coupling g_c can in principle be calculated from a particular higher dimensional solution. For the specific ansatz (including the radion) chosen above one obtains [Wetterich, 2010a]

$$g_c^{-2} = a_1(\varphi_\xi/\varphi_l)^2 + a_2 \ , \tag{3.81}$$

with some constants a_1 and a_2. Clearly a non-vanishing gauge coupling requires a finite non-zero radion value $\varphi_l \neq 0$, or a limit $\varphi_l, \varphi_\xi \to 0$ where the ratio φ_ξ/φ_l remains constant. This can be added to the list of constraints for stable quasistatic solutions for this specific model.

If one includes this constraint the relevant solutions compatible with all demands can be summarized as follows [Wetterich, 2010a]:

- Flat solutions with $\tilde{F} = \tilde{Q} = \Lambda = 0$, $\varphi_\xi^2/\varphi_l^2 > 2\tilde{G}$.
- Non-flat solutions with $\tilde{F} \geq 0$, $\tilde{Q} > 0$, $\tilde{G} < 0$ and $\Lambda > 0$. These require $\varphi_\xi = 0$ and $\varphi_l \neq 0$.
- One stable solution with $\varphi_l = \varphi_\xi = \Lambda = 0$ always exists. Despite the fact that it leads to $\chi^2 = 0$, it can nonetheless be compatible with stable gravity. One should consider the approach $\varphi_l \to 0$ and $\varphi_\xi \to 0$. This still leads to an acceptable (non zero constant) gauge coupling if the ratio φ_ξ/φ_l remains constant in the limiting process. In this case the ratio between typical particle masses m_p and the effective Planck mass m_p^2/χ^2 also remains finite. However, as the fields approach their asymptotic values, it becomes clear the the scalar potential terms in V quickly becomes irrelevant, and thus these solutions are similar to the first case.

Thus stable quasistatic solutions with a non-zero cosmological constant are only possible for a specific dilaton value of $\varphi_\xi = 0$. Furthermore, the third case of solutions is not realistic for the ansatz (3.69), since $\varphi_l = 0$ corresponds to an internal space of infinite size. For our purposes, the first class of solutions is the relevant one. Note that they imply not only a vanishing cosmological constant, but in fact a completely vanishing scalar potential $V = 0$.

The issue of tuning

From a four dimensional point of view, it seems like an adjustment of the cosmological constant (and the parameters $\tilde{F}$ and $\tilde{Q}$) is happening, and one might wonder if such an effective theory can arise relatively independent of the values of the couplings appearing in the higher dimensional theory, or if these need to be tuned somehow. As is argued in great detail in [Wetterich, 2010b], this is not the case. In fact, it is the combination of the constraints derived from dilatation symmetry together with the higher dimensional setting which allows for this to happen:

> "Dilatation symmetry assures that any extremum of W has to occur for $W_0 = 0$ and therefore $\Gamma = 0$. In turn, the higher dimensional setting provides the flexibility that an

> extremum of exists independently of the precise values of the couplings in Γ." [Wetterich, 2010b] (In the original paper the higher dimensional action was denoted Γ, it is the same object we denote with $S^{(d)}$ in this thesis.)

A simple way to understand this is the following: The higher dimensional field equations are obtained through local variations of the action. Any solution to these field equations is then described by a number of integration constants, from which Λ can be calculated. However, not all the solutions correspond to extrema of the action, i.e. satisfy $\delta S^{(d)} = 0$. This demand gives rise to an additional constraint, which then restricts the range of integration constants, typically singling out the case $\Lambda = 0$. This additional constraint is given by an additional boundary condition

$$\int \mathrm{d}^D y \, \partial_{\hat{\mu}}(\sqrt{-\hat{g}}\xi\partial^{\hat{\mu}}\xi) = 0. \tag{3.82}$$

In the case of regular internal geometries this is always fulfilled, but in the presence of singularities it provides an additional equation.

Conclusion

We conclude that higher dimensional dilatation symmetry has very interesting consequences for the cosmological constant problem. In particular it provides both the constraints to allow for solutions to the field equations for which the four dimensional cosmological constant Λ vanishes, and the freedom for these solutions to exist independent of the precise couplings present in the higher dimensional action (i.e. in F). Specific higher dimensional finite volume spaces which are solutions of the field equations can be found in [Wetterich, 2010a,b]. These include a rather wide range of scenarios, Ricci-flat regular geometries, non-Ricci flat regular geometries and also non-regular geometries with singularities.

3.4 THE COSMON-BOLON MODEL

In the previous section we have seen how higher dimensional dilatation symmetric theories with two effective scalar four dimensional degrees of freedom naturally give rise to scenario in which both the cosmological constant and the effective four dimensional scalar potential vanish. What can we do with this insight? First we have to acknowledge that we do observe mass scales in nature, and therefore dilatation symmetry can not be the end of the story. In fact, it has to broken somehow. Nonetheless, the actions investigated in the previous section can be of relevance for cosmology, particularly in the a scenario of *asymptotic* dilatation symmetry, which we will now explain.

3.4.1 COSMIC SCENARIO: ASYMPTOTIC DILATATION SYMMETRY

Let us consider the quantum effective action $S^{(d)}[\hat{g}_{\hat{\mu}\hat{\nu}}, \xi]$ for higher dimensional scalar-tensor theories. All quantum corrections are included in this action, the field equations derived from it are exact. We

do not impose dilatation symmetry at this stage. One possibility is to consider a family of actions $S_\kappa^{(d)}$, obtained by rescalings

$$S_\kappa^{(d)}[\hat{g}_{\hat{\mu}\hat{\nu}}, \xi] = S^{(d)}[\kappa^{-2}\hat{g}_{\hat{\mu}\hat{\nu}}, \kappa^{d(d-2)/2}\xi]\,. \tag{3.83}$$

One can now propose that this action should become dilatation symmetric in the limit $\kappa \to \infty$. Then, the asymptotic form of the action remains invariant under the transformations (3.83) (they are precisely dilatations), and it could therefore reasonably correspond to a fixed point of the quantum effective gravitational action. This is a scenario which can lead to interesting and realistic cosmologies and we will move on to investigate it. We should note, however, that the existence of such a fixed point in quantum gravity is far from established, even though first investigations in this direction appear promising [Henz et al., 2013]. Our assumption could therefore be considered quite a leap.

The conclusions drawn for the quasistatic solutions in the previous section only apply at the fixed point. For cosmology, they are relevant if the fixed point is approached asymptotically, i.e. for $\tau \to \infty$. In terms of eq. (3.83), one may imagine that a dynamical runaway solution drives κ effectively to infinity, for example by a monotonic increase of the cosmological value of the scalar ξ. In a similar fashion, the metric $\hat{g}_{\hat{\mu}\hat{\nu}}$ needs to be decreasing in time, so that the field equations obtained from $S^{(d)}$ in the limit $\kappa \to \infty$ become valid. It is then the approach to the fixed point which describes the cosmological evolution for finite time and is of particular interest.

We can thus use the results from section 3.3 to draw conclusions for the asymptotic state of cosmology: It should correspond to one of the stable quasistatic solutions. We have seen that the asymptotic effective four dimensional theory (under the assumption of two scalar degrees of freedom, one of which is the dilaton) has a vanishing cosmological constant and no scalar potential. Therefore, at the fixed point, both the dilaton and the radion are massless scalar degrees of freedom.

What would such a theory look like for finite times? There would be 'dilatation anomalies', i.e. terms in the action which are not dilatation symmetric. These terms are of course expected to vanish in the limit $\xi \to \infty$. In the effective four dimensional theory, such anomalous terms are realized as a common potential for the scalar fields $V(\varphi_\xi, \varphi_l)$. These potential terms break dilatation symmetry and asymptotic dilatation symmetry implies

$$\lim_{\varphi_\xi \to \infty} V(\varphi_\xi, \varphi_l) = 0\,. \tag{3.84}$$

Thus the dilaton acquires a small mass, it is now the 'pseudo-Goldstone boson' of broken dilatation symmetry. In general we can expect such anomalous terms to be small whenever we are close to the fixed point. This is typically the case when the universe is old compared to the Planck time, so basically for all times which are of interest to us. We therefore expect the dilaton mass to be small and slowly decreasing in time. A natural realization of this setting are quintessence scenarios, where the dilaton acts as the cosmon field. In fact, in [Wetterich, 2010a] it was shown that the anomalous potential to leading order in arising for the dilaton in the higher dimensional Einstein frame is of the following shape

$$V_{\mathrm{an}}^{(d)} = f\frac{d-2}{2d}h_d\,\mu^d \exp\left(-h_d\delta\right)(\delta + c_\mu) \tag{3.85}$$

where $f > 0$, c_μ is a constant and μ is the scale of anomalous dilatation symmetry breaking. This is in fact only the leading order contribution in an expansion of the anomalous potential in $m_\delta^2/\hat{M}_p^2$, where m_δ is the anomalous dilaton mass

$$m_\delta^2 = \frac{1}{2}\frac{\partial^2 V_{\rm an}^{(d)}}{\partial\delta^2}\,. \tag{3.86}$$

It vanishes in the limit $\delta \to \infty$ when dilatation symmetry gets restored. Further anomalous terms are suppressed for sufficiently large values of δ and we ignore these terms for now.

The resulting effective four dimensional theory in the Einstein frame is particularly simple if we assume that the ratio φ_ξ/φ_l settles to a constant value, as is appropriate for constant gauge couplings. In this case one is left with only one scalar degree of freedom and obtains the following anomalous potential

$$V_{\rm an} = M_p^4\, {\rm e}^{-\alpha(\varphi)\varphi/M_p}\,, \tag{3.87}$$

where

$$\varphi = \sqrt{c_\xi(1+D^2/2)^2+6}\,M_p \ln(\varphi_\xi/\bar{\mu})\,, \tag{3.88}$$

and $\bar{\mu}$ is a mass scale resulting from a combination of the symmetry breaking scale μ and the constants h_d, f and c_μ. This redefinition was made in order to obtain a field with canonical kinetic terms. The φ-dependence is such that α decreases with increasing values of φ. As the cosmon rolls towards higher field values, the exponent $\alpha(\varphi)$ slowly decreases and it is conceivable that this decrease leads to a tracker scenario with late time cosmic acceleration. The change in $\alpha(\varphi)$ then leads to the transition between the 'tracker phase' during which the cosmon is in the steep part of the potential with $|\alpha(\varphi)+\varphi\alpha'(\varphi)| \gg 1$ and cosmon dominated cosmic acceleration reached for $|\alpha(\varphi)+\varphi\alpha'(\varphi)| \lesssim 1$. We have thus recovered a rather common quintessence scenario with an exponential potential.

3.4.2 COSMON & BOLON

We now want to extend the scenario described above to include a second dynamical four dimensional scalar degree of freedom. This effectively means that we relax the assumption that φ_ξ/φ_l adjusts to a constant value. One might be concerned about the consequences for the resulting gauge couplings. We have a few comments on this.

First, the gauge coupling can be almost constant in time, even if the ratio φ_ξ/φ_l is changing. If, for example, we have $a_2 \gg a_1\varphi_\xi^2/\varphi_l^2$ in eq. (3.81), the gauge coupling remains constant to very good approximation independent of the precise evolution of φ_ξ and φ_l. At first sight this condition may seem a bit unnatural, since we require $\varphi_\xi \to \infty$ for $\tau \to \infty$ in order to restore dilatation symmetry. But one should keep in mind that is is still possible that $\varphi_l \to \infty$ also, and this limiting process might be faster than the one for the dilaton.
Second, the second four dimensional degree of freedom need not necessarily be the radion, it could be something else. In that case, the gauge couplings may depend on the effective four dimensional fields in a completely different manner, or not depend on them at all. As we have argued above, our conclusions about the asymptotic state of cosmology do not change in such a scenario, as long as one of the two fields is the dilaton.

In such a setting, the question remains what the common anomalous four dimensional potential for the two scalar fields should look like. We have very little input to guide us here, other than the fact that it should vanish in the limit $\varphi \to \infty$ and contain the part derived in Wetterich [2010a], i.e.

$$V(\varphi,\chi) = V_1(\varphi) + V_2(\varphi,\chi)\,, \tag{3.89}$$

with $V_1(\varphi)$ being the exponential quintessence potential

$$V_1(\varphi) = M_p^4 \mathrm{e}^{-\alpha\varphi/M_p}\,, \tag{3.90}$$

where we have neglected the φ-dependence of the exponent, and

$$\lim_{\varphi\to\infty} V_2(\varphi,\chi) = 0\,. \tag{3.91}$$

Here we use the nomenclature χ for the second scalar field. One can imagine it being related to the field φ_l is a similar way as φ to φ_ξ. We will further assume that both fields have canonical kinetic terms. Within a specific scenario of dimensional reduction this may or may not happen, as we have seen in eq. (3.76) we would generally expect mixed kinetic terms. We choose to ignore this additional complication for now.

Particularly interesting cosmologies arise if the potential $V_2(\varphi,\chi)$ has a local minimum in the χ-direction. In that case, χ will stabilize around this minimum during the later stages of its evolution and act like dark matter, as we will see below in more detail. We therefore dub the χ-field *bolon* (from the greek *bolos* meaning 'lump'), since it is ultimately responsible for the emergence of cosmic structures within this model. A simple model would therefore be

$$V_2(\varphi,\chi) = \mathrm{e}^{-2\beta\varphi/M_p} m_0^2 \chi^2\,, \tag{3.92}$$

with $\beta > 0$. This model has been analyzed in [Beyer et al., 2011] and can give rise to realistic cosmologies, but the the cosmic evolution is strongly dependent on the initial conditions for the bolon χ. While realistic cosmologies emerge for initial conditions which seem to be rather natural, a different scenario in which such a tuning problem does not arise seems more desirable.

This can be achieved if the bolon-potential V_2 is modified to be much steeper for larger field values, so that tracker solutions for both the bolon and the cosmon in the early universe become possible. We therefore employ a specific form of the potential similar to one originally introduced in [Matos and Urena-Lopez, 2000, 2001], but with an additional coupling to the cosmon field:

$$V_2(\varphi,\chi) = M_p^4 c^2 \mathrm{e}^{-2\beta\varphi/M_p}\left(\cosh\left(\frac{\lambda\chi}{M_p}\right) - 1\right). \tag{3.93}$$

The dimensionless constant c in this potential is closely related to the scale of anomalous symmetry breaking of dilatation symmetry, as is discussed in more detail in [Beyer et al., 2011]. Asymptotically

the bolon-dependence of this potential can be decomposed as follows

$$\cosh(\lambda\chi/M_p) - 1 \approx \begin{cases} \frac{1}{2}e^{|\lambda\chi/M_p|} & |\lambda\chi/M_p| \gg 1 \\ \frac{1}{2}\frac{\lambda^2\chi^2}{M_p^2} & |\lambda\chi/M_p| \ll 1 \end{cases}, \tag{3.94}$$

which ensures the required quadratic χ-dependence for small field values, with a cosmon-dependent bolon mass given by

$$m_\chi(\varphi)^2 = c^2 M_p^2 \lambda^2 \mathrm{e}^{-2\beta\varphi/M_p}. \tag{3.95}$$

For larger field values the potential gets much steeper, which is a necessary feature for a model exhibiting scaling solutions that lead to an insensitivity of the cosmological evolution to initial conditions for a wide range of initial field values.

We will refer to the cosmological model with two scalar fields and a common potential defined by equations (3.89), (3.90) and (3.93) as the *coupled cosmon-bolon model*, where χ is the bolon (meaning 'lump'), since it will act as dark matter and be ultimately responsible for the formation of structures in the universe. We choose $\alpha > 0$ and $\lambda > 0$ throughout this work, which can always be achieved by a suitable redefinition of φ and χ. Our motivation by asymptotic dilatation symmetry then requires $\beta > 0$ also. We will however at some stages refrain from this constraint and consider $\beta < 0$ as well. Much of this thesis will be concerned with the analysis of its cosmological consequences of this model. In addition to the two scalar fields, which make up the entire dark sector in our model, we also include baryons, photons and neutrinos into our cosmology.

In the remainder of this chapter we will provide a short outline of the evolution of the two scalar fields in a FLRW universe, mainly to give the reader an overview over the situation at hand. In doing so, we will draw heavily from the results presented in more detail in the coming chapters, in particular chapters 4 and 5. In chapter 4 we will anaylze the evolution of linear perturbations during the late universe, when the quadratic approximation for the bolon potential is valid, in some detail, while in chapter 5 we focus on the evolution of both the background and linear perturbations in the early universe, when the exponential approximation for the bolon potential is valid.

In the ensuing presentation we follow section III of [Beyer, 2014b] closely. Copyright for the figures and excerpts of this preprint resides, at the time of writing this, with the author, but will be transferred to the American Physical Society upon acceptance of the paper.

3.4.3 COSMOLOGICAL EVOLUTION

Cosmology with coupled scalar fields

Before we go to describe the dynamics of the cosmon bolon model, we need to introduce some nomenclature about cosmological scalar fields. Generically, the action for two canonical scalar fields which couple through their common potential reads:

$$S_{(\mathrm{sc})} = -\int \sqrt{-g}\left[\frac{1}{2}\mathcal{D}_\mu\varphi\mathcal{D}^\mu\varphi + \frac{1}{2}\mathcal{D}_\mu\chi\mathcal{D}^\mu\chi + V(\varphi,\chi)\right]. \tag{3.96}$$

Variation of this action with respect to the scalar field yields the Klein-Gordon equations

$$\mathcal{D}_\mu \mathcal{D}^\mu \varphi - V_{,\varphi} = 0\,, \quad \mathcal{D}_\mu \mathcal{D}^\mu \chi - V_{,\chi} = 0\,. \tag{3.97}$$

There is no canonical way to define separate energy momentum tensors for the two scalar fields in such a coupled scenario, in particular it is unclear how the potential energy should be split up. Let us nonetheless introduce an arbitrary splitting

$$V(\varphi,\chi) = V_1(\varphi,\chi) + V_2(\varphi,\chi)\,, \tag{3.98}$$

after which the energy momentum tensors can be readily defined as follows:

$$T^{\mu\nu}_\varphi = \mathcal{D}_\mu\varphi\mathcal{D}^\mu\varphi - g^{\mu\nu}\left[\frac{1}{2}\mathcal{D}_\tau\varphi\mathcal{D}^\tau\varphi + V_1(\varphi,\chi)\right], \tag{3.99}$$

$$T^{\mu\nu}_\chi = \mathcal{D}_\mu\chi\mathcal{D}^\mu\chi - g^{\mu\nu}\left[\frac{1}{2}\mathcal{D}_\tau\chi\mathcal{D}^\tau\chi + V_2(\varphi,\chi)\right]. \tag{3.100}$$

In a spatially homogeneous and isotropic FLRW universe we can insert the FLRW-metric and drop all spatial derivatives in the scalar field equations (3.97) to obtain:

$$\varphi'' + 2\mathcal{H}\varphi' + a^2 V_{,\varphi} = 0\,, \quad \chi'' + 2\mathcal{H}\chi' + a^2 V_{,\chi} = 0\,. \tag{3.101}$$

The energy momentum tensor is then again of the perfect fluid form, with the following identifications:

$$\rho_\varphi = \frac{1}{2a^2}\varphi'^2 + V_1(\varphi,\chi)\,, \quad \rho_\chi = \frac{1}{2a^2}\chi'^2 + V_2(\varphi,\chi)\,, \tag{3.102}$$

$$p_\varphi = \frac{1}{2a^2}\varphi'^2 - V_1(\varphi,\chi)\,, \quad p_\chi = \frac{1}{2a^2}\chi'^2 - V_2(\varphi,\chi)\,. \tag{3.103}$$

The dimensionless couplings governing the equations of energy conservation (see eq. (2.54)) then simply read:

$$q_\varphi = \frac{V_{1,\chi}\chi' - V_{2,\varphi}\varphi'}{3\mathcal{H}(1+\omega_\varphi)\rho_\varphi}\,, \tag{3.104}$$

$$q_\chi = -\frac{V_{1,\chi}\chi' - V_{2,\varphi}\varphi'}{3\mathcal{H}(1+\omega_\chi)\rho_\chi}\,. \tag{3.105}$$

Having set up the basics, we now move on to discuss the evolution of the cosmon bolon model. We will split the analysis into two parts, the early universe, when the approximation of the common potential for large field values is valid, and the late universe, when we can employ the quadratic approximation for small field values (see eq. (3.94)).

Tracking in the early universe

The dynamics of the evolution of the cosmon-bolon system in the early universe will be investigated in detail in chapter 5, here we will only use the relevant results. Using a dynamical system analysis one can show that attractive exact scaling solutions exist for the coupled exponential, in fact, these solutions split the parameter space of this model into disjunct sections. There is one particular scaling solution which is relevant for the early universe dynamics in our scenario, we have denoted it by R4 in Table 5.1 (see next chapter). This is the only stable scaling solution which allows for a radiation-like expansion for early times with a continuous range of couplings extending from the negative to the positive realm. It is also the unique stable scaling solution which covers the range of model parameters which are phenomenologically interesting, in particular the range of small couplings. All other stable fixed points do either not provide a realistic early cosmology (i.e. a radiation-like expansion) or only exist for large couplings, which can be observationally excluded, as we discuss below. Table 5.2 provides the constraints on the model-parameters arising from the demands of existence and stability of this fixed point, which are given by

$$\beta/\alpha < \frac{1}{2}\,,\ \frac{\alpha\beta}{\lambda^2+4\beta^2} \leq \frac{1}{2}\,,\ \alpha > 2\,,\ \lambda^2 > \frac{4(2\beta-\alpha)^2}{\alpha^2-4}\,. \tag{3.106}$$

For the range of positive couplings $0 < \beta/\alpha < 1/2$ the additional condition

$$\lambda^2 > 2\beta(\alpha-2\beta) \tag{3.107}$$

is required. We will stick to this parameter range from now on.

The evolution of the scalar fields during this early phase of the cosmic evolution can be obtained from the dynamical system analysis as well, under the assumption that baryons can be ignored, which is a valid assumption for early times. The results presented in Table 5.1 and a straightforward calculation give

$$\varphi(\mathcal{H}) = -\frac{M_p}{\alpha}\ln\left[\mathrm{f}(\alpha,\beta,\lambda)\frac{\mathcal{H}^2}{a^2M^2}\right], \tag{3.108}$$

$$\chi(\mathcal{H}) = \frac{M_p}{\lambda}\ln\left[8(1-2\beta/\alpha)\frac{\mathcal{H}^2}{a^2 m_\chi(\varphi)^2}\right], \tag{3.109}$$

where

$$\mathrm{f}(\alpha,\beta,\lambda) = \frac{4(\lambda^2+4\beta^2-2\alpha\beta)}{\alpha^2\lambda^2}\,. \tag{3.110}$$

The density parameters of the cosmon and the bolon corresponding to this solution can cover a large range of values, depending on the choices of the model parameters α, β and λ. They are given by

$$\Omega_{\varphi,\mathrm{es}} = \frac{4}{\alpha^2} + \frac{8}{3}\frac{\beta/\alpha(-1+2\beta/\alpha)}{\lambda^2}\,, \tag{3.111}$$

$$\Omega_{\chi,\mathrm{es}} = \frac{4}{\lambda^2} + \frac{8}{3}\frac{\beta/\alpha(-5+4\beta/\alpha)}{\lambda^2}\,, \tag{3.112}$$

where the subscript "es" stands for "early scaling".

The stability of this scaling solution is subject to two conditions: First, we neglected baryons in the derivation. Second, we assumed that the exponential approximation for the bolon-potential is valid. Both of these assumptions are valid for sufficiently early times (and a suitable range of initial conditions), but will eventually be violated. When this happens, the scaling behavior will be broken by a transition to a matter dominated era, where the bolon gets transferred towards the minimum of its potential and starts to perform quick oscillations, effectively acting like dark matter. Let us estimate when this takes place. Extrapolating the early scaling solution to the time when the bolon reaches a field value of M_p/λ gives a good estimate. According to equation (3.109) we have at this time

$$\mathcal{H}^2/a^2 m_\chi(\varphi)^2 \approx \mathrm{e}/8(1-2\beta/\alpha)\,, \tag{3.113}$$

which is of order 1.

The late universe

For sufficiently late times the cosmic evolution drives the bolon towards the minimum of its potential, so that it eventually acquires very small field values χ/M_p. For such small deviations from the minimum we can approximate the bolon potential by

$$V_2(\varphi,\chi) = \frac{m_\chi(\varphi)^2}{2}\chi^2\,, \tag{3.114}$$

with

$$m_\chi(\varphi) = m_0 \exp(-\beta\varphi/M_p) \quad \text{and} \quad m_0 \equiv M_p c\lambda\,. \tag{3.115}$$

The dynamics of the bolon in this regime depend on the ratio $\mu \equiv \mathcal{H}/a m_\chi(\varphi)$.[4] For $\mu > 1$ the Hubble friction is strong enough to keep the bolon field frozen at some (almost) constant value, whereas for $\mu < 1$ we expect rapid oscillations to occur. As we have just seen, a scaling scenario in the early universe will deliver the bolon to field values of the order M_p/λ when $\mu \approx 1$. We can track the subsequent behavior of this parameter by investigating the time evolution of μ, which is governed by the following relations:

$$\mu = \frac{\mathcal{H}}{a m_0}\mathrm{e}^{\beta\varphi/M_p} = \frac{\mathcal{H}}{a m_0}\left(3\frac{\mathcal{H}^2}{a^2 M_p^2}\Omega_{\varphi,\mathrm{pot}}\right)^{-\beta/\alpha}\,, \tag{3.116}$$

$$\mu' = \mu\mathcal{H}\left(-\frac{3}{2}(1+\omega_{\mathrm{eff}}) + \beta\sqrt{6\Omega_{\varphi,\mathrm{kin}}}\right)\,, \tag{3.117}$$

where $\Omega_{\varphi,\mathrm{kin}} = \varphi'^2/6M_p^2\mathcal{H}^2$ and $\Omega_{\varphi,\mathrm{pot}} = a^2 V_1/3M_p^2\mathcal{H}^2$. Here eq. (3.117) is valid independent of the precise shape of the potential V_1 and therefore for all quintessence scenarios coupled to the cosmon, whereas eq. (3.116) requires an exponential cosmon potential.

If the quintessence field exhibits a scaling or tracking behavior, i.e. the the density parameter Ω_φ is (almost) constant and not bigger than a few percent, equation (3.117) directly tells us that μ is

[4] This should not be confused with the symmetry breaking scale also called μ used above. From here on out μ always refers to the ratio of the Hubble rate to the bolon mass.

decreasing as long as β is not too large. During radiation and matter domination when $\omega_{\text{eff}} \geq 0$ this covers a wide range of couplings. Nonetheless, for very late times, this condition can be violated even for small couplings. In fact, we might quite generally expect this to happen. To see this, simply consider a very late cosmology which is dominated by the cosmon and has an (almost) de-Sitter like expansion, i.e. $\omega_{\text{eff}} \approx -1$. This necessarily requires $\Omega_{\varphi,\text{kin}} \ll 1$ and one can calculate that μ will start to increase again if

$$\beta > \sqrt{3\Omega_{\varphi,\text{kin}}/2}\,, \tag{3.118}$$

where we made the simplifying assumption that $\Omega_\varphi = 1$, i.e. this should be considered the leading order contribution in $\Omega_{\varphi,\text{kin}}$. Therefore any quintessence scenario which converges toward $\omega_\varphi = -1$ for $\tau \to \infty$ will eventually lead to arbitrarily small $\Omega_{\varphi,\text{kin}}$ and 'refreeze' the bolon field for non-zero positive coupling. We will not be concerned with this process however, as it lies in the far future.

We can draw deduce a direct constraint on the coupling β from equation (3.116) in conjunction with the requirement of a decreasing μ. It reads:

$$\beta/\alpha < 1/2\,. \tag{3.119}$$

The same restriction was already found earlier by requiring the existence of a radiation-dominated scaling solution in the early universe (see equation (3.106)). We have therefore shown that a decreasing μ is a quite generic feature in the cosmon-bolon model for a wide range parameters which give rise to realistic early cosmologies. We will therefore now consider the dynamics in the regime $\mu \ll 1$.

These dynamics contain very fast oscillations of the bolon field around its minimum, which are very expensive to resolve numerically. The oscillations transfer, in principle, to all other dynamical through Einstein's equations and explicitly to the cosmon through the coupling β. In chapter 4 we provide an analytical mechanism how to average over these oscillations, which have a period of the order $1/m_\chi$, a timescale much shorter than a Hubble time. What we end up with is an effective description valid for sufficiently late times, i.e. sufficiently small values of μ. Leaving the details of this mechanism for later, the resulting equations are the following:

The cosmon evolution is governed by the field equation

$$\varphi'' = -2\mathcal{H}\varphi' - a^2 V_{1,\varphi} + \frac{\beta}{M_p} a^2 \rho_\chi\,, \tag{3.120}$$

whereas the bolon energy density follows

$$\rho_\chi' + 3\mathcal{H}\rho_\chi = -\beta\frac{\varphi'}{M_p}\rho_\chi\,. \tag{3.121}$$

Friedmann's equation now reads

$$\mathcal{H}^2 = \frac{a^2}{3M_p^2}\left(\rho_\chi + \rho_\varphi + \rho_{\text{ext}}\right)\,. \tag{3.122}$$

All dynamical quantities used in these equations evolve adiabatically to leading order, i.e. do not change considerably on a timescale $1/m_\chi$. The only exception at the background level would be the

bolon pressure p_χ (see next chapter for more details). The energy density ρ_{ext} contains all additional energy densities, i.e. photons, neutrinos and baryons. We have thus come to the result that the cosmon and bolon form a system of coupled quintessence, which was already analyzed in [Amendola, 2000a] and described in section 3.2. For the range of parameters we are investigating (in particular $\alpha > \sqrt{2}$) it allows for accelerated expansion only for large negative β, specifically $\alpha < -2\beta$ (see Table 3.1). This is not only inconsistent with our original motivation of an asymptotically vanishing bolon mass, but also excludes the possibility of a prolonged matter dominated epoch in our scenario, as we have checked numerically. For such large negative couplings the universe simply transitions quickly from radiation-domination to an accelerated expansion. This problem is connected to the fact that the coupled quintessence scenario does not describe our model in the early universe. Within a pure coupled quintessence model realistic accelerated cosmologies are of course possible and were discussed by Amendola [2000a]. Furthermore current bounds on coupled quintessence models already rule out such strong couplings (see e.g. [Pettorino et al., 2012]), as we will discuss further below. We therefore exclude this possibility as unrealistic and focus on smaller couplings.

For these our cosmology will quickly adjust itself to a matter-dominated scaling solution, with the bolon energy-density scaling slightly differently than baryons due to the coupling. The parameter bounds resulting from the conditions of existence and stability of this solution can be found in Table 3.2 and read:

$$|\alpha-\beta| > \sqrt{\frac{3}{2}}, \quad \alpha > \sqrt{\frac{2}{3}}4\beta \quad \text{and} \quad \alpha > \frac{1}{2}\left(\beta + \sqrt{12+\beta^2}\right). \tag{3.123}$$

For positive β we additionally require

$$\alpha < (\beta + 3/\beta). \tag{3.124}$$

None of these constraints are in conflict with the ones we found above from considerations of an attractive radiation dominated era in the early universe or the condition of a decreasing μ. All parameter choices used in this thesis will respect all the bounds mentioned in this section. This is important, because we will end up using the averaged description in our numerics below, which would possibly become incorrect it we violated the parameter bounds derived here.

Before we move on we would like to say a few words concerning baryons. The coupled quintessence model studied in [Amendola, 2000a] considered a universal coupling to all matter. In the model introduced here, we have recovered a coupling only between dark matter and the quintessence field, the baryons remain uncoupled. Thus, we can not expect the scaling solutions in Table 3.1 to hold precisely, a small correction due to baryonic effects should be present. Furthermore, a coupling to all matter, including baryons, is tightly constrained by experiments testing the equivalence principle, since the coupling can be interpreted as a 'fifth force' on the matter particles. One way around this would be to change the setting in such a way that the 'fifth force' is shielded within dense matter accumulations (this is known as the *Chameleon mechanism* [Brax et al., 2004, Khoury and Weltman, 2004b,a, Brax et al., 2005]). For a coupling only between dark matter and the quintessence field, the observational constraints are much weaker.

FIGURE 3.3: **Density parameters in the cosmon bolon model**

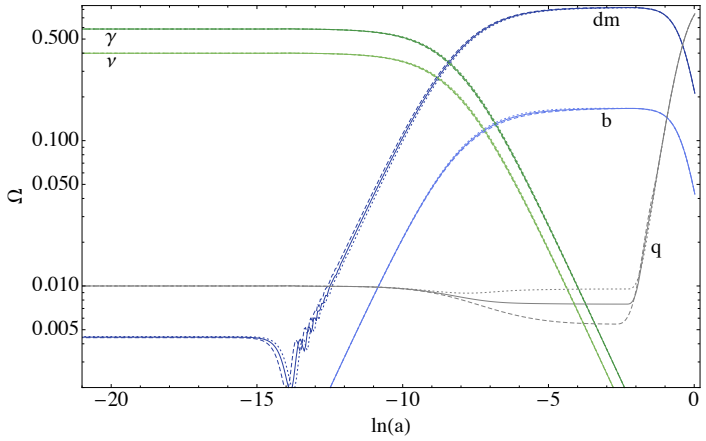

We show the density parameters for neutrinos (ν), photons (γ), baryons (b), the bolon (dm) and the cosmon (q) in the cosmon bolon model. The bolon exponential is chosen to be $\lambda = 30$, the quintessence exponential $\alpha = 20$. The coupling β takes the values 0, 0.05 and -0.05 for the solid, dashed and dotted lines respectively. The cosmon evolution was stopped by an φ-dependent exponential in the cosmon potential (see chapter 4 for more details).

Accelerated expansion

As was already pointed out, the specific model with an exponential potential treated here, with the restrictions on the parameters just derived, does not result in an accelerated expansion. The cosmon field simply adjusts itself to a scaling solution and will remain there. We are not too concerned about this problem, we have already seen several ways out of it in section 3.2. We could for example assume a slightly different form of the quintessence potential by reintroducing a φ-dependent exponential $\alpha(\varphi)$ [Wetterich, 1995], alternatively a non-standard kinetic term [Hebecker and Wetterich, 2001], a φ-dependent minimum in the bolon-potential [Beyer et al., 2011], a φ-dependent coupling $\beta(\varphi)$ [Tocchini-Valentini and Amendola, 2002] or an additional coupling to other components of the cosmic fluids (e.g. neutrinos, see [Amendola et al., 2008]) can break the scaling behavior and effectively stop the evolution of the cosmon, leading to an accelerated expansion. A detailed investigation of such scenarios is not the topic of this thesis. In order to arrive at realistic results, we will choose one of these possibilities in our numerics in the following chapter. An exemplary evolution of the density parameters in this model is given in Figure 3.3.

Observational parameter bounds

So far all the parameter bound we cited originated from the desire to obtain a realistic cosmology independent of model parameters. Current experimental bounds on these parameters go far beyond these theoretical limits. To our knowledge the most stringent observational bounds on a coupled theory such as ours come from big bang nucleosynthesis (BBN) [Ferreira and Joyce, 1997, 1998, Bean et al., 2001] and cosmic microwave background (CMB) observations [Calabrese et al., 2011,

Reichardt et al., 2012, Xia et al., 2013, Pettorino et al., 2013]. These bounds concern two quantities in our model: The density parameters for the scalar fields in their scaling solution (early dark energy) and the coupling β.

Let us start with bounds on early dark energy. We have already sketched how a tracker quintessence field modifies big bang nucleosynthesis and how observations of the abundances of the lightest elements in the cosmos can put an upper bound on the quintessence density parameter. Let us quickly recall the bound from Bean et al. [2001], which is at 0.045, the tightest constraint known to us . In our model this should be seen as a bound for the combined scalar density parameter $\Omega_{sc,es} = \Omega_{\varphi,es} + \Omega_{\chi,es}$ as given in equations (3.111) and (3.112), as both fields act as early dark energy in our scenario. On the other hand, the CMB constraints on early dark energy should be applied only to the cosmon field, as the bolon already acts as dark matter at the time of CMB emission. The tightest bound comes from the Planck cooperation [Ade et al., 2013b], and from Table 3.1 one directly obtains

$$\Omega_{\varphi,cq} = \frac{3 - \alpha\beta + \beta^2}{(\alpha - \beta)^2} \lesssim 0.01\,. \tag{3.125}$$

The subscript "cq" stands for coupled quintessence, indicating that we are in the regime where the averaged late time dynamics are valid.

Furthermore CMB analyses of coupled quintessence models also put a bound on the coupling [Pettorino et al., 2012], currently at the order of $\beta^2 \lesssim 0.01$. Interestingly, the best fit values for such a coupling from CMB data are inconsistent with zero at around $2-3\sigma$ [Pettorino et al., 2012] and favor a positive coupling. Future constraints using Planck and Euclid data sets are expected to improve bounds on the coupling by about two orders of magnitude [Amendola et al., 2012] and should be able to sort out if this is a real effect or not.

These CMB bounds, both for the coupling and for early dark energy, were derived for standard cold dark matter coupled to quintessence, but we expect similar constraints to hold in our scenario. As we will see in chapter 4, the evolution of perturbations in our model is different than in coupled cold dark matter models, but we expect these differences to be largely irrelevant for the CMB constraints, as they are only important for scales much smaller than the ones corresponding the multipole moments where the CMB has the most constraining power.

Parameter adjustment

At the background level our model has 4 parameters determining the behavior of the two scalar fields, the exponents α and λ, the coupling β and the mass-parameter c^2. To fully determine the background evolution (after some suitable very early time, in particular after neutrino-decoupling and electron-positron annihilation) we also have to fix the current radiation density $\rho_{r,0}$ (or, equivalently, the CMB temperature) and the baryon density $\rho_{b,0}$. We can now predict the current density parameters for both the bolon and the cosmon from the fundamental model parameters, adopting a procedure similar to one introduced in [Matos and Urena-Lopez, 2001]. This is an important step if one wants adjust the model parameters to values leading to realistic cosmologies.

First, we define a scale factor a^* as the scale-factor at which $\chi = M_p/\lambda$, i.e. roughly the time when bolon oscillations start. Extrapolating the analytically known bolon-evolution for the early scaling solution (eq. (3.109)) up to that point directly gives (see eq. (3.113))

$$\mathcal{H}(a^*)^2 = \frac{e}{8(1-2\beta/\alpha)}\, a^{*2}\, m_\chi(\varphi^*)^2\,, \tag{3.126}$$

where $\varphi^* = \varphi(a^*)$. Furthermore we can evaluate Friedmann's equation to obtain under the assumption that the cosmon also still follows its early scaling solution up to a^*:

$$\mathcal{H}(a^*)^2 = \frac{a^{*2}}{3M_p^2}\frac{\rho_r(a^*)}{1-\Omega_{sc,es}} = \frac{a^{*-2}}{3M_p^2}\frac{\rho_{r,0}}{1-\Omega_{sc,es}}\,. \tag{3.127}$$

Now we can set the last two equations equal, plug in the estimate for the cosmon value $\varphi^* = \varphi(a^*)$ by extending the analytic formula for the early scaling solution given by equation (3.108) and obtain the following estimate for a^*:

$$a^* = \left(\frac{\rho_{r,0}}{3M_p^4}\right)^{\frac{1}{4}} \left[\frac{8(1-2\beta/\alpha)\,f^{-2\beta/\alpha}}{e c^2\lambda^2(1-\Omega_{sc,es})^{1-2\beta/\alpha}}\right]^{\frac{1}{4(1-2\beta/\alpha)}} \tag{3.128}$$

where $\Omega_{sc,es} = \Omega_{\varphi,es} + \Omega_{\chi,es}$ and $f = f(\alpha,\beta,\lambda)$ as defined in eq. (3.110).
To make contact with the current bolon energy density, we can assume that from a^* onwards, the bolon will follow its evolution determined by eq. (3.121). Since the coupling causes the bolon-density to scale slightly differently than the baryons, we can not simply fix the ratio of the two energy densities, but have to specify ρ_χ at some redshift, say at $z = 0$. Once this is set, all that remains to consider is the cosmon energy density, which should dominate the cosmic evolution at late times. In particular we need to stop the evolution of the cosmon at some low redshift $\tilde{z}$ (appoximately 5). The value of the cosmon $\varphi_0 = \varphi(z=0) \approx \varphi(\tilde{z})$ can the simply be obtained by extending the late time cosmon scaling solution for coupled quintessence to $\tilde{z}$. For sufficiently late times we thus have

$$\frac{\rho_\chi}{\rho_r} \propto a^{-1} e^{-\beta\varphi/M_p}\,. \tag{3.129}$$

Extrapolating this evolution back to a^* and estimating the bolon energy-density at a^* by the one given by the scaling solution then gives

$$a^* = \frac{\rho_{r,0}}{\rho_{\chi,0}}\frac{\Omega_{\chi,es}}{1-\Omega_{sc,es}} e^{\beta(\varphi*-\varphi_0)/M_p}\,, \tag{3.130}$$

where we have not yet inserted the cosmon evolution in order to keep the equation simple. Plugging in this information using the approximations described above and equating the right hand sides of (3.128) and (3.130) gives us an approximate expression for the current bolon energy density $\rho_{\chi,0}$ given a set of model parameters. We can make this and exact expression by including a numerical

FIGURE 3.4: **Adjustment of the bolon energy density**

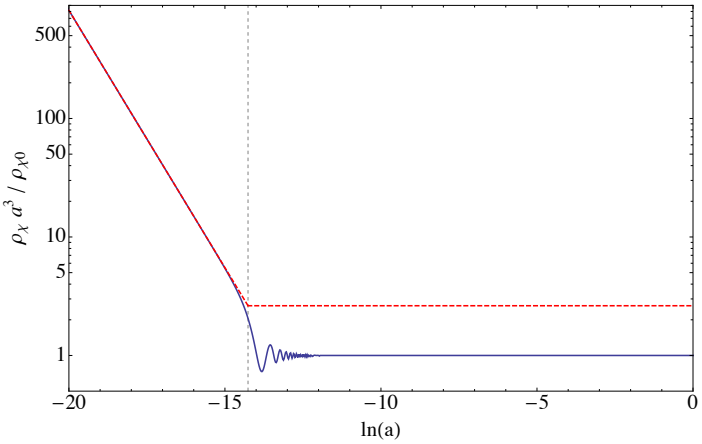

We show the bolon energy density in its correct evolution, determined numerically (blue line) and the approximation we made in eq. (3.131) without the numerical adjustment factor N. Cleary we overestimate the current bolon energy density by a factor of roughly 2.5, which is why $N \approx 0.4$. The dashed gridline represents a^*. The model parameters are the same as in Figure 3.3 with $\beta = 0$.

adjustment factor N:

$$\left(\frac{\rho_{\chi,0}}{\rho_{r,0}}\right)^{1-\beta/\alpha} = N\,\Omega_{\chi,es}(1-\Omega_{sc,es})^{-3/4}\left(\frac{\rho_{r,0}}{M^4}\right)^{-\frac{1}{4}+\beta/\alpha}\left(\frac{8(1-2\beta/\alpha)}{3e\lambda^2c^2}\right)^{-\frac{1-4\beta/\alpha}{4(1-2\beta/\alpha)}} \left(\frac{f}{3}\right)^{\frac{-\beta/\alpha}{2(1-2\beta/\alpha)}}\left(6^3(1+\tilde{z})\frac{g}{2-g}\tilde{g}\right)^{\beta/\alpha}, \tag{3.131}$$

where

$$g = g(\alpha,\beta,\lambda) = 1 + \frac{6\beta^2 - 6\alpha\beta + 18}{6(\alpha-\beta)^2} \quad \text{and} \tag{3.132}$$

$$\tilde{g} = \tilde{g}(\alpha,\beta,\lambda) = g(\alpha,\beta,\lambda) - \frac{3}{2(\alpha-\beta)^2}\,. \tag{3.133}$$

The adjustment factor N is of order 1, but always smaller, roughly 0.4. This is due to the fact that estimating the bolon energy density at a^* by the scaling solution is quite accurate, but using the averaged evolution from that point on leads to an overestimate of $\rho_{\chi,0}$ since the bolon energy dilutes faster than non-relativistic matter during the early oscillatory phase. This is visualized in Figure 3.4. Furthermore N is a function of the model parameters α, β and λ as well as the energy densities $\rho_{r,0}$, $\rho_{\chi,0}$ and $\tilde{z}$. It of course will also take (slightly) different values depending on which scenario is chosen to stop the cosmon evolution for late times. For practical purposes, we will choose one such scenario in the following chapter where we present numerical results and determine N (for fixed $\tilde{z} = 5$, $\rho_{r,0}$ and $\rho_{\chi,0}$) by running through a grid on c^2 and the remaining model parameters. We will give the precise value of N whenever discussing a specific choice of parameters.

We have therefore recovered a model in which the dynamics of the dark sector are determined by

four parameters. Actually, stopping the cosmon evolution introduces another one, so we should be honest and say that we have five parameters describing the dark sector. This may seem like a lot when compared to the cosmological standard model, in which essentially only two parameters, the cosmological constant and the current dark matter energy density appear as free parameters at the background level. We should, however, keep a few things in mind: This coupled scalar field model can be considered to be a complete particle physics model of the dark sector, and therefore should be compared with particle physics models of CDM, which typically include additional parameters. For example, in WIMP models, one needs to specify at least the mass and weak interaction cross section of the dark matter particle in order to predict its abundance in the universe.

Splitting the scalar field potential

Before we move on to study linear perturbations in this model in the next chapter, we want to come back to one fundamental point: The assignment of energy densities to the two scalar fields. We have already mentioned that this assignment is, on a mathematical level, completely arbitrary, there is no reason to prefer a specific splitting of the potential. So one might wonder if it even makes sense to talk about the two scalar fields separately and consider quantities like the bolon density parameter and the cosmon density parameter. After all, a different potential splitting would result in a very different evolution of these quantities. While that is true, we want to give a few arguments in favor of the splitting used above. First, any splitting should attempt to separate possibly different physical behaviors of the scalar fields. For a potential with a valley, such as ours, one may hope to find one degree of freedom describing the direction of the valley and the second one perpendicular to it. This is not always analytically possible (see e.g. [Beyer, 2011, Beyer et al., 2011]), but for our simple potential the splitting (3.89) achieves this precisely. Furthermore, as we have seen by the effective coupled quintessence description above, cosmon and bolon do indeed have very different physical roles in the late universe, which are well captured by our definitions.

4 THE INHOMOGENEOUS UNIVERSE 1: LINEAR PERTURBATIONS

The universe is not homogeneous. Any realistic cosmological model should therefore not only produce a realistic expansion history, but also a growth of cosmological perturbations which is compatible with current observational constraints. The data about cosmological inhomogeneities is plentiful, and growing quickly.

Small temperature fluctuations in the CMB of the order $\Delta T/T \approx 10^{-5}$ have been observed by many experiments, both satellite and balloon-based [Mather et al., 1994, Fixsen et al., 1996, Hanany et al., 2000, de Bernardis et al., 2000, Kovac et al., 2002, Readhead et al., 2004, Hinshaw et al., 2013, Ade et al., 2013a,b, 2014]. These provide an (almost) direct picture of the universe when it was only ~ 380000 years old. Milestones in CMB observations were its discovery [Penzias and Wilson, 1965a], the detection of a Planckian temperature spectrum [Mather et al., 1994, Fixsen et al., 1996], the detection of anisotropies at a level consistent with the existence of cold dark matter [Hanany et al., 2000, de Bernardis et al., 2000], detection of E-mode polarization [Kovac et al., 2002, Readhead et al., 2004] and, possibly, a recent detection of B-mode polarization which could constrain inflationary scenarios [Ade et al., 2014].
Since the temperature perturbations are small, CMB features can (mostly) be calculated from linear perturbation theory. Non-linear structure formation enters only through effects on CMB photon propagation, the most prominent ones are the *integrated Sach-Wolfe effect* [Sachs and Wolfe, 1967] and the (kinetic and thermal) *Sunyaev-Zel'dovich effects* [Sunyaev and Zeldovich, 1972]. Today, CMB data analysis is very far advanced and provides very strong constraints on cosmological models.

Other probes of cosmic structure formation include *galaxy surveys* [Lahav and Suto, 2004] *weak lensing* [Bartelmann and Schneider, 2001, Refregier, 2003], or the *Lyman* α*-forest* [Weinberg et al., 2003]. Galaxy redshift surveys record the distribution of galaxies (within a limited observable volume) by determining their redshifts. The resulting data traces the baryon density and can in principle be used as a tracer of the dark matter density as well. This last step requires knowledge about the relation between dark matter structures and baryonic structures, the so called *luminosity bias*, a quantity which depends on galaxy formation processes [Baugh, 2013] .
Weak lensing can probe the dark (or rather the total) matter distribution more directly, opening up the possibility to reconstruct the three-dimensional matter distribution, at least in principle [Hu, 1999].
Finally the absorption lines in the continuous emission spectra of distant quasars can also be used as a probe of structure formation models [Weinberg et al., 2003]. As the photons emitted from the quasar

redshift, each intergalactic gas cloud they pass through creates an absorption line at a wavelength below the Lyman-alpha line, according to the respective redshift of absorption.

The aim of this chapter is to describe the evolution of linear perturbations in the coupled cosmonbolon model introduced in the previous section. This requires several steps. First, we need to derive the linear perturbation equations for this model, for both the two scalar fields and for photons, neutrinos and baryons. This will be done in a gauge-invariant manner in section 4.1. Afterwards, the equations have to solved numerically in a Boltzmann-code. We have opted not to use one of the existing codes like CLASS [Blas et al., 2011, Lesgourgues, 2011a] or CAMB [Lewis and Bridle, 2002], but have written a new one instead which is particularly adapted to fit our model. Nonetheless, we rely heavily on the techniques employed in these codes, in particular on the approximation schemes described in [Blas et al., 2011] for baryons, photons and neutrinos. Since we employ a manifestly gauge-invariant setting, these schemes had to be adapted to our variables. We describe how this is done in section 4.2.

Finally, the scalar field perturbation equations (in fact, even the background equations) do not lend themselves well to a direct numerical evolution. This is due to very quick oscillations arising at both the background and perturbative level during the later stages of the cosmic evolution. Resolving these correctly, in particular the interferences between background and perturbations, would require a huge computational effort. Therefore we first derive a set of effective averaged perturbation equations analytically, which we then use in our code for sufficiently late times. This process is described in section 4.3, where we compare the resulting equations to those of standard cold dark matter. Finally, we describe how the different approximations are integrated into our code in section 4.4.1 and present the results of of the numerical runs, the bolon power spectrum, in section 4.4.2.

The first part of this chapter contains a short introduction to linear cosmological perturbation theory. This is standard material, we rely on a mixture of [Kodama and Sasaki, 1984, Gorbunov and Rubakov, 2011a, Amendola and Tsujikawa, 2010] and [Mukhanov et al., 1992]. Parts of the contents of this chapter have been published in [Beyer, 2014b]. In sections 4.1 and 4.3 we draw heavily from the appendix of [Beyer, 2014b], in section 4.3 we closely follow the presentation of section IV of this paper. Copyright for the figures and excerpts of this preprint resides, at the time of writing this, with the author, but will be transferred to the American Physical Society upon acceptance of the paper. One issue we omit in this chapter is that of initial conditions. These are analyzed in chapter 5 in some detail, here we simply use the adiabatic perturbation mode derived there as input for our simulations.

4.1 BASICS

In cosmological linear perturbation theory, every dynamical quantity $\mathcal{A}$ (e.g. the metric, scalar fields or fluid quantities in the energy-momentum tensor) gets split up into a background quantity $\bar{\mathcal{A}}(\tau)$ and a perturbation $\delta\mathcal{A}(\tau,\vec{x})$. In order for linear perturbation theory to be valid, we need to require $\delta\mathcal{A}/\bar{\mathcal{A}} \ll 1$. The background field $\bar{\mathcal{A}}(\tau)$ then follows its evolution according to the equations of motion in a FLRW universe, and the perturbations $\delta\mathcal{A}(\tau,\vec{x})$ follow the equations of motion linearized around this background. The latter will contain partial derivatives with respect to the comoving coordinates $\vec{x}$ as well as conformal time τ, so they form a set of partial differential equations. These

are hard to deal with, but luckily one can improve matters by going to Fourier space, i.e. by expanding the perturbations as follows:

$$\delta\mathcal{A}(\tau,\vec{x}) = \int \frac{\mathrm{d}^3k}{(2\pi)^3}\, \delta\mathcal{A}(\tau,\vec{k})\mathrm{e}^{-i\vec{k}\cdot\vec{x}}. \tag{4.1}$$

As is common practice, we do not make a difference in nomenclature between $\delta\mathcal{A}(\tau,\vec{x})$ and its Fourier transform $\delta\mathcal{A}(\tau,\vec{k})$. In Fourier space, the equations for the different wavenumbers $\vec{k}$ decouple and we are left with a set of ordinary differential equations in τ. To go from real space to Fourier space one simply can replace the spatial derivatives as follows:

$$\frac{\partial}{\partial x^i}\delta\mathcal{A}(\tau,\vec{x}) \to -ik_i\delta\mathcal{A}(\tau,\vec{k})\,. \tag{4.2}$$

As we will soon see, the resulting evolution equations for the linear perturbations do not depend on the direction of $\vec{k}$, but only on its absolute value $k \equiv |\vec{k}|$, further simplifying the problem.

Any dynamical quantity appearing in Einstein equations can be categorized according to its transformation behavior under spatial rotations in $SO(3)$. In this context we differentiate between scalars, 3-vectors and rank 2 3-tensors, and denote these by $\mathcal{A}$, $\mathcal{B}_i$ and $\mathcal{C}_{ij}$ respectively. The 3-vectors can now be written as a gradient (the scalar part) and a divergence-free vector:

$$\mathcal{B}_i = \underbrace{\partial_i\mathcal{B}}_{\text{scalar}} + \underbrace{\tilde{\mathcal{B}}_i}_{\text{vector}}, \quad \text{with} \quad g^{ij}\partial_i\tilde{\mathcal{B}}_j = 0\,. \tag{4.3}$$

Similarly, rank 2 3-tensors can be decomposed as follows:

$$\mathcal{C}_{ij} = \underbrace{C\delta_{ij} + (\partial_i\partial_j - \frac{1}{3}\delta_{ij}\nabla^2)\mathcal{C}}_{\text{scalar}} + \underbrace{2\partial_{(i}\tilde{\mathcal{C}}_{j)}}_{\text{vector}} + \underbrace{\tilde{\mathcal{C}}_{ij}}_{\text{tensor}}, \tag{4.4}$$

where the vector and tensor parts are divergence-free, i.e. $g^{ij}\partial_i\tilde{\mathcal{C}}_j = g^{ij}\partial_i\tilde{\mathcal{C}}_{jl} = 0$. Here we also used the symmetric operator

$$\partial_{(i}\tilde{\mathcal{C}}_{j)} = \frac{1}{2}\left(\partial_i\tilde{\mathcal{C}}_j + \partial_j\tilde{\mathcal{C}}_i\right). \tag{4.5}$$

Note that, slightly confusingly, both 3-vectors and rank 2 3-tensors have a scalar part and a vector part in the decomposition, we used the nomenclature 3-vector and 3-tensor precisely to avoid confusion concerning this matter. Hopefully it worked.

In linear perturbation theory, the scalar, vector and tensor perturbations decouple and can be analyzed separately. In this thesis we are exclusively concerned with the scalar sector of perturbations, since we analyze a theory of scalar fields and those do not source vector or tensor modes.

Generally speaking, vector perturbations do not play an important role in cosmology, as they can be shown to decay. So even if they were present in the early universe, they become irrelevant very quickly. The situation is different for tensor perturbations. They are the source of primordial gravitational waves, which be created during the era of inflation and can in principle be observed through polarization patterns in the CMB sky. In fact, the ratio of the primordial amplitudes of tensor and

scalar perturbations might be observable in the near future and can be used to discriminate between different inflationary scenarios [Gorbunov and Rubakov, 2011a, Ade et al., 2013c].

4.1.1 PERTURBING EINSTEIN-GRAVITY

We now quickly describe how to perturb dynamical quantities in Einstein gravity which are relevant to our model, i.e. the metric, a generic energy momentum tensor and cosmological scalar fields.

Metric perturbations

Generically, the perturbed metric around a FLRW solution in four dimensional spacetime has 10 degrees of freedom, 4 scalar, 4 vector and two tensor degrees. We are only interested in the scalar part here, and the generic line element not including vector or tensor contributions is given by

$$ds^2 = a(\tau)^2 \left\{ -(1+2\phi)d\tau^2 + 2G_{,i}\, d\tau dx^i + [(1-2\psi)\delta_{ij} + F_{,ij}]\, dx^i dx^j \right\} , \tag{4.6}$$

where a comma denotes a partial derivative, e.g. $G_{,i} = \partial_i G$.

Energy-momentum perturbations

For any (non-minimally coupled) component of the cosmic fluid the most generic form of the linearly perturbed energy momentum tensor reads

$$T^{\mu}_{\alpha\nu} = (\rho_\alpha + p_\alpha) u^{\mu}_{\alpha} u_{\alpha\nu} + p_\alpha \delta^{\mu}_{\nu} + \pi^{\mu}_{\alpha\nu} . \tag{4.7}$$

Here ρ_α, p_α and u_α have the usual meanings of the total (i.e. background and perturbed) energy density, pressure density and four-velocity, respectively. $\pi^{\mu}_{\alpha\nu}$ is the anisotropic stress tensor. It can always be chosen to be orthogonal to the four-velocity, i.e. $u_{\alpha\mu}\pi^{\mu}_{\alpha\nu} = 0$, which means we can set $\pi^0_{\alpha 0} = \pi^0_{\alpha i} = 0$. Furthermore the remaining spatial part can be chosen to be traceless, as any trace can be reabsorbed into a redefinition of the pressure. The resulting traceless rank 2 3-tensor can therefore be decomposed as follows (again ignoring the vector and tensor contributions):

$$\pi^{i}_{\alpha j} = \Pi_{\alpha,ij} - \frac{1}{3}\nabla^2 \Pi_\alpha \delta_{ij} , \tag{4.8}$$

while all other components vanish. Concerning the four-velocity, we can write the irrotational part (again neglecting vector modes) of u^μ as

$$(u^{\mu}_{\alpha}) = \frac{1}{a}\left\{ (1-\phi)\, ,\, v^{i}_{\alpha} \right\} . \tag{4.9}$$

We thus obtain for the scalar part of the stress energy tensor to linear order:

$$T^0_{\alpha 0} = -\bar{\rho}_\alpha - \delta\rho_\alpha\,, \tag{4.10}$$
$$T^0_{\alpha i} = (\bar{\rho}_\alpha + \bar{p}_\alpha)(G_{,i} + v_{\alpha,i})\,, \tag{4.11}$$
$$T^i_{\alpha 0} = -(\bar{\rho}_\alpha + \bar{p}_\alpha)(v^{,i}_\alpha)\,, \tag{4.12}$$
$$T^i_{\alpha j} = (\bar{p}_\alpha + \delta p_\alpha)\delta^i_j + \pi^i_{\alpha j}\,. \tag{4.13}$$

Here we have used a bar (like $\bar{\rho}$) to mark background quantities.

Gauge transformations

Before we continue to write down the perturbed Einstein equations, we want to address one important issue: The splitting of both the metric and the energy-momentum tensor in a background part and a perturbation introduced above is not uniquely defined. In particular, we defined the spatial coordinates on a preferred time slicing. Changing the time slicing corresponds to a simple coordinate change, and since we keep the FLRW background fixed, this change translates to the perturbative quantities only. This may appear to be a subtlety, but different coordinate choices, or *gauges*, can have striking consequences. They can change the values of perturbation variables considerably and even introduce fictitious perturbations, i.e. degrees of freedom which are non-physical, as they can be eliminated by a gauge transformation.

Let us make this explicit. A gauge-transformation is simply a coordinate transformation given by

$$\tau \to \tilde{\tau} = \tau + \xi^0(\tau, \vec{x})\,,\; x^i \to \tilde{x}^i = x^i + \xi^{,i}(\tau, \vec{x})\,. \tag{4.14}$$

Here we already limited ourselves to the scalar part of the transformation, i.e. we dropped a possible vector contribution to the change of the spatial coordinates. Clearly the coordinate change needs to be 'small', meaning that it should still be possible to consider the resulting perturbations as small around the FLRW solution. The transformation rules for the metric perturbations can be obtained from the generic metric transformation rule,

$$g_{\mu\nu} \to \tilde{g}_{\mu\nu} = \frac{\partial x^\rho}{\partial \tilde{x}^\mu}\frac{\partial x^\sigma}{\partial \tilde{x}^\nu} g_{\rho\sigma}\,, \tag{4.15}$$

which needs to be linearized. One obtains:

$$\begin{aligned} \phi \to \phi - \mathcal{H}\xi^0 - \xi^{0\prime}\,, \quad \psi \to \psi + \mathcal{H}\xi^0\,, \\ G \to G + \xi^0 - \xi'\,, \quad F \to F - \xi\,. \end{aligned} \tag{4.16}$$

An evaluation of the same transformation rule for the energy-momentum tensor yields the following: The anisotropic stress tensor $\pi^i_{\alpha j}$ is already gauge-invariant, whereas a scalar quantity δs (like $\delta\rho_\alpha$ or δp_α) transforms like

$$\delta s \to \delta s - \bar{s}'\xi^0 \tag{4.17}$$

under a generic gauge transformation. The velocity potential obeys

$$v_\alpha \to v_\alpha + \xi'. \tag{4.18}$$

Gauge invariant variables

A very elegant way to deal with the gauge issue is to introduce gauge-invariant variables. This is what we will do for most of this thesis. For metric perturbations we will always resort to the commonly used gauge-invariant Bardeen potentials [Bardeen, 1980], defined as

$$\Phi \equiv \phi - \mathcal{H}\sigma - \sigma' \quad \text{and} \quad \Psi \equiv \psi + \mathcal{H}\sigma, \tag{4.19}$$

where σ is given by $\sigma \equiv -G + F'$, i.e. $\sigma \to \sigma - \xi^0$ under the above gauge transformation. For the energy momentum tensor we employ the following gauge-invariant versions of scalar quantities (i.e. $\delta\rho_\alpha$ and δp_α):

$$\delta s^{(\mathrm{gi})} \equiv \delta s - \bar{s}'\sigma, \tag{4.20}$$

and also define a gauge-invariant momentum-perturbation via

$$[(\rho + p)v]_\alpha^{(\mathrm{gi})} \equiv (\bar{\rho}_\alpha + \bar{p}_\alpha)(v_\alpha + F'). \tag{4.21}$$

Furthermore, we will often use the dimensionless density contrast, defined via

$$\delta_\alpha^{(gi)} = \frac{\delta\rho_\alpha^{(gi)}}{\bar{\rho}_\alpha}. \tag{4.22}$$

These definitions are of course not unique, one could employ a large number of gauge invariant metric and fluid quantities (see e.g. [Kodama and Sasaki, 1984] for an overview). We choose to work with the definitions that correspond to the standard quantities used when working in the longitudinal gauge (defined by $F = \sigma = 0$, see below).

Specific gauges

As an alternative to gauge invariant quantities, one can choose to fix the gauge specifically. There are many options to do this, here we will only discuss the two most popular ones, *synchronous gauge* and *longitudinal gauge*.

The longitudinal gauge is defined by $F = G = 0$. A quick look at the gauge transformations of metric perturbations in eq. (4.16) confirms that this is is always possible and completely fixes the gauge, there is no additional freedom left. Any coordinate transformation would lead to a violation of the gauge conditions. This gauge has the advantage that it is easy to make the connection to Newtonian gravity, as both remaining gravitational potential ψ and ϕ reduce to the Newtonian gravitational potential in the corresponding limit. Our definition of gauge invariant quantities is designed such that they precisely coincide with the corresponding longitudinal gauge quantities.

The synchronous gauge is defined by $\phi = G = 0$. Eq. (4.16) now tells us that this does not uniquely fix the gauge. In fact, a residual gauge freedom of the form

$$\xi^0 = f_1(\vec{x})\, a^{-1}, \quad \xi = f_1(\vec{x}) \ln(a) + f_2(\vec{x}) \tag{4.23}$$

is still present. This remaining gauge freedom needs to be eliminated somehow, otherwise it can give rise to unphysical fictitious gauge modes. This can be achieved if there is a component of the cosmic fluid with $v_\alpha \propto a^{-1}$ in synchronous gauge (see eq. (4.18)). Such a component is precisely given by minimally coupled cold dark matter, a fluid with $\omega_{\mathrm{CDM}} = \delta p_{\mathrm{CDM}} = 0$ and no couplings. In this case one can set $v_\alpha = 0$, leaving only $f_2(\vec{x})$ as a free function. This remaining gauge freedom is in fact meaningless, since it only changes the value of F by a constant (meaning a spatial distribution which is constant in time), but F itself never appears in the equations of motion, only its derivative F'. The remaining fictitious gauge mode in Fourier space is therefore one where F is constant in time and all other quantities are zero, which can be easily eliminated. In our coupled scalar field model we have no such simple component, making the partial gauge fixing impossible. Thus the synchronous gauge is particularly unsuited for our situation.
Despite its disadvantages, the synchronous gauge is still commonly used up to today in many Boltzmann codes (e.g. [Lewis and Bridle, 2002]) and for the display of results, like power spectra. We will do the same and thus need the transformation rules from the gauge-invariant description to the synchronous gauge. First we recall that our gauge-invariant quantities coincide precisely with the Newtonian gauge quantities, and the transformation to synchronous gauge quantities can therefore be obtained from the generic gauge transformations for metric and energy momentum tensor quantities given in equations (4.16) to (4.18) with the following coordinate change:

$$\xi^0 = a \int \mathrm{d}\tau \frac{\Phi}{a}, \quad \xi' = \xi^0 . \tag{4.24}$$

This does not determine the functions ξ^0 and ξ completely, reflecting the remaining gauge freedom in synchronous gauge.

> *In the following sections the superscript "(gi)" will be dropped since we will be using gauge-invariant quantities exclusively. We will also stop employing the bar to denote the background quantities, because the total densities will not appear in any of the equations anymore.*

Perturbation equations

Now we will present the equations of motion for the gauge invariant quantities introduced above. We will work in Fourier space and start with Einstein's equations. At linear order one obtains the

following equations around a FLRW-background for the two Bardeen potentials:

$$k^2\Psi = -\frac{a^2}{2M_p^2}\sum_\alpha (\delta\rho_\alpha - 3\mathcal{H}[(\rho+p)v]_\alpha)\,, \tag{4.25}$$

$$\Psi' + \mathcal{H}\Phi = -\frac{a^2}{2M_p^2}\sum_\alpha [(\rho+p)v]_\alpha\,, \tag{4.26}$$

$$\Psi'' + 2\mathcal{H}\Psi' + \mathcal{H}\Phi' + (2\mathcal{H}' + \mathcal{H}^2)\Phi = +\frac{a^2}{2M_p^2}\sum_\alpha \left(\delta p_\alpha - \frac{2}{3}k^2\Pi_\alpha\right). \tag{4.27}$$

The two Bardeen potential are related by

$$\Phi = \Psi - a^2\Pi_{\rm tot}/M_p^2\,, \tag{4.28}$$

where $\Pi_{\rm tot} = \sum_\alpha \Pi_\alpha$. In order to write down the generic perturbed equations of energy- and momentum-conservation, we first have to specify the generic forms for energy- and momentum transfer at the linear level. This is done by perturbing the coupling four-vector Q defined in eq. (2.52), which reads

$$\delta Q^0_\alpha = -aQ_\alpha(\phi + \varepsilon_\alpha)\,, \tag{4.29}$$

$$\delta Q^j_\alpha = a\,[Q_\alpha(v+G) + f_\alpha]^{,j}\,. \tag{4.30}$$

Note that we have again dropped a possible vector contribution to the spatial part of the perturbed coupling four-vector, which does not affect scalar perturbations. While f_α is already gauge-invariant, ε_α transforms as $\varepsilon_\alpha \to \varepsilon_\alpha - \frac{Q'_\alpha}{Q_\alpha}\xi^0$. We define a gauge-invariant momentum transfer via

$$\tau_\alpha = \varepsilon_\alpha - \frac{Q'_\alpha}{Q_\alpha}\sigma\,. \tag{4.31}$$

The equation of energy conservation then reads at the linear level

$$\begin{aligned}\delta\rho'_\alpha =& -3\mathcal{H}(\delta\rho_\alpha + \delta p_\alpha) + k^2\,[(\rho+p)v]_\alpha + 3(\rho_\alpha + p_\alpha)\Psi' \\ &+ 3\mathcal{H}(\rho_\alpha + p_\alpha)q_\alpha\Phi + 3\mathcal{H}(\rho_\alpha + p_\alpha)q_\alpha\tau_\alpha\,,\end{aligned} \tag{4.32}$$

where we have used the dimensionless coupling q_α defined in equation (2.54). The equation of momentum conservation gives

$$\begin{aligned}[(\rho+p)v]'_\alpha =& -4\mathcal{H}\,[(\rho+p)v]_\alpha - (\rho_\alpha + p_\alpha)\Phi - \delta p_\alpha \\ &+ \frac{2}{3}k^2\Pi_\alpha + 3\mathcal{H}q_\alpha\frac{(\rho_\alpha + p_\alpha)}{(\rho_{\rm tot} + p_{\rm tot})}\,[(\rho+p)v]_{\rm tot} + af_\alpha\,.\end{aligned} \tag{4.33}$$

The equations presented in this section are both not complete and redundant. On the one hand, we are missing an evolution equation for the anisotropic stress Π_α. We will discuss how this can be obtained for photons and neutrinos, the only constituents in our model which develop anisotropic stress, in the next section. On the other hand, Einstein's equations and the equations of energy and momentum conservation are not independent. In fact, is is sufficient to consider only the equations of energy-momentum conservation for each component of the cosmic fluid plus the Poisson equation

(4.25) and eq. (4.28), equations (4.26) and (4.27) are redundant.

4.1.2 Scalar field perturbations

We now want to discuss perturbations for cosmological scalar fields. We will directly start with the case of two canonical scalar fields φ and χ which couple through their common potential, as this is the relevant case for our analysis. At the background level, we have already seen how the energy momentum tensor for the scalar fields can be mapped onto a fluid description (see section 3.4). At the level of linear perturbations we can split the scalar fields into background parts and perturbations: $\varphi = \bar{\varphi} + \delta\varphi$ and $\chi = \bar{\chi} + \delta\chi$. In order to remain manifestly gauge-invariant we will work with the redefined field perturbations (cf. eq. (4.20))

$$X = \delta\varphi - \varphi'\sigma \quad \text{and} \quad Y = \delta\chi - \chi'\sigma\,. \tag{4.34}$$

Plugging this and the linearly perturbed FLRW-metric (eq. (4.6)) into the Klein-Gordon equations (3.97) yields the following (manifestly gauge invariant) linearized field equations:

$$X'' + 2\mathcal{H}X' + k^2X + a^2V_{,\varphi\varphi}X + a^2V_{,\varphi\chi}Y + 2a^2V_{,\varphi}\Phi - \varphi'\Phi' - 3\varphi'\Psi' = 0\,, \tag{4.35}$$

$$Y'' + 2\mathcal{H}Y' + k^2Y + a^2V_{,\varphi\chi}X + a^2V_{,\chi\chi}Y + 2a^2V_{,\chi}\Phi - \chi'\Phi' - 3\chi'\Psi' = 0\,. \tag{4.36}$$

Following section 3.4 we split the potential into two parts $V(\varphi,\chi) = V_1(\varphi,\chi) + V_2(\varphi,\chi)$, where the exact definitions of V_1 and V_2 are in principle arbitrary. We can now directly calculate the energy momentum tensor at linear order from eqs. (3.99) and (3.100). We again recover the fluid form given in equations (4.10) to (4.13), this time with the following assignments:

$$\delta\rho_\varphi = \frac{1}{a^2}\left(\varphi'X' - \Phi\varphi'^2 + a^2V_{1,\varphi}X + a^2V_{1,\chi}Y\right), \tag{4.37}$$

$$\delta\rho_\chi = \frac{1}{a^2}\left(\chi'Y' - \Phi\chi'^2 + a^2V_{2,\varphi}X + a^2V_{2,\chi}Y\right), \tag{4.38}$$

$$\delta p_\varphi = \frac{1}{a^2}\left(\varphi'X' - \Phi\varphi'^2 - a^2V_{1,\varphi}X - a^2V_{1,\chi}Y\right), \tag{4.39}$$

$$\delta p_\chi = \frac{1}{a^2}\left(\chi'Y' - \Phi\chi'^2 - a^2V_{2,\varphi}X - a^2V_{2,\chi}Y\right), \tag{4.40}$$

$$[(\rho + p)v]_\varphi = \frac{-1}{a^2}\varphi'X\,, \tag{4.41}$$

$$[(\rho + p)v]_\chi = \frac{-1}{a^2}\chi'Y\,. \tag{4.42}$$

Anisotropic stress is not produced by scalar fields.

In order to find the correct perturbative expressions for energy- and momentum-transfer we have to evaluate the equations of energy- and momentum conservation $\mathcal{D}_\mu T^{\mu\nu}_\alpha = Q^\nu_\alpha$ at the linear level. We can do this explicitly, using the linearized field equations (4.35) and (4.36) to finally obtain rather complicated expressions. Since we assume that no additional couplings are present for the scalar fields, except of course to gravity, we know that $\mathcal{D}_\mu T^{\mu\nu}_\varphi + \mathcal{D}_\mu T^{\mu\nu}_\chi = 0$. From this it is easy to see that

energy- and momentum transfer of the two fields are related by

$$f_\chi = -f_\varphi \quad \text{and} \quad \tau_\chi = \tau_\varphi\,, \tag{4.43}$$

and we can restrict ourselves to quoting only the expressions for the perturbed cosmon-coupling here:

$$\begin{aligned} a f_\varphi =& -\frac{a^2 V_{2,\varphi}}{\varphi'}\left[(\rho+p)v\right]_\varphi + \frac{a^2 V_{1,\chi}}{\chi'}\left[(\rho+p)v\right]_\chi \\ &+ \frac{2\left(\chi' V_{1,\chi} - \varphi' V_{2,\varphi}\right)}{3\mathcal{H}(1+\omega_{\rm eff})}\Phi + \frac{2\left(\chi' V_{1,\chi} - \varphi' V_{2,\varphi}\right)}{3\mathcal{H}^2(1+\omega_{\rm eff})}\Psi'\,, \end{aligned} \tag{4.44}$$

$$\begin{aligned} \left(\varphi' V_{2,\varphi} - \chi' V_{1,\chi}\right)\tau_\varphi =& + \frac{a^2 V_{2,\varphi}}{\varphi'}\delta\rho_\varphi - \frac{a^2 V_{1,\chi}}{\chi'}\delta\rho_\chi \\ &+ \frac{\left(a^2\chi' V_{1,\varphi}V_{2,\varphi} - a^2\varphi' V_{1,\chi}V_{2,\varphi} + \varphi'\chi'^2 V_{1,\varphi\chi} - \varphi'^2\chi' V_{2,\varphi\varphi}\right)}{(\rho_\varphi + p_\varphi)\chi'}\left[(\rho+p)v\right]_\varphi \\ &- \frac{\left(a^2\varphi' V_{1,\chi}V_{2,\chi} - a^2\chi' V_{1,\chi}V_{2,\varphi} + \varphi'^2\chi' V_{2,\varphi\chi} - \chi'^2\varphi' V_{1,\chi\chi}\right)}{(\rho_\chi + p_\chi)\varphi'}\left[(\rho+p)v\right]_\chi\,. \end{aligned} \tag{4.45}$$

4.1.3 ALTERNATIVE PERTURBATION VARIABLES

In this section we want to introduce alternative perturbation variables which we will use in both our numerics and analytical analyses below. Following [Malik, 2001] we introduce a redefined density contrast and velocity potential via

$$\Delta_\alpha \equiv \frac{\delta\rho_\alpha}{\rho_\alpha} + \frac{\rho'_\alpha}{\mathcal{H}\rho_\alpha}\Psi = \frac{\delta\rho_\alpha}{\rho_\alpha} - 3(1+\omega_\alpha)(1-q_\alpha)\Psi\,, \tag{4.46}$$

$$V_\alpha \equiv -\frac{\mathcal{H}\left[(\rho+p)v\right]_\alpha}{\rho_\alpha + p_\alpha}\,. \tag{4.47}$$

The equations of energy- and momentum-conservation can now be rewritten in terms of these new variables. This gives:

$$\begin{aligned} \Delta'_\alpha =& -\frac{k^2}{\mathcal{H}}(1+\omega_\alpha)V_\alpha + 3(1+\omega_\alpha)\left[q'_\alpha + 3\mathcal{H}(1+c^2_{a,\alpha})q_\alpha(q_\alpha-1)\right]\Psi + 3\mathcal{H}(1+\omega_\alpha)q_\alpha\tau_\alpha \\ &- 3\mathcal{H}\omega_\alpha\Gamma_\alpha + 3(1+\omega_\alpha)q_\alpha\left(\mathcal{H}\Phi + \Psi'\right) - 3\mathcal{H}\left(q_\alpha(1+\omega_\alpha) + c^2_{a,\alpha} - \omega_\alpha\right)\Delta_\alpha\,, \end{aligned} \tag{4.48}$$

$$\begin{aligned} V'_\alpha =& 3\mathcal{H}\left(c^2_{a,\alpha}(1-q_\alpha) - q_\alpha - \frac{1+\omega_{\rm eff}}{2}\right)V_\alpha + \frac{\mathcal{H}c^2_{a,\alpha}}{(1+\omega_\alpha)}\Delta_\alpha + 3\mathcal{H}c^2_{a,\alpha}(1-q_\alpha)\Psi \\ &- \frac{2}{3}\frac{k^2}{\mathcal{H}}\frac{\omega_\alpha\tilde{\Pi}_\alpha}{(1+\omega_\alpha)} + \frac{\mathcal{H}\omega_\alpha}{1+\omega_\alpha}\Gamma_\alpha - \frac{\mathcal{H}}{\rho_\alpha+p_\alpha}af_\alpha + \frac{2q_\alpha}{1+\omega_{\rm eff}}\left(\mathcal{H}\Phi + \Psi'\right) + \mathcal{H}\Phi\,. \end{aligned} \tag{4.49}$$

Here we have introduced the adiabatic sound speed $c^2_{a,\alpha}$ and the internal entropy perturbation Γ_α, which are given by

$$c^2_{a,\alpha} \equiv \omega_\alpha + \frac{\rho_\alpha}{\rho'_\alpha}\omega'_\alpha = \omega_\alpha - \frac{\omega'_\alpha}{3\mathcal{H}(1-q_\alpha)(1+\omega_\alpha)}\,, \tag{4.50}$$

$$\Gamma_\alpha \equiv \frac{1}{p_\alpha}\left(\delta p_\alpha - c^2_{a,\alpha}\delta\rho_\alpha\right)\,, \tag{4.51}$$

as well as a dimensionless quantity for the anisotropic stress

$$\tilde{\Pi}_\alpha \equiv \frac{\mathcal{H}^2\Pi_\alpha}{p_\alpha}\,. \tag{4.52}$$

Einstein's equations (4.25) - (4.28) can of course easily be adapted as well:

$$\Psi = -\frac{3}{2}\frac{\sum_\alpha \Omega_\alpha\,(\Delta_\alpha + 3(1+\omega_\alpha)V_\alpha)}{k^2/\mathcal{H}^2 + \frac{9}{2}(1+\omega_{\rm eff})}\,, \tag{4.53}$$

$$\Psi'/\mathcal{H} = -\Phi + \frac{3}{2}\sum_\alpha \Omega_\alpha(1+\omega_\alpha)V_\alpha\,, \tag{4.54}$$

$$\Phi = \Psi - 3\sum_\alpha \Omega_\alpha\omega_\alpha\tilde{\Pi}_\alpha\,. \tag{4.55}$$

We have not included eq. (4.27) here, since it is redundant and will not be used below. (Eq. (4.54) is also redundant, but we will nonetheless use it at one point.)

Scalar fields

Let us now rewrite the equations governing the linear scalar perturbations in our new variables. In particular we would like to remove all direct dependences on the potential and the field derivatives and replace them with the equations of state, the adiabatic sound-speeds and the couplings q_φ and q_χ. This setting is not necessary for our work in this chapter, but it will essential for our analysis of early universe perturbations in chapter 5, and we feel it fits in better here.

To simplify matters we make the assumption that $V_{1,\chi} = 0$. This is not limiting the general model, as the splitting of the potential is arbitrary and we can thus choose to assign the entire common part to $T^{\mu\nu}_\chi$.

As a first step we employ the following relations to replace the potential derivatives:

$$V_{1,\varphi}\varphi' = \frac{3}{2}\mathcal{H}(1+\omega_\varphi)(1-q_\varphi)\rho_\varphi(c^2_{a,\varphi}-1)\,, \tag{4.56}$$

$$V_{2,\varphi}\varphi' = -3\mathcal{H}(1+\omega_\varphi)\rho_\varphi q_\varphi\,, \tag{4.57}$$

$$V_{2,\chi}\chi' = -\frac{3}{2}\mathcal{H}(1+\omega_\chi)\rho_\chi\left[1 - c^2_{a,\chi} + q_\chi(1+c^2_{a,\chi})\right]\,. \tag{4.58}$$

The second derivatives can not be so easily replaced, but we can take the time derivative of equation (4.57) to obtain

$$V_{2,\varphi\chi} = \frac{\varphi'}{\chi'}\left[\frac{9}{2}\frac{\mathcal{H}^2}{a^2}q_\varphi C_\varphi - V_{2,\varphi\varphi} - 3\frac{\mathcal{H}}{a^2}q'_\varphi\right], \tag{4.59}$$

with $C_\varphi = \left(1+\omega_{\rm eff}+(1-q_\varphi)(1+c^2_{a,\varphi})\right)$.
The derivative $V_{2,\varphi\varphi}$ remains in the equations and cannot be replaced without introducing another second potential derivative like $V_{2,\chi\chi}$. Using these simplifications we can rewrite the perturbed couplings as follows:

$$af_\varphi = 3q_\varphi(1+\omega_\varphi)\rho_\varphi\left(\frac{2}{3}\frac{(\Psi'/\mathcal{H}+\Phi)}{(1+\omega_{\rm eff})} - V_\varphi\right), \tag{4.60}$$

$$\begin{aligned}\tau_\varphi =& \frac{1}{1+\omega_\varphi}\Delta_\varphi + \left(\frac{3}{2}(1-q_\varphi)(1-c^2_{a,\varphi}) - \frac{a^2V_{2,\varphi\varphi}}{3q_\varphi\mathcal{H}^2}\right)V_\varphi \\ &- \left(\frac{3}{2}C_\varphi - \frac{q'_\varphi}{q_\varphi\mathcal{H}} - \frac{a^2V_{2,\varphi\varphi}}{3q_\varphi\mathcal{H}^2}\right)V_\chi + 3(1-q_\varphi)\Psi\,.\end{aligned} \tag{4.61}$$

The internal entropy perturbations now read:

$$\omega_\varphi\Gamma_\varphi = (1-c^2_{a,\varphi})\left(\Delta_\varphi + 3(1+\omega_\varphi)(1-q_\varphi)\right)\Psi + 3(1+\omega_\varphi)(1-q_\varphi)(1-c^2_{a,\varphi})V_\varphi\,, \tag{4.62}$$

$$\begin{aligned}\omega_\chi\Gamma_\chi =& (1-c^2_{a,\chi})\left(\Delta_\chi + 3(1+\omega_\chi)(1-q_\chi)\right)\Psi - 6(1+\omega_\chi)q_\chi V_\varphi \\ &+ 3(1+\omega_\chi)\left(1-c^2_{a,\chi}+q_\chi(1+c^2_{a,\chi})\right)V_\chi\,.\end{aligned} \tag{4.63}$$

Now the generic perturbation equations can simply be obtained by inserting these results into the generic equations (4.48) and (4.49). However, we see that the perturbed momentum transfer cannot be fully specified without making some additional assumption about the coupling to eliminate the remaining potential derivative. In the case of the cosmon-bolon model we directly obtain

$$V_{2,\varphi\varphi} = \frac{4\beta^2}{M_p^2}V_2 = 6\beta^2(1-\omega_\varphi)\frac{\mathcal{H}^2}{a^2}\Omega_\varphi\,. \tag{4.64}$$

4.1.4 ENTROPY AND CURVATURE PERTURBATIONS

We have already talked about adiabatic and isocurvature perturbations several times, so let us quickly define what this actually means.

Entropy perturbations

The pressure perturbation δp_α can be decomposed into an adiabatic and a non-adiabatic pressure perturbation

$$\delta p_\alpha = \delta p_{\alpha,\rm nad} + \delta p_{\alpha,\rm ad}\,, \tag{4.65}$$

where

$$\delta p_{\alpha,\mathrm{ad}} = c^2_{a,\alpha}\delta\rho_\alpha\,. \tag{4.66}$$

Here $c^2_{a,\alpha}$ is the adiabatic sound speed introduced in eq. (4.50), which should be clearly distinguished from the *total sound speed*, defined as

$$c^2_{\mathrm{tot},\alpha} = \frac{\delta p_\alpha}{\delta\rho_\alpha}\,, \tag{4.67}$$

which is fundamentally a perturbative quantity. The non-adiabatic sound speed is often described using the intrinsic entropy perturbation Γ_α and defined via

$$\delta p_{\alpha,\mathrm{nad}} = p_\alpha\Gamma_\alpha\,. \tag{4.68}$$

In addition to intrinsic entropy perturbations there can also be entropy perturbations between different components of the cosmic fluid. Let us divide the total pressure perturbation as follows:

$$\delta p_{\mathrm{tot}} = c^2_{\mathrm{tot},a}\delta\rho_{\mathrm{tot}} + p_{\mathrm{tot}}\Gamma_{\mathrm{tot}} \tag{4.69}$$

where

$$c^2_{a,\mathrm{tot}} = p'_{\mathrm{tot}}/\rho'_{\mathrm{tot}} = \sum_\alpha (1-q_\alpha)c^2_{a,\alpha}\frac{\rho_\alpha + p_\alpha}{\rho_{\mathrm{tot}} + p_{\mathrm{tot}}} \tag{4.70}$$

and

$$p_{\mathrm{tot}}\Gamma_{\mathrm{tot}} = \sum_\alpha p_\alpha\Gamma_\alpha + p_{\mathrm{tot}}\Gamma_{\mathrm{rel}}\,. \tag{4.71}$$

A straightforward calculation now shows that the total relative entropy perturbation satisfies

$$p_{\mathrm{tot}}\Gamma_{\mathrm{rel}} = \sum_\alpha (c^2_{a,\alpha} - c^2_{a,\mathrm{tot}})\delta\rho_\alpha\,. \tag{4.72}$$

In terms of our new variables we have

$$p_{\mathrm{tot}}\Gamma_{\mathrm{rel}} = \frac{1}{2}\sum_{\alpha,\beta}\frac{(1-q_\alpha)(1-q_\beta)(\rho_\alpha+p_\alpha)(\rho_\beta+p_\beta)}{\rho_{\mathrm{tot}}+p_{\mathrm{tot}}} \times \left(c^2_{a,\alpha} - c^2_{a,\beta}\right) S_{\alpha\beta} \tag{4.73}$$

where

$$S_{\alpha\beta} = \frac{\Delta_\alpha}{(1+\omega_\alpha)(1-q_\alpha)} - \frac{\Delta_\beta}{(1+\omega_\beta)(1-q_\beta)}\,. \tag{4.74}$$

For this reason, $S_{\alpha\beta}$ is sometimes referred to as the relative entropy perturbation between the two fluid components labelled by α and β. The condition for a perturbation mode to be adiabatic is sometimes given by demanding that all relative and intrinsic entropy perturbations vanish and sometimes by demanding only that the total entropy perturbation vanishes. We will use the former definition in this thesis, which clearly implies the latter. Note that in some analyses [Doran et al., 2003] different definitions of the relative entropy perturbations are used, but demanding a vanishing for these alternative definitions does not ensure a vanishing relative entropy perturbation in coupled scenarios (and are not even gauge-invariant in this case), and thus they are not suitable for our analysis.

Curvature perturbations

We define the gauge-invariant total curvature perturbation as

$$\zeta = -\Psi - \mathcal{H}\frac{\delta\rho_{\rm tot}}{\rho'_{\rm tot}} = \frac{1}{\rho_{\rm tot}+p_{\rm tot}}\sum_\alpha \rho_\alpha \Delta_\alpha \,. \tag{4.75}$$

Perturbation modes for which $\zeta = 0$ are known as isocurvature modes. Some works employ a different definition of the curvature perturbation [Mukhanov et al., 1992], but all definitions agree in the superhorizon limit for a flat universe, which is what is relevant for us. Interestingly, it is easy to show that on the superhorizon scales

$$\zeta' = -\frac{\mathcal{H}}{\rho_{\rm tot}+p_{\rm tot}}\delta p_{\rm nad}\,, \tag{4.76}$$

i.e. the total curvature perturbation is constant for adiabatic modes (see e.g. [Malik, 2001]).

Another gauge invariant curvature variable, sometimes referred to as *comoving curvature perturbation* is defined via

$$\mathcal{R} \equiv \Psi - \frac{\mathcal{H}}{\rho_{\rm tot}+p_{\rm tot}}\delta q_{\rm tot}\,. \tag{4.77}$$

We employed this quantity in our brief discussion of inflation in chapter 3.

4.1.5 STATISTICS

Given specific initial conditions for all (gauge invariant) perturbation fields, i.e. a configuration $\delta\mathcal{A}_i(\tau_1,\vec{x})$ at some initial time τ_1, the equations given above can in principle be used to evolve this configuration to any time τ_2. This is, however, not what is done in Boltzmann codes, for the following reason: We have no way to predict what the specific initial field configuration should look like. What we do have, usually from some version of inflation, is a statement about the statistical properties of the initial conditions.

Perturbations as random fields

By definition, all linear perturbations satisfy

$$< \delta\mathcal{A}_i(\tau,\vec{x}) >= 0 \quad \text{for all } \vec{x} \text{ and } \tau\,, \tag{4.78}$$

where the average $< \cdots >$ is an ensemble average, which can be taken to mean 'averaged over different realizations of the universe' in theories like eternal inflation we discussed in chapter 3. Beyond this, one usually assumes the random fields to be Gaussian, meaning that their entire statistics (i.e. all statistical momenta) are defined by the knowledge of their (generally $\vec{x}$- and τ-dependent) two-point correlation functions

$$\xi_{ij}(\tau,\vec{x}_1,\vec{x}_2) \equiv < \delta\mathcal{A}_i(\tau,\vec{x}_1)\,\delta\mathcal{A}_j(\tau,\vec{x}_2) > \ . \tag{4.79}$$

This demand is non-trivial. In fact, Non-Gaussianities arise during non-linear structure formation, since some perturbative quantities, like the densities contrast, are bound below by -1 but can reach big positive values of roughly 200. Furthermore, Non-Gaussianities can arise in theories of inflation, but we will not consider such scenarios in this work. See e.g. [Chen, 2010] for a review.

Additional assumptions about the perturbations commonly include the extension of the principles of spatial homogeneity and isotropy to their statistical properties. Imposing statistical homogeneity simply means that

$$\xi_{ij}(\tau,\vec{x}_1,\vec{x}_2) = \xi_{ij}(\tau,\vec{x}_1-\vec{x}_1) \quad \text{for all } \tau\,, \tag{4.80}$$

and requiring statistical isotropy in addition to that gives

$$\xi_{ij}(\tau,\vec{x}_1,\vec{x}_2) = \xi_{ij}(\tau,|\vec{x}_1-\vec{x}_2|)\,. \tag{4.81}$$

The real space two-point correlators can be directly related to the two-point correlation functions in Fourier space. One can easily convince oneself that the demands of statistical homogeneity and isotropy lead to

$$< \delta\mathcal{A}_i(\tau,\vec{k})\,\delta\mathcal{A}_j^*(\tau,\vec{q}) >= (2\pi)^3\,\mathrm{P}_{ij}(\tau,|\vec{k}|)\,\delta^{(3)}(\vec{k}-\vec{q})\,, \tag{4.82}$$

where $\mathrm{P}_{ij}(\tau,k)$ is called the *cross correlation power spectrum* of $\delta\mathcal{A}_i$ and $\delta\mathcal{A}_j$, or simply the *power spectrum* of the quantity $\delta\mathcal{A}_i$ for $i=j$. Note that it is only possible to define it in this very simple way (i.e. as a function of $k=|\vec{k}|$ and τ only) under the symmetry assumptions made above. Its relation to the real space two-point correlator is simply given by

$$\xi_{ij}(\tau,|\vec{x}_1-\vec{x}_2|) = \int \mathrm{d}\ln k\,\mathcal{P}_{ij}(\tau,k)\frac{\sin(k\,|\vec{x}_1-\vec{x}_2|)}{k\,|\vec{x}_1-\vec{x}_2|}\,, \tag{4.83}$$

where we introduced the dimensionless power spectrum (it is dimensionless if the perturbations $\delta\mathcal{A}_i$ and $\delta\mathcal{A}_j$*are*)

$$\mathcal{P}_{ij}(\tau,k) \equiv \frac{k^3\mathrm{P}_{ij}(\tau,k)}{2\pi^2}\,. \tag{4.84}$$

Evolution of random fields

As we have seen above, the evolution equations for the perturbation modes in Fourier space are isotropic, they only depend on the modulus of the wavenumber $k=|\vec{k}|$. Putting perturbation quantities into a single perturbation vector and assuming we have n dynamical quantities governed by first order linear differential equations, i.e.

$$\delta\mathcal{A}(\tau,\vec{k}) = (\delta\mathcal{A}_1(\tau,\vec{k}),\ldots,\delta\mathcal{A}_n(\tau,\vec{k}))^T\,, \tag{4.85}$$

a basis of solutions for these equations (for a given wavenumber k) can be written as

$$\delta\mathcal{A}_k^j(\tau) = (\delta\mathcal{A}_{1,k}^j,\ldots,\delta\mathcal{A}_{n,k}^j)^T\,, \quad j=1,\ldots,n. \tag{4.86}$$

The overall normalization of these solutions is of course arbitrary, lets fix it to $\delta\mathcal{A}^j_{1,k} = 1$, i.e. to the first perturbation variable for each mode. The generic solution for the quantity $\mathcal{A}$ then reads

$$\delta\mathcal{A}(\tau,\vec{k}) = \alpha^j(\vec{k})\,\delta\mathcal{A}^j_k(\tau)\,, \tag{4.87}$$

where a sum over j is implicit. Now we clearly have

$$< \delta\mathcal{A}_i(\tau,\vec{k})\,\delta\mathcal{A}^*_j(\tau,\vec{q}) >= \sum_{n,m} \delta\mathcal{A}^n_{i,k}(\tau)\delta\mathcal{A}^{m*}_{j,q}(\tau) < \alpha^n(\vec{k})\alpha^{m*}(\vec{q}) >\,, \tag{4.88}$$

and can define a set of primordial power spectra at some initial time τ_1 through

$$< \alpha^n(\vec{k})\alpha^{m*}(\vec{q}) >= (2\pi)^3 P^{nm}_{\rm prim}(k)\delta^3(\vec{p}-\vec{q})\,. \tag{4.89}$$

These primordial power spectra determine all the statistics of the Gaussian perturbations and the cross-correlation power spectrum at any time τ can be obtained by the mode functions as follows:

$$P_{ij}(\tau,k) = \sum_{n,m} \delta\mathcal{A}^n_{i,k}(\tau)\delta\mathcal{A}^{m*}_{j,k}(\tau)P^{nm}_{\rm prim}(k)\,. \tag{4.90}$$

As a sidenote, we would like to mention that the coefficients $\alpha^j(\vec{k})$ can be chosen to be uncorrelated for different perturbation modes and are also uncorrelated for different wavenumbers under the assumption of statistical isotropy and homogeneity, i.e. [Weinberg, 2008]

$$< \alpha^j(\vec{k})\alpha^{*l}(\vec{q}) >= 0 \quad \text{for } \vec{k} \neq \vec{q} \text{ or } j \neq l. \tag{4.91}$$

However, this requires a specific choice of basic perturbation modes, which may not coincide with the commonly used classification into adiabatic and isocurvature modes. Thus it still makes sense to investigate potential cross-correlations between different perturbation modes (see e.g. [Langlois, 1999, Langlois and Riazuelo, 2000, Langlois, 2003]). We will restrict ourselves to a single mode, the growing adiabatic mode in this chapter. Why it is justified to do so will be discussed in chapter 5. Under this assumption all statistical properties if the linear Gaussian scalar fluctuations are determined by a single primordial power spectrum.

We employ a nearly scale invariant spectrum as predicted by inflation, i.e.

$$\mathrm{P}_{\rm prim}(k) = \frac{2\pi^2}{k^3} A_s \left(\frac{k}{k_{\rm piv}}\right)^{n_s-1}\,, \tag{4.92}$$

where $n_s \approx 0.96$ and the pivot scale $k_{\rm piv}$ is in principle arbitrary, since a change in $k_{\rm piv}$ can be absorbed into the normalization A_s. Since we are dealing with linear perturbation theory here, the overall normalization of the mode functions is arbitrary, and such is the normalization of the primordial power spectrum A_s. It should be fixed either by a prediction concerning the amplitude of perturbations from inflation or by observations constraining the overall normalization of the power spectum. We will choose to do the latter below.

Observations: Ensemble average and spatial average

When we observe cosmic perturbations, we can not observe an ensemble of realizations, we only have one universe at our disposal. Still, in order to compare observations with theory, we need to draw conclusions about statistical properties, like power spectra. Luckily, under very generic circumstances, the ensemble average can be replaced by a spatial average. This is guaranteed by the *ergodic theorem* under the conditions that the perturbations are statistically homogeneous and become uncorrelated at large distances, meaning

$$< \delta\mathcal{A}_i(x+y)\delta\mathcal{A}_j(x-y) > \to 0 \quad \text{for} \quad |y| \to \infty \tag{4.93}$$

sufficiently quickly. See e.g. Weinberg [2008] for more details.

4.2 Baryons, photons and neutrinos

In the next section we will employ a Boltzmann-code to evolve the linear perturbations in the cosmonbolon model numerically. This requires a treatment of perturbations in the baryon, photon and neutrino sectors in addition to the scalar fields. For the relativistic particle species it is not sufficient to consider only the perfect fluid approximation, one has to take higher momenta of the phase space distribution function into account. Furthermore, acceptable numerical runtimes of the numerical code can only be achieved through the implementation of various approximations.

All existing Boltzmann-codes deal with these issues in very similar ways, the treatment has become (more or less) standard [Ma and Bertschinger, 1995, Lewis and Bridle, 2002, Blas et al., 2011]. However, our code uses a manifestly gauge-invariant setting, deviating from other Boltzmann-codes in this respect. This requires a re-calculation of the various approximations employed, which we will present in this section. As this is mainly a technical exercise and not particularly interesting, we will keep this presentation rather short. Essentially all approximations are derived following the same steps (only slightly adapted) that were used for the synchronous gauge calculation in [Blas et al., 2011], for the basics we draw heavily from [Ma and Bertschinger, 1995].

4.2.1 Full equations

Let us start by writing down the full equations governing the evolution of perturbations for neutrinos. First, let us recall the connection between the energy momentum tensor and the phase space distribution function (see eq. (2.58))

$$T^{\mu\nu}_{\alpha} = g_{\alpha} \int \frac{\mathrm{d}^3 P}{(2\pi)^3} \frac{1}{\sqrt{-g}} \frac{P^{\mu} P^{\nu}}{|P_0|} f_{\alpha}(\vec{x}, \vec{p}, \tau) \,. \tag{4.94}$$

In linear perturbation theory we can now decompose $f(\vec{x}, \vec{p}, \tau)$ into the background part given in eq. (2.57) and a perturbation:

$$f_{\alpha}(\vec{x}, \vec{p}, \tau) = \bar{f}_{\alpha}(|\vec{p}|, \tau) \left[1 + \delta f_{\alpha}(\vec{x}, \vec{p}, \tau)\right] . \tag{4.95}$$

Now the perturbed energy momentum tensor (4.94) is related to the perturbed phase space distribution function via

$$\delta T^0_{\alpha 0} = -g_\alpha a^{-4} \int \mathrm{d}^3 p \, \sqrt{\vec{p}^{\,2} + m^2} \bar{f}_\alpha(|\vec{p}|,\tau)\delta f_\alpha \,, \tag{4.96}$$

$$\delta T^i_{\alpha 0} = g_\alpha a^{-4} \int \mathrm{d}^3 p \, p_i \bar{f}_\alpha(|\vec{p}|,\tau)\delta f_\alpha \,, \tag{4.97}$$

$$\delta T^j_{\alpha i} = g_\alpha a^{-4} \int \mathrm{d}^3 p \, \frac{p^i p_j}{\sqrt{\vec{p}^{\,2} + m^2}} \bar{f}_\alpha(|\vec{p}|,\tau)\delta f_\alpha \,. \tag{4.98}$$

The evolution of the phase space distribution function is governed by the Boltzmann equation:

$$\frac{\mathrm{D}f_\alpha}{\mathrm{d}\tau} = \frac{\partial f_\alpha}{\partial \tau} + \frac{\mathrm{d}x^i}{\mathrm{d}\tau}\frac{\partial f_\alpha}{\partial x^i} + \frac{\mathrm{d}p^i}{\mathrm{d}\tau}\frac{\partial f_\alpha}{\partial p^i} = \left(\frac{\partial f_\alpha}{\partial \tau}\right)_C \,, \tag{4.99}$$

where the right hand side includes all terms due to interactions, which have to specified on a case by case basis. After a Fourier transformation to $\vec{k}$-space and removing the $\partial p^i/\partial\tau$-terms by employing a linearized version of the geodesic equation (2.8), one obtains the following linearized equation for the function $\delta f_\alpha(\vec{k},\vec{p},\tau)$

$$\frac{\partial \delta f_\alpha}{\partial \tau} + i\frac{\vec{k}\cdot\vec{p}}{\sqrt{\vec{p}^{\,2} + a^2 m^2}}\delta f_\alpha + \frac{\mathrm{d}\ln \bar{f}_\alpha}{\mathrm{d}\ln|\vec{p}|}\left[\Psi' - i\frac{\sqrt{\vec{p}^{\,2}+m^2}(\vec{p}\cdot\vec{k})}{\vec{p}^{\,2}}\Phi\right] = \frac{1}{\bar{f}_\alpha}\left(\frac{\partial f_\alpha}{\partial \tau}\right)_C \,, \tag{4.100}$$

where m is the particle mass of the species in question and the Fourier-space momenta $\vec{k}$ should not be confused with the physical momenta $\vec{p}$. Note that this equation depends on the physical three-momentum only through $|\vec{p}|$ and the product $\vec{k}\cdot\vec{p}$. Therefore any phase space distribution which is initially axially symmetric around $\vec{k}$ will remain so, and we will assume this to be the case. This is generally done in linear cosmic perturbation theory.

Now we specialize to neutrinos. We assume them to be massless in this work, meaning we can set $m = 0$. Furthermore they propagate freely after neutrino decoupling, thus the term $(\partial f_\nu/\partial\tau)_C$ vanishes. Since we assume that the phase space distribution function only depends on $|\vec{p}|$ and $\vec{k}\cdot\vec{p}$, we can expand it in Legendre polynomials:

$$F_\nu(\vec{k},\hat{e}_p,\tau) \equiv g_\nu \frac{\int \mathrm{d}p\, p^3 \bar{f}(p)\delta f(\vec{k},\vec{p},\tau)}{\int \mathrm{d}p\, p^3 \bar{f}(p)} = \sum_{l=0}^{\infty}(-i)^l(2l+1)F_{\nu l}(\vec{k},\tau)P_l\left(\frac{\vec{k}\cdot\vec{p}}{kp}\right) \,, \tag{4.101}$$

where $\hat{e}_p = \vec{p}/|\vec{p}|$, $k = |\vec{k}|$ and $p = |\vec{p}|$. A comparison to the perturbed energy momentum tensor (4.94) then quickly yields

$$\delta_\nu = \Delta_\nu + 4\Psi = \frac{1}{4\pi}\int \mathrm{d}\Omega F_\nu(\vec{k},\hat{e}_p,\tau) = F_{\nu 0} \,, \tag{4.102}$$

$$V_\nu = \frac{3i\mathcal{H}}{16\pi k^2}\int \mathrm{d}\Omega \left(\vec{k}\cdot\hat{e}_p\right) F_\nu(\vec{k},\hat{e}_p,\tau) = \frac{3\mathcal{H}}{4k}F_{\nu 1} \,, \tag{4.103}$$

$$\tilde{\Pi}_\nu = -\frac{9\mathcal{H}^2(1+\omega_\nu)}{32\pi k^2\omega_\nu}\int \mathrm{d}\Omega F_\nu(\vec{k},\hat{e}_p,\tau)\left[(\hat{e}_k\cdot\hat{e}_p)^2 - \frac{1}{3}\right] = \frac{3\mathcal{H}^2(1+\omega_\nu)}{4k^2\omega_\nu}F_{\nu 2} \,. \tag{4.104}$$

The evolution equations for the momenta $F_{\nu l}$ can now be obtained by plugging the Legendre-expansion into eq. (4.100) and comparing coefficients. This gives:

$$\Delta_\nu' = -\frac{4}{3}\frac{k^2}{\mathcal{H}}V_\nu\,, \tag{4.105}$$

$$V_\nu'/\mathcal{H} = +\frac{1}{4}\Delta_\nu - \frac{1}{2}F_{\nu 2} + \Psi + \Phi - \frac{1+3\omega_{\rm eff}}{2}V_\nu\,, \tag{4.106}$$

$$F_{\nu l}' = \frac{k}{2l+1}\left[lF_{\nu(l-1)} - (l+1)F_{\nu(l+1)}\right] \quad \text{for } l \geq 2\,. \tag{4.107}$$

Let us now move on to photons. The situation is somewhat similar to neutrinos, but with two important differences. First, photons are coupled to baryons through Thomson scattering with electrons before recombination (and strictly speaking after recombination as well, but very weakly). Thus the right hand side of eq. (4.100) is not zero for photons. Second, photons have two polarization states. This means we need to introduce two phase space distribution functions, one for the sum of the sum of the two linear polarization components and one for their difference. The momentum averaged versions of these distributions will be called F_γ and G_γ respectively, both functions can be expanded in a Legendre series (see eq. (4.101)). These will not evolve in the same way, as the Thomson cross section is polarization dependent. The linearized collision operators for the process of Thomson scattering were derived in [Bond and Efstathiou, 1984, 1987, Kosowsky, 1996] and rewritten in terms of Legendre-Polynomials in [Ma and Bertschinger, 1995]. The results read:

$$\left(\frac{\partial F_\gamma}{\partial \tau}\right)_C = an_e\sigma_T\left[\frac{4i\mathcal{H}}{k}(V_\gamma - V_b)P_1 + \left(\frac{9}{2}F_{\gamma 2} - \frac{1}{2}G_{\gamma 0} - \frac{1}{2}G_{\gamma 2}\right)P_2 - \sum_{l\geq 3}^{\infty}(-i)^l(2l+1)F_{\gamma l}P_l\right], \tag{4.108}$$

$$\left(\frac{\partial G_\gamma}{\partial \tau}\right)_C = an_e\sigma_T\left[\frac{1}{2}(F_{\gamma 2} + G_{\gamma 0} + G_{\gamma 2})(1-P_2) - \sum_{l\geq 0}^{\infty}(-i)^l(2l+1)G_{\gamma l}P_l\right], \tag{4.109}$$

where n_e is the mean electron density and $\sigma_T = 0.6652 \times 10^{-24}\mathrm{cm}^2$ is the integrated Thomson cross section. Plugging this into the linearized Boltzmann equation (4.100) gives the following evolution equations:

$$\Delta_\gamma' = -\frac{4}{3}\frac{k^2}{\mathcal{H}}V_\gamma\,, \tag{4.110}$$

$$V_\gamma'/\mathcal{H} = \frac{1}{4}\Delta_\gamma - \frac{1}{2}F_{\gamma 2} + \Psi + \Phi - \frac{1+3\omega_{\rm eff}}{2}V_\gamma + \frac{an_e\sigma_T}{\mathcal{H}}(V_b - V_\gamma)\,, \tag{4.111}$$

$$F_{\gamma 2}' = \frac{8}{15}\frac{k^2}{\mathcal{H}}V_\gamma - \frac{3}{5}kF_{\gamma 3} - \frac{9}{10}an_e\sigma_T F_{\gamma 2} + \frac{1}{10}an_e\sigma_T(G_{\gamma 0} + G_{\gamma 2})\,, \tag{4.112}$$

$$F'_{\gamma l} = \frac{k}{2l+1}\left[lF_{\nu(l-1)} - (l+1)F_{\nu(l+1)}\right] - an_e\sigma_T F_{\gamma l} \quad \text{for } l \geq 3\,, \tag{4.113}$$

$$G'_{\gamma l} = \frac{k}{2l+1}\left[lG_{\nu(l-1)} - (l+1)G_{\nu(l+1)}\right] + an_e\sigma_T\left[-G_{\gamma l} + \frac{1}{2}(F_{\gamma 2} + G_{\gamma 0} + G_{\gamma 2})\left(\delta_{l0} + \frac{\delta_{l2}}{5}\right)\right]. \tag{4.114}$$

The photon density contrast, velocity potential and anisotropic stress are related to the function F_γ by the same relations that hold for neutrinos (see equations (4.102) to (4.104)), the function G_γ does not enter here.

Finally we also have to add baryons. They are modeled by a barotropic fluid with $\omega_b = c^2_{\mathrm{tot},b} = c^2_{\mathrm{a},b} \ll 1$, $q_b = \tau_b = 0$ and a momentum transfer to photons which is given by

$$af_\gamma = -af_b = \frac{4}{3}\frac{\rho_\gamma}{\mathcal{H}} an_e\sigma_T\left(V_\gamma - V_b\right), \tag{4.115}$$

which follows from momentum conservation of the combined baryon-photon fluid. The equations of energy- and momentum conservation now read at the linear level (see eq. (4.48) and (4.49)):

$$\Delta'_b = -\frac{k^2}{\mathcal{H}}V_b\,, \tag{4.116}$$

$$V'_b = -\frac{3}{2}\mathcal{H}(1+\omega_{\mathrm{eff}})V_b + \mathcal{H}\Phi + \mathcal{H}c^2_{\mathrm{a},b}(\Delta_b + 3\Psi) + \frac{4}{3}\frac{\rho_\gamma}{\rho_b} an_e\sigma_T\left(V_\gamma - V_b\right), \tag{4.117}$$

where we dropped all terms of order $O(\omega_b, c^2_{\mathrm{a},b})$ except in the third term on the right hand side of the second equation, where it is the leading order contribution. The adiabatic sound speed can be calculated from

$$c^2_{\mathrm{a},b} = \frac{p'_b}{\rho'_b} = \frac{k_b T_b}{m_\mu}\left(1 - \frac{1}{3}\frac{\mathrm{d}\ln T_b}{\mathrm{d}\ln a}\right), \tag{4.118}$$

where m_μ is the mean molecular weight of the baryons, which can be assumed to be constant for the period of interest. Finally the baryon temperature follows the following evolution equation [Ma and Bertschinger, 1995]

$$T'_b = -2\mathcal{H}T_b + \frac{8}{3}\frac{m_\mu}{m_e}\frac{\rho_\gamma}{\rho_b} an_e\sigma_T(T_\gamma - T_b)\,, \tag{4.119}$$

where m_e is the electron mass.

4.2.2 TIGHT COUPLING APPROXIMATION

For sufficiently early times the electron density in the universe is very high, and therefore the inverse Thomson interaction timescale $\tau_c^{-1} \equiv an_e\sigma_T$ is huge. This causes numerical difficulties, which can be avoided through the so called *tight coupling approximation* (TCA). We will now discuss this scheme.

First, after some algebra, one can eliminate τ_c^{-1} from equations (4.111) and (4.117) to obtain

$$V_b' = \frac{-1}{1+R}\left[\frac{3}{2}(1+\omega_{\rm eff})\mathcal{H}V_b - c_{{\rm a},b}^2\mathcal{H}(\Delta_b+3\Psi) - \mathcal{H}\Phi \right.$$
$$\left. - R\left(\frac{-(1+3\omega_{\rm eff})}{2}\mathcal{H}V_\gamma + \mathcal{H}\Phi + \frac{1}{4}\mathcal{H}\Delta_\gamma + \mathcal{H}\Psi - \frac{1}{6}\frac{k^2}{\mathcal{H}}\tilde{\Pi}_\gamma\right) + RV_{\gamma b}'\right], \tag{4.120}$$

$$V_\gamma' = -\frac{1}{2}(1+3\omega_{\rm eff})\mathcal{H}V_\gamma + \frac{1}{4}\mathcal{H}\Delta_\gamma + \mathcal{H}(\Psi+\Phi) - \frac{1}{6}\frac{k^2}{\mathcal{H}}\tilde{\Pi}_\gamma$$
$$- \frac{1}{R}\left[V_b' + \frac{3}{2}(1+\omega_{\rm eff})\mathcal{H}V_b - \mathcal{H}\Phi - c_{{\rm a},b}^2\mathcal{H}(\Delta_b+3\Psi)\right], \tag{4.121}$$

where we introduced $R = 4\rho_\gamma/3\rho_b$ and the baryon-photon slip $V_{\gamma b} = V_\gamma - V_b$. The TCA now consists of finding approximations for the anisotropic stress $\tilde{\Pi}_\gamma$ and the derivative $V_{\gamma b}'$ to the desired order in $\varepsilon = \mathcal{H}\tau_c \ll 1$. These quantities are governed by the following evolution equations:

$$\tau_c\tilde{\Pi}_\gamma' = \mathcal{H}\tau_c\left(\frac{8}{5}V_\gamma - \frac{9}{5}\frac{\mathcal{H}}{k}F_{\gamma 3}\right) + \frac{3}{10}\frac{\mathcal{H}^2}{k^2}(G_{\gamma 0}+G_{\gamma 2}) - \left(\frac{9}{10} + (1+3\omega_{\rm eff})\mathcal{H}\tau_c\right)\tilde{\Pi}_\gamma = 0\,, \tag{4.122}$$

$$\tau_c V_{\gamma b}' = -\mathcal{H}\left[\left(\frac{3}{2}(1+\omega_{\rm eff})+R\right)V_{\gamma b} - V_b - \frac{1}{4}\Delta_\gamma - \Psi + c_{{\rm a},b}^2(\Delta_b+3\Psi)\right] - \frac{1}{6}k^2\tau_c\tilde{\Pi}_\gamma = 0\,. \tag{4.123}$$

A look at the equations for the higher momenta $G_{\gamma l}$ and $F_{\gamma l}$ (see equations (4.114)) shows that $G_{\gamma 0}$ and $G_{\gamma 2}$ are of order $O(\varepsilon)$ and $F_{\gamma 3}$ is of order $O(\varepsilon^2)$, and thus both equations can be written in the form

$$\varepsilon y' + y/f + \varepsilon g = 0\,. \tag{4.124}$$

The solution to this equation (to any order in ε) is then given by [Blas et al., 2011]

$$y = \sum_{n=1}^{\infty}\varepsilon^n y_n \quad \text{with} \quad y_1 = -fg, \quad y_{n+1} = -fy_n'\,, \tag{4.125}$$

where we ignored a solution of the homogeneous differential equation which is decaying quickly for $f > 0$, a condition that is guaranteed for both equations.

To zeroth order we simply have $\tilde{\Pi}_\gamma = V_{\gamma b} = 0$. In this case $V_\gamma = V_b$ and the evolution equations (4.120) and (4.121) coincide. To first order one obtains

$$\tilde{\Pi}_\gamma = \frac{3\mathcal{H}^2}{k^2}F_{\gamma 2} = \frac{32}{15}\mathcal{H}\tau_c V_\gamma\,, \tag{4.126}$$

$$\frac{V_{\gamma b}'}{\mathcal{H}} = \frac{2R}{1+R}V_{\gamma b} + \frac{\mathcal{H}\tau_c}{1+R}\left[\frac{k^2}{\mathcal{H}^2}\left(c_{{\rm a},b}^2 V_b - \frac{1}{3}V_\gamma\right) + \frac{\Delta_\gamma}{2} + \frac{\Psi'}{\mathcal{H}} + \frac{(1-3\omega_{\rm eff})}{2}V_b + \Phi\right]. \tag{4.127}$$

For higher order solutions one needs to consider the evolution of the higher momenta $G_{\gamma l}$ and $F_{\gamma l}$ to subleading order, which requires some additional analysis. Second order results (in synchronous gauge) can be found in [Blas et al., 2011], but we will not use them for our numerics. The advantage of higher order approximations lies in the fact that they allow the TCA to be used to later times without losing accuracy, thereby improving the runtime of the Boltzmann code.

4.2.3 RELATIVISTIC FLUID APPROXIMATION

The infinite hierarchy for the momenta of the phase space distribution function for relativistic particles needs to be truncated at some $l_{\max}$. The truncation schemes (which we will describe below) work well only for times $\tau < l_{\max}/k$, which means that in order to gain sufficient accuracy for large k we need very high values of $l_{\max}$. This is computationally expensive. It is thus advantageous to employ approximations for late times which effectively decrease the number $l_{\max}$. The first one we employ is the *ultrarelativistic fluid approximation* (UFA), as introduced in [Blas et al., 2011]. This scheme is based on the fact that the collisionless Boltzmann equation for the massless neutrino phase space distribution function takes the following form in Fourier space:

$$\partial_\tau F_\nu(\vec{k},\hat{e}_p,\tau) + i\vec{k}\cdot\hat{e}_p F_\nu(\vec{k},\hat{e}_p,\tau) = 4\left(\Psi' - i\vec{k}\cdot\hat{e}_p\Phi\right). \tag{4.128}$$

After an expansion in Legendre-Polynomials (see eq. (4.101)) the formal solution for the coefficients can be shown to be

$$F_{\nu l}(\vec{k},\tau) = \alpha(\vec{k})\, j_l(k\tau) + \beta(\vec{k})\, j_l'(k\tau) - 4\Phi\delta_{l0} + 4\int_0^\tau j_l(k(\tau-\tilde{\tau}))(\Psi'+\Phi')\mathrm{d}\tilde{\tau}, \tag{4.129}$$

$$\alpha(\vec{k}) - i(\hat{e}_k\cdot\hat{e}_p)\beta(\vec{k}) = F_\nu(\vec{k},\hat{e}_p,0) + 4\Phi|_{\tau=0}. \tag{4.130}$$

The real coefficients $\alpha(\vec{k})$ and $\beta(\vec{k})$ characterize the initial conditions and change according to which modes are assumed to present. This formal solution is exact, we can use it to derive an integro-differential equation which will contain F_l', F_m for $m \leq l$ and the gravitational potentials Ψ and Φ:

$$\begin{aligned}(F_{\nu l} + 4\Phi\delta_{l0})' &= k\left(F_{\nu(l-1)} + 4\Phi\delta_{(l-1)0}\right) - \frac{l+1}{\tau}\left(F_{\nu l} + 4\Phi\delta_{l0}\right) + \beta\frac{l+1}{k\tau^2}j_l(k\tau) \\ &+ 4\left(\Psi' - \frac{l+1}{\tau}\Phi\right)\delta_{l0} + 4k\Phi\delta_{l1} - 4\frac{l+1}{\tau}\int_0^\tau \frac{\tilde{\tau}}{\tau-\tilde{\tau}} j_l(k(\tau-\tilde{\tau}))(\Psi'+\Phi')\mathrm{d}\tilde{\tau}.\end{aligned} \tag{4.131}$$

The task now is to approximate the remaining integral. On subhorizon scales and for low l, the convolution of the Bessel function with the metric perturbations picks up its dominant contribution only near the peak of the Bessel function, i.e. for $\tilde{\tau}$ close to τ. For these late times the metric perturbations evolve very slowly on a timescale $1/k \ll \tau$, and we can thus approximate them as constant (i.e. $\Phi'(\tilde{\tau}) \to \Phi'(\tau)$, $\Psi'(\tilde{\tau}) \to \Psi'(\tau)$). Now we can solve the integral an obtain for $l = 2$:

$$F_{\nu 2}' = \frac{4}{3}\frac{k^2}{\mathcal{H}}V_\nu - \frac{3}{\tau}F_{\nu 2} - 6(\Psi'+\Phi'). \tag{4.132}$$

This approximation takes into account the transfer of power from higher to lower momenta to some extent, but of course not completely. It is however accurate enough for our purposes.

4.2.4 RADIATION STREAMING APPROXIMATION

For sufficiently late times and on subhorizon scales, the perturbations of relativistic species perform rapid oscillations which are numerically expensive to resolve. We will therefore employ a second

approximation scheme for these late times, called *radiation streaming approximation* (RSA). This approximation effectively reduces all relativistic perturbative degrees of freedom from the set of equations. Let us start with the neutrinos. For sufficiently late times we can ignore the anisotropic stress and all higher momenta of the phase space distribution function and derive a second order equation for Δ_ν from equations (4.105) and (4.106). Demanding for the averaged density contrast that $|\Delta_\nu''| \ll |k^2\Delta_\nu|$, one directly obtains

$$\Delta_\nu = -4\Phi - 4\Psi\,. \tag{4.133}$$

Using eq. (4.105) we can infer the value of V_ν from this approximation. Through differentiation one obtains

$$V_\nu = 3\frac{\mathcal{H}}{k^2}(\Psi' + \Phi')\,, \tag{4.134}$$

which can be neglected on subhorizon scales. Thus the RSA for neutrinos simply consists of replacing the density contrast by equation (4.133) and setting the velocity potential to zero in the equations for the gravitational potentials.

The situation for baryons is slightly more complicated, because the Thomson interaction terms can become relevant again during reionization. Still, for sufficiently late times we have $\mathcal{H}\tau_c \gg 1$ and we can employ an approximation valid to first order in $(\mathcal{H}\tau_c)^{-1}$. To zeroth order the replacement for photons would correspond precisely to the one for neutrinos given above. For the first order we can investigate the second order equation for the density contrast Δ_γ (from eq. (4.110) and eq. (4.111)) and obtain after replacing V_γ in the coupling terms by the zeroth order approximation (and again ignoring anisotropic stress)

$$\Delta_\gamma = -4\Psi - 4\Phi - \frac{4}{\mathcal{H}\tau_c}V_b\,. \tag{4.135}$$

We can again recover the corresponding first order approximation for V_γ through eq. (4.110), which gives (after replacing the derivative V_b' to the relevant order)

$$V_\gamma = 3\frac{\mathcal{H}}{k^2}\left(\Phi' + \Psi' + \frac{1}{\mathcal{H}\tau_c}\left[-\mathcal{H}V_b + \mathcal{H}\Phi + \mathcal{H}c_{\mathrm{a},b}^2(\Delta_b + 3\Psi) - \frac{\tau_c'}{\tau_c}V_b\right]\right)\,. \tag{4.136}$$

We should note that ignoring the anisotropic stress terms for both photons and neutrinos means that $\Phi = \Psi$, but we kept both gravitational potentials implicit in all the equations, so that they would remain valid in a model introducing additional anisotropic stress.

As a final comment we want to note that the matter power spectrum, which is the quantity we will be ultimately after, is much more sensitive to the RSA approximation than the C_ls of the CMB [Blas et al., 2011]. We will therefore be somewhat conservative in our choices of onset triggers for this approximation (see below).

4.3 Cosmon and bolon

In this section we want to analyze perturbations in the coupled cosmon-bolon system. The equations governing the evolution of perturbations are, on a fundamental level, the scalar field equations (4.35)

and (4.36), with the scalar potential given by

$$V(\varphi,\chi) = V_1(\varphi) + V_2(\varphi,\chi)\,, \tag{4.137}$$

where we leave the precise shape of the quintessence potential V_1 undetermined for now. The full form of the bolon potential is given by eq. (3.93), we are, however only, interested in late time perturbations in this section, which means that it can be approximated by

$$V_2(\varphi,\chi) = m_\chi(\varphi)^2\chi^2\,, \quad \text{with} \quad m_\chi(\varphi)^2 = m_0^2 \mathrm{e}^{-2\beta\varphi/M_p}\,, \tag{4.138}$$

where $m_0^2 = c^2 M_p^2 \lambda^2$. As we have already discussed in chapter 3, the evolution of the scalar fields will naturally transition to a regime where $\mathcal{H}/am_\chi(\varphi) \ll 1$, during which the bolon will oscillate quickly around the minimum of its potential. In this section we derive averaged effective equations for the relevant background and perturbative quantities for this stage of the evolution, which allow us to implement this model into our Boltzmann code with acceptable runtimes. We make a list of assumptions here:

- We do not specify the quintessence potential V_1 explicitly during this analysis. As will become apparent below, any quintessence potential which satisfies $V_{1,\varphi\varphi} \ll m_\chi(\varphi)^2$ during the relevant stages of the cosmic evolution can be inserted. This should be a generic feature of all quintessence potentials giving rise to a realistic dark energy scenario.
- We will explicitly assume that baryons, photons and neutrinos are present in addition to the scalar fields below, however, any additional component not explicitly coupled to the scalar fields can in principe be added to these equations, as long as the relevant mass scales introduced into the perturbation equations are much less than the bolon mass $m_\chi(\varphi)$.
- Finally, our analysis does not work for arbitrarily large wavenumbers, but the range is more than sufficient to cover the observable scales.

The derivation is rather technical, so let us declare what we are aiming for. The important results are equations (4.152), (4.159) and (4.160), which show that the treatment of the cosmon-bolon system as coupled quintessence is justified for sufficiently late times at the background level, and equations (4.193), (4.200) to (4.202) and (4.226) to (4.227), which provide an effective fluid description for the cosmon-bolon model at late times and have, as far as we know, not been studied before.

4.3.1 EFFECTIVE THEORY NEAR THE MINIMUM

Let us now move on to average the equations. The method we employ is in principle very simple: We make use of the fact that the ratio $\mu = \mathcal{H}/am_\chi(\varphi)$ is tiny, and therefore we should be able to expand the solution as a Taylor-series in μ. Essentially the same ansatz was used to treat a single scalar field in a harmonic potential (see e.g. [Gorbunov and Rubakov, 2011a]), we will now generalize it to our coupled scenario. Other approaches in the literature do exist, but they do not lend themselves well to a generalization to coupled scalar field models [Matos and Urena-Lopez, 2001].

The basic idea is to first expand all dynamical quantities in a Taylor-series in $\tilde{\mu} = \mathcal{H}_0/m_0$. Since $\tilde{\mu} = \mu e^{-\beta\varphi/M_p} a\mathcal{H}_0/\mathcal{H}$, this quantity is always smaller than μ for $a < 1$, but has the advantage of being time-independent. To give an example, the bolon-field χ can be expanded as follows:

$$\chi = \sum_j \tilde{\mu}^j \chi_j \,. \tag{4.139}$$

We then segment all the Taylor-Coefficients χ_j into a Fourier-type sum, given by

$$\chi_j = \sum_{n\in\mathbb{N}} \chi_{j1,n}\cos(nx) + \chi_{j2,n}\sin(nx)\,, \tag{4.140}$$

with $n \in \mathbb{N}$. Here the coefficients $\chi_{i1,n}$ and $\chi_{i2,n}$ are of course time-dependent, but are evolving slowly, i.e. remain almost constant at a time scale $1/m_\chi(\varphi)$. The oscillation frequencies are also time-dependent and given by multiples of the base frequency

$$x(\tau) = \int_{t_0}^{t(\tau)} m_\chi(\varphi(t'))dt'\,, \tag{4.141}$$

with t being the cosmic time and t_0 being some suitable early time, chosen such that any phase potentially appearing in the trigonometric functions gets cancelled. The whole expression should of course be read as a function of conformal time. We should not that there is a priori no guarantee that the expansion (4.140) is valid. However, as we will see explicitly below, it does provide a solution to the field equations to subleading order in $\tilde{\mu}$, which is what we are interested in.

Background

Let us start with the background evolution and quickly recall the relevant equations. The scalar fields obey the scalar field equations

$$\varphi'' + 2\mathcal{H}\varphi' + V_{,\varphi} = 0\,, \quad \chi'' + 2\mathcal{H}\chi' + V_{,\chi} = 0\,, \tag{4.142}$$

and we use the Friedmann-equations

$$\mathcal{H}^2 = \frac{a^2}{3M_p^2}\sum_\alpha \rho_\alpha\,, \quad \mathcal{H}' = -\frac{a^2}{6M_p^2}\sum_\alpha (\rho_\alpha + 3p_\alpha)\,. \tag{4.143}$$

We assign the scalar energy density and pressure as follows:

$$\rho_\varphi = \frac{1}{2a^2}\varphi'^2 + V_1(\varphi)\,, \quad \rho_\chi = \frac{1}{2a^2}\chi'^2 + V_2(\varphi,\chi)\,, \tag{4.144}$$

$$p_\varphi = \frac{1}{2a^2}\varphi'^2 - V_1(\varphi)\,, \quad p_\chi = \frac{1}{2a^2}\chi'^2 - V_2(\varphi,\chi)\,. \tag{4.145}$$

Furthermore we combine all other constituents of the cosmic fluid into a single component with energy density $\rho_{\rm ext}$ and (time-dependent) equation of state $\omega_{\rm ext}$.

Now we simply put the most general ansatz into the equations and compare coefficients, with the aim to find out which terms in the Fourier expansion need to be present at which order in $\tilde{\mu}$ in order to find a solution. This yields the following decomposition for the scalar fields:

$$\chi = \chi_0 \cos(x) + \chi_1 \sin(x) + \chi_2 \cos(3x) + \chi_{\rm ig}\,, \tag{4.146}$$

$$\varphi = \bar{\varphi} + \varphi_1 \cos(2x) + \varphi_2 \sin(2x) + \varphi_{\rm ig}\,, \tag{4.147}$$

and consistency requires that χ_1 is of the order $O(\tilde{\mu}\chi_0)$, χ_2 is of the order $O(\tilde{\mu}^2\chi_0)$, φ_1 is of the order $O(\tilde{\mu}^2\bar{\varphi})$ and φ_2 is of the order $O(\tilde{\mu}^3\bar{\varphi})$. The leading order contributions are formally related by setting χ_0 to be of the order $O(\tilde{\mu}\bar{\varphi})$, so that the energy densities for both scalar fields are of the same order, as is appropriate for a scaling quintessence scenario. The terms $\chi_{\rm ig}$ and $\varphi_{\rm ig}$ represent higher order contributions, they will not play a role in our analysis.

We introduced a notation here which we will keep consistently throughout this section: For all quantities which are slowly evolving to leading order we will mark the leading order quantity with a bar (like $\bar{\varphi}$ above). This will turn out to be helpful in the final equations, where we will also encounter quantities averaged over one oscillation period, which we will indicate using triangular brackets: $< . >$. This may seem unnecessary, since of course $\bar{\varphi} =< \varphi >$ holds, but we find it useful to make this distinction in order to indicate quantities which evolve adiabatically at leading order.

The oscillatory terms present in (4.146) and (4.147) do of course leave an imprint on the scale factor and we can deduce from Einsteins equations that the expansion for $a(\eta)$ reads

$$a = \bar{a} + a_{\rm osc} + a_{\rm ig}\,, \tag{4.148}$$

where $a_{\rm osc}$ is of the order $O(\tilde{\mu}^2\bar{a})$ and $a_{\rm ig}$ represents higher order contributions which will not concern us. For the conformal Hubble rate this directly implies

$$\mathcal{H} = \bar{\mathcal{H}} + \mathcal{H}_{\rm osc} + \mathcal{H}_{\rm ig}\,, \quad \text{where} \quad \mathcal{H}_{\rm osc} = \frac{a'_{\rm osc}}{\bar{a}}\,. \tag{4.149}$$

It is important to note that taking the derivative of an oscillatory quantity decreases the order in $\tilde{\mu}$ by one and therefore $\mathcal{H}_{\rm osc}$ is of order $O(\tilde{\mu}\bar{\mathcal{H}})$ ($\mathcal{H}_{\rm ig}$ again stands for higher order terms which we ignore). For the dimensionless coupling parameter q_χ the expansion directly gives

$$(1+\omega_\chi) q_\chi = -\beta \frac{\bar{\varphi}'}{3\bar{\mathcal{H}} M_p} \left(1 + \cos(2x)\right) \tag{4.150}$$

to leading order. Averaging this expression over one oscillation period gives:

$$< (1+\omega_\chi) q_\chi >= -\beta \frac{\bar{\varphi}'}{3\bar{\mathcal{H}} M_p}\,. \tag{4.151}$$

With these solutions we directly obtain from Friedmann's equation to leading order

$$\bar{\mathcal{H}}^2 = \frac{\bar{a}^2}{3M_p^2}\left(\bar{\rho}_\chi + \bar{\rho}_\varphi + \bar{\rho}_{\rm ext}\right)\,, \tag{4.152}$$

where $\bar{\rho}_\chi$ and $\bar{\rho}_\varphi$ denote the (non-oscillatory) leading order contributions to the bolon- and cosmon energy-densities, respectively. These are given by

$$\bar{\rho}_\chi = \frac{1}{2}\bar{m}_\chi^2(\bar{\varphi})\chi_0^2, \tag{4.153}$$

$$\bar{\rho}_\varphi = V_1(\bar{\varphi}) + \frac{1}{2\bar{a}^2}\bar{\varphi}'^2, \tag{4.154}$$

where $\bar{m}_\chi(\bar{\varphi})$ simply denotes the leading order term in the $\tilde{\mu}$-expansion for the mass, which is of course only $\bar{\varphi}$-dependent:

$$\bar{m}_\chi(\bar{\varphi}) = m_0 e^{-\beta\bar{\varphi}/M_p}. \tag{4.155}$$

Starting here we will drop the explicit $\bar{\varphi}$-dependence of $\bar{m}_\chi$ in all the formulas.

Before moving on, a short comment concerning the additional components of the cosmic fluid might be in order. We assume ρ_{ext} and ω_{ext} evolve adiabatically to subleading order on a timescale $1/\bar{m}_\chi$. This is consistent with the equations of energy conservation for all standard cosmological components to the order which we consider here:

$$\rho'_{\text{ext}} + 3\mathcal{H}(1+\omega_{\text{ext}})\rho_{\text{ext}} = 0. \tag{4.156}$$

The conformal Hubble rate introduces oscillations into this equation only at subleading order, which means they are present in ρ_{ext} only to subsubleading order, which does not concern us.

Evaluating the scalar field equations with the above expansion gives:

$$\chi_0' = -\frac{3}{2}\bar{\mathcal{H}}\chi_0 + \frac{\beta}{2}\frac{\chi_0}{M_p}\bar{\varphi}', \tag{4.157}$$

$$\varphi_1 = -\frac{\beta}{8}\frac{\chi_0^2}{M_p}, \tag{4.158}$$

$$\bar{\varphi}'' = -2\bar{\mathcal{H}}\bar{\varphi}' - \bar{a}^2 V_{1,\bar{\varphi}} + \frac{\beta}{M_p}\bar{a}^2\bar{\rho}_\chi. \tag{4.159}$$

From eq. (4.157) we can directly see that $\ln(\chi_0) \propto \ln(\bar{a}^{-3/2}) + \frac{\beta}{2}\frac{\bar{\varphi}}{M_p}$, i.e. $\chi_0 \propto \bar{a}^{-3/2}\exp(\beta\bar{\varphi}/2M_p)$ and therefore

$$\bar{\rho}_\chi \propto \bar{a}^{-3}\exp(-\beta\bar{\varphi}/M_p), \tag{4.160}$$

which is the standard evolution of cold dark matter coupled to quintessence we already discussed in chapter 3.

While not being particularly relevant at the background level, in order to obtain averaged evolution equations for the perturbations we need the next to leading order equations. Using the above results we get from Einsteins equations

$$\mathcal{H}_{\text{osc}} = \frac{1}{8}\bar{a}\bar{m}_\chi\frac{\chi_0^2}{M_p^2}\sin(2x), \quad a_{\text{osc}} = -\frac{1}{16}\bar{a}\frac{\chi_0^2}{M_p^2}\cos(2x), \tag{4.161}$$

and the field equation for the bolon gives at this order

$$\chi_2 = \frac{3}{128}\frac{\chi_0^3}{M_p^2}\left(1-\frac{2}{3}\beta^2\right), \tag{4.162}$$

$$\chi_1' = -\left(\frac{3}{2}\bar{\mathcal{H}} - \frac{\beta}{2}\frac{\bar{\varphi}'}{M_p}\right)\chi_1 - \frac{1}{2\bar{m}_\chi\bar{a}}\left(\chi_0'' + 2\bar{\mathcal{H}}\chi_0'\right) + \frac{3-2\beta^2}{32M_p^2}\bar{m}_\chi\bar{a}\chi_0^3. \tag{4.163}$$

Finally the cosmon field equation gives

$$\varphi_2 = -\frac{\chi_0}{16\bar{m}_\chi\bar{a}M_p}\left(4\beta\bar{m}_\chi\bar{a}\chi_1 - 2\beta\bar{\mathcal{H}}\chi_0 - \chi_0\bar{\varphi}'/M_p\right). \tag{4.164}$$

Linear Perturbations

We will now extend the procedure given above to the linear perturbations. The aim to construct effective perfect fluid equations, which arise from the scalar field equations after averaging over one oscillation period. The final set of equations should be accurate to subleasing order in $\tilde{\mu}$ and we thus have to careful to consider all interference effects, because at this order the background quantities no longer evolve adiabatically.

Our starting point are the exact gauge-invariant linearly perturbed scalar field equations which we now briefly recall:

$$X'' + 2\mathcal{H}X' + k^2X + a^2V_{,\varphi\varphi}X + a^2V_{,\varphi\chi}Y + 2a^2V_{,\varphi}\Phi - \varphi'\Phi' - 3\varphi'\Psi' = 0, \tag{4.165}$$

$$Y'' + 2\mathcal{H}Y' + k^2Y + a^2V_{,\varphi\chi}X + a^2V_{,\chi\chi}Y + 2a^2V_{,\chi}\Phi - \chi'\Phi' - 3\chi'\Psi' = 0. \tag{4.166}$$

We also employ the Poisson equation

$$k^2\Psi = -\frac{a^2}{2M_p^2}\sum_\alpha\left(\delta\rho_\alpha - 3h[(\rho+p)v]_\alpha\right), \tag{4.167}$$

and relate the two gravitational potentials via

$$\Phi = \Psi - 3\omega_{\rm eff}\tilde{\Pi}_{\rm tot}, \tag{4.168}$$

with $\tilde{\Pi}_{\rm tot} = \sum p_\alpha\tilde{\Pi}_\alpha/p_{\rm tot}$. Even though scalar fields do not produce anisotropic stress, we differentiate between Ψ and Φ, since anisotropic stress can be introduced through neutrino- and photon-contributions. The equations for the momenta of the corresponding phase space distribution functions (possibly in some approximation) have to be added to the system in order to complete it, the same holds for the equations of energy- and momentum-conservation for baryons.

The remaining Einstein equations are not necessary to analyze the evolution of linear perturbations, but they can provide useful trivial checks of the calculations. We will employ equation (4.26) several times, as it simplifies some steps. Using equation (4.168) it reads:

$$\Psi' + \mathcal{H}\Psi = -\frac{a^2}{2M_p^2}\sum_\alpha[(\rho+p)v]_\alpha + 3\mathcal{H}\omega_{\rm eff}\tilde{\Pi}_{\rm tot}. \tag{4.169}$$

As we will see below, the combined Taylor-Fourier expansion required to solve the perturbation equations at subleading order looks different depending on the size of the wavenumber k and we have to split up our analysis into two regimes: Large wavelength perturbations for which $\mu k^2/\mathcal{H}^2 \ll 1$ and small wavelength perturbations which have $\mu k^2/\mathcal{H}^2 \gtrsim 1$.

a) $\mu k^2/\mathcal{H}^2 \ll 1$

For large wavelengths the only consistent expansion in terms of trigonometric functions is given by

$$X = P + Q\cos(2x) + R\sin(2x) + X_{\rm ig}\,, \tag{4.170}$$

$$Y = A\cos(x) + B\sin(x) + C\sin(3x) + Y_{\rm ig}\,, \tag{4.171}$$

$$\Psi = \bar{\Psi} + \Psi_{\rm osc} + \Psi_{\rm ig}\,. \tag{4.172}$$

The linearized field equations require Q to be of the order $O(\tilde{\mu}^2 P)$, R to be of order $O(\tilde{\mu}P)$, A to be of order $O(\tilde{\mu}B)$, C to be of order $O(\tilde{\mu}^2 B)$, $\Psi_{\rm osc}$ to be of order $O(\tilde{\mu}\bar{\Psi})$ and finally P to be of order $O(B)$ and $\bar{\Psi}$ to be of order $O(B/M)$. The terms $X_{\rm ig}$, $Y_{\rm ig}$ and $\Psi_{\rm ig}$ again represent higher order contributions which we ignore.

As for the background, the presence of additional non-scalar field components may merit some additional discussion. We always assume that all additional energy density perturbations, i.e. the ones for photons, neutrinos and baryons, evolve slowly to leading order in $\tilde{\mu}$ on a timescale $1/\bar{m}_\chi$, the corresponding momentum perturbations and the higher momenta in the multipole-expansion of the Boltzmann-equations for photons and neutrinos even to subleading order. We emphasize that this is consistent with all the evolution equations for non-scalar field quantities, since the quick oscillations only enter these indirectly through the background and the gravitational potentials. To make this more precise, simply not that we can combine all non scalar quantities into a single fluid with $q_{\rm ext} = \tau_{\rm ext} = f_{\rm ext} = 0$. For such a fluid eq. (4.32) directly shows that $\delta\rho_{\rm ext}$ is evolving adiabatically at leading order, wheres eq. (4.33) guarantees that this is the case for $[(\rho + p)v]_{\rm ext}$ at subleading order. The same holds for the higher momenta of the photon- and neutrino phase space distribution function, as can be directly seen from the equations presented in the previous section. This reasoning is of course only justified as long as $k \ll \bar{m}_\chi$, because the only additional energy-scales present in the equations are the Hubble parameter and the wavenumber, both of which are much smaller than the bolon mass. Thus our approximation breaks down for very large wavenumbers, but this does not concern us. The range of validity is big enough to cover all relevant scales.

As scalar fields do not produce anisotropic stress, this reasoning directly implies that Φ can be expanded just as Ψ

$$\Phi = \bar{\Phi} + \Phi_{\rm osc} + \Phi_{\rm ig}\,, \tag{4.173}$$

where the terms are related by

$$\bar{\Phi} = \bar{\Psi} - 3\omega_{\rm eff}\bar{\tilde{\Pi}}_{\rm tot} \quad \text{and} \quad \Phi_{\rm osc} = \Psi_{\rm osc}\,. \tag{4.174}$$

Evaluating the scalar field equations (4.165) and (4.166) to leading order gives

$$B' = \bar{a}\bar{m}_\chi\chi_0(\beta P/M_p - \bar{\Phi}) - \frac{1}{2}B(3\bar{\mathcal{H}} - \beta\bar{\varphi}'/M_p)\,, \tag{4.175}$$

$$R = -\frac{\beta}{4}B\chi_0/M_p\,, \tag{4.176}$$

while the Poisson equation (4.167) yields

$$\begin{aligned}\bar{\Psi} = \frac{-\bar{a}^2}{2k^2M_p^2 - \bar{\varphi}'^2}\Big(&\overline{\delta\rho}_{\rm ext} - 3\bar{\mathcal{H}}\overline{[(\rho+p)v]}_{\rm ext} + \bar{m}_\chi^2 A\chi_0 - \frac{3}{2}\bar{m}_\chi\frac{\bar{\mathcal{H}}}{\bar{a}}B\chi_0 + \bar{m}_\chi^2\chi_1 B \\ &+ V_{1,\bar{\varphi}}P - \beta\bar{m}_\chi^2\chi_0^2\frac{P}{M_p} + 3\frac{\bar{\mathcal{H}}\bar{\varphi}'}{\bar{a}^2}P + \frac{\bar{\varphi}'P'}{\bar{a}^2} + 3\omega_{\rm eff}\frac{\bar{\varphi}'^2}{a^2}\tilde{\bar{\Pi}}_{\rm tot}\Big)\,.\end{aligned} \tag{4.177}$$

We need to go to subleading order, however, as will become apparent from the results below. From the Poisson equation we then obtain

$$\Psi_{\rm osc} = \frac{1}{8}\frac{\chi_0 B}{M_p^2}\sin(2x)\,. \tag{4.178}$$

Note that this expression is most easily obtained by evaluating equation (4.169) to leading order, instead of going to next to leading order in the Poisson equation. Both ways are of course equivalent, and we did both calculations in order to verify our results.

From the bolon field equation we get at this order

$$\begin{aligned}A' = &-\frac{3}{2}\bar{\mathcal{H}}A - \frac{3}{32}\bar{a}\bar{m}_\chi\frac{\chi_0^2}{M_p^2}B + \bar{a}\bar{m}_\chi\chi_1\bar{\Phi} + \frac{\bar{\mathcal{H}}}{\bar{a}\bar{m}_\chi}B' + \frac{1}{2\bar{m}_\chi\bar{a}}B'' + \frac{k^2}{2\bar{a}\bar{m}_\chi}B \\ &+ \frac{\beta^2}{16}\bar{a}\bar{m}_\chi\frac{\chi_0^2}{M_p^2}B - \beta\bar{a}\bar{m}_\chi\frac{\chi_1}{M_p}P + \frac{\beta}{2}\frac{\bar{\varphi}'A}{M_p}\,,\end{aligned} \tag{4.179}$$

$$C = \frac{13+2\beta^2}{128}\frac{\chi_0^2}{M_p^2}B\,, \tag{4.180}$$

whereas the cosmon field equation gives

$$Q = -\frac{\chi_0\bar{\varphi}'}{4\bar{a}\bar{m}_\chi M_p^2}\left(1+\frac{\beta^2}{2}\right)B - \frac{\beta}{4}\left(\frac{\chi_0}{M_p}A - \frac{\chi_1}{M_p}B\right) + \frac{3\beta}{8}\frac{\bar{\mathcal{H}}}{\bar{a}\bar{m}_\chi}\frac{\chi_0}{M_p}B\,, \tag{4.181}$$

$$\begin{aligned}P'' = &-2\bar{\mathcal{H}}P' - k^2P - \bar{a}^2V_{1,\bar{\varphi}\bar{\varphi}}P - 2\bar{a}^2V_{1,\bar{\varphi}}\bar{\Phi} + \bar{\varphi}'\bar{\Phi}' + 3\bar{\varphi}'\bar{\Psi}' \\ &+ \beta\bar{a}^2\bar{m}_\chi^2\left(\frac{\chi_0}{M_p}A + \frac{\chi_1}{M_p}B\right) - \beta^2\bar{a}^2\bar{m}_\chi^2\frac{\chi_0^2}{M_p^2}P + \beta\bar{a}^2\bar{m}_\chi^2\frac{\chi_0^2}{M_p}\bar{\Phi}\,.\end{aligned} \tag{4.182}$$

At this point we are ready to write down the effective averaged fluid equations for the bolon. We could in prinicple do the same for the cosmon, but it is more common to treat the cosmon field perturbations directly and we will adopt the same approach here. We have already seen in section 4.1 how the scalar field perturbations can be mapped directly onto a fluid description with an energy density perturbation, a pressure perturbation and a momentum perturbation. We can thus use the

above subleading order solutions, plug them into the fluid evolution equations and average them term by term, taking care to treat the interference terms between the background and the perturbations correctly. As it turns out, all such interference terms cancel precisely, and we could thus simply have averaged the fluid quantities and use the equations with adiabatically evolving background quantities, but that is not clear a priori.

Let us start by calculating the averaged perturbative fluid quantities for the bolon to subleading order:

$$< \delta\rho_\chi >= \bar{m}_\chi^2 (\chi_0 A + \chi_1 B) - 2\beta\bar{\rho}_\chi \frac{P}{M_p}, \tag{4.183}$$

$$< \delta p_\chi >= 0, \tag{4.184}$$

$$< [(\rho + p)v]_\chi >= \frac{\bar{m}_\chi \chi_0}{2\bar{a}} B. \tag{4.185}$$

Note that all these quantities have oscillatory contributions at leading order. Now we average over the equation of energy conservation for the bolon term by term to obtain:

$$< 3\mathcal{H}\delta\rho_\chi >= 3\bar{\mathcal{H}} < \delta\rho_\chi >, \tag{4.186}$$

$$< k^2 [(\rho + p)v]_\chi >= k^2 < [(\rho + p)v]_\chi >, \tag{4.187}$$

$$< 3\mathcal{H}\delta p_\chi >= -\frac{3}{16}\bar{a}\bar{m}_\chi^3 \frac{\chi_0^3}{M_p^2} B, \tag{4.188}$$

$$< 3(1+\omega_\chi)\rho_\chi \Psi' >= 3\bar{\rho}_\chi \bar{\Psi}' - \frac{3}{16}\bar{a}\bar{m}_\chi^3 \frac{\chi_0^3}{M_p^2} B, \tag{4.189}$$

$$< 3\mathcal{H}(1+\omega_\chi)\rho_\chi q_\chi \Phi >= -\beta\bar{\rho}_\chi \frac{\bar{\varphi}'}{M_p}\bar{\Phi}, \tag{4.190}$$

$$< 3\mathcal{H}(1+\omega_\chi)\rho_\chi q_\chi \tau_\chi >= -\beta\frac{\bar{\varphi}'}{M_p} < \delta\rho_\chi > -\beta\frac{\bar{\rho}_\chi}{M_p}\left(P' - \bar{\varphi}'\bar{\Psi}\right). \tag{4.191}$$

The interference terms arising during the averaging procedure in lines 3 and 4 of the above set of equations precisely cancel each other in the equation of energy conservation (4.32). Since

$$< \delta\rho_\chi' >=< \delta\rho_\chi >' \tag{4.192}$$

is obvious to all orders, we can directly write down the equations of energy conservation in terms of the density contrast δ_χ and velocity potential V_χ:

$$< \delta_\chi >' = -\frac{k^2}{\mathcal{H}}\bar{V}_\chi + 3\bar{\Psi}' - \beta P'/M_p + \beta\frac{\bar{\varphi}'}{M_p}\left(\bar{\Psi} - \bar{\Phi}\right). \tag{4.193}$$

We should not that the velocity potential is strictly speaking not well defined in this case, it is periodically divergent. We thus simply define the averaged version to be

$$\bar{V}_\chi \equiv -\mathcal{H}\frac{< [(\rho + p)v]_\chi >}{\bar{\rho}_\chi + < p_\chi >} = -\mathcal{H}\frac{< [(\rho + p)v]_\chi >}{\bar{\rho}_\chi}. \tag{4.194}$$

Let us move on to the equation of momentum conservation for the bolon. We get to subleading order:

$$< 4\mathcal{H}[(\rho+p)v]_\chi >= 4\bar{\mathcal{H}} < [(\rho+p)v]_\chi >, \tag{4.195}$$

$$< \delta p_\chi >= 0, \tag{4.196}$$

$$< (1+\omega_\chi)\rho_\chi\Phi >= \bar{\rho}_\chi\bar{\Phi}, \tag{4.197}$$

$$< 3\mathcal{H}q_\chi\frac{(\rho_\chi+p_\chi)}{(\rho_{\rm tot}+p_{\rm tot})}[(\rho+p)v]_{\rm tot}+af_\chi >= \beta\bar{\rho}_\chi P/M_p. \tag{4.198}$$

Since again

$$< [(\rho+p)v]'_\chi >=< [(\rho+p)v]_\chi >' \tag{4.199}$$

is obvious to all orders we can easily obtain the following equation for $\bar{V}_\chi$:

$$\bar{V}'_\chi = -\frac{3}{2}(1+\omega_{\rm eff})\bar{\mathcal{H}}\bar{V}_\chi + \mathcal{H}\bar{\Phi} + \beta\frac{\bar{\varphi}'}{M_p}\bar{V}_\chi - \beta\bar{\mathcal{H}}P/M_p. \tag{4.200}$$

Finally we obitain for the cosmon field equation and the Poission equation the following expressions in terms of the averaged bolon density contrast and velocity potential:

$$P'' = -2\bar{\mathcal{H}}P' - \left(k^2+\bar{a}^2V_{1,\bar{\varphi}\bar{\varphi}}\right)P - 2\bar{a}^2V_{1,\bar{\varphi}}\bar{\Phi} + \bar{\varphi}'\left(\bar{\Phi}'+3\bar{\Psi}'\right) + \frac{\beta\bar{a}^2}{M_p}\bar{\rho}_\chi\left(<\delta_\chi>+2\bar{\Phi}\right), \tag{4.201}$$

and

$$\bar{\Psi} = \frac{-\bar{a}^2}{2M_p^2k^2-\bar{\varphi}'^2}\left[\bar{\rho}_{\rm ext}\left(\bar{\delta}_{\rm ext}+3(1+\bar{\omega}_{\rm ext})\bar{V}_{\rm ext}\right)+\bar{\rho}_\chi\left(<\delta_\chi>+3\bar{V}_\chi\right)\right.$$
$$\left.+3\omega_{\rm eff}\frac{\bar{\varphi}'^2}{a^2}\bar{\bar{\Pi}}_{\rm tot}+V_{1,\bar{\varphi}}P+3\bar{\mathcal{H}}\frac{\bar{\varphi}'P}{\bar{a}^2}+\frac{\bar{\varphi}'P'}{\bar{a}^2}\right]. \tag{4.202}$$

One can compare these equation with the ones for standard cold dark matter coupled to quintessence in [Amendola, 2000b]. After adjusting for the different definitions of the velocity potential and the time variable used, one finds that these equations do precisely coincide to the ones for cold dark matter coupled to quintessence.

b) $\mu k^2/\mathcal{H}^2 \gtrsim 1$

In the regime of smaller wavelengths we obtain a different result. The expansion in terms of trigonometric functions, however, remains the same:

$$X = P + Q\cos(2x) + R\sin(2x) + X_{\rm ig}, \tag{4.203}$$

$$Y = A\cos(x) + B\sin(x) + C\cos(3x) + D\sin(3x) + Y_{\rm ig}, \tag{4.204}$$

$$\Psi = \bar{\Psi} + \Psi_{\rm osc} + \Psi_{\rm ig}, \tag{4.205}$$

$$\Phi = \bar{\Phi} + \Phi_{\rm osc} + \Phi_{\rm ig}, \tag{4.206}$$

but the orders of magnitude change. This time we have Q and R both of order $O(\tilde{\mu}P)$, while $Y_{\rm ig}$ is still of order $O(\tilde{\mu}^3P)$, A and B are of the order $O(P)$ while C and D are of the order $O(\tilde{\mu}^2P)$ and $X_{\rm ig}$ is of the order $O(\tilde{\mu}^3P)$. For the gravitational potential we again have $\bar{\Psi}$ of the order $O(P/M)$, but this time

with subleading order contributions as well, $\Psi_{\rm osc}$ of the order $O(\tilde{\mu}\bar{\Psi})$ and $\Psi_{\rm ig}$ of the order $O(\tilde{\mu}^2\bar{\Psi})$. Furthermore our assumptions about the additional (non scalar field) components of the cosmic fluid remains the same, which means the the relations (4.174) still hold. Note that A, B, Q and R all have corrections at next to leading order which will be relevant below, but we have not included them here explicitly. Instead we we split up A according to $A = A_0 + A_1$ with A_1 of the order $O(\tilde{\mu}A_0)$ and accordingly for B, Q and R.

When evaluating the field equations we have to deal with the fact that there are oscillations with frequency k present in the cosmon perturbations (and possibly in the other components of the cosmic fluid as well). Since we are setting k^2 to be of the order $O(\bar{\mathcal{H}}^2/\tilde{\mu})$, we restrict ourselves to the case $k^2 \ll \bar{m}_\chi^2$, so that we can still consider all the the quantities P, Q, R, A, B, C and $\bar{\Psi}$ to be almost constant on the timescale $1/\bar{m}_\chi$. (We have already discussed that our approximation becomes inconsistent for very small wavelengths.) Due to these additional (lower frequency) oscillations one has to take into account that P' is of the order $O(\tilde{\mu}^{-1/2}\bar{\mathcal{H}}P)$ and P'' is of the order $O(\tilde{\mu}^{-1}\bar{\mathcal{H}}^2P)$. When evaluating the field equations we will always include the next "half order" in the lower order in $\tilde{\mu}$, e.g. if we evaluate an equation at the order $O(\tilde{\mu}^0 M_p\bar{\mathcal{H}})$ we will also include terms of the order $O(\sqrt{\tilde{\mu}}M_p\bar{\mathcal{H}})$.

Applying this scheme to the cosmon field equation (4.165) yields to leading order

$$Q_0 = -\frac{1}{4}\beta\frac{\chi_0}{M_p}A_0\,, \tag{4.207}$$

$$R_0 = -\frac{1}{4}\beta\frac{\chi_0}{M_p}B_0\,, \tag{4.208}$$

$$P'' = -2\bar{\mathcal{H}}P' - k^2P + \beta\bar{a}^2\bar{m}_\chi^2\frac{\chi_0}{M_p}A_0\,. \tag{4.209}$$

A comparison of coefficients in the bolon field equation (4.166) results in the following two equations:

$$A_0' = -\frac{3}{2}\bar{\mathcal{H}}A_0 + \frac{k^2}{2\bar{a}\bar{m}_\chi}B_0 + \beta\frac{\varphi_0'}{2M_p}A_0\,, \tag{4.210}$$

$$B_0' = -\frac{3}{2}\bar{\mathcal{H}}B_0 - \frac{k^2}{2\bar{a}\bar{m}_\chi}A_0 - \bar{a}\bar{m}_\chi\chi_0\bar{\Phi} + \beta\bar{a}\bar{m}_\chi\frac{\chi_0}{M_p}P + \beta\frac{\bar{\varphi}'}{2M_p}B_0\,. \tag{4.211}$$

Evaluating the Poisson equation (4.167) to leading order gives

$$\bar{\Psi} = -\frac{1}{2}\frac{\bar{a}^2}{k^2M_p^2}\left(\overline{\delta\rho}_{\rm ext} - 3\overline{[(\rho+p)v]}_{\rm ext}\right) - \frac{\bar{a}^2\bar{m}_\chi^2\chi_0}{2M_p^2k^2}A_0 - \frac{\bar{\varphi}'}{2M_p^2k^2}P' - \frac{3}{2}\frac{\bar{\varphi}'^2}{k^2M_p^2}\omega_{\rm eff}\bar{\tilde{\Pi}}_{\rm tot}\,. \tag{4.212}$$

We can now again evaluate equation (4.169) to leading order and identify the oscillatory part of the gravitational potential to obtain

$$\Psi'_{\rm osc} = \frac{\bar{a}\bar{m}_\chi\chi_0}{4M_p^2}A_0\sin(2x) - \frac{\bar{a}\bar{m}_\chi\chi_0}{4M_p^2}B_0\cos(2x)\,, \tag{4.213}$$

i.e.

$$\Psi_{\rm osc} = \frac{\chi_0}{8M_p^2}A_0\cos(2x) + \frac{\chi_0}{8M_p^2}B_0\sin(2x)\,. \tag{4.214}$$

As a trivial check one can easily verify that the slowly evolving part of equation (4.169) is indeed satisfied with the $\bar{\Psi}$-solution given above. When doing that, on should however take into account next-to-leading order terms in P, since they yield P'-terms which have to be included in the $\bar{\Psi}'$-expression in order to remain consistent. Otherwise, this check does not work.

We will again require the results from the next to leading order calculation in order to come up with effective fluid equations below. The bolon field equation gives us:

$$\begin{aligned}
A_1' =& -\frac{3}{2}\bar{\mathcal{H}}A_1 + \frac{k^2}{2\bar{a}\bar{m}_\chi}B_1 - \frac{3}{32M_p^2}\bar{a}\bar{m}_\chi\chi_0^2 B_0 + \frac{\bar{\mathcal{H}}}{\bar{a}\bar{m}_\chi}B_0' + \bar{a}\bar{m}_\chi\chi_1\bar{\Phi} + \frac{1}{2}\chi_0\left(3\bar{\Psi}' + \bar{\Phi}'\right) \\
&+ \frac{1}{2\bar{a}\bar{m}_\chi}B_0'' + \frac{\beta\bar{\varphi}'}{2M_p}A_1 + \frac{\beta^2}{16M_p^2}\bar{a}\bar{m}_\chi\chi_0^2 B_0 - \frac{\beta}{M_p}\bar{a}\bar{m}_\chi\chi_1 P\,, \qquad (4.215)\\
B_1' =& -\frac{3}{2}\bar{\mathcal{H}}B_1 - \frac{k^2}{2\bar{a}\bar{m}_\chi}A_1 + \frac{9}{32M_p^2}\bar{a}\bar{m}_\chi\chi_0^2 A_0 - \frac{\bar{\mathcal{H}}}{\bar{a}\bar{m}_\chi}A_0' - \frac{3\beta^2}{16M_p^2}\bar{a}\bar{m}_\chi\chi_0^2 A_0 \\
&+ \frac{\beta\bar{\varphi}'}{2M_p}B_1 - \frac{1}{2\bar{a}\bar{m}_\chi}A_0'\,, \qquad (4.216)\\
C =& \frac{\left(13+2\beta^2\right)}{128M_p^2}\chi_0^2 A_0\,, \qquad (4.217)\\
D =& \frac{\left(13+2\beta^2\right)}{128M_p^2}\chi_0^2 B_0\,. \qquad (4.218)\\
& \qquad (4.219)
\end{aligned}$$

The cosmon field equation gives:

$$\begin{aligned}
R_1 =& -\frac{\beta}{4M_p}\chi_0 B_1 - \beta\frac{k^2}{16\bar{a}^2\bar{m}_\chi^2}\frac{\chi_0}{M_p}B_0 + \frac{\beta}{4M_p\bar{a}\bar{m}_\chi}\chi_0' A_0 + \frac{1}{4\bar{a}\bar{m}_\chi}\frac{\chi_0\bar{\varphi}'}{M_p^2}A_0 - \frac{\beta}{4M_p}\chi_1 A_0 \\
&+ \frac{\beta}{4\bar{a}\bar{m}_\chi M_p}\chi_0 A_0' + \frac{1}{16\bar{a}\bar{m}_\chi}\frac{\chi_0^2}{M_p^2}P' - \frac{\beta^2}{8\bar{a}\bar{m}_\chi}\frac{\chi_0\bar{\varphi}'}{M_p^2}A_0 + \frac{3\beta\bar{\mathcal{H}}}{8\bar{a}\bar{m}_\chi}\frac{\chi_0}{M_p}A_0\,, \qquad (4.220)\\
Q_1 =& -\frac{\beta}{4M_p}\chi_0 A_1 - \beta\frac{k^2}{16\bar{a}^2\bar{m}_\chi^2}\frac{\chi_0}{M_p}A_0 - \frac{3\beta\bar{\mathcal{H}}}{8\bar{a}\bar{m}_\chi M_p}\chi_0 B_0 + \frac{\beta^2}{4M_p^2}\chi_0^2 P + \frac{\beta}{4M_p}\chi_1 B_0 \\
&- \frac{\beta\chi_0^2}{4M_p}\bar{\Phi} - \frac{\beta}{4\bar{a}\bar{m}_\chi M_p}\chi_0 B_0' - \frac{\chi_0\bar{\varphi}'}{4\bar{a}\bar{m}_\chi M_p^2}B_0 + \frac{\beta^2\chi_0\bar{\varphi}'}{8M_p^2\bar{a}\bar{m}_\chi}B_0 - \frac{\beta\chi_0'}{4\bar{a}\bar{m}_\chi M_p}B_0\,. \qquad (4.221)
\end{aligned}$$

We can use these results to perform the same averaging we already executed for large wavelengths. We will only quote the results here, the calculation proceeds in exactly the same fashion as in the small-k regime and the details are not particularly enlightening. The averaged quantities now read

(to subleading order):

$$< \delta\rho_\chi >= \bar{m}_\chi^2 (\chi_0 A_0 + \chi_1 B_0) - 2\beta\bar{\rho}_\chi \frac{P}{M_p} + \frac{k^2}{4\bar{a}^2}\chi_0 A_0 + \bar{m}_\chi^2 \chi_0 A_1 \,, \tag{4.222}$$

$$< \delta p_\chi >= \frac{k^2}{4\bar{a}^2}\chi_0 A_0 \,, \tag{4.223}$$

$$< [(\rho + p)v]_\chi >= \frac{\bar{m}_\chi}{2\bar{a}} (\chi_0 B_0 - \chi_1 A_0) + \frac{3\bar{\mathcal{H}}}{4\bar{a}^2}\chi_0 A_0 - \frac{\beta\chi_0\varphi_0'}{4\bar{a}^2 M_p} A_0 + \frac{\bar{m}_\chi}{2\bar{a}}\chi_0 B_1 \,. \tag{4.224}$$

All these quantities contain oscillatory parts at the order considered here, but in the case of $\delta\rho_\chi$ only at subleading order. Note that since $< \delta p_\chi >$ is surpressed by a factor of $\tilde{\mu}$ compared to $< \delta\rho_\chi >$, we can write

$$< \delta p_\chi >= \frac{k^2}{4\bar{a}^2\bar{m}_\chi^2} < \delta\rho_\chi > \tag{4.225}$$

to subleading order. We have recovered a small, scale-dependent sound speed $c_{s,\chi}^2 = k^2/4\bar{a}^2\bar{m}_\chi^2$, which generalizes earlier findings in [Hu et al., 2000, Matos and Urena-Lopez, 2001]. However, we still need to verify this by averaging the full equations of energy-and momentum conservation, taking care of all possible interferences between background and perturbative oscillations to subleading order in $\tilde{\mu}$, as we did above in the case of large wavelength. Doing this yields the following final equations for the density contrast and the velocity potential:

$$< \delta_\chi >' = -\frac{k^2}{\mathcal{H}}\bar{V}_\chi + 3\bar{\Psi}' - \beta\frac{P'}{M_p} + \frac{\beta\bar{\varphi}'}{M_p}\left(\bar{\Psi} - \bar{\Phi}\right) - \left(3\bar{\mathcal{H}} - \beta\frac{\bar{\varphi}'}{M_p}\right) c_{s,\chi}^2 < \delta_\chi > \,, \tag{4.226}$$

$$\bar{V}_\chi' = -\frac{3}{2}(1 + \omega_{\rm eff})\bar{\mathcal{H}}\bar{V}_\chi + \mathcal{H}\bar{\Phi} + \beta\frac{\bar{\varphi}'}{M_p}\bar{V}_\chi - \beta\mathcal{H}\frac{P}{M_p} + \mathcal{H}c_{s,\chi}^2 < \delta_\chi > \,. \tag{4.227}$$

The Poisson equation reads as in equation (4.202) if we include subleading non-oscillatory terms, and we will note repeat it here.

We should mention one important fact at this point. The effective fluid equations we just derived for small wavelengths can not be derived from equations (25) to (30) in [Amendola, 2000b]. This is due to the fact that the equations in [Amendola, 2000b] were derived for a barotropic fluid, i.e. for a fluid without non-adiabatic pressure perturbations. Since we have $< \omega_\chi >=< \omega_\chi' >= 0$ to the order considered here, we can directly deduce that the adiabatic sound speed is zero, and the small sound speed we recovered is therefore non-adiabatic. As can be seen from comparing equations (4.226) and (4.227) to [Amendola, 2000b], this makes no difference in the uncoupled scenario, as expected. The coupling however enters the equations differently, and the evolution equations we have just written down have, to our knowledge, not been investigated before. They constitute a new system.

4.3.2 RSA FOR THE COSMON

Before we move on the numerics we want to discuss one last approximation we employ in our Boltzmann code, which concerns the late time evolution of the cosmon perturbations. Similar to neutrinos and photons, the perturbed cosmon field will perform high frequency oscillations (of frequency $\sim k$)

for late times, the resolution of which requires much computational power. Fortunately, we can extend the RSA introduced above for photons and neutrinos to the cosmon. This was effectively done in [Amendola, 2004], if not under the same name. In our conventions we can directly obtain:

$$P = 3\beta M_p \frac{\bar{\mathcal{H}}^2}{k^2}\bar{\Omega}_\chi < \delta_\chi > . \tag{4.228}$$

We have checked numerically that this indeed approximates the averaged evolution of the cosmon perturbations very well for sufficiently late times.

4.4 NUMERICAL EVOLUTION

4.4.1 THE BOLTZMANN CODE

We have already described the various approximations we employ in our Boltzmann code. In this section we quickly want to describe how they are implemented, what we choose our initial conditions to be and how we achieve a realistic cosmology including late time cosmic acceleration.

Let us start with cosmic acceleration. For our numerics we go back to a specific quintessence potential, the exponential potential given in eq. (3.90). As we already discussed in chapter 3, a constant α does not lead to a scenario of cosmic acceleration in our model. We have already mentioned several possible ways to fix this, for our numerics we use a simply way which may seem slightly ad-hoc: We introduce an φ-dependent exponent of the form

$$\alpha(\varphi) = \begin{cases} \alpha & \varphi < \varphi_0 \\ \alpha - t(\varphi) & \varphi_0 < \varphi < \varphi_1 \\ 0.1 & \varphi_1 < \varphi \end{cases} , \tag{4.229}$$

with

$$t(\varphi) = \left(3\frac{(\varphi-\varphi_0)^2}{(\varphi_1-\varphi_0)^2} - 2\frac{(\varphi-\varphi_0)^3}{(\varphi_1-\varphi_0)^3} \right)(\alpha - 0.1) . \tag{4.230}$$

This effectively introduces a minimum in the cosmon potential around which the cosmon will stabilize for late times. The values of φ_0 and φ_1 do of course have to be adjusted in order to gain a realistic cosmology. We would like to stress that this scenario does not solve the coincidence problem at all, it is very much a construction tuned to fit observations. In fact, the author is of the opinion that possibly the most promising ansatz to address this issue is the growing neutrino quintessence model mentioned in chapter 3. However, due to the strong backreaction effect present in this model [Ayaita et al., 2012b] this is not straightforward to implement in a realistic fashion. We do want to point out that possible solutions of the coincidence problem are not the topic of this work, and thus we are not too concerned about this ad-hoc adjustment.

It may, however, be appropriate to return to the issue of separating the scalar field potential. As the cosmon field stabilizes in the minimum of its potential, it starts to oscillate as well and it is justified to ask whether our potential splitting still remains meaningful or not. We have a few comments on this.

- First, the splitting of the potential is completely arbitrary in nature. A different splitting would simply introduce a different form of the coupling, the dynamics of the Hubble parameter at the background level or the gravitational potentials at the level of perturbations are not affected by a redefinition.

- One could, however, reasonably ask if the approximations introduced above remain valid for the late stages of the cosmon evolution. Concerning this we merely want to mention that the cosmon mass is of order $\mathcal{H}/a \ll \bar{m}_\chi$. This is sufficient to ensure that the approximations derived in section 4.3 for both the background evolution and the perturbations remains valid.

- Finally one can argue about the physical meaning of the splitting of the two fields. As we mentioned above, at the background level it is justified by the fact that we recovered two components behaving as quintessence and coupled cold dark matter to high accuracy, as we explicitly showed by the analytic approximations in the previous section. For late times one could argue that the oscillatory part of the cosmon starts to act like dark matter as well, so we should use a different splitting of the fields. There are two facts ameliorating this concern: First, the oscillatory part of the cosmon energy density is tiny, both compared to the total energy density and compared to the bolon energy density. Second, it makes no difference which splitting definition we employ, as long as we do it consistently at both the background and the perturbative level. Even if the splitting is not unique or may not even canonical anymore, the resulting evolution is valid.
  A more serious issue concerns observable quantities. For example, one could ask if the matter power spectrum, constructed from the bolon and baryonic density contrast, remains a useful quantity to study. The easiest way to deal with this issue is to simply include all density contrasts into the total matter power spectrum and see that it makes no difference on the observable subhorizon scales. Very similar to neutrinos and photons, the cosmon does not make a sizable contribution, even for the late times when it oscillates during the adjustment to the potential minimum. Basically what this tells us that our splitting remains 'accurate enough' for all our purposes, as is made clear by the huge difference between the cosmon mass and the bolon mass.

Let us now move on to the initial conditions. In the very early universe we can employ the simplest (zeroth order) version of the TCA for photons and baryons and truncate the expansion of the phase space distribution function for neutrinos after the quadrupole [Kodama and Sasaki, 1984]. In chapter 5 we will derive the precise form of the adiabatic perturbation mode and show that it is stable, i.e. that there exists no isocurvature mode which is growing faster than the adiabatic mode in the early universe. We thus focus on purely adiabatic perturbations and start with the following initial

conditions:

$$\begin{pmatrix} \Delta_\nu \\ V_\nu \\ \Delta_\gamma \\ \Delta_b \\ V_\gamma \\ \Delta_\varphi \\ V_\varphi \\ \Delta_\chi \\ V_\chi \\ \tilde{\Pi}_\nu \end{pmatrix}_{\text{adiab.}} = \mathcal{C} \begin{pmatrix} 1 \\ -5/4\,\mathcal{S}^{-1} \\ 1 \\ 3/4 \\ -5/4\,\mathcal{S}^{-1} \\ 1 \\ -5/4\,\mathcal{S}^{-1} \\ 1 \\ -5/4\,\mathcal{S}^{-1} \\ -\mathcal{S}^{-1} \end{pmatrix}, \tag{4.231}$$

where $\mathcal{S} = (15 + 4\Omega_\nu)$ and $\mathcal{C}$ is a constant. As our code uses the exact scalar field perturbations in the early universe instead of a fluid description, we need to translate this to scalar field perturbations, which yields:

$$\begin{pmatrix} X \\ X' \\ Y \\ Y' \end{pmatrix}_{\text{adiab.}} = \mathcal{C} \begin{pmatrix} -\frac{5}{\alpha(15+4\Omega_\nu)} \\ 0 \\ -\frac{5(\alpha-\beta)}{\alpha\lambda(15+4\Omega_\nu)} \\ 0 \end{pmatrix}. \tag{4.232}$$

One could of course go to subleading order in X' and Y' here, but for the starting time of our code the corresponding values lie below the numerical precision for all wavenumbers considered and we do not do so. Note that the baryon and photon velocity potential are equal, $V_b = V_\gamma$, in the zeroth order TCA.

For later times we switch to the first order TCA and then finally to the hierarchy of higher momenta of the phase space distribution functions for photons and neutrinos. We obviously cannot implement the full infinite hierarchy and have to truncate at some $l_{\max}$. We use the standard truncation introduced in [Ma and Bertschinger, 1995], which reads for massless neutrinos:

$$F_{\nu(l_{\max}+1)} \approx \frac{(2l_{\max}+1)}{k\tau} F_{\nu l_{\max}} - F_{\nu(l_{\max}-1)}\,, \tag{4.233}$$

whereas for photons we set

$$F'_{\gamma l_{\max}} = kF_{\gamma(l_{\max}-1)} - \frac{l_{\max}+1}{\tau} F_{\gamma l_{\max}} - an_e\sigma_T F_{\gamma l_{\max}}\,, \tag{4.234}$$

$$G'_{\gamma l_{\max}} = kG_{\gamma(l_{\max}-1)} - \frac{l_{\max}+1}{\tau} G_{\gamma l_{\max}} - an_e\sigma_T G_{\gamma l_{\max}}\,. \tag{4.235}$$

For even later times we employ the UFA and RSA respectively. When which set of equations is employed is determined by a set of triggers, which are exactly the same ones used in [Blas et al., 2011]:

- The first order TCA evolution starts when either $\mathcal{H}\tau_c >$ tca_start_hubble_tauc or $k/\mathcal{H} >$ tca_start_hubble_k.

- We switch to the full truncated set of equations for the higher momenta in the phase space distribution function (or directly the UFA or RSA) when either $\mathcal{H}\tau_c >$ tca_stop_hubble_tauc or $k\tau_c >$ tca_stop_k_tauc.
- The UFA is switched on when $k\tau >$ ufa_trigger.
- Finally the RSA is switched on when both $k\tau >$ rsa_k_tau and $\tau_c/\tau >$ rsa_tauc_tau.

Clearly the triggers should be chosen carefully. Our standard choices are summarized in Table 4.1. These values are basically the same as the ones used in the class code reference files for a better than permille accuracy for both the C_ls and the matter power spectrum, except for the TCA-stop triggers. Since we use only a first order TCA (whereas CLASS uses a second order scheme) we set these considerably lower. Furthermore we are more conservative with the UFA, setting a higher start trigger. In order to avoid truncation effects during the phase when the truncated Boltzmann hierarchy is used, one should choose $l_{\max}$ slightly bigger than the trigger ufa_trigger. Our standard setting is $l_{\max} = 35$.

The switching from the exact scalar field evolution of the scalar fields to the fluid description happens at roughly $10a^*$ (cf. eq. (3.128)). To be more precise: We numerically search for the next oscillation period after $10a^*$ and determine the precise time of transition and the initial values for the fluid description through explicit numerical integration. The value of $10a^*$ is chosen such that the value of μ is small enough for the fluid approximation to be valid and at the same time the numerical inaccuracies resulting from the presence of quick oscillations are still under excellent control ($\mu(10a^*) \lesssim 10^{-3}$). For much later times these can become very big, in fact pushing the exact scalar field evolution to much later times leads to numerical errors in the bolon background energy density ρ_χ, because the constructive interference terms do not get resolved with sufficient accuracy anymore.

Finally we need to determine the free electron density $n_e(\tau)$. We do this by employing the Fortran-version of recfast from september 2012 (version 1.5.2). As recfast is programmed to work for ΛCDM models we had to modify it slightly. In our version the Hubble rate (and its derivative) is not calculated directly from the ΛCDM parameters but read in from a table created by the Boltzmann code. We should mention here that reionization effects are not included in recfast, and also not implemented in our Boltzmann code. The effects of reionization on the matter power spectrum come from the baryonic sound-speed, which gets increased during this period. However, as was shown by a comparison between CLASS, which includes this effect, and CAMB, which does not in [Lesgourgues, 2011b], the effect is at the sub-percent level for $k < 50\ \mathrm{Mpc}^{-1}$, which is an error we are willing to accept.

We adjust the cosmological parameters to the WMAP7-values [Jarosik et al., 2011], i.e.

$$h = 0.71\,, \quad \Omega_{\chi,0} = 0.222\,, \quad \Omega_{b,0} = 0.0449\,, \tag{4.236}$$

$$T_{CMB} = 2.728\,\mathrm{K}\,, \quad n_s = 0.961\,, \quad \sigma_8 = 0.801\,. \tag{4.237}$$

The normalization of the power spectrum is imposed after actually running the code.

Runtime and accuracy

The runtime of our code is, plainly, terrible. When compared to a state-of-the-art code like CLASS, it is slower by a factor of roughly 200 already for the ΛCDM model, and runtimes get slower by another factor of ~ 5 for the cosmon-bolon model, due to its increased complexity. There are several reasons for this: First, we programmed the code in Mathematica, which is comparatively high level programming language and can generally be expected to produce inferior runtimes when compared to a C or Fortran code. Second, we do not use an integrator specifically designed to optimize the speed of the code, but refer to the standard Mathematica option. Finally, there are probably many small things we have not implemented in an ideal fashion in the code.

To check the validity of the approximations employed and their implementation we compare the results of our Boltzmann-Code for the standard ΛCDM model with the results of the CLASS-code [Lesgourgues, 2011a, Blas et al., 2011]. To see that both codes agree to excellent accuracy, we simply plot the absolute value of the relative error for the matter power-spectrum at $z = 0$, which is the quantity we are interested in in this work, i.e.

$$\Delta P = \frac{\left|P_m(k) - P_m^{\mathrm{CLASS}}(k)\right|}{P_m^{\mathrm{CLASS}}(k)}\,. \tag{4.238}$$

The results for a run with the precision settings of CLASS adapted to ours (and reionization turned off) for the WMAP-7 parameters are shown in Figure 4.1. For some reason we have an error of about 1% an low k, which is a little bit strange, because this is the regime where the fewest approximations are employed. For larger k however, which is the regime of interest for us, the error is below half a percent everywhere up to $k \approx 50\ \mathrm{Mpc}^{-1}$, which is more than good enough for our purposes. This is roughly the same order of magnitude as the error that gets introduced by switching between different approximation schemes within CLASS (see [Blas et al., 2011]).

4.4.2 THE BOLON POWER SPECTRUM

Let us now discuss the evolution of linear perturbations in the coupled cosmon-bolon model. The evolution of the bolon density contrast can be understood fairly easily, at least in its most basic

TABLE 4.1: **Approximation triggers for the Boltzmann code: Standard values**

Trigger	Standard value
tca_start_hubble_tauc	0.004
tca_start_hubble_k	0.15
tca_stop_hubble_tauc	0.002
tca_stop_k_tauc	0.003
ufa_trigger	30
rsa_k_tau	120
rsa_tauc_tau	40

FIGURE 4.1: **Matter power spectrum comparison with CLASS**

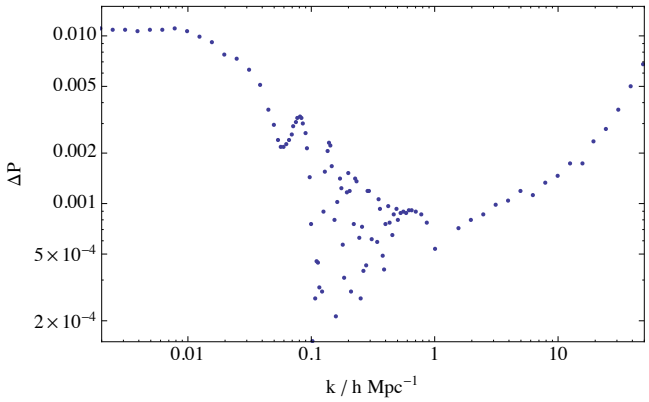

The absolute value of the relative error for our matter power spectrum when compared to the results of the CLASS-code.

features. Perturbations with wavenumbers in the regime $\mu k^2/\mathcal{H}^2 \ll 1$ follow the evolution of a coupled cold dark matter component, whereas perturbations in the regime $\mu k^2/\mathcal{H}^2 \gtrsim 1$ are suppressed due to the small sound speed. This is a time-dependent condition, so let us see how the quantity $\mu k^2/\mathcal{H}^2$ evolves during the main stages of the cosmic evolution. We can generally assume that $\bar{\mathcal{H}} \propto \bar{a}^{\eta}$, where $\eta = -1, -1/2$ and 1 during radiation-domination, matter domination and de-Sitter expansion respectively. The coupling between the bolon and the cosmon will of course change this behavior slightly, but that is not crucial for our argument. We then have

$$\mu k^2/\bar{\mathcal{H}}^2 \propto \bar{a}^{-1-\eta} e^{\beta\bar{\varphi}/M_p}, \tag{4.239}$$

which shows that during the eras of bolon- or cosmon-domination (and for not too large couplings), this quantity is decreasing, whereas it is (almost) constant during radiation domination. We can thus draw the following picture concerning the evolution of linear perturbations in the cosmon-bolon model: Immediately after the onset of bolon oscillations, essentially all subhorizon modes are suppressed in their evolution by the small sound speed (as $\mu \approx 1$ at this stage). Eventually all modes will leave this regime and start to grow like a coupled cold dark matter component, with smaller wavenumbers exiting the suppression stage first.

Due to the delayed onset of growth for short wavelength modes, the power spectrum exhibits a sharp cutoff at a scale which can be approximated by the horizon size at the time when the bolon oscillations start, i.e.

$$k_J^2 = m_0 e^{-\beta\bar{\varphi}^*/M} \sqrt{\frac{\rho_{r,0}}{3M^2(1-\Omega_{sc,es})}}, \tag{4.240}$$

where the value φ^* of the cosmon at a^* can once again be approximated by extrapolating the early scaling solution given in eq. (3.108). A similar formula was found in [Matos and Urena-Lopez, 2001] for a different model (see eq. (63) in this work), our result can be considered a generalization. It is of course only an estimate, but it is the best definition of a Jeans length available in our model as

it describes the smallest wavenumber for which the pressure balances out the gravitational attraction during some stage of the cosmic evolution. We can assign a corresponding Jeans mass in the usual way:

$$M_{\rm J} = \frac{4\pi}{3}\left(\frac{\pi}{k_{\rm J}}\right)^3 \bar{\rho}_\chi \,. \tag{4.241}$$

At this point we want to mention one feature of the numerics we have not yet discussed, and that is the matching of the two perturbation regimes. We have derived effective fluid perturbation equations in the two regimes $\mu k^2/\mathcal{H}^2 \ll 1$ and $\mu k^2/\mathcal{H}^2 \gtrsim 1$, and should somehow interpolate between these two cases. What we argue is that the details of this matching are utterly unimportant for any physically interesting results. To see this, consider that the point in time determining the position of the cutoff in the bolon power spectrum is the scale factor a^* when the bolon oscillations start. At this time (and for some considerable period ensuing it) we use the scalar field perturbations directly in our code. The transition to the fluid description happens sufficiently late, that all modes which are suppressed compared to a CDM evolution, i.e. which are in the vicinity of the cutoff, have already been suppressed when the switching occurs. We have checked three interpolation schemes between the perturbative regimes, one where we impose a sharp transition at $\mu k^2/\mathcal{H}^2 = 1$, one where we use a smooth interpolation function and one where we keep the small sound speed in the equations for all modes. All schemes give essentially identical results. For the last case the sound speed becomes numerically so small for the relevant modes in the vicinity of the cutoff that it does not influence their growth.

To visualize the connection between the evolution of the bolon density contrast and the quantity $\mu k^2/\mathcal{H}^2$ we show both in Figure 4.2. The plot shows numerical results for two different wavenumbers, $k = 0.96$ h/Mpc (green) and $k = 10.7$ h/Mpc (blue). The solid lines represent the bolon evolution, the dashed lines standard cold dark matter modes with the same wavenumbers evolved in the same background, given here for comparison. The normalization for both modes is arbitrary. First one should note the slightly elevated initial density contrast in the adiabatic mode for the bolon compared to standard CDM. Also clearly visible is the onset of oscillations in both modes, but while the $k = 0.96$ h/Mpc mode, when averaged, follows the evolution of the cold dark matter mode exactly, the growth of the $k = 10.7$ h/Mpc mode is suppressed during a prolonged period of time. This can be understood from the evolution of $\mu k^2/\mathcal{H}^2$, which can be seen in the lower panel of the picture. For the $k = 0.96$ h/Mpc mode we have $\mu k^2/\mathcal{H}^2 \ll 1$ throughout the entire evolution, whereas for $k = 10.7$ h/Mpc we have $\mu k^2/\mathcal{H}^2 > 1$ initially, but the value decreases for later times and growth sets in.

The power spectrum

The synchronous gauge matter power spectrum resulting from this evolution, which we reconstructed from our gauge-invariant quantities, is shown in Figure 4.3 (colored lines). For comparison we also show a number of additional power spectra. The solid black line represents the power spectrum obtained for a cold dark matter component, evolved in the same background cosmology. The colored lines represent bolon power spectra for different choices of the bolon exponent, from $\lambda = 30$ on the left to $\lambda = 70$ on the right, but with c^2 adjusted to give the same late background cosmology. Furthermore we show a warm dark matter power spectrum, obtained by modifying the transfer function

FIGURE 4.2: **Evolution of the bolon density contrast**

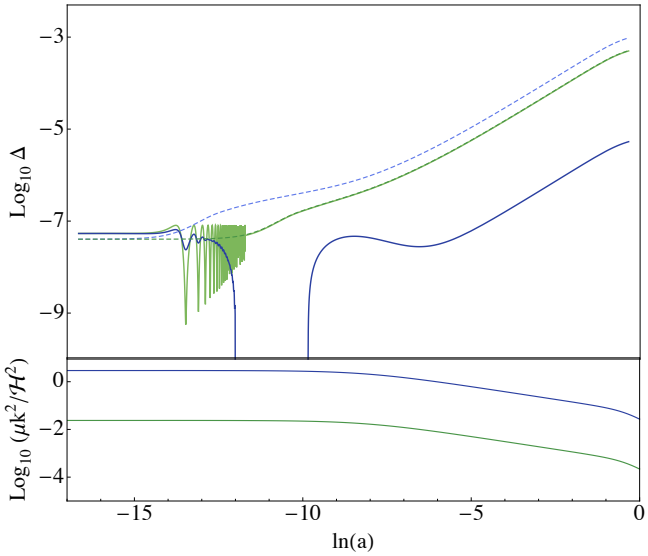

The upper panel shows the evolution of the linear density contrast for the bolon (solid lines) and a standard cold dark matter evolution (dashed lines) in the same background. The green lines show a $k = 0.96$ h/Mpc mode, whereas the blue ones represent $k = 10.7$ h/Mpc. In the lower panel we show the corresponding evolution of the quantity $\mu k^2/\mathcal{H}^2$. The bolon exponential is $\lambda = 30$ for this plot, the coupling is $\beta = 0$. Figure is almost identical to Figure 2 in [Beyer, 2014b].

for the cold dark matter component (gray line) in a manner suggested in [Barkana et al., 2001, Bode et al., 2001], i.e.

$$P_{\rm wdm}(k) = P_{\rm cdm}(k)\left(1 + (0.361k/k_{\rm wdm})^{2.4}\right)^{-4.17}, \tag{4.242}$$

where

$$k_{\rm wdm}^{-1} = 0.201\left(\frac{\Omega_{\rm wdm,0}h^2}{0.15}\right)^{0.15}\left(\frac{\hat{g}_{\rm wdm}}{1.5}\right)^{-0.29}\left(\frac{m_{\rm wdm}}{1\,\rm keV}\right)^{-1.15}\rm Mpc\,. \tag{4.243}$$

This transfer function is a numerical fit to the WDM power spectrum obtained at $z = 0$ for thermally produced warm dark matter. Here $\hat{g}_{\rm wdm}$ denotes the effective number of degrees of freedom for the WDM particle entering the calculation of the number density, which is 1.5 for a fermion, which we assume to be the case here.[1] The mass of the wdm-particle we use throughout this section is

$$m_{\rm wdm} = 2.284\,\rm keV\,. \tag{4.244}$$

All power spectra have been normalized to the value of $\sigma_8 = 0.801$ given above.

The cutoff in the bolon power spectrum is initially much steeper than in warm dark matter models, which is typical for scalar field dark matter. Furthermore is gets shifted to smaller wavenumbers

[1] This is not the same number of degrees of freedom as we employed in chapter 2, which of course is 2 for fermions. In this definition, the factor $3/4$ resulting from the momentum integration for the number densities is already included (cf. eq. (2.61)).

FIGURE 4.3: **Matter power spectra for different λ**

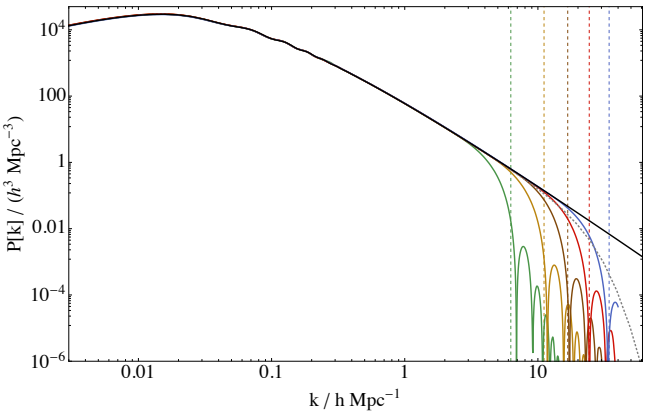

Power spectra for standard cold dark matter (black), warm dark matter with $m_{\mathrm{wdm}} = 2.284$ keV (grey, dotted) and the bolon (colored) for different masses. The corresponding values are from left to right $\lambda = 30$ (green line, $N = 0.3793$), $\lambda = 40$ (orange line, $N = 0.3804$), $\lambda = 50$ (brown line, $N = 0.3792$), $\lambda = 60$ (red line, $N = 0.3791$) and $\lambda = 70$ (blue line, $N = 0.3784$). The coupling is $\beta = 0$, the scalar field transition values are $\varphi_0 = 13.806$ and $\varphi_1 = 15.493$ for all curves. We also show the estimates of the corresponding Jeans wavenumbers in the same colors (dashed gridlines). Figure taken from [Beyer, 2014b].

for smaller λ, which can be easily understood in terms of the bolon mass. Decreasing the bolon-exponential λ leads to an effective decrease of the bolon mass. Keeping all other parameters fixed we would obtain $m_0 \propto \lambda$, but a more realistic comparison is to investigate this effect after adjusting the mass-parameter c^2 using equation (3.131) to a realistic current bolon energy density. Evaluating equation (3.131) for $\beta = 0$ then directly gives $c^2 \propto \lambda^6$, i.e. $m_0 \propto \lambda^4$, an even stronger growth of the mass with λ. The resulting effect is a larger sound speed as λ decreases and as a consequence a suppression of growth extending to smaller wavenumbers. The opposite effect for larger values of λ is also clear.

Effect of the coupling

We now want to move on to study the influence the coupling β has on the evolution of the bolon density contrast. It can be summarized in four effects:

First, there are effects from the background evolution. The coupling causes the energy density of the bolon to scale slightly differently from a standard cold dark matter one, for a positive coupling it scales away faster then a^{-3} and therefore the bolon energy density exceeds the one obtained for the $\beta = 0$ case for $z > 0$ after adjusting $\rho_{\chi,0}$, leading to shift of matter-radiation equality to earlier times. This results in a shift of the maximum in the matter-power-spectrum to larger wavenumbers, since the horizon size at matter-radiation-equality is suppressed, an effect only boosted by the effect the coupled evolution has on the Hubble parameter. Similarly, a negative coupling has the opposite effect, shifting the maximum to smaller wavenumbers.

FIGURE 4.4: **Growth of the matter density contrast in coupled quintessence**

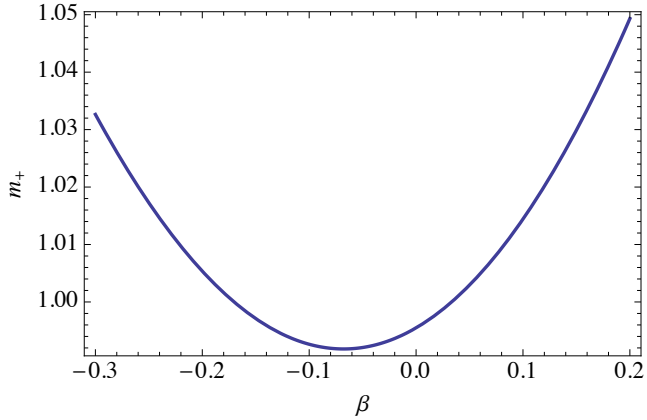

Growth of the matter density contrast in coupled quintessence models during matter domination with a cosmon scaling solution. We shown the exponent m_+, where $\delta \propto a^{m_+}$. This plot was created for an exponential quintessence potential with $\alpha = 20$ and displays the formula for m_+ given in eq. (60) in [Amendola, 2000b].

Second, the growth of bolon perturbations during bolon-domination also gets changed by the coupling. The evolution of the growth of linear perturbations in a coupled quintessence scenario with a scaling solution during matter domination was analyzed in [Amendola, 2000b], and the results can be applied to to our model in the $\mu k^2/\mathcal{H}^2 \ll 1$ regime. For not too large coupling the effect can be summarized as follows: A positive coupling increases the growth of linear perturbations, whereas a negative coupling decreases the growth compared to the uncoupled case. This effect leads to an increase of power for large k modes in the power spectrum for positive coupling, and a suppression for a negative one.We have visualized this effect in Figure 4.4.
For larger couplings this no longer holds true. The growth rate now starts to increase even for negative couplings and a growth faster than $\delta \propto a$ also becomes possible. Note that this is not in conflict with the results found in [Amendola, 2000a], where a suppression of growth for all couplings was found. The difference arises from the background evolution, since in our model the quintessence field adjusts itself to a different fixed point than the one analyzed in [Amendola, 2000a].

Finally the coupling also changes the evolution of the bolon-mass and thus of the sound-speed present in the $\mu k^2/\mathcal{H}^2 \gtrsim 1$ regime. Adjusting the background cosmology according to equation (3.131) leads to an increase in the value of the bolon mass at $a = 1$ (i.e. today) with a positive coupling, in contrast to what one might expect naively from the $e^{-\beta\varphi/M}$-dependence. Similarly, it decreases for a negative coupling. This leads to a decrease of the soundspeed for a positive coupling and thus to the cutoff in the power spectrum shifted to larger wavenumbers. The opposite of course holds for a negative coupling.

As a last effect, the growth of perturbations during the radiation dominated in era and during transition from radiation domination to matter domination also gets affected by the coupling. This is difficult to access analytically, and the important modifications of the power spectrum can be understood in terms of the previously discussed points alone. We will therefore not go into this any further.

All these effects can be seen in Figures 4.5 and 4.6. In Figure 4.5 we show the evolution of the bolon density contrast with wavenumber $k = 10.7$ h/Mpc for a model with $\lambda = 40$ and three different choices of the coupling plus a standard CDM evolution evolved in the same background (black solid line). Clearly a positive coupling leads to an earlier onset of perturbation growth, thus shifting the cutoff to larger wavenumbers.

The matter power spectra for the same models are shown in Figure 4.6, where we have also added the WDM-modification (gray dotted line). Otherwise the coloring is the same as in Figure 4.5. One can clearly see the small shift of the maximum of the power spectrum depending on the coupling, as well as the growth modification, epitomized by the different slopes in the power spectra for large k. Furthermore the shift in the position of the cutoff to larger wavenumbers for a positive coupling is also evident. The difference in the spectra for smaller superhorizon wavenumbers are an effect resulting from the normalization in conjunction with the different high-k slopes and position of the maximum. The position of the cutoff (as long as it is at large enough k) has very little influence on the normalization.

Finally we have attempted to find a simple fitting function for the form of the cutoff, motivated by the fact that simple fitting was found in similar models in [Hu et al., 2000, Matos and Urena-Lopez, 2001]. However, a fitting of such a simple form as was proposed there does not yield good results in our case. A good result is obtained by the following function:

$$P_\chi(k) = P_{\rm cdm}(k)\left\{\frac{\cos\left[(bx)^a\right]}{1+\sqrt{c}\,(x^{d_1}+x^{d_2})}\right\}^2, \tag{4.245}$$

where $x = k/k_J$ and the parameters a, b, c, d_1 and d_2 are functions of the model parameters λ and β. We assumed a linear dependence for all functions here, optimized the parameters numerically and eliminated all terms the inclusion of which would not yield a significant improvement of the fitting. The resulting best estimate is given by

$$a(\beta) = 4.105 + 0.428\beta\,, \tag{4.246}$$
$$b(\lambda,\beta) = 0.827 + 0.098\beta + 0.006\lambda + 0.0025\lambda\beta\,, \tag{4.247}$$
$$c(\lambda,\beta) = -0.46 - 1.9\beta + 0.053\lambda + 0.152\lambda\beta\,, \tag{4.248}$$
$$d_1(\beta) = 4.31 - 1.2\beta\,, \tag{4.249}$$
$$d_2(\beta) = 7.66 + 1.49\beta\,. \tag{4.250}$$

This gives a fitting better than 18% up to suppression of $1/500$. More details on the fitting procedure including a comparison to the functions proposed in [Hu et al., 2000, Matos and Urena-Lopez, 2001] can be found in appendix B.

Summary

To sum up, in this chapter we have introduced an analytical averaging procedure to arrive at an effective fluid description of the cosmon-bolon model valid for sufficiently late times, which allowed us to implement the model into a Boltzmann code with high accuracy. The resulting matter power

FIGURE 4.5: **Evolution of the bolon density contrast for different couplings**

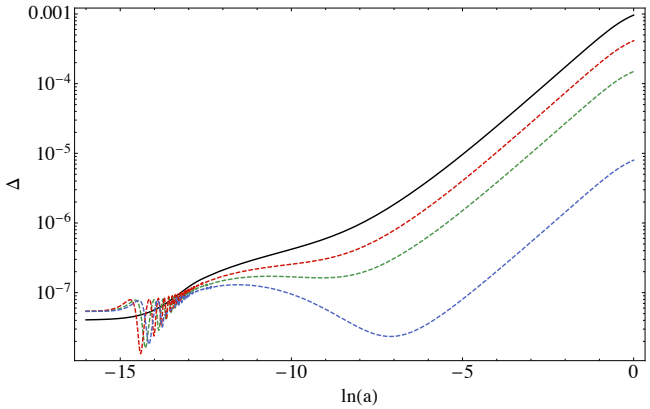

Evolution of the bolon density contrast with $k = 10.7$ h/Mpc for varying couplings. The black line represents standard uncoupled cold dark matter, the dashed green line an uncoupled bolon model, the red line a model with $\beta = 0.05$ ($N = 0.3716$, $\varphi_0 = 13.786$ and $\varphi_1 = 16.248$) and the blue line $\beta = -0.1$ ($N = 0.3777$, $\varphi_0 = 13.789$ and $\varphi_1 = 16.168$). The bolon exponential is $\lambda = 40$. Figure taken from [Beyer, 2014b].

FIGURE 4.6: **Matter power spectra for different couplings**

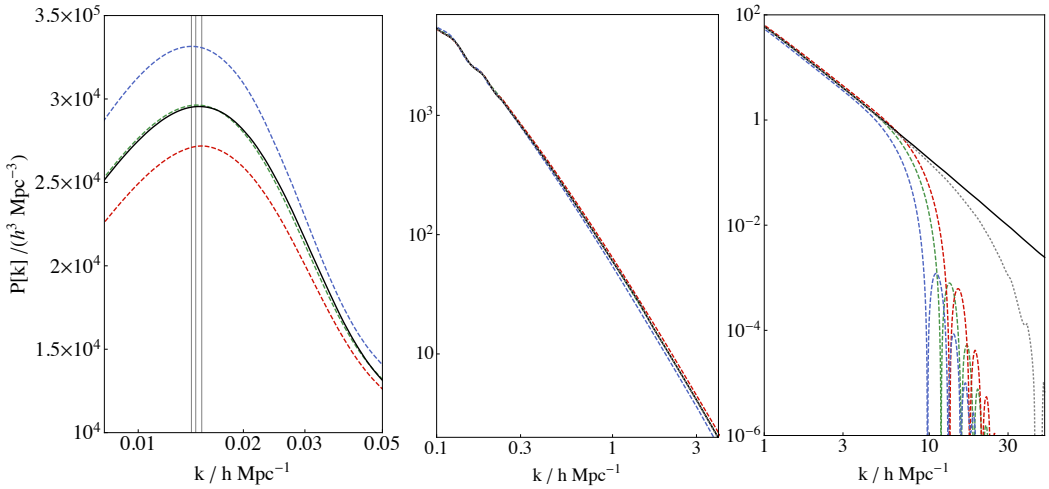

The black solid and gray dotted lines represent cold and warm dark matter spectra respectively, just as in Figure 4.3. The dotted lines represent cosmon-bolon models with $\lambda = 40$ and $\beta = 0, 0.05$ and -0.1 for the green, red and blue lines respectively. The three gridlines in the left hand figure show the positions of the maxima of the power spectra. Figure very similar to Figure 5 in [Beyer, 2014b].

spectra could be understood, at least qualitatively, by analytical means. A cutoff as we find in this model is expected to suppress the formation of structure on the corresponding scales, similar to WDM models. We will investigate these consequences more closely in chapter 6.

5 PERTURBATIONS ALONG MULTIPLE-FIELD SCALING SOLUTIONS

In the previous chapter we have discussed the evolution of linear perturbations in the cosmon-bolon model in the late universe, i.e. during the era when the bolon is performing fast oscillations around the minimum of its potential. In this entire treatment we have assumed that the perturbations are purely adiabatic, an assumption which is non-trivial and deserves some attention. Furthermore we still need to derive the specific forms of both the adiabatic perturbation mode we used as initial conditions in the numerics and the early scaling solution for the coupled cosmon-bolon model, which is essential for both the background evolution and the determination of the position of the power-spectrum cutoff, i.e. the Jeans scale.

In this chapter we will address all these issues as part of a larger analysis, which has its own scientific merits independent of the connection to the cosmon-bolon model. We will focus on the following questions:

- First, in cosmological models containing multiple canonical scalar fields, what is the most generic form of common potential that allows for the existence of exact scaling solutions, and what do these solutions look like?
- Second, how do perturbations around such scaling solutions behave? In particular, are adiabatic perturbations stable?

The last point is of particular relevance, since current observational constraints clearly indicate that cosmological perturbations have to be largely adiabatic [Enqvist et al., 2000, 2002, Beltran et al., 2005a, Seljak et al., 2006, Keskitalo et al., 2007, Kawasaki and Sekiguchi, 2008, Castro et al., 2009, Valiviita and Giannantonio, 2009, Li et al., 2011, Ade et al., 2013c], meaning that the amount of isocurvature perturbations present should be small. If adiabatic perturbations are unstable already in the early universe, i.e. there exist isocurvature modes which grow faster than the adiabatic mode, any, presumably initially small, admixture of such modes could in principle eventually outgrow the adiabatic perturbations and become dominant. An example of such a growth of isocurvature perturbations can be found during the 'adjustment phases' in minimally coupled tracking quintessence models when the quintessence field does not yet follow the tracker trajectory, but a sufficiently long tracking regime typically erases these modes [Malquarti and Liddle, 2002a]. If, however, such a 'fast growing' isocurvature mode is present throughout the era of radiation domination, the initial amplitude of this mode would have to be essentially completely eliminated in order to reconcile the theory

with observations. This is possible, in fact the simplest models of inflation based on a single scalar field predict purely adiabatic perturbations, but more complicated scenarios with multiple fields can lead to substantial isocurvature contributions. It is therefore highly preferable, from a model-building point of view, to avoid scenarios which include fast growing isocurvature modes during the radiation dominated era.

While standard minimally coupled one-field scaling quintessence models seem to generically generate stability of the adiabatic mode [Doran et al., 2003], the situation in coupled models of quintessence appears to be more complicated. We are aware of only one study which systematically analyzes the evolution of superhorizon-perturbations in a coupled quintessence model [Majerotto et al., 2010]. It appears that in such scenarios there are certain sections of parameter space for which the adiabatic mode becomes unstable, i.e. faster growing isocurvature perturbation modes exist. Since this analysis includes a conventional cold dark matter component and employs a specific commonly used form of the coupling given by $Q_\varphi = -\beta M_p \rho_{\rm cdm}$, the question remains if similar issues will arise in coupled scalar field models of dark matter. For the case of the cosmon-bolon model and other models originating from two-scalar field scaling solutions in the early universe, it will be answered below.

Before moving on to our analysis, let us recap some relevant results from previous studies. These have been limited to cosmologies containing either no scalar fields [Ma and Bertschinger, 1995], only scalar fields (usually in the context of inflation) [Gordon et al., 2001] or a single quintessence field [Malik et al., 2003, Malquarti and Liddle, 2002a, Bartolo et al., 2004, Doran et al., 2003, Majerotto et al., 2010], and therefore differ considerably from our setting. We include neutrinos, photons and baryons into our model in addition to the two scalar fields, but exclude a possible cold dark matter contribution, as is appropriate for the cosmon-bolon model. Nonetheless, some important conclusions can be drawn from these works.
As was shown in [Malik et al., 2003], even in generic non-minimally coupled models (which of course includes ours), purely adiabatic perturbations remain purely adiabatic on superhorizon scales, no matter what the interaction is. Here a mode is called adiabatic if all entropy perturbations vanish. This includes relative entropy perturbations between different components of the cosmic fluid as well as internal entropy perturbations for a single component - these can exist for non-perfect fluids (see section 4.1.4 for more details). However, as was noted in [Doran et al., 2003], the existence of such an adiabatic mode is non-trivial, since demanding all entropy perturbations to vanish typically introduces more constraints than we have degrees of freedom in the equations, in particular if the number of species considered is large. One should understand that this is not in conflict with the theorem found by Weinberg in [Weinberg, 2003, 2004], which states that an adiabatic superhorizon mode always exists, no matter the content of the universe. The apparent contradiction stems from Weinberg's definition of an adiabatic superhorizon-mode, which he takes to mean a mode for which the total curvature perturbation ζ remains constant, which is the case if the total entropy perturbation $\Gamma_{\rm tot} = 0$ (see section 4.1.4). This is a weaker condition than demanding all entropy perturbations to vanish, which is what we take adiabatic to mean in this thesis.

The contents of this chapter have been published in [Beyer, 2014a]. We follow this work both in content and in line of presentation with only minor deviations and include only few additions. Copyright for the figures and excerpts of this preprint resides, at the time of writing this, with the author, but will be transferred to the American Physical Society upon acceptance of the paper.

5.1 GENERIC MULTI-FIELD SCALING SOLUTIONS

5.1.1 SHAPE OF THE COMMON POTENTIAL

In this section we investigate exact scaling solutions in FLRW-cosmologies involving multiple coupled canonical scalar fields and a background matter fluid, defined by an energy density ρ_m and a constant equation of state ω_m. Let us quickly recall what we mean by that: We consider an exact scaling solution to be a scenario in which all scalar energy densities present scale exactly like the background fluid.
It is well known that the only potential providing an exact scaling solution for a single canonical scalar field is an exponential potential. This even holds true in the presence of a coupling to the background fluid [Amendola, 1999, Uzan, 1999, Copeland et al., 2005, Tsujikawa and Sami, 2004]. Furthermore, even in the presence of non-canonical kinetic terms - however still restricted to those yielding second order field equations - the form of possible Lagrangians yielding scaling solutions can be strongly restricted [Tsujikawa and Sami, 2004].
We will now show that in the case of multiple canonical coupled scalar fields similar restrictions for the common potential can be found. To do this we employ an approach already used in the earlier papers cited above, slightly adjusted to fit our scenario. We start by considering the following action

$$S = \int \mathrm{d}^4x\sqrt{-g}\left[\frac{R}{2} + \sum_{i=1}^{n} X_{\varphi_i} + V(\varphi_1,...,\varphi_n)\right] + S_\mathrm{m}\,, \tag{5.1}$$

where $X_{\varphi_i} = \frac{1}{2}\mathcal{D}_\mu\varphi_i\mathcal{D}^\mu\varphi_i$, n denotes the number of scalar fields φ_i present and S_m denotes the matter action. The scalar field equations for this action in the FLRW-background read

$$\varphi_i'' + 2\mathcal{H}\varphi_i' + a^2V_{,\varphi_i} = 0\,. \tag{5.2}$$

The common potential V can in principal be identified with any one of the scalar field energy densities or even split in some arbitrary fashion, but we choose to assign it to φ_1 for simplicity and define scalar energy densities and pressure densities as follows:

$$\rho_{\varphi_1} = X_{\varphi_1} + V\,, \quad p_{\varphi_1} = X_{\varphi_1} - V\,, \tag{5.3}$$

$$\rho_{\varphi_j} = p_{\varphi_j} = X_{\varphi_j}\,, \quad j = 2,...,n\,. \tag{5.4}$$

As we assume no direct coupling between the background fluid and the scalar sector, the equations governing the background-evolution can be written as

$$\frac{\mathrm{d}\rho_m}{\mathrm{d}N} + 3(1+\omega_m)\rho_m = 0\,, \tag{5.5}$$

$$\frac{\mathrm{d}\rho_{\varphi_i}}{\mathrm{d}N} + 3(1+\omega_{\varphi_i})\rho_{\varphi_i} = 3(1+\omega_{\varphi_i})q_i\rho_{\varphi_i}\,, \tag{5.6}$$

where $N = \ln(a)$ and conservation of the total energy-momentum tensor implies that the scalar couplings have to satisfy

$$\sum_i (1+\omega_{\varphi_i})\rho_{\varphi_i} q_i = 0\,. \tag{5.7}$$

In an exact scaling scenario we demand

$$\omega_{\varphi_i} = \frac{p_{\varphi_i}}{\rho_{\varphi_i}} = \text{const.} \quad \text{and} \quad \frac{\rho_{\varphi_i}}{\rho_m} = \text{const.} \quad \text{for } i = 1\ldots n\,. \tag{5.8}$$

Note that the scalar equations of state can differ from the background equation of state even in an exact scaling scenario if a coupling between the scalar fields is present, only the combined scalar equation of state has to fulfill

$$\omega_{\text{sc}} = \frac{\sum_i \rho_{\varphi_i}\omega_{\varphi_i}}{\sum_i \rho_{\varphi_i}} = \omega_m\,, \tag{5.9}$$

if the scalar density parameters are non-zero. From equations (5.5) and (5.8) we can directly conclude that

$$\frac{\mathrm{d}\ln\rho_{\varphi_i}}{\mathrm{d}N} = \frac{\mathrm{d}\ln\rho_m}{\mathrm{d}N} = -3(1+\omega_m)\,, \tag{5.10}$$

and

$$\frac{\mathrm{d}\ln X_{\varphi_i}}{\mathrm{d}N} = -3(1+\omega_m)\,. \tag{5.11}$$

Since $X_{\varphi_i} \propto (\mathrm{d}\varphi_i/\mathrm{d}N)^2\,\rho_{\text{tot}}$, equations (5.10) and (5.11) directly give

$$\mathrm{d}\varphi_i/\mathrm{d}N = c_i = \text{const.} \quad \text{for all } i\,. \tag{5.12}$$

Furthermore all couplings have to be constant by virtue ofequations (5.6) and (5.10):

$$q_i = \frac{(\omega_{\varphi_i} - \omega_m)}{1+\omega_{\varphi_i}}\,. \tag{5.13}$$

Now we can easily derive a differential equation for the potential V by again employing equations (5.6) and (5.10):

$$\frac{\mathrm{d}\ln V}{\mathrm{d}N} = \frac{\mathrm{d}\ln V}{\mathrm{d}\varphi_i} c_i = -3(1+\omega_m), \tag{5.14}$$

which directly gives

$$\ln V = -\frac{3(1+\omega_m)}{c_1}\varphi_1 + f\,(\xi_2, ..., \xi_n)\,, \tag{5.15}$$

where $\xi_i = \varphi_i - \frac{c_i}{c_1}\varphi_1$ and f is some arbitrary (smooth) function. One can quickly check that this solution is not in conflict with the the demand of constant couplings simply by noting that by virtue of equation (5.12) all ξ_i have to be constant for a scaling solution and by convention (5.3) we therefore have

$$q_j = \frac{-V_{,\varphi_j} c_j}{3(1+\omega_{\varphi_j})\rho_{\varphi_j}} = -\frac{(1-\omega_{\varphi_1})c_j\rho_{\varphi_1}}{6(1+\omega_{\varphi_j})\rho_{\varphi_j}}\frac{\partial f}{\partial \xi_j} = \text{const.} \tag{5.16}$$

for $j > 2$ and dynamics corresponding to a scaling solution.

One comment might be in order here: In the derivation of equation (5.15) we made some implicit

assumptions. The most obvious one is that $\omega_{\varphi_1} \neq 1$, i.e. the scalar potential energy density should be non-vanishing. As we will see in section 5.1.2, purely kinetic fixed points with $\omega_{\varphi_1} = 1$ do exist, and we expect them to be present for a large class of potentials, including many not of the shape derived here. All that is required for this feature is that the common potential should become zero somewhere, at least asymptotically. We consider this to be the generic case, as any non-zero minimum potential value can be reabsorbed into a cosmological constant, which we assume to be zero. Furthermore one might suggest that we have excluded solutions for which the cosmological expansion is purely scalar field dominated. This is however not the case, as one can simply replace all ω_m appearing in the above equations with a constant effective equation of state ω_{eff} and reach the same conclusions concerning the potential shape.

To clarify this result: The construction of a potential allowing for exact scaling solution with non-vanishing potential energy density involving n multiple coupled canonical scalar fields requires the common potential to fulfill equation (5.15) for some set of constants $c_1, ..., c_n$. If that is the case, a scaling solution can exist.

5.1.2 Exact scaling solutions

Let us now move on to find explicit examples for exact scaling solutions during radiation domination for coupled two scalar field cosmologies. Since we are limiting the number of scalar fields to two from here on out, we will slightly deviate from the nomenclature used above and define

$$\varphi \equiv \varphi_1\,, \quad \chi \equiv \varphi_2\,, \quad \xi \equiv \xi_2 = \chi - \frac{c_2}{c_1}\varphi\,. \tag{5.17}$$

We start out with a coupled exponential potential and move on to different shapes later.

Coupled exponential potential

Let us first consider a potential of the shape

$$V(\varphi,\chi) = M_p^4 \left[\mathrm{e}^{-\alpha\varphi/M_p} + \mu \mathrm{e}^{-2\beta\varphi/M_p} \mathrm{e}^{\lambda\chi/M_p} \right], \tag{5.18}$$

where μ is some constant. We chose this particular shape for two reasons. First, it describes the cosmon-bolon model in the early universe. Second, as we will show later in this section, this simple potential is already the most generic case, in the sense that all exact scaling solutions which may arise for other potentials are already present for this exponential form.
One can easily check that this potential fulfills equation (5.15) with $c_1 = 3(1+\omega_{\text{eff}})/\alpha$, $c_2 = 4(2\beta - \alpha)/\alpha\lambda$ and

$$f(\xi) = \ln\left[M_p^4 \left(1 + \mu \mathrm{e}^{\lambda\xi/M_p} \right) \right]. \tag{5.19}$$

For the subsequent analysis we split the potential as follows

$$V(\varphi,\chi) = V_1(\varphi) + V_2(\varphi,\chi) \tag{5.20}$$

with

$$V_2(\varphi,\chi) = M_p^4 \mu \mathrm{e}^{-2\beta\varphi/M} \mathrm{e}^{\lambda\chi/M_p}\,, \tag{5.21}$$

and assign energy- and pressure-densities accordingly:

$$\rho_\varphi = X_\varphi + V_1\,, \quad p_\varphi = X_\varphi - V_1\,, \tag{5.22}$$

$$\rho_\chi = X_\chi + V_2\,, \quad p_\chi = X_\chi - V_2\,. \tag{5.23}$$

We are interested finding all exact scaling solutions for the case of two coupled canonical scalar fields φ and χ in the presence of a radiation fluid, which is the relevant case for studying physics in the early universe. The equations of motion governing this system can be directly read off from equations (5.2) and (5.5). As is common when trying to find exact scaling solutions, we now employ the dynamical systems approach introduced in chapter 3 [Copeland et al., 1998, Gumjudpai et al., 2005] and introduce the following new variables:

$$x = \frac{\varphi'}{\sqrt{6}M_p\mathcal{H}}\,, \quad y = \frac{a\sqrt{V_1}}{\sqrt{3}M_p\mathcal{H}}\,, \quad u = \frac{\chi'}{\sqrt{6}M_p\mathcal{H}}\,, \quad v = \frac{a\sqrt{V_2}}{\sqrt{3}M_p\mathcal{H}}\,, \quad z = \frac{a\sqrt{\rho_r}}{\sqrt{3}M_p\mathcal{H}}\,, \tag{5.24}$$

where these variables are subject to the constraint

$$z^2 = 1 - x^2 - y^2 - u^2 - v^2\,, \tag{5.25}$$

since are assuming a flat universe. The equations of motion can now be rewritten as

$$\frac{\mathrm{d}x}{\mathrm{d}N} = 2x\left(1-u^2-v^2-x^2-y^2\right) + 3u^2x + \sqrt{6}\beta v^2 + 3x^3 - 3x + \frac{1}{2}\sqrt{6}\alpha y^2\,, \tag{5.26}$$

$$\frac{\mathrm{d}y}{\mathrm{d}N} = 2y\left(1-u^2-v^2-x^2-y^2\right) + 3u^2y + 3x^2y - \frac{1}{2}\sqrt{6}\alpha xy\,, \tag{5.27}$$

$$\frac{\mathrm{d}u}{\mathrm{d}N} = 3u^3 + 2u\left(1-u^2-v^2-x^2-y^2\right) + 3ux^2 - 3u - \frac{1}{2}\sqrt{6}\lambda v^2\,, \tag{5.28}$$

$$\frac{\mathrm{d}v}{\mathrm{d}N} = 2v\left(-u^2-v^2-x^2-y^2+1\right) + 3u^2v + \frac{1}{2}\sqrt{6}\lambda uv + 3vx^2 - \sqrt{6}\beta vx\,, \tag{5.29}$$

and a fixed point is characterized by $\mathrm{d}x/\mathrm{d}N = \mathrm{d}y/\mathrm{d}N = \mathrm{d}u/\mathrm{d}N = \mathrm{d}v/\mathrm{d}N = 0$. When solving the resulting algebraic equations we can reduce the number of fixed points by eliminating some redundancies. First we assume that $\alpha > 0$ and $\lambda > 0$, both can be easily achieved by a suitable sign-change in the fields φ and χ. We exclude the case $\alpha = 0$, as this would lead to a cosmological constant term for V_1, and come back to $\lambda = 0$ below. Furthermore we have $y \geq 0$ and $v \geq 0$ by definition. Restricting ourselves to these ranges, the complete set of all fixed points is given in Table 5.1.

These fixed points can be split up into the purely scalar field dominated fixed points K_1 to S_3 and radiation-like fixed points R_1 to R_4. We expect the kinetically dominated fixed points K_1 and K_2 to always exist, irrespective of the exact shape of the scalar potential, as long as it exhibits a root, possibly asymptotically. The same holds for the point $R1$, which corresponds to both scalar fields sitting at a root of the potential, in the case of the potential (5.18) φ sits at infinity. The kinetically dominated fixed points are always unstable, as one can see directly by the fact that the scalar energy densities scales away $\propto a^{-6}$ and therefore faster than radiation (or matter). The point R_1 is also

unstable for the coupled exponential potential, as we will see below.
The remaining points S_1 to S_3 and R_2 to R_4 are the ones only existing for potentials of the form derived in section 5.1 and among these, only the ones exhibiting a radiation-like expansion, i.e. R_2 to R_4, can result in a realistic early cosmology.

The stability of the fixed points can be analyzed by investigating the Jacobian matrix for x, y, u and v for each fixed point. We are not interested in the typical classification into nodes, spirals and saddle-points here, we merely distinguish stable and unstable points [Copeland et al., 1998, Gumjudpai et al., 2005]. Points for which the Jacobian matrix has only positive (or zero) eigenvalues are unstable, and points for which all eigenvalues are negative are stable. The conditions for existence and stability of the fixed points are given in Table 5.2.

As is common in scenarios such as ours, the stable fixed points split up the parameter space into disjunct sections. For a given set of parameters α, λ and β we therefore have a unique attractive scaling solution towards which the cosmological evolution will adjust itself relatively quickly in the early universe. To avoid this fixed point for the prolonged period of radiation domination, one would necessarily have to start with initial conditions very far away from the fixed point configuration. The splitting of the parameter space can be seen in Figures 5.1 and 5.2. The region allowing for a realistic early radiation dominated scaling solution is quite large, in particular for $\lambda > 2$. However, only the point R_4 allows for a radiation-like expansion and arbitrarily small absolute values of the coupling.

Let us quickly return to the case $\lambda = 0$ ignored above. In this special case the potential does not depend on χ. The results are almost the same as before, however, all fixed points except for R_4 still exist, and the conditions for stability are the same as given in Table 5.2. We will not be concerned with this special case any further for the remainder of this chapter.

Non-exponential potentials

We now move on to show that all exact scaling solutions for coupled two scalar field cosmologies are effectively the ones found above for the coupled exponential potential. We start by recalling the generic shape of the common scalar potential required for the existence of scaling solutions given in equation (5.15). As before, we use a the splitting of the potential given by (5.20), which means it is useful to rewrite $f(\xi)$ as

$$f(\xi) = \ln\left(\mu_1 + \mu_2 g(\xi)\right), \tag{5.30}$$

where μ_1 and μ_2 are some suitable constants. Note that this already shows that V_1 has to be an exponential potential. With these definitions the common potential is given by

$$V_2(\varphi, \chi) = \mu_2\, g(\xi)\, \mathrm{e}^{-\alpha\varphi/M_p}, \tag{5.31}$$

with $\alpha = 3(1+\omega_{\mathrm{eff}})M_p/c_1$. Our aim is to rewrite the field equations in the same form used in the discussion of the exponential coupling potential, in order to recover a set of algebraic equations whose fixed points determine the existing scaling solutions. For non-exponential potentials we can of course not express the potential derivatives in terms of the potential, and we therefore need a new set of variables, defined by

TABLE 5.1: **Fixed points for coupled exponential potentials**

Point	x	y	u	v	z	ω_{eff}
K_1	$\sqrt{6}/\alpha$	0	$\pm\left(1-\frac{6}{\alpha^2}\right)^{1/2}$	0	0	1
K_2	$\frac{2\sqrt{6}\beta\pm\lambda\sqrt{f-6}}{f}$	0	$\frac{\pm 2\beta\sqrt{f-6}-\sqrt{6}\lambda}{f}$	0	0	1
S_1	$\sqrt{\frac{2}{3}}\beta$	0	$-\lambda/\sqrt{6}$	$\left(1-\frac{f}{6}\right)^{1/2}$	0	$-1+f/3$
S_2	$\alpha/\sqrt{6}$	$\left(1-\frac{\alpha^2}{6}\right)^{1/2}$	0	0	0	$-1+\alpha^2/3$
S_3	$\frac{\alpha\lambda^2}{\sqrt{6}g}$	$\left(\frac{h_1}{6g^2}\right)^{1/2}$	$\frac{\alpha(2\beta-\alpha)\lambda}{\sqrt{6}g}$	$\left(\frac{h_2}{6g^2}\right)^{1/2}$	0	$-1+\frac{\alpha^2\lambda^2}{3g}$
R_1	0	0	0	0	1	$1/3$
R_2	$\sqrt{\frac{2}{3}}\frac{4\beta}{f}$	0	$-\sqrt{\frac{2}{3}}\frac{2\lambda}{f}$	$\left(\frac{4}{3f}\right)^{1/2}$	$1-\frac{4}{f}$	$1/3$
R_3	$\sqrt{\frac{2}{3}}\frac{2}{\alpha}$	$\frac{2}{\sqrt{3}\alpha}$	0	0	$1-\frac{4}{\alpha^2}$	$1/3$
R_4	$\sqrt{\frac{2}{3}}\frac{2}{\alpha}$	$\frac{2\sqrt{f-2\alpha\beta}}{\sqrt{3}\alpha\lambda}$	$-\sqrt{\frac{2}{3}}\frac{2(\alpha-2\beta)}{\alpha\lambda}$	$\left(\frac{4(\alpha-2\beta)}{3\alpha\lambda^2}\right)^{1/2}$	$1-\frac{4g}{\alpha^2\lambda^2}$	$1/3$

Here $f(\beta,\lambda)=4\beta^2+\lambda^2$, $g(\alpha,\beta,\lambda)=(\alpha-2\beta)^2+\lambda^2$, $h_1=(f-2\beta\alpha)(6g-\alpha^2\lambda^2)$, $h_2=\alpha(\alpha-2\beta)(6g-\alpha^2\lambda^2)$ and the sign change for the point K_2 should be taken simultaneously in x and y. Table taken from [Beyer, 2014a].

TABLE 5.2: **Existence and stability of the fixed points for coupled exponential potentials**

Point	Existence	Stability
K_1	$\alpha^2\geq 6$	unstable $\forall\alpha,\beta,\lambda$
K_2	$f(\beta,\lambda)\geq 6$	unstable $\forall\alpha,\beta,\lambda$
S_1	$f(\beta,\lambda)\leq 6$	$f(\beta,\lambda)<\min(4,2\alpha\beta)$
S_2	$\alpha^2\leq 6$	$\alpha<\min(2,2\beta)$
S_3	$f(\beta,\lambda),\alpha^2\geq 2\alpha\beta$, $6g\geq\alpha^2\lambda^2$	$f(\beta,\lambda),\alpha^2>2\alpha\beta$ $4g>\alpha^2\lambda^2$
R_1	always	unstable $\forall\alpha,\beta,\lambda$
R_2	$f(\beta,\lambda)\geq 4$	$2\alpha\beta>f(\beta,\lambda)>4$
R_3	$\alpha^2\geq 4$	$2<\alpha<2\beta$
R_4	$f(\beta,\lambda),\alpha^2\geq 2\alpha\beta$, $4g\leq\alpha^2\lambda^2$	$4g<\alpha^2\lambda^2$, $\alpha\lambda^2>2\beta g$

For definitions of f and g see caption of Table 5.1. Table taken from [Beyer, 2014a].

FIGURE 5.1: **Parameter space of stable fixed points for the exponential coupling potential with $\lambda = 1$**

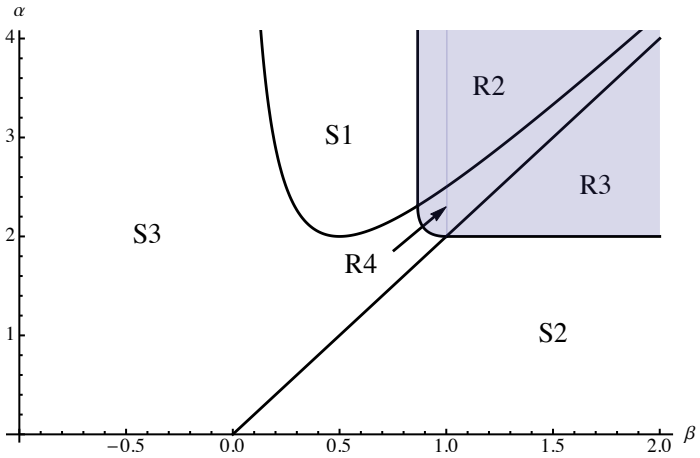

The phase space structure remains valid for all $\lambda < 2$. The shaded region shows the points which allow for a realistic early universe cosmology, i.e. a radiation-like expansion. Figure taken from [Beyer, 2014a].

FIGURE 5.2: **Parameter space of stable fixed points for the exponential coupling potential with $\lambda = 3$**

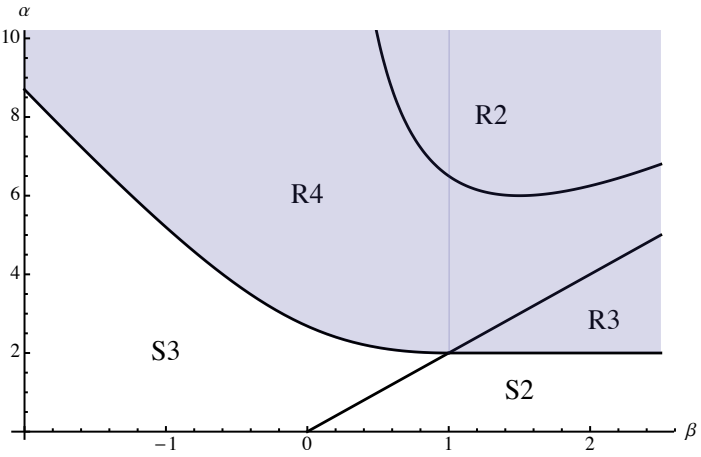

The phase space structure remains valid for all $\lambda > 2$. The shaded region shows the points which allow for a realistic early universe cosmology, i.e. a radiation-like expansion. Figure taken from [Beyer, 2014a].

$$s_n \equiv \frac{g^{(n)}(\xi) M_p^n}{g(\xi)} \quad \text{for} \quad n > 1\,. \tag{5.32}$$

Since ξ is constant for an exact scaling solution, it is clear that all the quantities s_n also have to be constant for such dynamics. The generic evolution equations for these variables are very simple and read

$$\frac{\mathrm{d}s_n}{\mathrm{d}N} = (s_{n+1} - s_1 s_n)\sqrt{6}\,(u - \sigma x)\,, \tag{5.33}$$

where we introduced $\sigma = c_2/c_1$. For an exact scaling solution we thus have to require

$$\frac{\mathrm{d}s_n}{\mathrm{d}N} = 0 \quad \text{for all } n\,. \tag{5.34}$$

Note that this does not exclude the possibility of algebraic relations between the s_n, which might render some of these equations redundant. For example, in the case of the exponential coupling potential we have $g(\xi) \propto \exp(\lambda\xi/M_p)$, which implies $s_n = \lambda^n v$, automtically satisfying eq. (5.34). In addition to the s_n-equations we have to add the following field equations to complete the system:

$$\frac{\mathrm{d}x}{\mathrm{d}N} = -x + x^3 - 2xy^2 + xu^2 - 2xv^2 + \frac{\sqrt{6}}{2}\alpha y^2 + \frac{\sqrt{6}}{2}(\alpha + \sigma s_1)v^2\,, \tag{5.35}$$

$$\frac{\mathrm{d}y}{\mathrm{d}N} = \left[-\frac{\sqrt{6}}{2}\alpha x + 2 + x^2 - 2y^2 + u^2 - 2v^2\right] y\,, \tag{5.36}$$

$$\frac{\mathrm{d}u}{\mathrm{d}N} = -u - \frac{\sqrt{6}}{2}s_1 v^2 + x^2 u - 2uy^2 + u^3 - 2uv^2\,, \tag{5.37}$$

$$\frac{\mathrm{d}v}{\mathrm{d}N} = \left[2 + x^2 - 2y^2 + u^2 - 2v^2 + \frac{\sqrt{6}}{2}s_1 u\right] v - \frac{\sqrt{6}}{2}(\alpha + \sigma s_1)xv\,. \tag{5.38}$$

As before, the scaling solutions can now be found algebraically by demanding $\mathrm{d}x/\mathrm{d}N = \mathrm{d}y/\mathrm{d}N = \mathrm{d}u/\mathrm{d}N = \mathrm{d}v/\mathrm{d}N = \mathrm{d}s_n/\mathrm{d}N = 0$ for $n \leq m$ with some suitable $m \in \mathbb{N}$, if the set of s_n-evolution equations truncate at m, i.e.

$$\frac{\mathrm{d}s_m}{\mathrm{d}N} = f(x, y, u, v, z, s_1, \ldots, s_m)\,. \tag{5.39}$$

This clearly does not hold for all potentials, but we can still make progress in the general case. Luckily, the only s_n-term relevant for the x, y, u and v-equation is s_1, which has to be a constant. Thus, equations (5.35) to (5.38) give exactly the same system of algebraic equations as equations (5.26) to (5.29), with the replacements

$$s_1 = \lambda \quad \text{and} \quad \sigma\lambda = -\alpha + 2\beta\,. \tag{5.40}$$

Let us pause for a moment to reconsider the logic of our approach. At first sight it may seem strange that we have apparently extended the equations of motion to include $m + 4$ dynamical variables governed by first order differential equations, instead of just the 4 present originally. In fact, the variables s_n are not truly free variables, they depend on y and v in some, typically non-algebraic, way.

In order to determine this dependence the relation

$$g(\xi) = \frac{\mu_1}{\mu_2}\frac{v^2}{y^2} \tag{5.41}$$

needs to be inverted (if possible). We could then simply replace s_1 in equations (5.35) to (5.38) by the corresponding non-algebraic expression and recover the equations of motion, without need for the higher derivatives s_n. However, the equations of motion in this non-algebraic form do not usually allow us to find any fixed points. The extended closed algebraic system of equations including the quantities s_n also describes the full dynamics of the system and is perfectly valid. In order to find a generic solution one can either integrate the system of four non-algebraic equations, or the system of $4+m$ algebraic equations, where the initial conditions for the quantities s_1 to s_m are given by the initial values for y and v in some non-algebraic way. We can therefore make the following statements:

- By analyzing the fixed points of extended set of algebraic equations we do capture all possible scaling solutions. However, since the s_n are treated as free constants in this approach, we still have to check that the non-algebraic relations relating them to y and v (i.e. the scalar potential) can indeed be fulfilled for a given fixed point within a given model. This may give additional non-trivial constraints.
- The stability analysis for each fixed point has to be extended to include the variables s_n, as they are dynamical in general, and constant only for exact scaling solutions.

With this in mind, let us quickly clarify what the relation (5.40) is telling us. The equivalency of the equations for x, y, u and v directly shows that any exact scaling solution for two coupled canonical scalar fields is effectively given by one of the points found above for the exponential cross-coupling potential. One should be careful not to take this conclusion too far. We emphasize that the conditions that all s_n have to be static are not necessarily met by all the points above for all potentials of the shape given in equation (5.31) and furthermore the non-algebraic relations fixing the s_n to y and v might be in conflict with the requirements of existence or stability for the fixed points. These issues have to be checked on a case by case basis. However, equations (5.33) and (5.40) tell us that all points for which $u = x(2\beta - \alpha)/\lambda$, i.e. $S3$ and $R4$, do exist for all such models, as long as the non-algebraic relations between the s_n and v and y do not violate the conditions of existence. Furthermore, the points $K1, K2$ and $R1$ exist if V_2 vanishes somewhere, at least asymptotically. We stress once again that the stability conditions may look very different than for the coupled exponential case, since stability of the s_n provides new constraints, which depend on the functional form of the potential.
Finally, there almost certainly exist potentials for which the series of s_n-equations never truncates. In this case we can still conclude that all possible fixed points are given in Table 5.1, but we cannot check whether they really do exist or are stable within our approach.

To sum up: We have shown that all scaling solutions for two coupled canonical scalar fields are included in the set of fixed points found for the coupled exponential potential, and that two of these points, $S3$ and $R4$, appear to exist rather generically. However, the stability conditions for the fixed points can change for different potentials, and have to be analyzed on a case by case basis.

Power law couplings

As an example of models with non-exponential potentials allowing for stable scaling solutions, we now investigate potentials with a power law coupling. By this we mean models for which $g(\xi) = \kappa\xi^m/M_p^m$, where obviously m has to be even in order for the potential to be bound from below. In this case the system of algebraic equations is closed after adding the equation for s_1, since

$$s_n = \frac{m!}{(m-n)!\,m^n} s_1^n \quad \text{for } n \leq m\,, \tag{5.42}$$

and of course $s_n = 0$ for $n > m$. In this case the evolution equations for s_1 reads

$$\frac{\mathrm{d}s_1}{\mathrm{d}N} = -\frac{\sqrt{6}}{m} s_1^2 (u - \sigma x)\,. \tag{5.43}$$

Let us quickly draw some conclusions concerning the fixed points for this type of coupling. First, eq. (5.43) is clearly solved for $s_1 = 0$. This is a special case, as we can not make the identification (5.40) anymore and thus not apply the correspondence to the exponential coupling potential anymore. However, for a power law coupling potential this is only possible when the field ξ is 'sitting at ∞'. This requires '$\varphi = \infty$' also, in order to keep V_2 finite. Thus the only fixed points available in this case are the kinetically dominated points K_1 and K_2 as well as the point R_1, all of which are unstable. (In the case of $R1$ this requires a stability analysis employing the extended set of equations, which we do not present here.)

For $s_1 \neq 0$ we can use the list of fixed points from the exponential coupling potential and a solution of eq. (5.43) requires $u = x(2\beta - \alpha)/s_1$, which is only satisfied for $S3$ and $R4$. The stability analysis for S_3 is quite complicated, and as this point does not provide a radiation-like expansion it is not of particular interest for the early universe and we omit it here. The only remaining fixed point is thus $R4$. A stability analysis reveals that stability of $R4$ for the power-law coupling requires

$$\alpha^2 > 4(1+\sigma^2)\,, \quad 4\sigma s_1 + m\alpha > 0\,, \tag{5.44}$$

$$-\sigma\left((m-2)s_1 + m\sigma(\alpha + \sigma s_1)\right) > 0\,. \tag{5.45}$$

Finally, for the point $R4$ the relation (5.41) can be shown to give

$$s_1^m + m^m \frac{1+\sigma^2}{\sigma\alpha\tilde{\kappa}} s_1 + m^m/\tilde{\kappa} = 0\,, \tag{5.46}$$

where $\tilde{\kappa} = \kappa\mu_1/\mu_2$. For $m = 2$ this can be solved explicitly for s_1, but the conditions for stability for $R4$ are not met for any of the two solutions. For higher values of m, one needs to analyze the situation numerically. The equation (5.46) has up to two real roots, which can serve as values for s_1 given a set of parameters α, $\tilde{\kappa}$ and σ. In terms of the original fields these two roots can be interpreted as follows: For any set of given model parameters we can find two sets of initial conditions corresponding to the scaling solution $R4$, with different values for x, y, u and v in each case. These two sets of initial conditions correspond to the two roots of equation (5.46). We have analyzed the situation for $m = 4, 6, 8, 10$ and 12 numerically, and found that the scaling solution $R4$ exists and is stable for suitable parameter choices in all these cases. As an example we present a cut through parameter

FIGURE 5.3: **The fixed point *R*4 for the power law coupling potential**

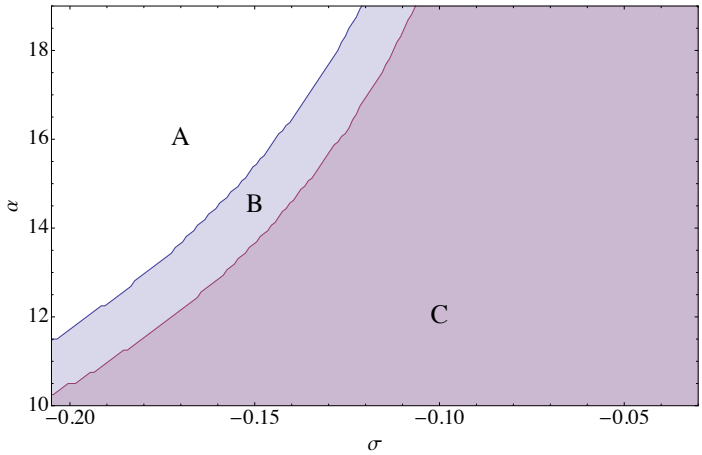

We have fixed the parameters $m = 4$ and $\tilde{\kappa} = 1$. In the region *A* the equation (5.46) has no real solution, in the region *B* the fixed point *R*4 exists but is unstable for both real roots of (5.46), in the region *C* existence is guaranteed for both real roots of (5.46), but stability only for one of the two.

space in Figure 5.3. This plot shows explicitly that the fixed point *R*4 exists and is stable for a suitable choice of parameters.

5.2 PERTURBATIONS ALONG SCALING SOLUTIONS

We will now turn our attention to the evolution of perturbations in the early universe in models containing two non-minimally coupled canonical scalar fields. We adopt the same conventions as in the previous section, i.e. denote the fields by φ and χ, and split the potential according to eq. (5.20). By "early universe" we mean an era during which the cosmic expansion proceeds as if dominated by radiation, i.e. $\mathcal{H}(\tau) = \tau^{-1}$, with τ being conformal time. We will consider a background-evolution during which both fields follow an exact scaling bahavior, in particular the equations of state are assumed to be constant. We stress again that this does not imply a strongly subdominant role of the scalar fields or equations of state of exactly $1/3$. The coupling between the two fields enables a wide range of possible ω_φ's and ω_χ's while still allowing for a radiation-like expansion ($a(\tau) \propto \tau$) and non-negligible scalar field contributions to the energy-densities already in very simple models, as we have seen above. In addition to the two coupled scalar fields we include neutrinos, photons and baryons into our model, but exclude a possible cold dark matter contribution, as is appropriate in coupled scalar field models of dark matter and dark energy.

5.2.1 BASIC FORMALISM

The basic idea we employ to study the early universe evolution of superhorizon perturbations is one already used in earlier works [Malquarti and Liddle, 2002a, Bartolo et al., 2004, Doran et al., 2003].

We write the differential equations governing the evolution of linear perturbations in a convenient matrix form, i.e.

$$\frac{\mathrm{d}U(x)}{\mathrm{d}\ln(x)} = A(x)U(x)\,. \tag{5.47}$$

Here we introduced a convenient new time variable $x \equiv k/\mathcal{H}$ and combined all relevant perturbative quantities into a single perturbation vector $U(x)$. Which quantities these are depends on the approximations one choses to use in the neutrino-, photon- and baryonic sectors. Here we employ the simplest (lowest order) version of the tight-coupling approximation for photons and baryons, which yields a common velocity potential for both components and excludes all higher momenta of the phase space distribution function for photons (see section 4.2 for a derivation). In the case of neutrinos we truncate the Boltzmann-expansion after the quadrupole, leaving an additional anisotropic stress contribution. This is justified for sufficiently early times (see e.g. [Kodama and Sasaki, 1984]). The perturbation variables we employ are consistent with the definitions given in section 4.1.

Since the scalar fields only have two degrees of freedom, the components of the perturbation vector can be chosen to be the energy density contrasts Δ_α and velocity potentials V_α for all components of the cosmic fluid as well as anisotropic stress for neutrinos, i.e.

$$U = \{\Delta_\nu, V_\nu, \Delta_\gamma, \Delta_b, V_\gamma, \Delta_\varphi, V_\varphi, \Delta_\chi, V_\chi, \tilde{\Pi}_\nu\}\,. \tag{5.48}$$

The common velocity potential for photons and baryons is denoted by V_γ here. The entries of the perturbation matrix A can now be read off from the differential equations governing the evolution of these variables. For the photon-, baryon- and neutrino-sector they read

$$\frac{\mathrm{d}\Delta_\gamma}{\mathrm{d}\ln(x)} = -\frac{4}{3}x^2 V_\gamma\,, \tag{5.49}$$

$$\frac{\mathrm{d}\Delta_\nu}{\mathrm{d}\ln(x)} = -\frac{4}{3}x^2 V_\nu\,, \tag{5.50}$$

$$\frac{\mathrm{d}\Delta_b}{\mathrm{d}\ln(x)} = -x^2 V_\gamma\,, \tag{5.51}$$

$$\frac{\mathrm{d}V_\nu}{\mathrm{d}\ln(x)} = \frac{1}{4}\Delta_\nu - V_\nu + 2\Psi - \left(\frac{1}{6}x^2 + \Omega_\nu\right)\tilde{\Pi}_\nu \tag{5.52}$$

$$\frac{\mathrm{d}V_\gamma}{\mathrm{d}\ln(x)} = \frac{4\Omega_\gamma}{4\Omega_\gamma + 3\Omega_b}\left(\frac{1}{4}\Delta_\gamma + \Psi\right) - \frac{4\Omega_\gamma + 6\Omega_b}{4\Omega_\gamma + 3\Omega_b}V_\gamma + \Phi\,, \tag{5.53}$$

$$\frac{\mathrm{d}\tilde{\Pi}_\nu}{\mathrm{d}\ln(x)} = \frac{8}{5}V_\nu - 2\tilde{\Pi}_\nu\,. \tag{5.54}$$

These equations can be derived from the generic equations given in section 4.2 by setting $\omega_{\mathrm{eff}} = 1/3$ and employing

$$\frac{\mathrm{d}}{\mathrm{d}\tau} = -\frac{1}{2}\mathcal{H}(1 + 3\omega_{\mathrm{eff}})\frac{\mathrm{d}}{\mathrm{d}\ln(x)}\,. \tag{5.55}$$

The equation for the velocity potential V_γ is different from the one employed in [Doran et al., 2003, Majerotto et al., 2010]. This version is the correct one if one makes no assumption about the ratio Ω_b/Ω_γ, as should be clear from the generic derivation given in chapter 4. Both version agree in the limit $\Omega_b/\Omega_\gamma \to 0$.

The gravitational potentials are then given by

$$\Psi = -\frac{3}{2}\frac{\sum_\alpha \Omega_\alpha \left(\Delta_\alpha + 3(1+\omega_\alpha)V_\alpha\right)}{x^2+6}, \tag{5.56}$$

$$\Psi'/\mathcal{H} = -\Phi + \frac{3}{2}\sum_\alpha \Omega_\alpha (1+\omega_\alpha)V_\alpha, \tag{5.57}$$

$$\Phi = \Psi - 3\sum_\alpha \Omega_\alpha \omega_\alpha \tilde{\Pi}_\alpha = \Psi - \Omega_\nu \tilde{\Pi}_\nu. \tag{5.58}$$

The generic equations of motion for the scalar fields are quite complicated (see equations (4.48), (4.49) and (4.60) to (4.63) in section 4.1), but they can be simplified considerably in an exact scaling scenario. The background quantities appearing in the scalar sector are the equations of state ω_φ and ω_χ, the adiabatic sound speeds $c^2_{a,\varphi}$ and $c^2_{a,\chi}$, the couplings q_φ and q_χ, their time-derivatives and the second derivative of the common potential $V_{2,\varphi\varphi}$.
In an exact scaling scenario we assume constant equations of state, i.e. we set $\omega'_\varphi = \omega'_\chi = 0$. This implies that the adiabatic sound speeds are given by $c^2_{a,\varphi} = \omega_\varphi$ and $c^2_{a,\chi} = \omega_\chi$. Furthermore the couplings q_φ and q_χ have to be constant by equation (5.13) and are of course related by equation (5.7). Finally the scalar equations of state are related by equation (5.9) and we only have to deal with the second derivative $V_{2,\varphi\varphi}$ of the common potential. For a generic scalar field evolution this can of course take any, in principle time-dependent, form, but in a scaling scenario it merely introduces another constant into the equations, which can be seen as follows.

We start by investigating the generic potential for exact scaling solutions given by equation (5.15). Let us recall the generic shape of the potential V_2 introduced above in eq. (5.31)

$$V_2(\varphi,\chi) = \mu_2\, g(\xi)\, \mathrm{e}^{-\alpha\varphi/M_p}. \tag{5.59}$$

We can now take the second derivative of this potential with respect to φ and recall $\alpha = 3(1+\omega_{\rm eff})M_p/c_1$, to obtain (for $\omega_{\rm eff} = 1/3$)

$$V_{2,\varphi\varphi} = \mu_2 \mathrm{e}^{-4\varphi/c_1}\left[\frac{16}{c_1^2}g(\xi) + \frac{8c_2}{c_1^2}g'(\xi) + \frac{c_2^2}{c_1^2}g''(\xi)\right]. \tag{5.60}$$

Since ξ is constant during a scaling solution, it is clear that $V_{2,\varphi\varphi} \propto V \propto \rho_{\rm tot}$ in such scenarios and we can thus define

$$V_{2,\varphi\varphi} = 3q_\varphi \frac{\mathcal{H}^2}{a^2} r_\varphi, \tag{5.61}$$

with some constant r_φ. Note that r_φ is in principle a new independent constant depending on the functional form of g and can generally generally not be related to q_φ, as it depends on the second derivative g'', whereas only the first derivative g' enters into q_φ.

Now we can finally write down the equation for the scalar sector in a form where the only remaining constant parameters are ω_φ, r_φ and the density parameters. They read

$$\begin{aligned}
\frac{\mathrm{d}\Delta_\varphi}{\mathrm{d}\ln(x)} =& \frac{\omega_\varphi - 3}{1+\omega_\varphi}\Delta_\varphi + (3\omega_\varphi - 1)\left(\Psi'/\mathcal{H} + \Phi\right) + (3\omega_\varphi - 1)(r_\varphi - 4)V_\chi + \frac{4(\omega_\varphi - 3)}{1+\omega_\varphi}\Psi \\
&+ \left((1-3\omega_\varphi)r_\varphi - x^2(1+\omega_\varphi) + \frac{2(\omega_\varphi - 1)(7+3\omega_\varphi)}{1+\omega_\varphi}\right)V_\varphi\,, \qquad (5.62)\\
\frac{\mathrm{d}V_\varphi}{\mathrm{d}\ln(x)} =& \frac{1}{1+\omega_\varphi}\Delta\varphi + \Phi + \frac{2(1-\omega_\varphi)}{1+\omega_\varphi}V_\varphi + \frac{4}{1+\omega_\varphi}\Psi\,, \qquad (5.63)\\
\frac{\mathrm{d}\Delta_\chi}{\mathrm{d}\ln(x)} =& -2\Delta_\chi + \frac{\Omega_\varphi}{\Omega_\chi}(1-3\omega_\varphi)\left(\Psi'/\mathcal{H} + \Phi\right) - 4\left(2 + \frac{\Omega_\varphi}{\Omega_\chi}\frac{1-3\omega_\varphi}{1+\omega_\varphi}\right)\Psi \\
&- \left(\frac{(r_\varphi - 6)(3\omega_\varphi - 1)\Omega_\varphi + 8\Omega_\chi}{\Omega_\chi} + \frac{4\Omega_\chi + \Omega_\varphi(1-3\omega_\varphi)}{3\Omega_\chi}x^2\right)V_\chi \\
&+ \frac{\Omega_\varphi}{\Omega_\chi}(3\omega_\varphi - 1)\left(4\frac{2+\omega_\varphi}{1+\omega_\varphi} - r_\varphi\right)V_\varphi + \frac{\Omega_\varphi}{\Omega_\chi}\frac{1-3\omega_\varphi}{1+\omega_\varphi}\Delta_\varphi\,, \qquad (5.64)\\
\frac{\mathrm{d}V_\chi}{\mathrm{d}\ln(x)} =& \frac{3(1-3\omega_\varphi)\Omega_\varphi}{(3\omega_\varphi - 1)\Omega_\varphi - 4\Omega_\chi}V_\varphi + \frac{12\Omega_\chi}{\Omega_\varphi(1-3\omega_\varphi) + 4\Omega_\chi}\Psi \\
&+ \frac{3\Omega_\chi}{\Omega_\varphi(1-3\omega_\varphi) + 4\Omega_\chi}\Delta_\chi + \Phi + V_\chi\,. \qquad (5.65)
\end{aligned}$$

The coefficients of the matrix $A(x)$ can be read off from equations, (5.49) - (5.54) and (5.62) - (5.65) after replacing the gravitational potentials.

Before analyzing the solutions for the perturbations we have to investigate the background quantities appearing in $A(x)$. Those are generally x-dependent, but in this analysis we are interested only in the superhorizon-limit defined by $x \ll 1$ and we can therefore work with Taylor-expansions in x. To see that, first note that we assume a radiation-like expansion with a scalar scaling solution in the early universe, a scenario only slightly disturbed by the baryonic density parameter, which is small, but grows linearly in x:

$$\Omega_b = \Omega_{b,\mathrm{in}}\frac{a}{a_\mathrm{in}} = \Omega_{b,\mathrm{in}}\frac{\mathcal{H}_\mathrm{in}}{k}x\,. \qquad (5.66)$$

This implies that all the other density parameters are constant to leading order, but decrease slowly at linear order in x . Evaluating Friedmanns equations for a flat universe in the form $\Omega_\nu + \Omega_\gamma + \Omega_\varphi + \Omega_\chi + \Omega_b = 1$ order by order in x then yields to leading order

$$\Omega_\alpha = \Omega_{\alpha,0}\,(1-x) \quad \text{for all } \alpha \neq b. \qquad (5.67)$$

Using this, one can directly deduce that we can expand the matrix $A(x)$ as a Taylor-series in x and recover a constant matrix at leading order:

$$A(x) = A_0 + A_1 x + A_2 x^2 + O(x^3)\,. \qquad (5.68)$$

With this approximation we can immediately write down the leading order solution for equation (5.47), which reads

$$U_0(x) = \sum_i c_i x^{\lambda_i} U_0^{(i)}\,, \tag{5.69}$$

where $U_0^{(i)}$ are eigenvectors of the matrix A_0 and λ_i the corresponding eigenvalues. With this as a starting point, one can now easily determine higher order corrections to the found solution by expanding the eigenvectors as follows:

$$U^{(i)}(x) = U_0^{(i)} + U_1^{(i)} x + U_2^{(i)} x^2 + O(x^3)\,, \tag{5.70}$$

where the first order correction is then given by

$$U_1^{(i)} = ((\lambda_i + 1)\mathbb{I} - A_0)^{-1} A_1 U_0^{(i)}\,, \tag{5.71}$$

and the other corrections can be calculated in a similar fashion, but we will not need them here. Of course, the general solution is given by

$$U(x) = \sum_i c_i x^{\lambda_i} U^{(i)}(x)\,. \tag{5.72}$$

A short comment concerning the different approximations used here might be in order. As explained in section 4.2, we use the simplest version of the tight coupling approximation for photons and baryons, i.e. we only include coupling terms to leading order (that is zeroth order) of $\mathcal{H}\tau_c \ll 1$, where $\tau_c = (a n_e \sigma_T)^{-1}$ is the Thomson interaction timescale. One might question whether it is consistent to go to next to leading order in the x-expansion of the matrix $A(x)$, but not include the next order in the TCA, i.e. terms suppressed by $\mathcal{H}\tau_c$. As it turns out, for the relevant wavenumbers we have $x = k/\mathcal{H} \gg \mathcal{H}\tau_c$ during radiation domination. To see this, note the following: The Thomson interaction timescale is given by $\tau_c = (a n_e \sigma_T)^{-1}$. During radiation domination, but after electron-positron annihilation, we can approximate the electron density by

$$n_e \approx n_b = \frac{\Omega_b\, 3M_p^2 \mathcal{H}^2}{a^2 m_p}\,, \tag{5.73}$$

where m_p is the proton mass (which is roughly the hydrogen mass, we ignore other light elements in this estimate). Since we have $\mathcal{H} \propto a^{-1}$ during this time, we obtain

$$x \gg \mathcal{H}\tau_c \Leftrightarrow k \gg \frac{m_p}{3M_p^2 \sigma_T} \frac{a}{\Omega_b}\,. \tag{5.74}$$

The ratio a/Ω_b remains constant during radiation domination, we estimate it by its value at matter-radiation equality, i.e. $a_{\mathrm{eq}}/\Omega_b(a_{\mathrm{eq}}) \approx 1/320$. Plugging in numbers then yields that our approximation appears to be valid for $k \gg 0.2 \times 10^{-4}\ \mathrm{Mpc}^{-1}$. This breaks down for very small k, but $10^{-4}\ \mathrm{Mpc}^{-1}$ is already far below what is currently observable.

5.2.2 EIGENVALUES AND EIGENMODES

Eigenvalues

In order to determine the dominant perturbation modes in the early universe in coupled two scalar field models one simply has to determine the eigenvalues λ_i of the matrix A_0 with the largest real parts and the corresponding eigenvectors. In principle these depend on 4 parameters, which can be taken to be ω_φ, r_φ, Ω_φ and Ω_χ. Here ω_φ, Ω_φ and Ω_χ determine the scaling solution and r_φ appears only at the perturbative level. The remaining density parameters for neutrinos and photons are fixed by the fact that we assume a FLRW metric without curvature, i.e. $\Omega_\nu + \Omega_\gamma + \Omega_\varphi + \Omega_\chi = 1$ and the well known relation $\Omega_\nu = 21/8 \times (4/11)^{4/3}\,\Omega_\gamma$, which is valid after electron-positron annihilation (see chapter 2). However, four of the eigenvalues are always given by

$$\{\lambda_1, \lambda_2, \lambda_3, \lambda_4\} = \{0, 0, 0, -1\}\,, \tag{5.75}$$

irrespective of the values of these parameters. The remaining 6 eigenvalues are very complicated functions of the 4 free parameters. Four of them, say λ_5 to λ_8, are given by the roots of a fourth order polynomial, which can be explicitly written down, but the resulting equations are quite complicated and not enlightening at all. Instead, we treat those eigenvalues numerically by running through a grid of the four free parameters $\{\omega_\varphi, r_\varphi, \Omega_\varphi, \Omega_\chi\}$. We find that they appear to be bound above by -0.5. This finding is subject only to the constraint that r_φ is not bound in general, in our numerics we chose an interval of $[-10, 10]$ for this parameter. The other three parameters are bound and thus our grid coveres the entire allowed parameter range and can be considered 'complete' in this sense. Still, it seems unlikely that this conclusion will change for very large absolute values of r_φ, and in fact, for the specific models we discuss below, this will not be an issue.

The remaining two eigenvalues are given by

$$\lambda_{9,10} = \frac{\left(-3\omega_\varphi^2 - 2\omega_\varphi + 1\right)\Omega_\varphi\Omega_\chi + 4\omega_\varphi\Omega_\chi^2 + 4\Omega_\chi^2 \mp \sqrt{F}}{2(\omega_\varphi + 1)\Omega_\chi((3\omega\varphi - 1)\Omega_\varphi - 4\Omega_\chi)}\,, \quad \text{with} \tag{5.76}$$

$$\begin{aligned} F = -(\omega_\varphi + 1)\Omega_\chi^2(-3\omega_\varphi\Omega_\varphi + \Omega_\varphi + 4\Omega_\chi)\big[&(3\omega_\varphi - 1)\Omega_\varphi(16r_\varphi - 15\omega_\varphi - 79) \\ &+ 4\Omega_\chi(-4r_\varphi(1 - 3\omega_\varphi) - 33\omega_\varphi + 31)\big]\,. \end{aligned} \tag{5.77}$$

Only these two 'critical' eigenvalues can have a real part bigger than zero, a case will will call *strongly growing* from now on. As we will see below, the nullspace of A_0 always contains an adiabatic mode. It is precisely the two potentially strongly growing modes which can render the adiabatic mode unstable, which would make the corresponding scenario difficult to reconcile with observations [Enqvist et al., 2000, 2002, Beltran et al., 2005a, Seljak et al., 2006, Keskitalo et al., 2007, Kawasaki and Sekiguchi, 2008, Castro et al., 2009, Valiviita and Giannantonio, 2009, Li et al., 2011, Ade et al., 2013c]. One could of course conceivably come up with reasons why these modes are initially strongly suppressed compared to the adiabatic mode, so that it does not become dominant during the radiation dominated era, but such a fine-tuning of initial conditions is often not very natural and generally undesirable.

To visualize the effect of the coupling between the two scalar fields we have plotted the real part of the two critical eigenvalues in Figures 5.4 and 5.5. Clearly, one of the values can become bigger than zero for large deviations of ω_φ from the uncoupled value of $1/3$, i.e. for big couplings. Furthermore, as one would expect, this effect becomes stronger for larger scalar field density parameters. In the uncoupled case, even the critical eigenvalues have real parts bound by -0.5 from above and the corresponding modes are thus subdominant. This shows that a strong coupling can be relevant for early universe perturbations, because it can potentially change the dominant perturbation mode, rendering the adiabatic mode unstable.

One should note however, that just because we can find a set of parameters which yield a strongly growing eigenvalue in this numerical treatment does not necessarily mean that we can construct a model actually yielding a scaling solution with such a feature. The problem is of course, that for any given scaling solution some of the parameters treated here as free might well be related, or scaling solutions with a radiation like expansion might not even exist or be confined to specific regions of parameter-space. Let us therefore investigate the models introduced in section 5.1.2 with regard to this issue.

Exponential coupling potential

The values of the critical eigenvalues for the exponential coupling potential can now be obtained directly from the general results. First, we note that the constant r_φ can be related to the the potential parameters through equation (5.60). We obtain after a short computation:

$$r_\varphi = \sqrt{3(1+\omega_\varphi)\Omega_\varphi}(\alpha+\sigma s_1)\left[1-\frac{\sigma^2(s_1^2-s_2)}{(\alpha+\sigma s_1)^2}\right]. \tag{5.78}$$

For the exponential coupling potential this simplifies since we have $s_1^2 = s_2 = \lambda^2$ and $\alpha+\sigma s_1 = 2\beta$. Furthermore, the coupling β is related to q_φ by equations (3.104) and (5.13), which can be combined to give

$$\beta = \frac{\sqrt{3}\Omega_\varphi(3\omega_\varphi-1)}{\sqrt{(1+\omega_\varphi)\Omega_\varphi}\left(2\Omega_\chi+\Omega_\varphi(3\omega_\varphi-1)\right)}. \tag{5.79}$$

With this the function r_φ for the exponential coupling potential can be shown to be:

$$r_\varphi^{exp} = \frac{6\Omega_\varphi(3\omega_\varphi-1)}{2\Omega_\chi+\Omega_\varphi\left(3\omega_\varphi-1\right)}. \tag{5.80}$$

First we note that the range for r_φ is in this case restricted to $-6 \leq r_\varphi^{exp} \leq 6$, and therefore the range of r_φ investigated numerically for the eigenvalues $\lambda_5,\ldots,\lambda_8$ is more than sufficient. It is thus guaranteed that they do not correspond to strongly growing modes. Furthermore we have checked numerically that the same holds true for the two critical eigenvalues λ_9 and λ_{10}, they are bound above by 0. This can be seen in Figures 5.4 and 5.5. The particular shape of the potential leads to a form of the coupling term r_φ that excludes the region of strongly growing eigenvalues as indicated by the solid red lines.

FIGURE 5.4: **Real part of the critical eigenvalue λ_9**

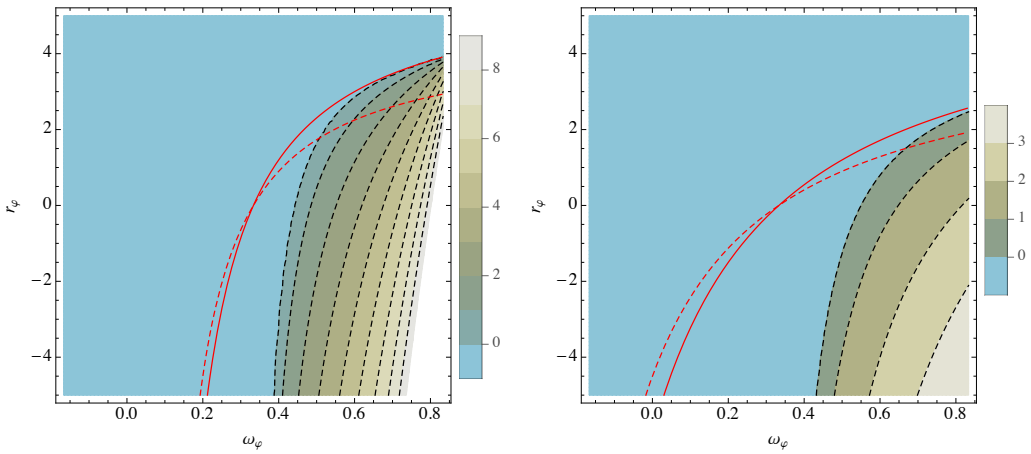

The left panel shows the real part of the critical eigenvalue λ_9 for $\Omega_\varphi = 0.05$ and $\Omega_\chi = 0.02$, the right panel for $\Omega_\varphi = \Omega_\chi = 0.002$. The solid red line represents a model with an exponential coupling potential, the dashed red line a power-law coupling potential with $m = 4$. Both models are introduced and discussed in section 5.1.2. Figure taken from [Beyer, 2014a].

FIGURE 5.5: **Real part of the critical eigenvalue λ_{10}**

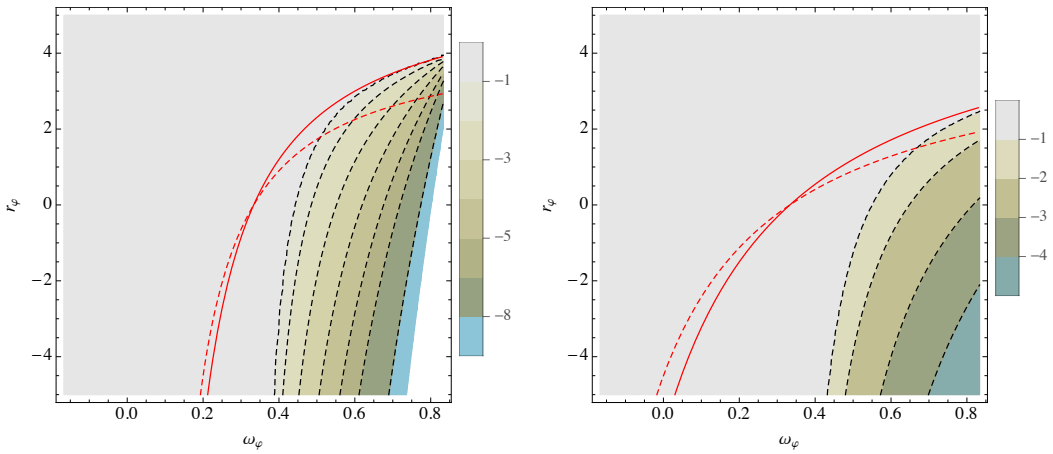

The left panel shows the real part of the critical eigenvalue λ_{10} for $\Omega_\varphi = 0.05$ and $\Omega_\chi = 0.02$, the right panel for $\Omega_\varphi = \Omega_\chi = 0.002$. The solid red line represents a model with an exponential coupling potential, the dashed red line a power-law coupling potential with $m = 4$. Both models are introduced and discussed in section 5.1.2.

However, in this case a numerical treatment of the two critical eigenvalues is not necessary, we can determine the eigenvalues analytically in this case. First, we plug eq. (5.80) into eq. (5.76) to obtain

$$\lambda_{9,10} = \frac{1}{2}\left(-1 \pm \frac{\sqrt{\frac{\left(45\omega_\varphi^2-66\omega_\varphi+17\right)\Omega_\varphi+(62-66\omega_\varphi)\Omega_\chi}{(\omega_\varphi+1)(-3\omega_\varphi\Omega_\varphi+\Omega_\varphi-2\Omega_\chi)}}}{\mathrm{sgn}(-3\omega_\varphi\Omega_\varphi+\Omega_\varphi+4\Omega_\chi)}\right). \tag{5.81}$$

This still looks rather involved, but we can evaluate the expression for each stable fixed point with a radiation like expansion separately.

First, for the point R_2 we have $\omega_\varphi = 1$, from which we directly obtain $\Re(\lambda_{9,10}) \in \{-1,0\}$. Second, for $R3$ we have $\omega_\varphi = 1/3$, which directly gives $\Re(\lambda_{9,10}) = -1/2$. Finally, the point R_4 is slightly more complicated. But we still simply plug in the solutions for Ω_φ, Ω_χ and ω_φ for this fixed point and obtain the eigenvalues as a function of α, λ and β. After some algebra, one comes to the conclusion that

$$\Re(\lambda_{9,10}) \leq 0 \Leftrightarrow \alpha\lambda^2 \geq 2\beta(\alpha-2\beta)^2 + 2\beta\lambda^2, \tag{5.82}$$

which is guaranteed by the conditions of existence for the fixed point $R4$ alone.

Thus for the coupled exponential potential there is a huge region of the parameter space which is not only viable as an early cosmology at the background level, but for which no strongly growing perturbation modes exist and the adiabatic mode is therefore stable. With the results presented here one can therefore directly write down the early universe background evolution for any set of parameters α, β and λ with the density parameters replaced by the ones given in Table 5.1 for the relevant fixed point, which we have done in chapter 4. Furthermore, the dominant perturbation modes are given by the nullspace of A_0, which we will analyze in the next subsection.

Power law coupling potential

Let us now move on to see how perturbations around scaling solutions for the power law coupling potential behave. First we need to determine r_φ^{pc}, for which can be directly deduced from equation (5.78) with the help of (5.42):

$$r_\varphi^{pc} = r_\varphi^{exp}\left(1 - \frac{(\sigma s_1)^2}{(\alpha+\sigma s_1)^2 m}\right). \tag{5.83}$$

Clearly a power law coupling lowers the $r_\varphi(\omega_\varphi)$ curve for positive values of r_φ compared to the exponential coupling model, which suggests that it might push the perturbations into a regime where the critical eigenvalue λ_9 can become positive. We have visualized this in Figures 5.4 and 5.5 by a dashed red line, obtained for $m = 4, \alpha = 4$ and $\sigma s_1 = -2$.
Before claiming that strongly growing isocurvature modes exist along scaling solutions in this model we have to check a few things. First, can we really just adjust the value of σs_1? After all s_1 is not a model parameter, but needs to obey equation (5.46). This is, however, not an issue, since for $\sigma s_1 = -\zeta$ the parameter choice

$$\tilde{\kappa} = -\frac{m^m \sigma^m}{(-\zeta)^m}\left[1 - \zeta\frac{1+\sigma^2}{\alpha\sigma^2}\right] \tag{5.84}$$

guarantees that equation (5.46) is satisfied for $s_1 = -\zeta/\sigma$. Second, in our analysis of the growth of perturbations we have chosen our parameters to be Ω_φ, Ω_χ and ω_φ. Whether or not the range of existence (and stability) of the fixed point $R4$ allows for the parameter range where the adiabatic mode becomes unstable still needs to be checked. We have done this numerically, with the following result: Strongly growing isocurvature modes can exist for the power law coupling potential around the fixed point $R4$, however, only for one of the two real roots of equation (5.46). This is precisely the root for which the fixed point is never stable. For the second root, which guarantees stability of the fixed point in a given parameter range, strongly growing modes do not exist. In other words: We can choose initial conditions corresponding to a scaling solution in this model which allows for parameters Ω_φ, Ω_χ and ω_φ in the range where the a strongly growing isocurvature mode exists, but this solution is unstable. We can also construct a stable scaling solution, but this does not allow for the range of Ω_φ, Ω_χ and ω_φ with a strongly growing isocurvature mode.
These conclusions are of course subject to the constraint that or numerical grid is of finite size. We show the real part of the eigenvalue λ_9 for the fixed point $R4$ in Figure 5.6, where we chose the root of equation (5.46) leading to an unstable scaling solution.

Eigenvectors

Since the generic eigenvalues have very complicated forms in general, so do the corresponding eigenvectors. This also holds for the eigenvectors belonging to the two critical eigenvalues, representing potentially dominant modes. Things look a lot better for the nullspace of A_0, which of course includes

FIGURE 5.6: **Eigenvalue λ_9 for the power law coupling potential**

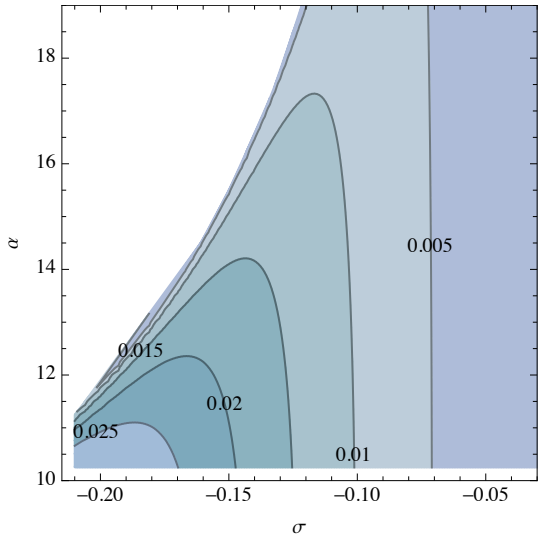

The critical eigenvalue λ_9 for the fixed point $R4$ for the power law coupling potential, corresponding to the 'unstable root' of equation (5.46). We show a cut through parameter space for $m = 4$ and $\tilde{\kappa} = 1$. The white region denotes the section of parameter space where the fixed point does not exist (cf. Figure 5.3).

all dominant perturbations modes in the absence of strongly growing modes. One is free to choose any suitable basis of this three-dimensional space, we choose to categorize the modes following Doran et al. [2003], i.e. by means of the total curvature and relative entropy perturbations.

In this categorization a mode is called an isocurvature mode if the total curvature perturbation vanishes, i.e.

$$\zeta = \sum_{\alpha} \frac{\rho_\alpha \Delta_\alpha}{\rho_{\rm tot} + p_{\rm tot}} = 0\,, \tag{5.85}$$

and adiabatic if all relative and internal entropy perturbations, i.e.

$$S_{\alpha\beta} = \frac{\Delta_\alpha}{(1+\omega_\alpha)(1-q_\alpha)} - \frac{\Delta_\beta}{(1+\omega_\beta)(1-q_\beta)} = 0\,, \tag{5.86}$$

$$\Gamma_\alpha = \frac{1}{p_\alpha}\left(\delta p_\alpha - c^2_{a,\alpha}\delta\rho_\alpha\right) = 0 \quad \text{for all } \alpha, \beta\,. \tag{5.87}$$

There are some deviating definitions of the total curvature pertubation in the literature [Mukhanov et al., 1992], but they agree in the superhorizon limit in a flat universe.

This categorization splits the nullspace into a two-dimensional isocurvature space and one adiabatic mode. The adiabatic eigenvector is given by

$$\begin{pmatrix} \Delta_\nu \\ V_\nu \\ \Delta_\gamma \\ \Delta_b \\ V_\gamma \\ \Delta_\varphi \\ V_\varphi \\ \Delta_\chi \\ V_\chi \\ \tilde{\Pi}_\nu \end{pmatrix}_{\rm adiab.} = \mathcal{C} \begin{pmatrix} 1 \\ -5/4\,\mathcal{S}^{-1} \\ 1 \\ 3/4 \\ -5/4\,\mathcal{S}^{-1} \\ 1 \\ -5/4\,\mathcal{S}^{-1} \\ 1 \\ -5/4\,\mathcal{S}^{-1} \\ -\mathcal{S}^{-1} \end{pmatrix}, \tag{5.88}$$

where $\mathcal{S} = (15 + 4\Omega_\nu)$. This is very similar to the adiabatic mode in minimally coupled quintessence scenarios [Doran et al., 2003].

The isocurvature-subspace can be further decomposed into one baryon-isocurvature and one neutrino/ scalar-isocurvature mode.

The baryon isocurvature mode is characterized by the demand that all species except for baryons should be adiabatic, i.e. $S_{b,\alpha} \neq 0$ for all α, but $S_{\alpha,\beta} = 0$ for $\alpha, \beta \neq b$. For our set of scaling scenarios this necessarily implies that the scalar internal entropy perturbations also vanish, i.e. $\Gamma_\varphi = \Gamma_\chi = 0$. In the corresponding eigenvector all entries except for Δ_b vanish at leading order, we therefore quote

the result to subleading order in x here:

$$\begin{pmatrix} \Delta_\nu \\ V_\nu \\ \Delta_\gamma \\ \Delta_b \\ V_\gamma \\ \Delta_\varphi \\ V_\varphi \\ \Delta_\chi \\ V_\chi \\ \tilde{\Pi}_\nu \end{pmatrix}_{\text{bar.iso.}} = \mathcal{C} \begin{pmatrix} 0 \\ -45/8\,\Omega_b \mathcal{P}^{-1}/(15+2\Omega_\nu) \\ 0 \\ 1 \\ -45/8\,\Omega_b \mathcal{P}^{-1}/(15+2\Omega_\nu) \\ -3/4\,(\omega_\varphi - 3)\Omega_b \mathcal{P}^{-1} \\ -45/8\,\Omega_b \mathcal{P}^{-1}/(15+2\Omega_\nu) \\ -2\Omega_b/\Omega_\chi\, \mathcal{P}^{-1}\mathcal{X} \\ -45/8\,\Omega_b \mathcal{P}^{-1}/(15+2\Omega_\nu) \\ -3\Omega_b \mathcal{P}^{-1}/(15+2\Omega_\nu) \end{pmatrix}, \tag{5.89}$$

where we defined the quantities

$$\mathcal{P} = (1 + 2\Omega_\gamma + 2\Omega_\nu) \quad \text{and} \tag{5.90}$$

$$\mathcal{X} = \left(-2(1-\Omega_\chi) + (1-3\omega_\varphi)\Omega_\varphi/4\right). \tag{5.91}$$

This vector differs considerably from the ones found in previous studies [Doran et al., 2003], which is due not only to the presence of two coupled scalar fields, but also to the improved treatment of the tight coupling approximation, which changes the subleading order contributions to the perturbation matrix $A(x)$.

Finally, the neutrino/scalar isocurvature mode is characterized by which $S_{\gamma,b} = 0$, as this is the only relative entropy perturbation not involving neutrinos or scalar fields. Enforcing this necessarily implies $S_{\varphi,\chi} = \Gamma_\varphi = \Gamma_\chi = 0$, with all other relative entropy perturbations non-vanishing. The corresponding eigenvector reads at leading order:

$$\begin{pmatrix} \Delta_\nu \\ V_\nu \\ \Delta_\gamma \\ \Delta_b \\ V_\gamma \\ \Delta_\varphi \\ V_\varphi \\ \Delta_\chi \\ V_\chi \\ \tilde{\Pi}_\nu \end{pmatrix}_{\text{neut.iso.}} = \mathcal{C} \begin{pmatrix} \mathcal{S} \\ 15/4 \\ -\Omega_\nu/\Omega_\gamma \mathcal{S} \\ 3\Omega_\nu/4\Omega_\gamma \mathcal{S} \\ -\Omega_\nu/4\Omega_\gamma(\mathcal{S}+4\Omega_\gamma) \\ 0 \\ -\Omega_\nu \\ 0 \\ -\Omega_\nu \\ 3 \end{pmatrix}, \tag{5.92}$$

Note that due to the convenient choice of perturbation variables, the dependence on the coupling only appears at subleading order in the baryon isocurvature mode through ω_φ. At leading order, the nullspace of the leading order perturbation matrix A_0 is completely independent of r_φ or q_φ.

6 THE INHOMOGENEOUS UNIVERSE 2: STRUCTURE FORMATION

A huge amount of cosmological observations concerns virialized objects, such as galaxies or clusters of galaxies. Any good cosmological theory should be aiming not only to produce a valid background expansion and evolution of linear perturbations, but also to give rise to a theory of structure formation in concordance with observations of such objects. This clearly goes beyond the scope of linear perturbation theory, as virialized objects typically have an overdensity of roughly 200. So how can one compare structure growth in a cosmological model with observations?

From the simulation side, the state-of-the-art method to investigate non-linear structure formation are N-body simulations, which have have advanced considerably during recent years and can by now not only account for the physics of cold dark matter, but also include quite sophisticated models for the baryonic physics of galaxy formation (see e.g. [Genel et al., 2014, Vogelsberger et al., 2014a]) or (coupled) quintessence models (see e.g. [Baldi, 2012]). The continuously growing precision of these simulations allows a comparison with observational data in ever increasing detail. Some of the results raise questions about the validity of the ΛCDM model concerning structure formation on small scales (see e.g. [Weinberg et al., 2013a] for a short recent review).

It would, in principle, be desirable to perform similar simulations for our coupled scalar field dark matter model in order to figure out how the linear suppression of power on small scales translates to structure formation. This would, however, constitute a quite involved project, which goes beyond the scope of this thesis. The basic problem is the following: All modern N-body codes are based on a Newtonian simulation of particles, which trace the distribution of cold (or warm) dark matter. It is a priori unclear how to translate this concept to a coupled scalar field model such as ours. Clearly modeling the scalar fields directly is out of the question, as this already failed at the background level and the level of linear perturbations. It would thus be desirable to come up with a an effective description of our model which is valid in the regime of non-linear perturbations and try to evolve the corresponding equations. This could possibly be achieved by a similar averaging procedure as we introduced in chapter 4, and we have in fact started this project, but not achieved any presentable results at the time of writing this thesis.

Instead, we take a different approach in this chapter, which is technically a lot less involved: We study the formation of structures in our model using the extended Press-Schechter (ePS) formalism. This allows us to make predictions about structure formation in our model from the linear power spectrum, with very little input from non-linear structure formation. We will discuss the assumptions made in our calculations and their limits in detail below.

We start this chapter with a very short and non-technical review about the current situation concerning the small scale problems of the ΛCDM model and discuss some alternatives to cold dark matter which might help to alleviate them. In this part we roughly follow [Weinberg et al., 2013a]. We then move on to introduce the ePS formalism and discuss the technical issues which arise when trying to apply it to our model. Finally we use the results to put constraints on the current bolon mass and discuss possible observational signatures. For all models discussed here we use the same cosmological parameters as in chapter 4 (see equations (4.236) and (4.237)). The results presented here have been published in [Beyer and Wetterich, 2014, Beyer, 2014b]. In sections 6.2 to 6.5 we closely follow the presentation of section V in [Beyer, 2014b]. Copyright for the figures and excerpts of this preprint resides, at the time of writing this, with the author, but will be transferred to the American Physical Society upon acceptance of the paper.

6.1 STRUCTURE FORMATION ON SMALL SCALES

Let us not take much time talking about the successes of N-body simulations in cold dark matter scenarios on large scales, where they produce results which are in excellent agreement with observations. Instead, let us directly move on to smaller scales, where the cold dark matter paradigm might run into some trouble.

6.1.1 SMALL SCALE ISSUES

As the accuracy of cold dark matter N-body simulations and the amount of observational data to compare them with continuously increased in the late 90s, apparent discrepancies between the predictions of the cold dark matter scenario and observations started to emerge. Originally these problems were separated into two issues: the *cusp-core problem* and the *missing satellite problem*.

The cusp-core problem describes a discrepancy between simulations and observations concerning the matter distribution in the center of dark matter halos. In cold dark matter simulations the central density profile of halos is rising like r^{-b}, with $b = 1 - 1.5$ [Navarro et al., 1997, Moore et al., 1998]. Measurements of the circular velocities of stars within galactic halos, however, found that a flat density profile fits the observations much better [Flores and Primack, 1994, Moore, 1994].

The missing satellite problem is concerned with the distribution of subhalos within a larger cold dark matter halo. These smaller halos are expected to host satellites of the larger structures, such as dwarf galaxies surrounding a typical galaxy. Simulations suggest a huge number of such halos exist, but, until the year 2000, only 9 dwarf galaxies around the Milky way were observed. This lead to the conclusion that either these dark matter halos are not there, or they are for some reason void of stars.

In recent years much progress concerning both issues has been made. Probably the most important news in this context was the discovery of an additional ~ 15 'ultra faint' dwarf galaxies through analyses of SDSS data [Abazajian et al., 2009]. Since this survey covered only about 20% of the sky and these galaxies are so faint that they could be detected only out to a distance of roughly 50-100 kpc (the virial radius of the Milky way is roughly 300 kpc), some authors have proposed that the

number of actual dwarf galaxies in the Milky way should be several hundred [Tollerud et al., 2008]. Other studies, however, are more conservative, coming up with a bound of 66 [Lovell et al., 2014]. The situation is further complicated by the fact that baryonic physics may play an important role at small scales. We cannot even hope to scratch the surface of the complexities of galaxy formation theories here, but the basic results concerning the missing satellite problem are the following: The masses of the faintest dwarf galaxies (within a radius of 0.3 kpc) seem to be universal at around 10^7 $M_\odot$, whereas the luminosities vary considerably (about 10^3-10^7 $L_\odot$) [Strigari et al., 2008]. Models including baryonic physics through stellar feedback and photoionization have shown that galaxy formation on such small scales is a highly stochastic process, potentially leaving a large number of dark halos void of stars, and it is in fact possible to account for the luminosity mass relation [Koposov et al., 2009]. Despite the fact that there are some open issues, it is probably fair to say that the missing satellite problem is at this stage more a problem of understanding the physics of galaxy formation than one of the dark sector.
Things look different, however, if one takes a closer look at the most massive dwarf galaxies. Here ΛCDM simulations suggest that the Milky should contain a number of halos with a mass exceeding the one observed for the heaviest dwarf galaxies by a factor of ~ 5 [Springel et al., 2008]. The precise magnitude of the disagreement depends on the simulation parameters (such as, for example, the not very well known mass of the Milky way), but even for conservative assumptions the discrepancy seems to be persistent [Boylan-Kolchin et al., 2011, 2012]. As was concluded in [Weinberg et al., 2013a], this issue might well be a manifestation of the cusp-core problem in disguise. Since cuspy dark matter profiles generate larger masses, a simulation giving flatter density profiles might reduce the masses of the heaviest Milky way subhalos and potentially solve this problem. Whether or not this can be achieved through baryonic physics is currently a topic of scientific debate. While baryonic processes certainly flatten the inner density profiles of dark matter halos, it remains uncertain if they are able to do so for structures which are largely void of baryonic matter today. For more references on this issue see e.g. [Weinberg et al., 2013a].

Whether baryonic effects will ultimately be able to resolve the small scale issue of the cold dark matter model or not remains to be seen. In the meantime, however, one might be tempted to explore, as an alternative route, modifications of the dark sector itself.

6.1.2 Modifying dark matter

Many particle physics models of dark have been constructed in attempts to address the small scale issue of structure formation, we want to give a short (biased) overview over what are some of the most popular ones.

Warm dark matter

Probably the most popular alternative to cold dark matter is warm dark matter. In these models the dark matter particle is sufficiently light to retain a non-negligible velocity dispersion, which leads to a free streaming of particles out of gravitational wells and thereby erases small scale features in the matter power spectrum. The precise details of the cosmological implications depend on the specific

particle physics model, here we will focus on the simplest one: A single warm dark matter particle that is thermally produced in the early universe. Some other models, such as for example sterile neutrinos, exhibit similar features of power spectrum suppression and can be related to this simple case for the purposes of structure formation by assigning to them an 'effective thermal' WDM mass. It has been shown in recent years that a WDM particle of mass $1-3$ keV can solve a number of issues of small scale structure formation [Papastergis et al., 2011, Lovell et al., 2012, Menci et al., 2013], but the precise value of the particle mass required to address the individual observations varies considerably within this range. These discrepancies have let Schneider et al. [2013] to investigate whether or not a single WDM particle consistent with observational constraints from the Lyman-α forest [Viel et al., 2013] and SDSS data [Polisensky and Ricotti, 2011] can in fact improve the small scale inconsistencies of cold dark matter models. The answer is, essentially, no. The constraints force the WDM particle mass into a regime where the problems of small scale structure formation can no longer be effectively addressed. This finding is clearly not the end of warm dark matter models. The conclusions of [Schneider et al., 2013] may change, if the bounds on the WDM mass from observations turn out to be slightly weaker than assumed for some reason. Furthermore, one can easily construct models of non-thermal production or models containing particles of several masses in order to get around the bounds found in this paper.

Interacting dark matter

An alternative to warm dark matter are models of self-interacting dark matter [Spergel and Steinhardt, 2000]. Recent cosmological simulations suggest that it is possible to find a parameter range for the interaction strength and the particle mass for which observational constraints are met and yet the formation of structure on the relevant scales is suppressed [Peter et al., 2012, Rocha et al., 2013].

Scalar field dark matter

Finally, let us discuss models of ultra-light scalar field dark matter. Many models of scalar field dark matter have been proposed, but the cosmon-bolon model is, to out knowledge, the only one giving rise to a coupling to dark energy. The literature on these models is quite extensive, and when studying it, one should keep (at least) two basic distinctions between in mind:

1. Is the scalar field considered real or complex?
2. Is the scalar field action considered to be the classical action, such that quantum effects still have to considered in addition to the scalar field dynamics, or the effective action, such that the field equations are exact?

We stress that our model falls within the range of real scalar field models and we consider the action to be the effective action, with no additional quantum corrections present.

BEC models

Let us start with models of the sort where the action is considered to be the classical action. In these models the scalar field is usually assumed to form a Bose-Einstein-condensate (BEC) very early in the universe. The consequences of such a BEC dark matter model have been studied in great detail and in a variety of models (see e.g. [Suarez et al., 2013] for a review). The non-linear dynamics in the Newtonian regime of such models are effectively described by the Newton-Poisson system (see e.g. [Schive et al., 2014]). We will not be too concerned with this class of models, as it is unclear how the results relate, precisely, to the cosmon-bolon model, even in the uncoupled case.

Effective scalar fields models

These are models in which the scalar field equations obtained from the action are assumed to be exact, as in our case. We want to quickly summarize the results that were obtained concerning the formation of structure which are the most relevant for us.
First, static spherically symmetric solutions for the scalar field equations (excluding any additional matter) have been found for a variety models, including exact solutions for exponential potentials [Matos and Guzman, 2000, Matos et al., 2000b,a] and approximate ones for a χ^2-potential, so called oscillatons [Urena-Lopez, 2002]. As the latter ones are relevant for our purposes, let us take a closer look. In order to obtain these solutions, the full Einstein-Klein-Gordon system, consisting of Einstein's equations and the Klein-Gordon equation for a (real or complex) scalar field, needs to be reduced to the so called Newton-Schrödinger system (see e.g. [Alcubierre et al., 2002, Guzman and Urena-Lopez, 2003, 2004]), which effectively consists of an expansion of the scalar field into Fourier modes, very similar to what we have obtained in chapter 4. The resulting leading order system is then the Newton-Schrödinger system. This system allows for stable solutions, so called *oscillatons*. These form acceptable states for virialized dark halos, and, as was shown in [Alcubierre et al., 2002, Guzman and Urena-Lopez, 2003, 2004], dynamical collapse and stabilization of such structures is indeed possible for suitable initial configurations.
What do such results tell us? First, and this is important, stable spherically symmetric configurations do exists for simple scalar field dark matter models, and dynamics allowing for collapse and stabilization as well. We can therefore hope that similar structures arise in our coupled scenario, too. But, we should be remember the conditions under which these results were derived:

1. A spherical spatial symmetry was assumed for both the metric and the scalar field.
2. A weak field limit was assumed for both the deviations of the metric from a Minkowski-form and for the scalar field.
3. A post-Newtonian approximation was employed, where the time-derivative is assumed to be small in the sense that $\partial_t \sim \varepsilon\partial_r$ with $\varepsilon \ll 0$ (r being the radial coordinate).
4. The stabilization of collapsing structures requires the choice of suitable initial configurations.

This gives rise to the following issues: First, initial conditions for realistic collapse should be obtained from linear cosmological perturbation theory. Second, in an expanding FLRW universe, the collapse of a structure could look different than in the analyzed oscillaton models, where small departures from

Minkowski spacetime were considered. Third, the weak field limit is very similar to the expansion in $\mu \ll 1$ we employed in chapter 4. We have seen that second order effects matter already in the linear theory in our model and it therefore far from obvious that the first order approximation employed to derive the Schrödinger-Newton system is sufficient.

The only way to address these issues properly would be a full cosmological simulation. This is however technically very involved, and far beyond what we can do here. For the remainder of this chapter we will be more modest and consider a different approach to structure formation. Instead of trying to predict precisely the shapes or stability of bolon halos we turn the missing satellite problem around: The model should at least produce a sufficiently large number of subhalos within a Milky-way like halo in order to remain consistent with recent observations of dwarf galaxy counts. We can use this demand to put constraints on the model parameters.

6.2 EXTENDED PRESS-SCHECHTER FORMALISM

One way to make predictions about non-linear structure formation in the universe without computationally expensive N-body simulations is the so called *extended Press-Schechter formalism* (ePS). It was originally introduced by Press and Schechter [1974] and later refined and extended in several works [Bond et al., 1991, Bower, 1991, Lacey and Cole, 1993, Sheth et al., 2001, Sheth and Tormen, 2002]. The big advantage of this formalism is that it allows the prediction of halo number counts and merger histories from the linear power spectrum, with very little input from physics of non-linear structure formation. In this section we want to quickly review the basic formalism.

6.2.1 STRUCTURE FORMATION AS A RANDOM WALK

Let us start with the basic idea introduced by Press and Schechter [1974], which can be summarized as follows: Evolve the density contrast field to $z = 0$ using linear perturbation theory and identify regions of space with an averaged density contrast above a certain threshold with collapsed objects. To put this in more precise terms: One averages the linearly evolved matter density contrast field over a radius R and identifies the fraction of space which lies above a given threshold ω with the fraction of mass of the universe which is bound in objects with a mass greater than the mass associated with the size of the region, denoted by $M(R)$.
While this approach is certainly sensible, it suffers from one well known shortcoming, the so called *cloud in cloud problem*: A typical large halo with a big mass consists of a number of smaller, lighter halos. A region around a given spatial point in the linearly evolved density contrast field might therefore switch back and forth from being considered collapsed (i.e. above the threshold) and non-collapsed (below the threshold) depending on the filtering radius R. Thus it becomes unclear which mass it should be assigned to. We want to stress that this problem has no canonical solution. The most commonly used approach to get a unique prescription is described in [Bond et al., 1991] and has become known as the *excursion set formalism*.[1] In this approach one starts with the linearly

[1] Probably the most well known alternative to the excursion set formalism is the peak theory, originally developed by Bardeen et al. [1986]. We will not investigate this approach further here, since it will play no role for the remainder of this thesis.

evolved density contrast field filtered using very large radii, which leads to an effectively vanishing averaged density contrast everywhere. Subsequently one starts to decrease the filter radius step by step, thereby creating a random walk in R-space for each spatial point. Now the fraction of mass in the universe which is bound in collapsed objects of mass bigger than $M(R)$, denoted by $\Omega(\omega;R)$, is simply given by the fraction of trajectories which have crossed the threshold at some radius greater than R. Determining this quantity requires solving an *absorbing barrier problem*: As the random walk proceeds, more and more trajectories get absorbed by the threshold ω when they cross it for the first time.

Let us put this idea in precise mathematical terms. First of all, we can replace the filtering radius with a new variable, the variance, defined by

$$S(R) = \int \frac{\mathrm{d}k}{2\pi^2} k^2 P(k) \left|\widehat{W}_R(k)\right|^2 , \tag{6.1}$$

where where ρ_m is the homogeneous (average) matter density, $\widehat{W}_R(k)$ is the Fourier transform of the filtering function and $P(k)$ the matter power spectrum. Since the power spectrum is a positive definite quantity, this relation is always invertible, with large radii corresponding to small variances. We will from now on work with a mass-assignment $M(S) \equiv M(R(S))$ and a mass fraction of collapsed objects $\Omega(\omega;S) \equiv \Omega(\omega;R(S))$, as is common in this field. The number density of objects of mass M is then simply given by

$$n(\omega;M)\mathrm{d}\ln M = \rho_m f(\omega;S)\frac{\mathrm{d}S}{\mathrm{d}M}\,\mathrm{d}\ln M \tag{6.2}$$

where $f(\omega;S)$ is the first crossing rate at variance S, which can be calculated as follows:

$$f(\omega;S) \equiv \frac{\mathrm{d}\,\Omega(\omega;S)}{\mathrm{d}S} . \tag{6.3}$$

Note that equation (6.2) exhibits a clean splitting between linear perturbation theory and non-linear physics. The quantity $\mathrm{d}S/\mathrm{d}M$ can be calculated from the linear power spectrum alone, whereas non-linear physics are incorporated into the first crossing rate $f(\omega;S)$. How the first crossing rate can be determined depends on the choice of the filtering function $\widehat{W}_R(k)$, the barrier shape ω and the mass assignment $M(R)$, which we will now discuss.

6.2.2 Filter choices and mass assignments

While the choices of filtering functions are plentiful in principle, there are two particularly popular filters which get employed almost exclusively (with the possible addition of a Gaussian filter, which we ignore here). The first one is a real space tophat window function with Fourier transform given by

$$\widehat{W}_R^{th}(k) = \frac{3(\sin(kR) - kR\cos(kR))}{k^3R^3} . \tag{6.4}$$

This filter has the advantage that the assignment of a mass for a given radius $R(S)$ is canonical, the only sensible choice is

$$M(R) = \frac{4\pi}{3}\rho_m R^3 . \tag{6.5}$$

It does, however, also come with some issues: The random walk of density-trajectories in S-space, which one needs to analyze in order to calculate the first crossing rate, consists of correlated steps for this filter, making the calculation rather involved [Maggiore and Riotto, 2010a,b,c, Farahi and Benson, 2013]. We will come back to this issue below.

The second popular filter choice is a sharp window function in k-space given by

$$\widehat{W}_R^{sh}(k) = \Theta(1 - kR)\,. \tag{6.6}$$

For this filter choice the random walk in variance-space is uncorrelated, which allows for a relatively straightforward calculation of the first crossing rate. In fact, in the case of a constant barrier ω one can find an analytical solution (the one originally introduced in [Bond et al., 1991]) which reads

$$f_{\rm PS}(\omega;S) = \frac{\omega}{\sqrt{2\pi}S^{3/2}}\exp\left(-\omega^2/2S\right)\ . \tag{6.7}$$

However, the sharp-k filter also suffers from one disadvantage: It is completely unclear how to assign a mass to a filter radius. The only safe assumption one can make is that the integral should scale $\sim R^3$, i.e.

$$M(R) = \frac{4\pi}{3}\rho_m(AR)^3\,, \tag{6.8}$$

where $A = 1$ corresponds to the tophat filter choice. To clarify this issue, we simply note that trying to define the normalization for the real-space sharp-k filter gives

$$\int_0^{R_{up}} {\rm d}r\, 4\pi r^2\, W_R^{sh}(r) = 12\pi R^3\left(\int_0^{R_{up}/R} {\rm d}z \frac{\sin(z)}{z} - \sin(R_{up}/R)\right)\ , \tag{6.9}$$

which does not have a well defined limit $R_{up}\to\infty$ due to the sin-function (the integral has an asymptotic value of $\pi/2$). As we will see below, this is a very severe issue which introduces huge uncertainties for the cosmon-bolon model and will ultimately lead us to discard the sharp-k filter for our analysis.

6.2.3 BARRIERS

The shape of the barrier ω is obviously an important input into any ePS calculation. It is in fact the only point where information about non-linear structure formation enters into the formalism. Generally ω can be expected to be a function of the variance $S(M)$, since the physics of structure formation can reasonably depend on the mass of the collapsing halo. However, in the original setting, a constant barrier of the magnitude

$$\omega = \delta_{sc} \equiv \frac{3}{5}\left(\frac{3\pi}{2}\right)^{2/3} \approx 1.686 \tag{6.10}$$

was used, based on considerations of the spherical collapse model in an Einstein-de-Sitter universe [Peebles, 1967] (see e.g. chapter 8 of [Weinberg, 2008] for a more modern presentation). However, with the advent of N-body simulations it soon emerged that this barrier, in combination with the first

crossing rate for Markovian random walks (given by equation (6.7)) was not in good agreement with simulation results.
As was shown in [Sheth and Tormen, 2002], a remapping of the barrier according to

$$\omega(S) = \sqrt{A}\delta_{sc}\left[1 + b\left(\frac{S}{A\delta_{sc}^2}\right)^c\right] \tag{6.11}$$

with $A = 0.707$, $b = 0.5$ and $c = 0.6$ gives a more accurate fit. The parameters b and c are a result of a statistical analysis of the elliptical collapse model, which is more realistic than assuming a spherical symmetry. The parameter A on the other hand has to be put in manually and adjusted to fit the results of N-body simulations, but it can be argued that it is related to the way in which structures in these simulations are identified. Typically the method used to find bound structures allows for some variability with influences on the halo abundances.

6.2.4 Random walks

Before we move on we want to say a few more things about the calculations of the first crossing rates we will employ in this chapter. We will be using both a sharp-k filter and a tophat filter, at least up the point where it should become clear that the sharp-k filter results are very difficult to interpret correctly. We will, however, always consider the random walks to be uncorrelated. While this is correct for the sharp-k filter, it is not for the tophat filter. Let us therefore quickly explain why we do this anyway.
Essentially the reason is that the we want to employ the elliptical collapse barrier (6.11) and that this barrier shape was derived using a spatial tophat filter, but the corresponding first crossing rate was calculated using uncorrelated random walks. This is mathematically inconsistent, but since the barrier has been adjusted to fit N-body simulations by Sheth and Tormen [2002] in precisely this way we can only expect it to give correct results if we do the same. If we wanted to stay mathematically completely consistent and treat the random walk as non-Markovian, we would have to change the shape of the barrier in order to get results of acceptable accuracy. We want to point out that this has been done in a series of recent works [Maggiore and Riotto, 2010a,b,c, Corasaniti and Achitouv, 2011a,b, Farahi and Benson, 2013]. However, this procedure also involves several approximations along the way and finally requires a fitting of two parameters determining the barrier shape to N-body simulations. Since the final result is of comparable accuracy to the Sheth-Tormen mass function but computationally much more complex, we choose to ignore this issue at the cost of, and we should be clear about this, a (small) mathematical inconsistency. This is, however, a common approach within the ePS formalism.

6.3 Total number counts

Let us now start to apply the ePS formalism to the cosmon-bolon model. Essentially we have everything set up, except for one thing: the barrier. What should it look like? We have already seen the barriers used in the ePS formalism are derived from the spherical collapse model or generalizations

thereof. However, the model of spherical collapse runs into severe problems in a model such as ours, where the dynamics of the collapsing component are strongly scale-dependent already in the linear regime. Let us quickly outline why this is.

6.3.1 PROBLEMS WITH SPHERICAL COLLAPSE

First we should recall that the model of spherical collapse itself is of course an approximation. One assumes an initial overdensity which is spherically symmetric and homogeneous (i.e. has a tophat-profile), evolves this overdensity and determines the value of the linearly evolved overdensity at the time when the structure collapses. The full non-linear collapse equations usually get simplified in some way, either through an invocation of Birkhoff's theorem or some incarnation of Newtonian cosmology. In the first case one effectively treats the overdensity as an independent FLRW-universe, but now with a positive curvature constant which will ultimately lead to the collapse of the structure. Within the Newtonian approach there are gradient terms appearing in the equations, which are typically ignored with reference to either the lack of gradients in the initial density profile or to the size of the overall perturbation. Whichever approach one employs, it should clearly fulfill (at least) two basic criteria:

1. The perturbation should retain its (tophat-)profile, at least to very good approximation.
2. The evolution of the perturbation should agree with linear cosmological perturbation theory at early times.

Both of these demands cannot be met by either formalism for the cosmon-bolon model for structures with masses close to or below the Jeans scale. To see what the problems are, let us start with the first condition.

The evolution of linear perturbations in the cosmon-bolon model depends strongly on the wavenumber of the perturbation. This holds even under the simplifying assumption of a cosmology which is bolon-dominated throughout its evolution (a sort of Einstein-de-Sitter universe with bolon dark matter). The reason for this is simply the scale-dependent sound-speed present in the the effective fluid equations we obtained in chapter 4. This constitutes a fundamental difference to CDM-models, where perturbations have a universal growth proportional to the scale factor during matter domination. Thus it directly follows that an initially tophat-shaped perturbation will not retain its shape if modes where the soundspeed is relevant make up a sizable contribution to the Fourier-decomposition of the perturbation, not even in the linear regime. This is clearly the case if the size of the perturbation is close to the Jeans mass, which is the most interesting mass range. If we look at much larger masses however, the suppressed modes play (almost) no role for the evolution of the profile, because they are almost irrelevant in the Fourier-decomposition. We can therefore expect the spherical profile to be stable for large masses, at least as a very good approximation.

One might think that a useful way to get around this problem is to employ Birkhoff's theorem and treat the overdensity as an independent universe, forcing it to stay spherically symmetric. This is

however not justified, Birkhoff's theorem is not applicable, as should become clear by the following arguments. The soundspeed present in the averaged equations is non-adiabatic, it is a purely perturbative quantity (in contrast to the adiabatic sound-speed, which can be calculated from the background evolution only). Therefore the background equations can not reflect the suppression of growth present for large-k modes in our model. The background equations give rise to an $\omega_\chi = 0$ scenario, i.e. one where the perturbation behaves just like cold dark matter. It is possible to obtain a slightly delayed collapse time compared to a standard CDM collapse if one adjusts the initial conditions to fit the linear evolution at some early initial time, but not by much, and the delay depends on the initial time chosen. Simply put, the reason for this is that the spherical collapse model in its simplest form (i.e. with only one component collapsing) is determined completely by two parameters, the initial overdensity and its initial time derivative. When trying to adjust the time derivative to an initially suppressed evolution for small masses, one finds numerically that the evolution of the density contrast quickly adjusts itself to the standard CDM evolution, thus resulting in only a small delay in the collapse time. This is of course very different from the linear evolution recovered in cosmological perturbation theory and thus unrealistic.

The approach from Newtonian cosmology essentially suffers from the same shortcomings. One can easily find a version of Newtonian cosmology that recovers the cosmological linear perturbation equations in the subhorizon regime, but this just puts one back to the problem of stability of the tophat shape.

The problems just outlined indicate that finding the correct barrier for the bolon model could be a highly non-trivial issue. The one thing we can say for sure is that for large masses (corresponding to large radii), the modes which are suppressed in the linear regime play (almost) no role in the evolution of a tophat-perturbation, and we can thus suspect that the usual spherical collapse model is valid and recover the standard barrier. For smaller masses close to the Jeans mass however, things seem to be much more complicated. One might envision a procedure where one averages the full non-linear bolon perturbations over an oscillation period, much as we have done in the linear theory in chapter 4, to arrive at an effective description of the evolution of non-linear bolon perturbations, possibly in the Newtonian limit. However, the problem that the tophat profile remains unstable could be persistent. One could of course consider different radial profiles, but even then it is unclear if one can find a profile that retains its shape. One the one hand, the evolution of the linearized density contrast is oscillatory during the suppressed stage of the evolution and the oscillation frequency depends strongly on the wavenumber. In the interesting mass range these wavenumbers have to contribute to the density profile of the perturbation considerably, and it is hard to imagine a scenario where one can make profile-independent statements. On the other hand, the suppression of modes starts already in the radiation-dominated era, an in the matter dominated era the modes around the Jeans scale are already growing like cold dark matter modes. So one could reasonably assume that one can avoid this problem in a bolon-dominated setting. Which is the case can ultimately only be determined by writing down the non-linear theory explicitly.

6.3.2 THE BARRIERS WE EMPLOY

Still, we have to make some assumptions if we are to make any progress at all. From the arguments above the following should be clear: We expect the barrier to be indistinguishable from the cold dark matter barrier for large masses, but for smaller masses around the Jeans mass, modifications may become necessary.

To get an idea of what may happen there, let us look at the much better studied WDM models. Several authors have studied how to apply the ePS formalism to such models, see e.g. [Barkana et al., 2001, Benson et al., 2012]. Concerning the barrier shape, the following effects are relevant: The velocity dispersion of WDM particles leads to modifications in the spherical collapse model. As was shown in [Barkana et al., 2001], these effects lead to later virialization times and larger virialization radii, which need to be taken into account in the ePS formalism by modifying the collapse barrier. A fit for this modification (which is accurate for masses not too far below the Jeans mass) was given by [Benson et al., 2012] and reads

$$\delta_{WDM}(M) = \delta_{sc}\left[h(x)\,\frac{0.04}{\exp(2.3\mathrm{x})} + (1-h(x))\exp\left(\frac{0.31687}{\exp(0.809x)}\right)\right], \tag{6.12}$$

where $x = \ln(M/M_J)$, with M the halo mass in question and M_J the Jeans mass, defined in [Benson et al., 2012] as the halo mass for which pressure and gravity balance initially (in the linear regime). The function $h(x)$ is given by

$$h(x) = \left[1+\exp[(x+2.4)/0.1]\right]^{-1}. \tag{6.13}$$

This modification effectively increases the barrier dramatically for masses below the Jeans mass and thus suppresses the first crossing rate $f(\omega;S(M))$ in that regime, which has a distinct effect on the predicted number densities. One should note that the modification given in equation (6.12) was obtained from a 1-dimensional baryonic simulation, where the temperature was adjusted to fit the WDM velocity dispersion, and not from a spherical collapse model of WDM in the stricter sense. Still, it has been shown to give results which are in good agreement with WDM N-body simulations.

In a model of scalar field dark matter not dissimilar to ours, Marsh and Silk [2013] argued that a similar sharp upturn near the Jeans mass should present. The argument was that the ratio of the scalar field linear growth function $D_{\mathrm{scalar}}(k,a)$ when compared to CDM version $D_{\mathrm{CDM}}(a)$ should yield a scale-dependent critical density of the form

$$\delta_{sc}(k,a) = D_{\mathrm{CDM}}(a)/D_{\mathrm{scalar}}(k,a), \tag{6.14}$$

which clearly has a sharp upturn close to the Jeans scale. This is, however, not a good argument. The suppression of linear power in the ePS formalism is completely represented by the $\mathrm{d}S/\mathrm{d}M$ term in equation (6.2), one cannot draw any conclusions about the barrier shape from linear perturbation theory. To make this point clearer: The spherical collapse barrier is obtained precisely from a comparison between linear and non-linear perturbation growth, given an initial perturbations strength. The amount of initial perturbations at a given scale is then determined by the linear power spectrum. It does not enter into the spherical collapse model.

So we should be honest any say that it is unclear to us what the correct shape of the barrier is in our model, in particular whether or not it exhibits an increase around the Jeans mass or not. It is entirely possible that an effect similar to WDM models is present, i.e. the formation of non-linear structures is additionally suppressed. However, we have seen that linear perturbations around the Jeans scale evolve just like CDM perturbations during matter domination, and maybe the same holds true in the non-linear regime. In order to show the full range of possibilities and the effect of the barrier choice, we will present all calculations for both cases, once for the modified elliptical collapse barrier which works well for CDM described above and once for a barrier where the WDM-modification given in equation (6.12) is included. In the latter case we do of course insert the Jeans mass appropriate for our model, which is given by equations (4.240) and (4.241). Note that we modify the spherical collapse barrier, i.e. the barrier δ_{sc} before insertion into the elliptical barrier modification (6.11), not the other way around.

Finally we should mention a few additional complications present in our model which we ignore in our calculations, because their effect is small:

- First, we have a non-negligible fraction of early dark energy in our model. Spherical collapse with early dark energy has been studied in [Bartelmann et al., 2006, Pace et al., 2010], under the assumption that dark energy does not cluster. While the effects on the virial overdensity can be considerable, the effects on the critical density contrast are at the percent level (cf. Figure 4 in [Pace et al., 2010], our dark energy model is closest to the EXP2 model studied there, for which the effect is completely negligible).
- Second, if one assumes that dark energy can cluster, the critical overdensity in spherical collapse can also be modified [Abramo et al., 2007], in fact it might be lowered up to $\sim 10\%$. However, this typically requires an equation of state $\omega_0 > -1$, though scaling scenarios were not investigated in this paper. We ignore such effects as well.
- Third, a coupling between dark energy and dark matter also modifies the value for δ_{sc} [Bartelmann et al., 2006, Wintergerst and Pettorino, 2010], but for the comparatively small couplings we are interested in this effect is below the percent level (cf. e.g. Figure 8 in [Wintergerst and Pettorino, 2010]). We ignore this effect also.

6.3.3 Calculation of the first crossing rate

For barriers which are not constant or of one of a few other very simple forms, no analytical solution for the first crossing rate exists, even under the assumption of a Markovian random walk. We therefore have to resort to a numerical treatment.[2] A very suitable numerical scheme to do this was derived in [Benson et al., 2012].

First, we set up a grid in S-space, i.e. we define S_i for $i = 0,...,N$ by $S_0 = 0$ and $S_i = \sum_0^{i-1} \Delta S_i$ for $i > 0$. The ΔS_i for $i = 0,...,N$ can in principle be chosen arbitrarily, but obviously choosing the steps

[2] For the elliptical barrier (6.11) a fitting function for the first crossing rate was given in [Sheth et al., 2001], in fact the first crossing rate was originally fitted and the barrier constructed afterwards. However, for barriers including a sharp upturn near the Jeans mass no such fitting is available.

FIGURE 6.1: **Accuracy of the numerical first crossing rate calculation**

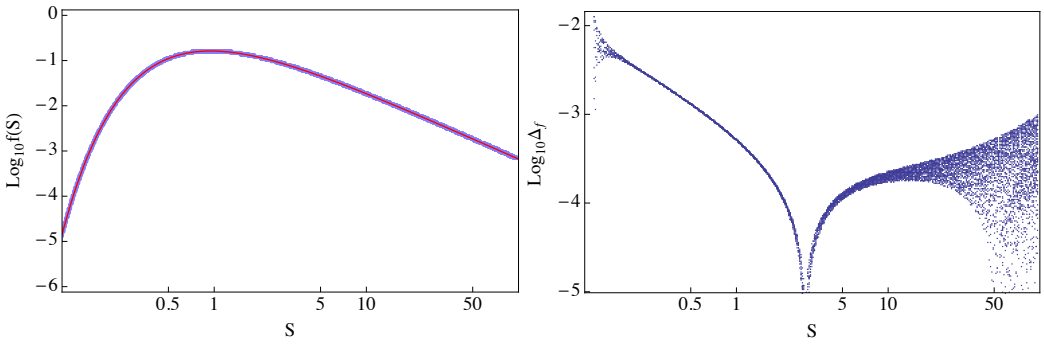

In the left hand panel we show the first crossing rate, calculated for a constant barrier $\omega = 1.686$ once with the analytical solution (6.7) (red line) and one numerically through equation (6.15) (blue dots). The panel on the right hand side shows the absolute value of the relative error Δ_f.

too big will cause numerical inaccuracies. Now we can iterate the first crossing rate at each S_i step by step employing the following formula:

$$f(S_j) = \frac{2}{\Delta S_{j-1}} \left[1 - \mathrm{erf}\left(\frac{\omega(S_j)}{\sqrt{2S_j}} \right) - \sum_{i=1}^{j-1} \left(1 - \mathrm{erf}\left(\frac{\omega(S_j) - \omega(S_i)}{\sqrt{2(S_j - S_i)}} \right) \right) f(S_i) \frac{\Delta S_{i-1} + \Delta S_i}{2} \right] . \tag{6.15}$$

For a derivation of this equation see [Benson et al., 2012]. For now let us quickly discuss its numerical accuracy. First, the accuracy is excellent in the case of a constant barrier, where we have the analytical solution (6.7) to compare it with. For small variances it takes a few steps to become accurate, as expected, bit for larger variances the absolute values of the relative error

$$\Delta_f \equiv \frac{|f_{\mathrm{num}}(S) - f_{\mathrm{PS}}(S)|}{f_{\mathrm{PS}}(S)} \tag{6.16}$$

becomes tiny. We show this in Figure 6.1.

For models exhibiting a cutoff in the power spectrum, the variance as a function of M will stagnate at small masses. To get a good mass-resolution for the number densities, the steps ΔS_i have to be chosen appropriately small in this regime. However, if at the same time the first crossing rate becomes very small due to a rise in the barrier, numerical accuracy becomes an issue. To see this, simply note that the product $f(S_j)\Delta S_{j-1}$ can become tiny in this case, and the sum on the right hand side of eq. (6.15) therefore needs to be determined with high accuracy. For our models, this happens at small masses (i.e. large variances), when this sum already contains several thousand terms. We optimize our stepsizes as follows: First, we calculate a variance-grid from the linear power spectrum with a very fine resolution. Then we choose a subgrid by imposing a minimal stepsize in order to avoid numerical issues. A good choice for the minimal stepsize in our model is $\sim 10^{-5}$, which allows for a sufficient mass-resolution around the Jeans scale and at the same time avoids numerical issues. This

FIGURE 6.2: **Stepsizes and resolution of the first crossing rate calculation**

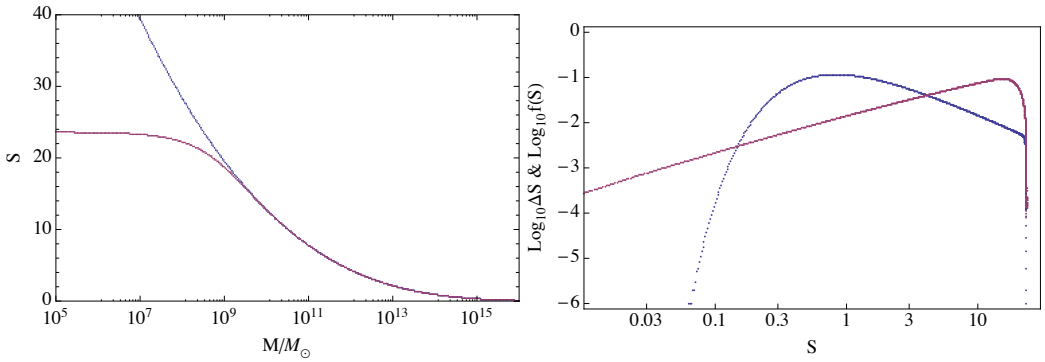

In the left hand panel we show the variance as a function of mass for a bolon model ($\lambda = 65$, $\beta = 0$, $\alpha = 20$) in red and a CDM model in blue for a tophat filter. The panel on the right hand side shows stepsizes used for the calculation of the first crossing rate for the bolon model (in red) and the corresponding first crossing rate (in blue). The barrier was chosen to include the upturn as given by equation (6.12).

leads to several thousand sampling points in S-space, which means that the sum one the right hand side of equation (6.15) can be expected to be accurate to $\sim 10^{-12} - 10^{-11}$ (the numerical accuracy of a single expression being somewhere at $10^{-15} - 10^{-14}$). Thus we can expect to resolve the first crossing rate correctly down to a magnitude of $\sim 10^{-6}$, and this is indeed the case, as can be seen in Figure 6.2.

6.3.4 TOTAL NUMBER COUNTS

Let us now move on to investigate total halo number counts for the cosmon-bolon model. Before we do that, however, we need to discuss one more subject: The barrier for the sharp-k filter.
We have already mentioned that the elliptical barrier modification introduced by Sheth et al. [2001] assumes an uncorrelated random walk combined with the usage of a spatial tophat filter, which is mathematically inconsistent. One might hope to avoid such inconsistencies for the sharp-k filter, where the the Markovian nature of the random walk is guaranteed. However, it is unclear what the barrier for such a filter should look like. Simply employing the same barrier as for the tophat filter (be it the barrier for spherical collapse or elliptical collapse) is clearly wrong, since the number densities obtained when using a sharp-k filter have a different shape, due to a different mass-dependence of the variance $S(M)$ (see Figure 6.3). We can not fix this discrepancy through an adjustment of the mass-assignment alone. In order to get number densities on agreement with the tophat-filter results for the CDM case we also have to modify the barrier used for the a sharp-k filter calculations. This does not come as a surprise, as the barrier motivated by spherical (or elliptical) collapse can only be expected to give good results when a tophat-filter is used. As it turns out, one can get very good agreement already for a very simple modification. Following Benson et al. [2012], we simply shift

the barrier upwards by multiplying it with a constant factor

$$\omega \to B\omega\,. \tag{6.17}$$

This rescaling needs to be applied after other barrier modifications, in particular after the non-linear elliptical modification in equation (6.11). A food fit to the total number densities for CDM spectra can be obtained by adjusting the parameters A in eq. (6.8) and B in the above rescaling. For the choices $A = 2.27$ and $B = 1.1$, the relative discrepancy is below 10% everywhere in the mass range from $10^6 M_\odot$ to $10^{16} M_\odot$ (cf. Figure 6.5).[3]
The different variances as a function of mass are shown in Figure 6.3, the corresponding barriers in Figure 6.4 and the resulting number densities in Figure 6.5. The ΛCDM model is shown in black, with the dashed curve representing the tophat filter and the solid line a sharp-k filter. In both cases we employed the elliptical barrier modification, in the case of the sharp-k filter the barrier and mass assignment were adjusted as described above. Both lines are almost indistinguishable. The green lines are results obtained for the bolon-model with $\lambda = 65$, $\alpha = 20$ and $\beta = 0$, where a tophat filter was used for the dashed line and a sharp-k filter for the solid one. For the dotted and dashed-dotted lines the additional modification of the barrier due to a possible upturn at the Jeans-mass was put in, for a sharp-k filter and a tophat filter respectively. Finally the red dotted line represents the WDM already used in chapter 4 for comparison, with a mass of

$$m_{\rm wdm} = 2.284\ {\rm keV}\,. \tag{6.18}$$

A number of effects are evident.

First, clearly the function $\mathrm{d}S/\mathrm{d}M$ are suppressed near the Jeans mass compared to the ΛCDM model for both the bolon and the WDM model, as expected. However, the sharp k-filter clearly leads to a much quicker decline of the function $\mathrm{d}S/\mathrm{d}M$ in the bolon case, in fact, the decline is so steep that the function is effectively zero already at masses above the Jeans mass. This is a first strong hint of a severe problem with the sharp-k filter. There is no unique way to adjust the mass assignment for this filter, and we have chosen one with the desire to obtain realistic results for CDM spectra. However, the resulting mass-assignment is clearly not suitable for the cosmon-bolon model, as it assigns a mass which is too large to the Jeans scale k_J.

Let us go on and take a look at the resulting number counts. For the tophat filter, using the elliptical collapse barrier without an upturn near the Jeans mass results in a suppression of the abundance of small scale structures, but the number density continues to grow with decreasing halo mass even below the Jeans scale. Using the modified barrier, however, a sharp cutoff in the number densities at the Jeans scale gets introduced. This seems to be more reasonable, as it is hard to imagine how sub-Jeans scale structures should form in considerable numbers in a purely hierarchical model of structure formation, when the linear power at these scales is strongly suppressed. For the sharp-k filter, the modification of the barrier is almost irrelevant for a prediction of the total number densities, since the

[3] Other mass assignments suggested for the sharp-k filter correspond to $A = 2.5$ in [Benson et al., 2012] or $A = 2.42$ in [Lacey and Cole, 1993], which are not too different from our fit. These assignments are however motivated by different considerations.

FIGURE 6.3: **Change of variance with mass for different filters**

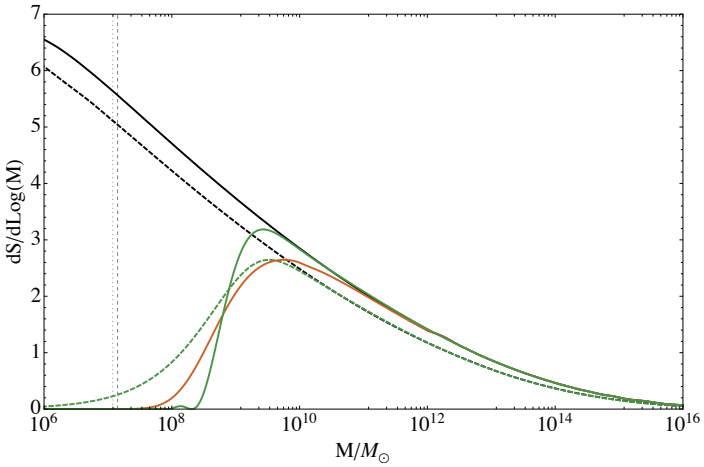

dS/dLog(M) for a tophat filter (dashed) and a sharp-k filter (solid) with the mass assignment given in eq. (6.5) for a standard CDM power spectrum (black) and the bolon model (green) with $\lambda = 65$, $\alpha = 20$ and $\beta = 0$. The red line represents a thermal WDM model with a 2.284 keV mass for a sharp-k filter. The dashed gridline represents the WDM Jeans mass, the dotted one the bolon Jeans mass. Figure taken from [Beyer, 2014b].

FIGURE 6.4: **Barriers for the ePS formalism**

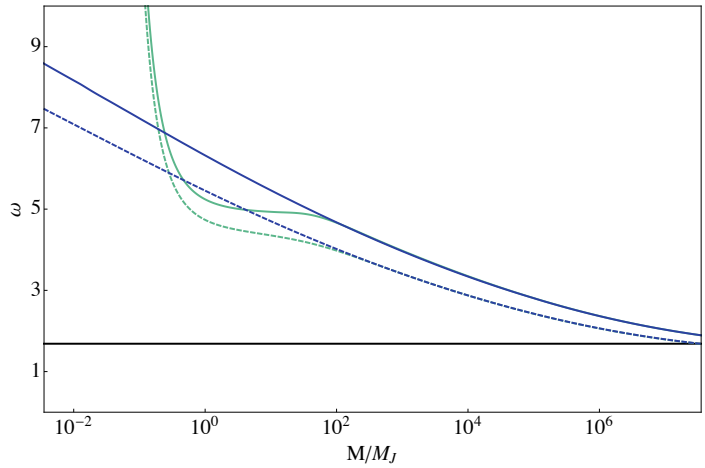

Different barriers used in this work. We show the spherical collapse barrier (black), the elliptical collapse barrier for the tophat-filter given in equations (6.11) (blue dashed) and the elliptical collapse barrier shifted by a factor of 1.1 (blue solid) for the sharp-k filter. Finally we show the barriers modified through equation (6.12) to get a sharp upturn near the Jeans mass for both the tophat elliptical barrier (green, dashed) and its raised version for the sharp-k filter (green, solid). All modifications have been calculated from a bolon power spectrum with $\lambda = 65$, $\alpha = 20$ and $\beta = 0$. Figure taken from [Beyer, 2014b].

FIGURE 6.5: **Total number densities**

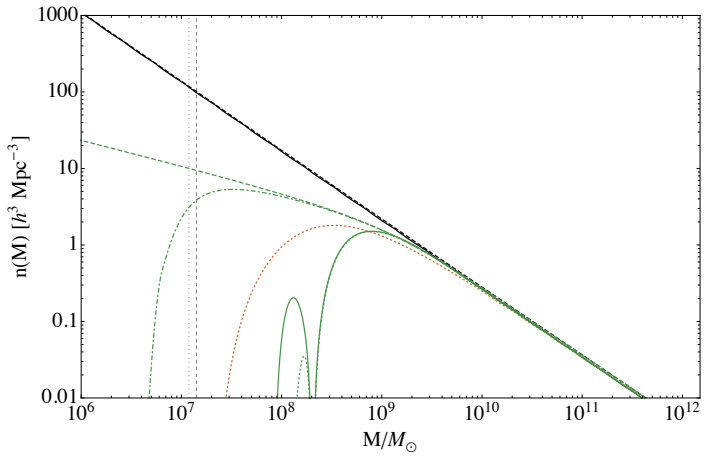

Total number densities predicted by the Press-Schechter excursion set formalism for different models and different filters. The black lines show the results for a CDM power spectrum with a tophat (dashed) and a sharp-k filter (solid) respectively. The elliptical barrier and mass assignment for the sharp-k filter has been successfully adjusted to fit the tophat results, both lines are (almost) indistinguishable. The green lines show the results for a bolon model with $\lambda = 65$, $\alpha = 20$ and $\beta = 0$. A tophat filter was used for the dashed line, and an additional upturn of the barrier near the Jeans mass inserted for the dashed-dotted one. The solid line shows the sharp-k filter results with an elliptical barrier, whereas the dotted line shows what happens if an upturn in the barrier is included. Finally the red line shows the WDM model with a sharp-k filter and Jeans mass modification already displayed in Figure 6.3 for comparison. The dashed gridline represents the Jeans mass for the WDM model, the dotted one the Jeans mass for the bolon model. Figure taken from [Beyer, 2014b].

cutoff is completely determined by the function $\mathrm{d}S/\mathrm{d}M$, which goes to zero at masses above the Jeans mass. The only difference is a slightly quicker suppression of the oscillatory part, resulting from the oscillatory shape of the power-spectrum cutoff, if the barrier is raised near the Jeans mass. However, with a different mass assignment the results would be dramatically different. A much lower choice of the parameter A would of course again lead to a bigger difference between the two barrier choices and at very low A the first crossing rate would once again determine the cutoff position, similar to the tophat filter case. From these simple observations it is clear that the mass-assignment for the sharp-k filter introduces huge uncertainties, which will translate from the total number densities to substructure abundances (which we treat below) as well. We know currently of no way to resolve this issue and will continue to use only the tophat filter from this point onward.

6.4 PROGENITORS AND SUBSTRUCTURES

We have not yet discussed how a redshift dependence gets introduced into the sPS formalism. Instead of evolving the density contrast field to different redshifts, it is far more common to work with the density contrast field (i.e. the linear power spectrum) at $z = 0$ and put the entire redshift dependence

into the barrier, i.e.

$$\omega(z) = \omega(z=0)/D(z)\,, \tag{6.19}$$

where $D(z)$ is the linear growth function. We should probably point out that the time-evolution of the elliptical barrier is not obtained by applying this relation directly, but by replacing the critical overdensity $\delta_{sc} \to \delta_{sc}(z)$ and applying the elliptical barrier modification (6.11) afterwards, which is consistent with the original motivation of the elliptical barrier. Exchanging these two modifications would lead to a strong underprediction of subhalo abundances at higher redshifts, i.e. a strongly accelerated version of hierarchical structure growth, which is not realistic.

6.4.1 Progenitor mass functions

Let us now move on to investigate what might be the most interesting aspect of small scale power suppression: the abundance of substructure within a typical galaxy such as the Milky way. The ePS formalism does not provide substructure abundances directly, but it does allow for the calculation of an object called the *conditional mass function*, which we denote by

$$g(M_1,z_1|M_2,z_2) = -f(\omega_1;S_1|\omega_2;S_2)\frac{\mathrm{d}S_1}{\mathrm{dlog}M}\Big|_{M=M_1}\,. \tag{6.20}$$

This function describes the fraction of mass bound in halos of mass $M_2 = M(S_2)$ at redshift z_2 (corresponding to the barrier ω_2) which is contained in progenitor halos of mass $M_1 = M(S_1)$ at redshift z_1 (corresponding to the barrier ω_1) per log M-interval. It is determined by two quantities: the variance as a function of mass and the conditional first crossing rate $f(\omega_1,S_1|\omega_2,S_2)$. The latter quantifies the first crossing rate of Langevin-trajectories through originating at $\omega_2(S_2)$ at variance S_2 through the barrier $\omega_1 > \omega_2$ at $S_1 > S_2$.

As one might expect, we can not obtain this function analytically for the complicated barriers depicted in Figure 6.4, this is again only possible for very simple barriers like a constant one [Bond et al., 1991]. Still, the elliptical barrier modification given in equation (6.11) has been shown to also give better results than the constant spherical collapse barrier for progenitor mass functions as well [Sheth and Tormen, 2002] and we should therefore use it. Luckily we can employ the same numerical strategy used above for the calculation of total number densities. The reason for that is the following: the conditional first crossing rate is the same as the unconditional first crossing rate with an adapted barrier shape [Benson et al., 2012]:

$$f(\omega_1;S_1|\omega_2;S_2) = f(\tilde{\omega};S_1-S_2)\,, \tag{6.21}$$

where

$$\tilde{\omega}(S) = \omega_1(S+S_2) - \omega_2(S_2)\,. \tag{6.22}$$

The change of the barrier with redshift is of course determined by the linear growth function $D(z)$, which we obtain numerically from our Boltzmann-code. It can be somewhat approximated by $D(z) = (1+z)^{-1}$, but this fails for low z due to dark energy and for medium z due to the modified structure growth if β is non-zero.

FIGURE 6.6: **Conditional mass functions**

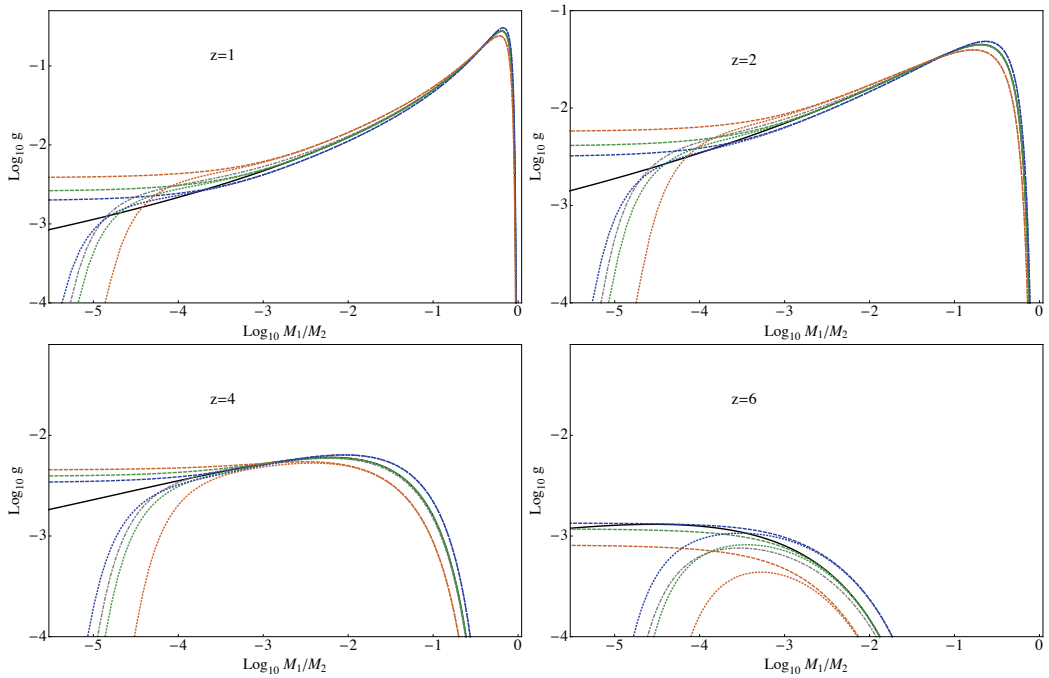

Conditional mass functions for different power spectra. The ePS-result for a tophat filter with the shifted barrier are shown in solid black for CDM and in dash-dotted gray for a wdm model with particle mass of 2.284 keV. The dashed lines represent the bolon-model with $\lambda = 65$, $\alpha = 20$ and $\beta = -0.1, 0., 0.05$ for the red, green and blue lines respectively, where the elliptical barrier was used. The dotted lines stand for the same models, but this time with an additional upturn of the barrier near the Jeans mass included. Figure taken from [Beyer, 2014b].

The conditional mass function can be seen for a number of redshifts and models in Fig. 6.6. The reference mass in this figure is of the order of the Milky way mass, we chose

$$M_2 = 1.8 \times 10^{12} M_\odot \,, \tag{6.23}$$

and the reference redshift is $z_2 = 0$. This will be our reference mass for all plots from here on out. We show the standard CDM prediction (black solid line), together with the WDM-model already used above (gray dash-dotted line) and three bolon models with modified barrier (dotted) and with an elliptical one (dashed). The three colors represent different couplings of $\beta = -0.1$ (red), $\beta = 0$ (green) and $\beta = 0.05$ (blue). The bolon exponent λ is 65 for all curves, while $\alpha = 20$.

6.4.2 MILKY WAY SUBHALOS

Let us now make the final step from progenitor mass functions to the abundance of substructure within our galactic halo. This quantity is not directly accessible to us via the ePS-approach and we have to do some additional work. Following the ansatz presented in [Giocoli et al., 2008], we

calculate the current number of subhalos by a simple integration in barrier space, i.e.

$$\frac{\mathrm{d}n}{\mathrm{d}M_1} = \int_{\omega_0}^{\infty} \frac{M_2}{M_1} f(\omega(\delta_{sc,1}); S_1 | \omega(\delta_{sc,2}); S_2) \mathrm{d}\delta_{sc,1} \,, \tag{6.24}$$

where ω_0 denotes the barrier $\omega(S_2)$ at redshift 0 and $\delta_{sc,i}$ denote the spherical collapse barriers at redshifts z_i. Afterwards the cumulative number of subhalos can be obtained by a simple integration over M_1:

$$n(>M_1) = \int_{M_1}^{M_2} \frac{\mathrm{d}n}{\mathrm{d}M_1} \mathrm{d}M_1 \,. \tag{6.25}$$

At this point a few comments are in order. First, eq. (6.24) necessarily overcounts the number of subhalos. This can be seen from the simple observation that a single progenitor may stay a progenitor for a prolonged amount of time before being absorbed into the halo, but it gets counted in the integral 'at every redshift step'. This causes us to lose the overall normalization of the cumulative number density. In order to regain the correct normalization we impose a constraint from [Diemand et al., 2005], which states that in CDM simulations about 10% of the the mass in bound structures of galactic size resides in halos in the mass range from $10^7 M_\odot$ to $10^{10} M_\odot$. We then simply impose the resulting normalization for the cosmon-bolon model as well. Second, we note that an additional assumption going into this ansatz is that the current distribution of subhalos corresponds directly to the distribution of progenitor halos when averaged over redshift. This essentially means that there should be no 'internal mergers' once a small halo gets absorbed into a bigger one, which appears to be a good approximation, as we recover the CDM N-body results to good accuracy (see below).

Results for cumulative number counts of subhalos for a Milky-way like structure can be seen in Figure 6.7. To gauge the accuracy of our assumptions, a comparison with the N-body results shown in Figure 11 in [Lovell et al., 2014] shows that the CDM result agrees to excellent accuracy.[4] This was expected, as we have adjusted our normalization accordingly. The results for the WDM model on the other hand looks slightly different, even though we employ the same WDM particle mass (uppermost WDM curve in Figure 11 in [Lovell et al., 2014]). For a barrier without an upturn near the Jeans mass we overestimate the abundance of halos with masses below the Jeans mass, which was to be expected for the WDM model. In fact, the cumulative number counts continue to rise, if very slowly, for ever smaller masses, which seems unrealistic. For the correct WDM barrier, however, our results seem agree rather well with the N-body results down to masses slightly above the Jeans mass, but for smaller masses the ePS results stagnate more quickly, whereas the N-body curve continues to give small numbers of additional halos below the Jeans mass. We seem to underestimate the asymptotic value by a factor of about 2. Two reasons which could potentially explain this come to mind. First, the ePS formalism assumes a strictly hierarchical model of structure formation, which is clearly not the case. There are violent mergers and disruptions which can strip mass from halos and give rise to structures below the Jeans scale, which could not have formed hierarchically. Such effects can not be properly included in the purely hierarchical ePS approach. Second, this is also the regime where spurious halos start to contaminate the simulation, in fact, this is the scale where spurious halos start

[4] We are aware of the fact that putting this figure into this thesis would be beneficial at this stage, but we are not sure if this would violate the journals copyright claims, as this thesis will be available online.

FIGURE 6.7: **Cumulative number of Milky way subhaloes**

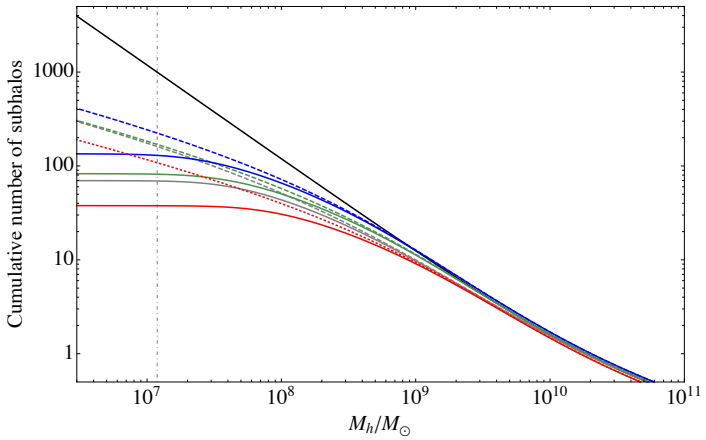

Cumulative number of Milky Way subhaloes as a function of halo mass M_h. The CDM power spectrum is represented by a solid black line, the gray lines show a WDM modification for a thermally produced WDM particle of mass $m_{\rm wdm} = 2.284$ keV. The green lines stands for a bolon power spectrum with $\beta = 0$ and $\lambda = 69$, the blue and red lines correspond to the same λ but with $\beta = 0.05$ and $\beta = -0.1$ respectively. For all WDM and bolon models, the dashed lines are results calculated without an upturn of the barrier near the Jeans mass, whereas such a modification is included for the solid lines. As an additional orientation we added the dashed-dotted gridline at the WDM Jeans mass. Figure taken from [Beyer, 2014b].

to be more abundant than real ones. Issues with the identification of such halos could introduce additional uncertainties to the N-body results.

Let us now use these results to put constraints on model parameters in the cosmon-bolon model. To do this, we simply demand that the number of subhalos should not fall below the number of dwarf galaxies estimated from observations. As we already mentioned in section 6.1, these estimates are still the subject ob ongoing debate, current numbers range from 66 [Lovell et al., 2014] to several hundred [Tollerud et al., 2008]. Since we want to set conservative bounds, we choose the lower value of 66. We also want to point out, again, that the baryonic physics can additionally suppress structure formation on small scales, a fact that we ignore. Such an additional suppression would only lead to tighter parameter bounds, we remain very cautious here. As a third point, we have seen some discrepancies between the results for substructure calculations arising from the ePS formalism and N-body calculations for warm dark matter. We count the cumulative number of structures at a halo mass of $10^7 M_\odot$, which appears to be a common lower mass for small dwarf galaxies. For this mass, we already underestimate the N-body result by a factor of about 1.5, which we artificially remedy by raising our obtained number counts by this factor when we use the modified spherical collapse barrier in order to remain extra cautious. The results for our parameter bounds can be seen in Figures 6.8 and 6.9.

As a first effect, the coupling β has a direct effect on the value of the current bolon masses $m_\chi(t_0)$ which are compatible with observations. The smallest current bolon masses are possible for the largest couplings β. However, we have already discussed in chapter 4 that we expect current coupling

FIGURE 6.8: **Number of Milky way subhalos in the bolon model**

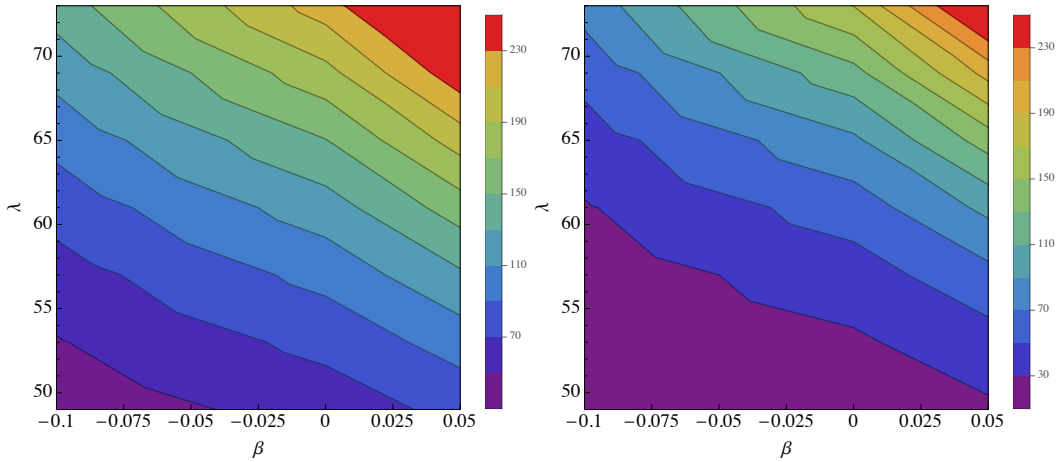

Cumulative number of Milky way subhalos above a mass of $10^7\ M_\odot$. In the left panel we show results for the elliptical barrier, in the right panel for the modified barrier where an upturn near the Jeans mass is included.

FIGURE 6.9: **Parameter bounds for the cosmon-bolon model**

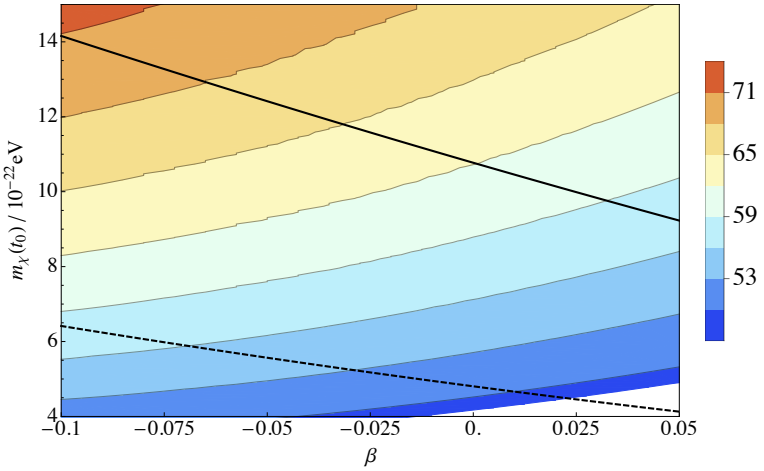

Allowed parameter range for the cosmon-bolon model. The colored contours show different bolon exponents λ. The solid line displays the lower boundary of parameters which yield more than 66 subhalos in the Milky way if the modified barrier is used, the dashed line shows the same exclusion curve for the standard elliptical barrier. Figure taken from [Beyer, 2014b].

constraints from CMB observations to apply to our model as well, as the wavenumbers for which the CMB has the most constraining power are much lower than the ones where linear structure formation is modified compared to CDM. In [Pettorino et al., 2012, Pettorino, 2013] the bounds on the coupling are roughly $|\beta| < 0.1$. From this constraint we can derive an upper bound for current bolon mass, which we estimate by evaluating the boundaries presented in Figure 6.9 for large couplings. For $\beta = 0.05$ the resulting bound is

$$m_\chi(t_0) \gtrsim 9.2\,(4.1) \times 10^{-22}\text{eV} \tag{6.26}$$

for the modified (ellitpical) barrier. This bound lies at the larger end of typical ultra-light scalar field dark matter masses, with important consequences for its observational signatures, as we will see in the next section.

But before we do this, let us compare this bound with another recent work in the field of scalar field dark matter, which points the way forward in this field. An N-body type cosmological simulation of structure formation for the Schrödinger-Poisson system, i.e. for the BEC dark matter model, was achieved very recently by Schive et al. [2014]. While it is unclear how this simulation precisely relates to our model, even the uncoupled one, they were able to resolve similar quick oscillation and interference issues which are typical for scalar field dark matter models. Thus it presents a big step forward. Interestingly, they use a simulation mass of the scalar field of about 8.1×10^{-23} eV, roughly an order of magnitude below the bound we derived, and apparently still find a large abundance of substructures in the mass range relevant for dwarf galaxies. A few comments might be in order here, since one might consider our findings in conflict with this simulation.

- First, it is unclear how exactly the Schrödinger-Poisson system relates to our model.
- Second, they do not choose this mass based on the results of their simulation, but based on fitting a soliton density profile arising in this model to data of the Fornax dwarf galaxy.
- Third, so far there is no precise statement concerning the amount of structure within a Milky-way like halo from the simulation. The statement they make that 80% of the halos formed in the simulation are in the range relevant for dwarf galaxies might even seem low, considering that the Milky way galaxy by itself is expected to have at least of the order 66 of them.
- Finally, they start their simulations with a cold dark matter power spectrum at $z = 1000$, but we have seen in our model the suppression of linear power is already sourced at much higher redshifts during the radiation dominated regime. Taking this into account should result in a stronger suppression of small scale power for a given scalar field mass.

Still, this work very much points in the direction one should go into in order to make predictions of models such as ours more robust and shows that a full cosmologically simulations might be within reach in the not-too-distant future.

6.5 OBSERVING THE OSCILLATIONS?

As a final comment, we want to discuss potential observational signatures of the cosmon-bolon model. We have seen that this model is, in many ways, similar to WDM models when it comes to the predictions of halo number densities and substructure abundances. The internal structure of bolon dark matter halos is, however, expected to look considerably different from CDM or WDM ones. We do not mean the density profile here, even though this would be interesting as well, we are talking about the quick bolon field oscillations which we expect to be present in virialized structures as well, similar to oscillatons [Urena-Lopez, 2002]. These oscillations are then expected to translate to the gravitational potentials.

In a recent work [Khmelnitsky and Rubakov, 2014] studied if oscillations arising from a scalar field dark matter halo (with a constant mass and under some simplifying assumptions) could potentially detected through time variations in pulsar timing signals. Such a time variation would be a very direct of the scalar nature of dark matter. Unfortunately, however, as can be seen by a quick look at Figure 1 in [Khmelnitsky and Rubakov, 2014], the bound we set on the current bolon mass clearly excludes a possible near future detection in this way by more than an order of magnitude. However, pending other smoking gun scenarios yet to be discovered, this also means that we can likely continue to consider such models for a while, as they are unlikely to be invalidated any time soon.

7 Conclusion

In this thesis we have travelled a long path, starting from models of higher dimensional dilatation symmetric theories of gravity and ending at the small scale problems of cosmic structure formation. We have almost arrived at the end of this thesis, so it is time to look back and recapitulate what has been achieved, and also what would be interesting to investigate in the future.

The starting point for our considerations was the cosmological constant problem. We have discussed in some detail in chapter 3 why the current value of the cosmological constant as inferred from observations is considered to be unnaturally small by many researchers, and why this problem is indeed hard to solve. Gravitational theories based on the concept of higher dimensional dilatation symmetry might provide a solution to this issue, but there is still a lot of work left to be done in this field. In particular, establishing the existence of a dilatation symmetric fixed of the quantum effective action of higher dimensional scalar tensor gravity would constitute a big step forward. First attempts in this direction have been made [Henz et al., 2013], but a substantial amount of additional work is still required.

As is good practice among theorists we have not shied away from such uncertainties and drawn up a cosmological scenario motivated by the assumption that this fixed point exists. If so, it constitutes a valid asymptotic state for cosmology, which is expected to be reached in the limit $t \to \infty$. Considerations of the asymptotic fixed point configuration are crucial for the motivation of our model. They give rise to the notion that in an effective four-dimensional theory containing two scalar fields, the effective common potential should vanish at the fixed point. For finite times, away from the fixed point, we expect anomalous terms breaking dilatation symmetry to be present, which results in the dilaton acquiring a small mass and acting like a cosmological cosmon field. We have then studied a scenario in which the second field, called the bolon, acts like dark matter, thus presenting a unified picture of the dark sector.

We have described at the end of chapter 3 in some detail what the background evolution in this model looks like, in particular how to achieve an independence of the cosmic evolution from the precise initial conditions and how to match the model parameters to observable parameters like the current dark matter energy density. We furthermore have determined the parameter ranges which are required to keep out model consistent with constraints for early dark energy from both big bang nucleosynthesis and CMB observations, and also with constraints on the coupling strength.

In chapter 4 we have discussed the evolution of linear perturbations in the cosmon-bolon model in some detail. The technical aspects included two major steps: First, the derivation of an effective fluid theory for the bolon perturbations, which is valid for sufficiently late times when the bolon

field values are small and quick oscillations around the minimum of the potential are present. The resulting equations for the coupled model have, to our knowledge, not been written down before. Second, we written a Boltzmann code evolving the perturbations of the two scalar fields as well as baryons photons and neutrinos. We believe that our code is quite accurate, as we have compared it with the state-of-the-art CLASS code for a ΛCDM cosmology and obtained good agreement. The effects of the coupled scalar field dark matter model on the power spectrum are twofold. First, the coupling modifies the growth of subhorizon perturbations, as for standard cold dark matter coupled to a cosmon field. Second, the small soundspeed introduced in the effective fluid theory effectively suppresses the evolution of modes below a Jeans mass, leading to cutoff in the matter power spectrum. This is similar to other scalar field dark matter or warm dark matter models discussed in the literature. We were able to get a quantitative understanding of this behavior, including the dependence of the cutoff position on model parameters, from precise knowledge of the background evolution. Such a cutoff in the power spectrum could potentially provide a solution to the small scale issues of structure formation in the cold dark matter scenario, but additional investigations are clearly required here.

Chapter 5 represents a slight detour from our path. Here we investigated exact scaling solutions involving multiple scalar fields in some detail, and were able to establish some rather interesting results. We could constrain the generic shape of the common potential for canonical scalar fields required by the existence of exact scaling solutions. Contrary to the case of a single scalar field, the potential is not limited to one single shape, but in fact allows for a variety of different functions. In a second step we obtained all possible scaling solutions for such potentials. This was achieved through a dynamical system analysis for one particular shape of potential, the exponential cross coupling potential which is relevant for the cosmon-bolon model, and an ensuing proof that all other possible potentials consistent with the existence of exact scaling solutions can not add any new solutions to the list. We showed that scaling solutions for other potentials are possible, even stable ones, by explicitly constructing one for a power law coupling potential.

In the second part of this chapter we investigated the evolution of perturbations around such scaling solutions. This was motivated by the recent finding that in models of quintessence coupled to cold dark matter, the stability of the adiabatic perturbation mode can be an issue for some regions of parameter space [Majerotto et al., 2010]. It is therefore an interesting question if similar problems can arise in coupled scalar field dark matter models originating in scaling solutions in the early universe. The answer we found is: Yes, but not for a suitable choice of potential. We were able to proof conclusively that the exponential cross coupling potential is free of such instabilities. However, for the power law coupling potential, we were able to explicitly show that strongly growing perturbation modes exist around a scaling solution, albeit only for an unstable one. Whether or not it is possible to construct models with strongly growing perturbation modes around stable two-field scaling solutions or whether there is some mechanism preventing this, remains an open question for now. The method we developed can however be applied to any potential allowing for two scalar field scaling solutions, so anyone can feel free to try out their favorite potential and see what happens.

We finally returned to the issue of cosmic structure formation in chapter 6. Here we employed the extended Press-Schechter excursion set formalism in order predict total halo numbers and substructure abundances within a typical Milky-way like halo. While this approach clearly has a number of shortcomings, the results of more accurate N-body simulations could be obtained with acceptable

accuracy for CDM and WDM models, indicating we are including essential physics. We were able to put bounds on the model parameters from demanding that the amount of Milky way satellites should not be suppressed so much as to become incompatible with recent findings from the Sloan Digital Sky survey data, and since we were very conservative with our estimates, we believe these bounds to be quite robust. Depending on the assumptions, we have shown that a current bolon mass should obey

$$m_\chi(t_0) \geq 9.2(4.1) \times 10^{-22}\mathrm{eV}\,. \tag{7.1}$$

This is at the larger end of typical scalar field dark matter masses.

Now, what could and should be done in the future? Clearly, in order to really understand the impact of a coupled scalar field dark matter model a full N-body like cosmological simulation of structure formation would be desirable. Ideally this should include effects of the baryonic physics of galaxy formation, since the effects of dark matter power suppression and baryonic feedback processes are somewhat degenerate in their effect on the formation of small scale structures. This type of simulation would however be computationally very demanding, but it might just be within reach in the forseeable future, if not quite yet. Researchers employing state-of-the art cold dark matter simulations which include baryonic physics come the conclusion that the modeling of baryons still requires improvement [Genel et al., 2014, Vogelsberger et al., 2014a], and thus it seems premature to exclude baryonic solutions from the range of possibilities to solve the small scale structure issues. At the same time, the first cosmological simulation of the Schrödinger-Poisson system has been achieved [Schive et al., 2014], and while it is unclear how this relates precisely to our model, the numerical difficulties that have been overcome are very similar to what we expect to be present in the cosmon-bolon model. Clearly combining both, state-of-the-art modeling of baryonic physics and the scalar field nature of dark matter into a single simulation may proof to be very challenging, but the fact that both ingredients work on an individual basis shows that this might be within reach.

If the small scale problems of cold dark matter structure formation can ultimately be solved by baryonic physics remains to be seen. We want to stress that even if that is the case, it does by no means invalidate scalar field dark matter models such as we have presented here. Very similar to WIMP models of dark matter, where one can interpolate between the warm dark matter and cold dark matter regime using the particle mass, we can do the same and choose a bolon mass in a regime where it essentially ends up being another cold dark matter candidate. If searches for weakly interacting dark matter particles should not provide conclusive results within the next ten years or so, such models may become more and more appealing. A direct signature of the scalar nature of dark matter would be a measurement of the time-variations in the gravitational potentials of bound structures, e.g. through time-variations in pulsar timing signals [Khmelnitsky and Rubakov, 2014]. Such a detection, however, appears to be out of reach for the cosmon-bolon model, as our constraints from structure formation considerations put an upper bound on the bolon mass in a range where such effects are expected to be undetectable given current observational possibilities. We want to point out that a detection of this kind becomes more and more challenging as one moves the mass of the scalar field dark matter particle further towards the cold dark matter regime.

As a last point we want to back to out original motivation. In an era when cosmological observations become increasingly precise and the simulation techniques are ever improving, one should not lose

track of the very fundamental problems in physics. The cosmological constant is most certainly one of the more persistent ones, and so are the nature of dark energy and dark matter. The fact that the cosmological standard model has proven to be so very resilient against virtually all observational probes means that, in the authors opinion, it is very likely to have secured its place in physics, even if it should be invalidated some day. A so simple model so consistent with a large number of observations is likely to remain useful for a long time, if only as an approximation. Nonetheless, we should never stop searching, doing our best to poke holes into the model and come up with alternatives. Ultimately the ingenuity of scientists will certainly be able to figure out what it is that makes up our universe. Currently, with 95% of it unknown, it is only fair to say: While we have many, many ideas, we have no clue which is the right one.

List of Figures

2.1 Energy densities in the ΛCDM model 34

3.1 Dependence of the SM vacuum energy on the renormalization scale 41
3.2 Cosmon field adjusting to a scaling solution 50
3.3 Density parameters in the cosmon bolon model 72
3.4 Adjustment of the bolon energy density 75

4.1 Matter power spectrum comparison with CLASS 117
4.2 Evolution of the bolon density contrast 119
4.3 Matter power spectra for different λ 120
4.4 Growth of the matter density contrast in coupled quintessence 121
4.5 Evolution of the bolon density contrast for different couplings 123
4.6 Matter power spectra for different couplings 123

5.1 Stable fixed points for the exponential coupling potential 1 133
5.2 Stable fixed points for the exponential coupling potential 2 133
5.3 The fixed point $R4$ for the power law coupling potential 137
5.4 Real part of λ_9 144
5.5 Real part of λ_{10} 144
5.6 Eigenvalue λ_9 for the power law coupling potential 146

6.1 Accuracy of the numerical first crossing rate calculation 162
6.2 Stepsizes and resolution of the first crossing rate calculation 163
6.3 Change of variance with mass for different filters 165
6.4 Barriers for the ePS formalism 165
6.5 Total number densities 166
6.6 Conditional mass functions 168
6.7 Cumulative number of Milky way subhaloes 170
6.8 Number of Milky way subhalos in the bolon model 171
6.9 Parameters bounds for the cosmon-bolon model 171

B.1 Fitting the power spectrum cutoff 189
B.2 Relative errors for the cutoff fitting 189

LIST OF TABLES

2.1 Annihilation events in the quark epoch. 27
2.2 Annihilation and decoupling events in the hadron epoch. 28
2.3 Cosmological events after big bang nucleosynthesis. 29
2.4 Parameters of the ΛCDM model. 33

3.1 Scaling solutions in Coupled Quintessence 54
3.2 Existence and Stability for Coupled Quintessence scaling solutions 54

4.1 Approximation triggers for the Boltzmann code: Standard values 116

5.1 Fixed points for coupled exponential potentials 132
5.2 Existence and stability of the fixed points for coupled exponential potentials 132

A.1 Fermions of the standard model 185
A.2 Bosons of the standard model 186
A.3 Lightest hadrons of the standard model 186

ABBREVIATIONS

GR	**G**eneral **R**elativtiy
CMB	**C**osmic **M**icrowave **B**ackground
EEP	**E**instein **E**quivalence **P**rinciple
FLRW	**F**riedmann-**L**emaître-**R**obertson-**W**alker
EDE	**E**arly **D**ark **E**nergy
BBN	**B**ig **B**ang **N**ucleosynthesis
SM	**S**tandard **M**odel
UV	**U**ltra **V**iolet
TCA	**T**ight **C**oupling **A**pproximation
UFA	**U**ltrarelativistic **F**luid **A**pproximation
RSA	**R**adiation **S**treaming **A**pproximation
BEC	**B**ose-**E**instein **C**ondensate
ePS	**e**xtended **P**ress-**S**chechter (formalism)

A PARTICLES OF THE STANDARD MODEL

In this appendix we give an overview over the fundamental particles of the standard model and the lightest hadrons. This is by no means comprehensive, we only provide the information necessary to understand the thermal history of the universe as presented in chapter 2.

TABLE A.1: **Fermions of the standard model**

	Name	Mass
Leptons	τ^-, τ^+	1777 MeV
	μ^-, μ^+	105 MeV
spin = 1/2	e^-, e^+	511 keV
d.o.f. = 4	$\nu_\tau, \bar{\nu}_\tau$	< 2 eV
	$\nu_\mu, \bar{\nu}_\mu$	< 2 eV
	$\nu_e, \bar{\nu}_e$	< 2 eV
Quarks	$t, \bar{t}$	173 GeV
	$b, \bar{b}$	4 GeV
spin = 1/2	$c, \bar{c}$	1 GeV
colors = 3	$s, \bar{s}$	95 MeV
d.o.f. = 12	$d, \bar{d}$	4.8 MeV
	$u, \bar{u}$	2.3 MeV

The masses are approximate values taken from [Beringer et al., 2012], where current best fits and errors are given.

TABLE A.2: **Bosons of the standard model**

	Name	Mass
Weak gauge bosons	W^+	80 GeV
spin = 1	W^-	80 GeV
d.o.f. = 3	Z^0	91 GeV
Photon	γ	0
spin=1		
d.o.f. = 2		
Gluons (8)		0
spin=1		
d.o.f. = 2		
Higgs	H^0	125 GeV
spin = 0		
d.o.f. = 1		

The masses are approximate values taken from [Beringer et al., 2012], where current best fits and errors are given.

TABLE A.3: **Lightest hadrons of the standard model**

	Name	Mass	Quark composition
Mesons	$\pi^{\pm}$	140 MeV	$u\bar{d}$, $d\bar{u}$
	π^0	135 MeV	$(u\bar{u}$ - $d\bar{d})/2$
Baryons	p, $\bar{p}$	938 MeV	uud, $\bar{u}\bar{u}\bar{d}$
	n, $\bar{n}$	940 MeV	udd, $\bar{u}\bar{d}\bar{d}$

The masses are approximate values taken from [Beringer et al., 2012], where current best fits and errors are given.

B FITTING THE POWER SPECTRUM CUTOFF

In this appendix we discuss the procedure employed to fit the power spectrum cutoff in the cosmon-bolon model in chapter 4. We compare numerically evolved power spectra for two models: A coupled CDM model and the coupled cosmon-bolon model, both for a wide range of parameters. The evolution equations for the coupled CDM model are equal to those presented for the averaged (late-time) coupled bolon model in chapter 4, except that the sound-speed is set to zero. The initial conditions for the adiabatic mode in the coupled CDM model differ from the ones for the cosmon-bolon model, but they are easy to derive or even guess from the results of chapter 5 and we will not quote them here. The grid we investigated runs through the the parameters λ and β for the cosmon-bolon model, the boundaries we chose to investigate are $[20,30]$ for λ and $[-0.2,0.1]$ for β. This covers (roughly) the range of observationally allowed couplings.

Building on the results of earlier works [Hu et al., 2000, Matos and Urena-Lopez, 2001], we first assumed that the cutoff can be well fit by the relation

$$P_\chi(k) = P_{\rm cdm}(k) \left\{ \frac{\cos\left[(bx)^a\right]}{1+cx^d} \right\}^2 , \tag{B.1}$$

where $x = k/k_J$. In [Matos and Urena-Lopez, 2001], a good fit of the cutoff in a similar model was reported to be given by $a = 3$, $c = 1$ and $d = 8$. However, in that work a slightly different definition of the Jeans scale k_J was used, we therefore adjusted the parameter b to fit the data. What we are aiming for in a good fit is a minimalization of the maximal absolute value of the relative error when the fitting is compared to the numerical results for the entire grid. This is of course only reasonable if we do not use the complete power spectra, but cut off wavenumbers for which the suppression compared to the CDM result is below a given threshold, which we denote by t_c.
For $t_c = 1/500$ the best fit is given by $b = 1.0725$, but this already gives a maximal relative error of order 3. Raising the threshold to $t_c = 1/100$ results in the same $b = 1.0725$, whereas the maximal relative error is still 0.99.

As these errors are still big, we have to improve the fitting function. We generalized it to be of the following form:

$$P_\chi(k) = P_{\rm cdm}(k) \left\{ \frac{\cos\left[(bx)^a\right]}{1+\sqrt{c}\,(x^{d_1}+x^{d_2})} \right\}^2 , \tag{B.2}$$

where this time the parameters a, b, c, d_1 and d_2 are functions of the model parameters λ and β. We 'optimized' the fitting procedure by assuming a linear dependence on the parameters for all functions at first, and eliminated all dependencies which would not yield a significant improvement for the

fitting with a threshold of $t_c = 1/500$. The resulting best estimate reads

$$a(\beta) = 4.105 + 0.428\beta\,, \tag{B.3}$$

$$b(\lambda,\beta) = 0.827 + 0.098\beta + 0.006\lambda + 0.0025\lambda\beta\,, \tag{B.4}$$

$$c(\lambda,\beta) = -0.46 - 1.9\beta + 0.053\lambda + 0.152\lambda\beta\,, \tag{B.5}$$

$$d_1(\beta) = 4.31 - 1.2\beta\,, \tag{B.6}$$

$$d_2(\beta) = 7.66 + 1.49\beta\,. \tag{B.7}$$

This gives a fitting better than 18% for $t_c = 1/500$. For $t_c = 1/100$ a fitting better than 8% can be achieved with the same parameterization. We show the results of our fittings in Figures B.1 and B.2. We show the numerically obtained ratio $P_\chi/P_{\rm cdm}$ for $\lambda = 28$ and $\beta = -0.2$ in Figure B.1: black points represent wavenumbers above the threshold $t_c = 1/500$, gray ones wavenumbers below it. We also show the estimated ratios given by equation (B.1) in red, and the more complicated one originating from equation (B.2) in blue. The parameters are chosen such that they give biggest errors for the optimized fitting within our grid, but not for the simple one. The corresponding relative errors can be seen in Figure B.2, again in blue for the optimized fitting, and in red for the simple one. This time the points that were excluded from the fitting by the threshold are shown in lighter colors.

FIGURE B.1: **Fitting the power spectrum cutoff**

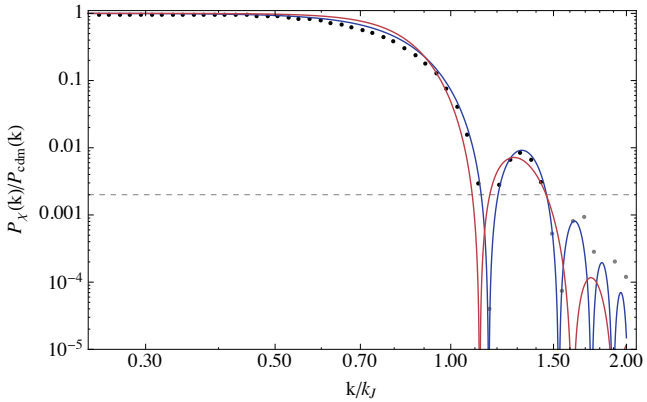

We show a fitting the power spectrum cutoff for $\lambda = 28$ and $\beta = -0.2$. The simple fitting (B.1) is shown in red, the optimized one (B.2) in blue. Figure taken from [Beyer, 2014b].

FIGURE B.2: **Relative errors for the cutoff fitting**

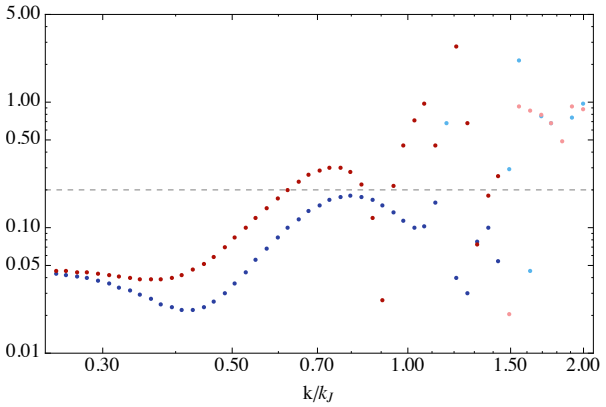

Relative errors for the fitting given in figure B.1. Again the simple fitting is shown in red, the improved one in blue. The light points are excluded by the threshold. Figure taken from [Beyer, 2014b].

BIBLIOGRAPHY

Aad, G., Abajyan, T., Abbott, B., Abdallah, J., Abdel Khalek, S., Abdelalim, A. A., Abdinov, O., Aben, R., Abi, B., Abolins, M., and et al. (2012). Observation of a new particle in the search for the Standard Model Higgs boson with the ATLAS detector at the LHC. *Physics Letters B*, 716:1–29, 1207.7214.

Abazajian, K. N., Adelman-McCarthy, J. K., Agüeros, M. A., Allam, S. S., Allende Prieto, C., An, D., Anderson, K. S. J., Anderson, S. F., Annis, J., Bahcall, N. A., and et al. (2009). The Seventh Data Release of the Sloan Digital Sky Survey. *Astrophys.J.Suppl.*, 182:543–558, 0812.0649.

Abramo, L., Batista, R., Liberato, L., and Rosenfeld, R. (2007). Structure formation in the presence of dark energy perturbations. *JCAP*, 0711:012, 0707.2882.

Ade, P. et al. (2013a). Planck 2013 results. I. Overview of products and scientific results. 1303.5062.

Ade, P. et al. (2013b). Planck 2013 results. XVI. Cosmological parameters. 1303.5076.

Ade, P. et al. (2013c). Planck 2013 results. XXII. Constraints on inflation. 1303.5082.

Ade, P. et al. (2014). Detection of B-Mode Polarization at Degree Angular Scales by BICEP2. *Phys.Rev.Lett.*, 112:241101, 1403.3985.

Ahmad, Q. R. et al. (2001). Measurement of the Rate of $\nu_e + d -> p + p + e^-$ Interactions Produced by ^{8}B Solar Neutrinos at the Sudbury Neutrino Observatory. *Physical Review Letters*, 87(7):071301, nucl-ex/0106015.

Albrecht, A. and Steinhardt, P. J. (1982). Cosmology for Grand Unified Theories with Radiatively Induced Symmetry Breaking. *Phys.Rev.Lett.*, 48:1220–1223.

Alcubierre, M., Becerril, R., Guzman, S. F., Matos, T., Nunez, D., et al. (2003). Numerical studies of Phi**2 oscillatons. *Class.Quant.Grav.*, 20:2883–2904, gr-qc/0301105.

Alcubierre, M., Guzman, F. S., Matos, T., Nunez, D., Urena-Lopez, L. A., et al. (2002). Galactic collapse of scalar field dark matter. *Class.Quant.Grav.*, 19:5017, gr-qc/0110102.

Alpher, R. A., Bethe, H., and Gamow, G. (1948). The Origin of Chemical Elements. *Physical Review*, 73:803–804.

Amendola, L. (1999). Scaling solutions in general nonminimal coupling theories. *Phys.Rev.*, D60:043501, astro-ph/9904120.

Amendola, L. (2000a). Coupled quintessence. *Phys.Rev.*, D62:043511, astro-ph/9908023.

Amendola, L. (2000b). Perturbations in a coupled scalar field cosmology. *Mon.Not.Roy.Astron.Soc.*, 312:521, astro-ph/9906073.

Amendola, L. (2004). Linear and non-linear perturbations in dark energy models. *Phys.Rev.*, D69:103524, astro-ph/0311175.

Amendola, L., Baldi, M., and Wetterich, C. (2008). Quintessence cosmologies with a growing matter component. *Phys.Rev.*, D78:023015, 0706.3064.

Amendola, L., Pettorino, V., Quercellini, C., and Vollmer, A. (2012). Testing coupled dark energy with next-generation large-scale observations. *Phys.Rev.*, D85:103008, 1111.1404.

Amendola, L. and Tsujikawa, S. (2010). *Dark energy: Theory and observations*. Cambridge Univ. Press, Cambridge.

Anderhalden, D., Schneider, A., Maccio, A. V., Diemand, J., and Bertone, G. (2013). Hints on the Nature of Dark Matter from the Properties of Milky Way Satellites. *JCAP*, 1303:014, 1212.2967.

Angloher, G., Bauer, M., Bavykina, I., Bento, A., Bucci, C., et al. (2012). Results from 730 kg days of the CRESST-II Dark Matter Search. *Eur.Phys.J.*, C72:1971, 1109.0702.

Aprile, E. et al. (2012). Dark Matter Results from 225 Live Days of XENON100 Data. *Phys.Rev.Lett.*, 109:181301, 1207.5988.

Armendariz-Picon, C., Damour, T., and Mukhanov, V. F. (1999). k - inflation. *Phys.Lett.*, B458:209–218, hep-th/9904075.

Armendariz-Picon, C., Mukhanov, V. F., and Steinhardt, P. J. (2000). A Dynamical solution to the problem of a small cosmological constant and late time cosmic acceleration. *Phys.Rev.Lett.*, 85:4438–4441, astro-ph/0004134.

Armendariz-Picon, C., Mukhanov, V. F., and Steinhardt, P. J. (2001). Essentials of k essence. *Phys.Rev.*, D63:103510, astro-ph/0006373.

Ayaita, Y., Schaefer, B. M., and Weber, M. (2012a). Investigating clustering dark energy with 3d weak cosmic shear. *Mon.Not.Roy.Astron.Soc.*, 422:3056–3066, 1110.1985.

Ayaita, Y., Weber, M., and Wetterich, C. (2012b). Structure Formation and Backreaction in Growing Neutrino Quintessence. *Phys.Rev.*, D85:123010, 1112.4762.

Ayaita, Y., Weber, M., and Wetterich, C. (2013). Neutrino Lump Fluid in Growing Neutrino Quintessence. *Phys.Rev.*, D87(4):043519, 1211.6589.

Baldi, M. (2012). Structure formation in Multiple Dark Matter cosmologies with long-range scalar interactions. 1206.2348.

Bania, T. M., Rood, R. T., and Balser, D. S. (2002). The cosmological density of baryons from observations of $^3He^+$ in the Milky Way. *Nature*, 415:54–57.

Bardeen, J. M. (1980). Gauge Invariant Cosmological Perturbations. *Phys.Rev.*, D22:1882–1905.

Bardeen, J. M., Bond, J., Kaiser, N., and Szalay, A. (1986). The Statistics of Peaks of Gaussian Random Fields. *Astrophys.J.*, 304:15–61.

Barkana, R., Haiman, Z., and Ostriker, J. P. (2001). Constraints on warm dark matter from cosmological reionization. *ApJ*, 558:482, astro-ph/0102304.

Bartelmann, M. (2010). The Dark Universe. *Rev.Mod.Phys.*, 82:331–382, 0906.5036.

Bartelmann, M., Doran, M., and Wetterich, C. (2006). Non-linear structure formation in cosmologies with early dark energy. *Astron.Astrophys.*, 454:27–36, astro-ph/0507257.

Bartelmann, M. and Schneider, P. (2001). Weak gravitational lensing. *Phys.Rept.*, 340:291–472, astro-ph/9912508.

Bartolo, N., Corasaniti, P. S., Liddle, A. R., and Malquarti, M. (2004). Perturbations in cosmologies with a scalar field and a perfect fluid. *Phys.Rev.*, D70:043532, astro-ph/0311503.

Basse, T., Bjaelde, O. E., and Wong, Y. Y. (2011). Spherical collapse of dark energy with an arbitrary sound speed. *JCAP*, 1110:038, 1009.0010.

Baugh, C. (2013). Luminosity bias: from haloes to galaxies. 1302.2768.

Baumann, D. (2009). TASI Lectures on Inflation. 0907.5424.

Bean, R., Dunkley, J., and Pierpaoli, E. (2006). Constraining Isocurvature Initial Conditions with WMAP 3-year data. *Phys.Rev.*, D74:063503, astro-ph/0606685.

Bean, R., Hansen, S., and Melchiorri, A. (2002a). Constraining dark energy.

Bean, R., Hansen, S. H., and Melchiorri, A. (2001). Early universe constraints on a primordial scaling field. *Phys.Rev.*, D64:103508, astro-ph/0104162.

Bean, R., Hansen, S. H., and Melchiorri, A. (2002b). Constraining the dark universe. *Nucl.Phys.Proc.Suppl.*, 110:167–172, astro-ph/0201127.

Beltran, M. (2008). Isocurvature, non-gaussianity and the curvaton model. *Phys.Rev.*, D78:023530, 0804.1097.

Beltran, M., Garcia-Bellido, J., Lesgourgues, J., Liddle, A. R., and Slosar, A. (2005a). Bayesian model selection and isocurvature perturbations. *Phys.Rev.*, D71:063532, astro-ph/0501477.

Beltran, M., Garcia-Bellido, J., Lesgourgues, J., and Viel, M. (2005b). Squeezing the window on isocurvature modes with the lyman-alpha forest. *Phys.Rev.*, D72:103515, astro-ph/0509209.

Benson, A. J., Farahi, A., Cole, S., Moustakas, L. A., Jenkins, A., et al. (2012). Dark Matter Halo Merger Histories Beyond Cold Dark Matter: I - Methods and Application to Warm Dark Matter. 1209.3018.

Beringer, J. et al. (2012). Review of Particle Physics (RPP). *Phys.Rev.*, D86:010001.

Bernabei, R. et al. (2008). First results from DAMA/LIBRA and the combined results with DAMA/-NaI. *Eur.Phys.J.*, C56:333–355, 0804.2741.

Bertone, G., Hooper, D., and Silk, J. (2005). Particle dark matter: Evidence, candidates and constraints. *Phys.Rept.*, 405:279–390, hep-ph/0404175.

Beyer, J. (2011). Coupled dark energy and dark matter from dilatation anomalies. Master's thesis, University of Heidelberg.

Beyer, J. (2014a). Adiabatic perturbations in coupled scalar field cosmologies. 1407.0186.

Beyer, J. (2014b). Linear Perturbations in a coupled cosmon-bolon cosmology. 1407.0497.

Beyer, J., Nurmi, S., and Wetterich, C. (2011). Coupled dark energy and dark matter from dilatation anomaly. *Phys.Rev.*, D84:023010, 1012.1175.

Beyer, J. and Wetterich, C. (2014). Small scale structures in coupled scalar field dark matter. 1407.0141.

Blas, D., Lesgourgues, J., and Tram, T. (2011). The Cosmic Linear Anisotropy Solving System (CLASS) II: Approximation schemes. *JCAP*, 1107:034, 1104.2933.

Bode, P., Ostriker, J. P., and Turok, N. (2001). Halo formation in warm dark matter models. *Astrophys.J.*, 556:93–107, astro-ph/0010389.

Bond, J., Cole, S., Efstathiou, G., and Kaiser, N. (1991). Excursion set mass functions for hierarchical Gaussian fluctuations. *Astrophys.J.*, 379:440.

Bond, J. and Efstathiou, G. (1984). Cosmic background radiation anisotropies in universes dominated by nonbaryonic dark matter. *Astrophys.J.*, 285:L45–L48.

Bond, J. and Efstathiou, G. (1987). The statistics of cosmic background radiation fluctuations. *Mon.Not.Roy.Astron.Soc.*, 226:655–687.

Bower, R. G. (1991). The Evolution of groups of galaxies in the Press-Schechter formalism. *Mon.Not.Roy.Astron.Soc.*, 248:332.

Boylan-Kolchin, M., Bullock, J. S., and Kaplinghat, M. (2011). Too big to fail? The puzzling darkness of massive Milky Way subhaloes. *Mon.Not.Roy.Astron.Soc.*, 415:L40, 1103.0007.

Boylan-Kolchin, M., Bullock, J. S., and Kaplinghat, M. (2012). The Milky Way's bright satellites as an apparent failure of LCDM. *Mon.Not.Roy.Astron.Soc.*, 422:1203–1218, 1111.2048.

Brans, C. and Dicke, R. H. (1961). Mach's Principle and a Relativistic Theory of Gravitation. *Physical Review*, 124:925–935.

Brax, P., van de Bruck, C., Davis, A., Khoury, J., and Weltman, A. (2005). Chameleon dark energy. *AIP Conf.Proc.*, 736:105–110, astro-ph/0410103.

Brax, P., van de Bruck, C., Davis, A.-C., Khoury, J., and Weltman, A. (2004). Detecting dark energy in orbit - The Cosmological chameleon. *Phys.Rev.*, D70:123518, astro-ph/0408415.

Calabrese, E., Huterer, D., Linder, E. V., Melchiorri, A., and Pagano, L. (2011). Limits on Dark Radiation, Early Dark Energy, and Relativistic Degrees of Freedom. *Phys.Rev.*, D83:123504, 1103.4132.

Caldwell, R. R., Kamionkowski, M., and Weinberg, N. N. (2003). Phantom energy and cosmic doomsday. *Phys.Rev.Lett.*, 91:071301, astro-ph/0302506.

Carroll, S. M. (2004). *Spacetime and geometry: An introduction to general relativity*. Cummings.

Carroll, S. M., Geddes, J., Hoffman, M. B., and Wald, R. M. (2002). Classical stabilization of homogeneous extra dimensions. *Phys.Rev.*, D66:024036, hep-th/0110149.

Carroll, S. M., Hoffman, M., and Trodden, M. (2003). Can the dark energy equation - of - state parameter w be less than -1? *Phys.Rev.*, D68:023509, astro-ph/0301273.

Castro, . P. et al. (2009). Cosmological Parameters from the QUaD CMB polarization experiment. *Astrophys.J.*, 701:857–864, 0901.0810.

Cavaliere, A. G., Gursky, H., and Tucker, W. H. (1971). Extragalactic X-ray Sources and Associations of Galaxies. *Nature*, 231:437–438.

Charbonnel, C. and Primas, F. (2005). The Lithium content of the Galactic Halo stars. *Astron.Astrophys.*, 442:961–992, astro-ph/0505247.

Chatrchyan, S., Khachatryan, V., Sirunyan, A. M., Tumasyan, A., Adam, W., Aguilo, E., Bergauer, T., Dragicevic, M., Erö, J., Fabjan, C., and et al. (2012). Observation of a new boson at a mass of 125 GeV with the CMS experiment at the LHC. *Physics Letters B*, 716:30–61, 1207.7235.

Chen, T.-j., Fasiello, M., Lim, E. A., and Tolley, A. J. (2013). Higher derivative theories with constraints: Exorcising Ostrogradski's Ghost. *JCAP*, 1302:042, 1209.0583.

Chen, X. (2010). Primordial Non-Gaussianities from Inflation Models. *Adv.Astron.*, 2010:638979, 1002.1416.

Chiba, T., Okabe, T., and Yamaguchi, M. (2000). Kinetically driven quintessence. *Phys.Rev.*, D62:023511, astro-ph/9912463.

Cho, Y. and Freund, P. G. (1975). Nonabelian Gauge Fields in Nambu-Goldstone Fields. *Phys.Rev.*, D12:1711.

Cho, Y. and Jang, P. S. (1975). Unified Geometry of Internal Space with Space-Time. *Phys.Rev.*, D12:3789.

Cole, S., Helly, J., Frenk, C. S., and Parkinson, H. (2007). The statistical properties of LCDM halo formation. *Mon.Not.Roy.Astron.Soc.*, 0708.1376.

Copeland, E. J., Lee, S.-J., Lidsey, J. E., and Mizuno, S. (2005). Generalised cosmological scaling solutions. *Phys.Rev.*, D71:023526, astro-ph/0410110.

Copeland, E. J., Liddle, A. R., and Wands, D. (1998). Exponential potentials and cosmological scaling solutions. *Phys.Rev.*, D57:4686–4690, gr-qc/9711068.

Copeland, E. J., Sami, M., and Tsujikawa, S. (2006). Dynamics of dark energy. *Int.J.Mod.Phys.*, D15:1753–1936, hep-th/0603057.

Copi, C. J., Huterer, D., Schwarz, D. J., and Starkman, G. D. (2009). No large-angle correlations on the non-Galactic microwave sky. *Mon.Not.Roy.Astron.Soc.*, 399:295–303, 0808.3767.

Corasaniti, P. and Achitouv, I. (2011a). Excursion Set Halo Mass Function and Bias in a Stochastic Barrier Model of Ellipsoidal Collapse. *Phys.Rev.*, D84:023009, 1107.1251.

Corasaniti, P. and Achitouv, I. (2011b). Toward a Universal Formulation of the Halo Mass Function. *Phys.Rev.Lett.*, 106:241302, 1012.3468.

Das, S., Corasaniti, P. S., and Khoury, J. (2006). Super-acceleration as signature of dark sector interaction. *Phys.Rev.*, D73:083509, astro-ph/0510628.

Davies, G. and Widrow, L. M. (1996). Test bed simulations of collisionless, selfgravitating systems using the Schrodinger method. *Astrophys. J.*, astro-ph/9607133.

Davis, R., Harmer, D. S., and Hoffman, K. C. (1968). Search for Neutrinos from the Sun. *Physical Review Letters*, 20:1205–1209.

de Bernardis, P., Ade, P. A. R., Bock, J. J., Bond, J. R., Borrill, J., Boscaleri, A., Coble, K., Crill, B. P., De Gasperis, G., Farese, P. C., Ferreira, P. G., Ganga, K., Giacometti, M., Hivon, E., Hristov, V. V., Iacoangeli, A., Jaffe, A. H., Lange, A. E., Martinis, L., Masi, S., Mason, P. V., Mauskopf, P. D., Melchiorri, A., Miglio, L., Montroy, T., Netterfield, C. B., Pascale, E., Piacentini, F., Pogosyan, D., Prunet, S., Rao, S., Romeo, G., Ruhl, J. E., Scaramuzzi, F., Sforna, D., and Vittorio, N. (2000). A flat Universe from high-resolution maps of the cosmic microwave background radiation. *Nature*, 404:955–959, astro-ph/0004404.

Dicke, R. H., Peebles, P. J. E., Roll, P. G., and Wilkinson, D. T. (1965). Cosmic Black-Body Radiation. *Astrophys. J.*, 142:414–419.

Diemand, J., Moore, B., and Stadel, J. (2005). Earth-mass dark-matter haloes as the first structures in the early Universe. *Nature*, 433:389–391, astro-ph/0501589.

Doran, M., Muller, C. M., Schafer, G., and Wetterich, C. (2003). Gauge-invariant initial conditions and early time perturbations in quintessence universes. *Phys.Rev.*, D68:063505, astro-ph/0304212.

Doran, M., Schwindt, J.-M., and Wetterich, C. (2001). Structure formation and the time dependence of quintessence. *Phys.Rev.*, D64:123520, astro-ph/0107525.

Drewes, M. (2013). The Phenomenology of Right Handed Neutrinos. *Int.J.Mod.Phys.*, E22:1330019, 1303.6912.

Duffy, L. D. and van Bibber, K. (2009). Axions as Dark Matter Particles. *New J.Phys.*, 11:105008, 0904.3346.

Einstein, A. (1905a). Ist die Trägheit eines Körpers von seinem Energieinhalt abhängig? *Annalen der Physik*, 323:639–641.

Einstein, A. (1905b). Zur Elektrodynamik bewegter Körper. *Annalen der Physik*, 322:891–921.

Einstein, A. (1915a). Die Feldgleichungen der Gravitation. *Sitzungsberichte der Königlich Preußischen Akademie der Wissenschaften (Berlin), Seite 844-847.*, pages 844–847.

Einstein, A. (1915b). Erklärung der Perihelbewegung des Merkur aus der allgemeinen Relativitätstheorie. *Sitzungsberichte der Königlich Preußischen Akademie der Wissenschaften (Berlin), Seite 831-839.*, pages 831–839.

Einstein, A. (1915c). Zur allgemeinen Relativitätstheorie. *Sitzungsberichte der Königlich Preußischen Akademie der Wissenschaften (Berlin), Seite 778-786.*, pages 778–786.

Einstein, A. (1917). Kosmologische Betrachtungen zur allgemeinen Relativitätstheorie. *Sitzungsberichte der Königlich Preußischen Akademie der Wissenschaften (Berlin), Seite 142-152.*, pages 142–152.

Enqvist, K., Kurki-Suonio, H., and Valiviita, J. (2000). Limits on isocurvature fluctuations from boomerang and MAXIMA. *Phys.Rev.*, D62:103003, astro-ph/0006429.

Enqvist, K., Kurki-Suonio, H., and Valiviita, J. (2002). Open and closed CDM isocurvature models contrasted with the CMB data. *Phys.Rev.*, D65:043002, astro-ph/0108422.

Farahi, A. and Benson, A. J. (2013). Excursion Set Theory for Correlated Random Walks. 1303.0337.

Ferreira, P. G. and Joyce, M. (1997). Structure formation with a selftuning scalar field. *Phys.Rev.Lett.*, 79:4740–4743, astro-ph/9707286.

Ferreira, P. G. and Joyce, M. (1998). Cosmology with a primordial scaling field. *Phys.Rev.*, D58:023503, astro-ph/9711102.

Fixsen, D., Cheng, E., Gales, J., Mather, J. C., Shafer, R., et al. (1996). The Cosmic Microwave Background spectrum from the full COBE FIRAS data set. *Astrophys.J.*, 473:576, astro-ph/9605054.

Fixsen, D. J. (2009). The Temperature of the Cosmic Microwave Background. *Astrophys. J.*, 707:916–920, 0911.1955.

Flores, R. A. and Primack, J. R. (1994). Observational and theoretical constraints on singular dark matter halos. *Astrophys. J. Lett.*, 427:L1–L4, astro-ph/9402004.

Flores, R. A. and Primack, J. R. (1994). Observational and theoretical constraints on singular dark matter halos. *Astrophys.J.*, 427:L1–4, astro-ph/9402004.

Forman, W., Kellogg, E., Gursky, H., Tananbaum, H., and Giacconi, R. (1972). Observations of the Extended X-Ray Sources in the Perseus and Coma Clusters from UHURU. *Astrophys. J.*, 178:309–316.

Friedmann, A. (1922). Über die Krümmung des Raumes. *Zeitschrift fur Physik*, 10:377–386.

Friedmann, A. (1924). Über die Möglichkeit einer Welt mit konstanter negativer Krümmung des Raumes. *Zeitschrift fur Physik*, 21:326–332.

Garriga, J. and Mukhanov, V. F. (1999). Perturbations in k-inflation. *Phys.Lett.*, B458:219–225, hep-th/9904176.

Genel, S., Vogelsberger, M., Springel, V., Sijacki, D., Nelson, D., et al. (2014). The Illustris Simulation: the evolution of galaxy populations across cosmic time. 1405.3749.

Giocoli, C., Moreno, J., Sheth, R. K., and Tormen, G. (2007a). An improved model for the formation times of dark matter haloes. *Mon.Not.Roy.Astron.Soc.*, 376:977–983, astro-ph/0611221.

Giocoli, C., Pieri, L., and Tormen, G. (2008). Analytical Approach to Subhaloes Population in Dark Matter Haloes. *Mon.Not.Roy.Astron.Soc.*, 387:689–697, 0712.1476.

Giocoli, C., Tormen, G., and Bosch, F. C. d. (2007b). The Population of Dark Matter Subhaloes: Mass Functions and Average Mass Loss Rates. 0712.1563.

Giocoli, C., Tormen, G., and Sheth, R. K. (2011). Formation times, mass growth histories and concentrations of dark matter haloes. 1111.6977.

Giocoli, C., Tormen, G., Sheth, R. K., and Bosch, F. C. d. (2009). The Substructure Hierarchy in Dark Matter Haloes. 0911.0436.

Gogberashvili, M. (1999). Four dimensionality in noncompact Kaluza-Klein model. *Mod.Phys.Lett.*, A14:2025–2032, hep-ph/9904383.

Gorbunov, D. S. and Rubakov, V. A. (2011a). Introduction to the theory of the early universe: Cosmological perturbations and inflationary theory.

Gorbunov, D. S. and Rubakov, V. A. (2011b). *Introduction to the theory of the early universe: Hot big bang theory*. World Scientific.

Gordon, C., Wands, D., Bassett, B. A., and Maartens, R. (2001). Adiabatic and entropy perturbations from inflation. *Phys.Rev.*, D63:023506, astro-ph/0009131.

Gribov, V. and Pontecorvo, B. (1969). Neutrino astronomy and lepton charge. *Physics Letters B*, 28:493–496.

Gumjudpai, B., Naskar, T., Sami, M., and Tsujikawa, S. (2005). Coupled dark energy: Towards a general description of the dynamics. *JCAP*, 0506:007, hep-th/0502191.

Guo, Z.-K., Piao, Y.-S., Cai, R.-G., and Zhang, Y.-Z. (2003a). Cosmological scaling solutions and cross coupling exponential potential. *Phys.Lett.*, B576:12–17, hep-th/0306245.

Guo, Z. K., Piao, Y.-S., and Zhang, Y.-Z. (2003b). Cosmological scaling solutions and multiple exponential potentials. *Phys.Lett.*, B568:1–7, hep-th/0304048.

Gursky, H., Kellogg, E., Murray, S., Leong, C., Tananbaum, H., and Giacconi, R. (1971). A Strong X-Ray Source in the Coma Cluster Observed by UHURU. *Astrophys. J., Letters*, 167:L81.

Guth, A. H. (1981). The Inflationary Universe: A Possible Solution to the Horizon and Flatness Problems. *Phys.Rev.*, D23:347–356.

Guth, A. H. and Weinberg, E. J. (1981). Cosmological Consequences of a First Order Phase Transition in the SU(5) Grand Unified Model. *Phys.Rev.*, D23:876.

Guzman, F. S. and Urena-Lopez, L. A. (2003). Newtonian collapse of scalar field dark matter. *Phys.Rev.*, D68:024023, astro-ph/0303440.

Guzman, F. S. and Urena-Lopez, L. A. (2004). Evolution of the Schrodinger-Newton system for a selfgravitating scalar field. *Phys.Rev.*, D69:124033, gr-qc/0404014.

Hanany, S., Ade, P., Balbi, A., Bock, J., Borrill, J., et al. (2000). MAXIMA-1: A Measurement of the cosmic microwave background anisotropy on angular scales of 10 arcminutes to 5 degrees. *Astrophys.J.*, 545:L5, astro-ph/0005123.

Hansen, F., Banday, A., Gorski, K., Eriksen, H., and Lilje, P. (2009). Power Asymmetry in Cosmic Microwave Background Fluctuations from Full Sky to Sub-degree Scales: Is the Universe Isotropic? *Astrophys.J.*, 704:1448–1458, 0812.3795.

Hawkins, M. (2011). The case for primordial black holes as dark matter. 1106.3875.

Hebecker, A. and Wetterich, C. (2000). Can quintessence be natural? pages 125–134.

Hebecker, A. and Wetterich, C. (2001). Natural quintessence? *Phys.Lett.*, B497:281–288, hep-ph/0008205.

Henz, T., Pawlowski, J. M., Rodigast, A., and Wetterich, C. (2013). Dilaton Quantum Gravity. *Phys.Lett.*, B727:298–302, 1304.7743.

Hilbert, D. (1915). Die grundlagen der physik. *Konigl. Gesell. d. Wiss. Göttingen, Nachr. Math.-Phys. Kl.*, pages 395–407.

Hinshaw, G. et al. (2013). Nine-Year Wilkinson Microwave Anisotropy Probe (WMAP) Observations: Cosmological Parameter Results. *Astrophys.J.Suppl.*, 208:19, 1212.5226.

Hoftuft, J., Eriksen, H., Banday, A., Gorski, K., Hansen, F., et al. (2009). Increasing evidence for hemispherical power asymmetry in the five-year WMAP data. *Astrophys.J.*, 699:985–989, 0903.1229.

Hu, W. (1999). Power spectrum tomography with weak lensing. *Astrophys.J.*, 522:L21–L24, astro-ph/9904153.

Hu, W., Barkana, R., and Gruzinov, A. (2000). Cold and fuzzy dark matter. *Phys.Rev.Lett.*, 85:1158–1161, astro-ph/0003365.

Hu, W., Scott, D., and Silk, J. (1994a). Power spectrum constraints from spectral distortions in the cosmic microwave background. *Astrophys.J.*, 430:L5–L8, astro-ph/9402045.

Hu, W., Scott, D., and Silk, J. (1994b). Reionization and cosmic microwave background distortions: A Complete treatment of second order Compton scattering. *Phys.Rev.*, D49:648–670, astro-ph/9305038.

Hubble, E. (1929). A Relation between Distance and Radial Velocity among Extra-Galactic Nebulae. *Proceedings of the National Academy of Science*, 15:168–173.

Jarosik, N., Bennett, C., Dunkley, J., Gold, B., Greason, M., et al. (2011). Seven-Year Wilkinson Microwave Anisotropy Probe (WMAP) Observations: Sky Maps, Systematic Errors, and Basic Results. *Astrophys.J.Suppl.*, 192:14, 1001.4744.

Joyce, M. (2001). *Habilitation thesis*. PhD thesis, Universite Paris XI.

Kaluza, T. (1921). Zum Unitätsproblem der Physik. *Sitzungsberichte der Königlich Preußischen Akademie der Wissenschaften (Berlin)*, K1:966–972.

Kamenshchik, A. Y., Moschella, U., and Pasquier, V. (2001). An Alternative to quintessence. *Phys.Lett.*, B511:265–268, gr-qc/0103004.

Kamionkowski, M. and Liddle, A. R. (2000). The Dearth of halo dwarf galaxies: Is there power on short scales? *Phys.Rev.Lett.*, 84:4525–4528, astro-ph/9911103.

Kawasaki, M. and Sekiguchi, T. (2008). Cosmological Constraints on Isocurvature and Tensor Perturbations. *Prog.Theor.Phys.*, 120:995–1016, 0705.2853.

Keskitalo, R., Kurki-Suonio, H., Muhonen, V., and Valiviita, J. (2007). Hints of Isocurvature Perturbations in the Cosmic Microwave Background. *JCAP*, 0709:008, astro-ph/0611917.

Khmelnitsky, A. and Rubakov, V. (2014). Pulsar timing signal from ultralight scalar dark matter. *JCAP*, 1402:019, 1309.5888.

Khoury, J. and Weltman, A. (2004a). Chameleon cosmology. *Phys.Rev.*, D69:044026, astro-ph/0309411.

Khoury, J. and Weltman, A. (2004b). Chameleon fields: Awaiting surprises for tests of gravity in space. *Phys.Rev.Lett.*, 93:171104, astro-ph/0309300.

Klein, O. (1926). Quantentheorie und fünfdimensionale Relativitätstheorie. *Zeitschrift fur Physik*, 37:895–906.

Klypin, A. A., Kravtsov, A. V., Valenzuela, O., and Prada, F. (1999). Where are the missing Galactic satellites? *Astrophys.J.*, 522:82–92, astro-ph/9901240.

Kodama, H. and Sasaki, M. (1984). Cosmological Perturbation Theory. *Prog.Theor.Phys.Suppl.*, 78:1–166.

Koksma, J. F. and Prokopec, T. (2011). The Cosmological Constant and Lorentz Invariance of the Vacuum State. 1105.6296.

Koposov, S. E., Yoo, J., Rix, H.-W., Weinberg, D. H., Maccio, A. V., et al. (2009). A quantitative explanation of the observed population of Milky Way satellite galaxies. *Astrophys.J.*, 696:2179–2194, 0901.2116.

Kopp, M., Appleby, S. A., Achitouv, I., and Weller, J. (2013). Spherical collapse and halo mass function in f(R) theories. *Phys.Rev.*, D88:084015, 1306.3233.

Kosowsky, A. (1996). Cosmic microwave background polarization. *Annals Phys.*, 246:49–85, astro-ph/9501045.

Kovac, J., Leitch, E., Pryke, C., Carlstrom, J., Halverson, N., et al. (2002). Detection of polarization in the cosmic microwave background using DASI. *Nature*, 420:772–787, astro-ph/0209478.

Kravtsov, A. and Borgani, S. (2012). Formation of Galaxy Clusters. *Ann.Rev.Astron.Astrophys.*, 50:353–409, 1205.5556.

Kregel, M., van der Kruit, P. C., and de Blok, W. (2004). Structure and kinematics of edge-on galaxy discs. 2. Observations of the neutral hydrogen. *Mon.Not.Roy.Astron.Soc.*, 352:768, astro-ph/0405173.

Labini, F. S., Vasilyev, N. L., and Baryshev, Y. V. (2009a). Persistent fluctuations in the distribution of galaxies from the Two degree Field Galaxy Redshift Survey. *Europhys.Lett.*, 85:29002, 0812.3260.

Labini, F. S., Vasilyev, N. L., Pietronero, L., and Baryshev, Y. V. (2009b). Absence of self-averaging and of homogeneity in the large scale galaxy distribution. *Europhys.Lett.*, 86:49001, 0805.1132.

Lacey, C. G. and Cole, S. (1993). Merger rates in hierarchical models of galaxy formation. *Mon.Not.Roy.Astron.Soc.*, 262:627–649.

Lahav, O. and Suto, Y. (2004). Measuring our universe from galaxy redshift surveys. *Living Rev.Rel.*, 7:8, astro-ph/0310642.

Lamb, W. E. and Retherford, R. C. (1947). Fine Structure of the Hydrogen Atom by a Microwave Method. *Physical Review*, 72:241–243.

Lambrecht, A. and Reynaud, S. (2012). Casimir Effect: Theory and Experiments. *Int.J.Mod.Phys.*, A27:1260013, 1112.1301.

Langlois, D. (1999). Correlated adiabatic and isocurvature perturbations from double inflation. *Phys.Rev.*, D59:123512, astro-ph/9906080.

Langlois, D. (2003). Isocurvature cosmological perturbations and the CMB. *Comptes Rendus Physique*, 4:953–959.

Langlois, D. and Riazuelo, A. (2000). Correlated mixtures of adiabatic and isocurvature cosmological perturbations. *Phys.Rev.*, D62:043504, astro-ph/9912497.

Lee, J.-w. and Koh, I.-g. (1996). Galactic halos as boson stars. *Phys.Rev.*, D53:2236–2239, hep-ph/9507385.

Lemaître, G. (1927). Un Univers homogène de masse constante et de rayon croissant rendant compte de la vitesse radiale des nébuleuses extra-galactiques. *Annales de la Societe Scietifique de Bruxelles*, 47:49–59.

Lemaître, G. (1931). Expansion of the universe, A homogeneous universe of constant mass and increasing radius accounting for the radial velocity of extra-galactic nebulae. *Mon.Not.Roy.Astron.Soc.*, 91:483–490.

Lesgourgues, J. (2011a). The Cosmic Linear Anisotropy Solving System (CLASS) I: Overview. 1104.2932.

Lesgourgues, J. (2011b). The Cosmic Linear Anisotropy Solving System (CLASS) III: Comparision with CAMB for LambdaCDM. 1104.2934.

Lewis, A. (2006). Observational constraints and cosmological parameters. astro-ph/0603753.

Lewis, A. and Bridle, S. (2002). Cosmological parameters from CMB and other data: a Monte- Carlo approach. *Phys. Rev.*, D66:103511, astro-ph/0205436.

Li, H., Liu, J., Xia, J.-Q., and Cai, Y.-F. (2011). Cold Dark Matter Isocurvature Perturbations: Cosmological Constraints and Applications. *Phys.Rev.*, D83:123517, 1012.2511.

Libeskind, N. I., Frenk, C. S., Cole, S., Helly, J. C., Jenkins, A., et al. (2005). The Distribution of satellite galaxies: The Great pancake. *Mon.Not.Roy.Astron.Soc.*, 363:146–152, astro-ph/0503400.

Liddle, A. R. and Scherrer, R. J. (1999). A Classification of scalar field potentials with cosmological scaling solutions. *Phys.Rev.*, D59:023509, astro-ph/9809272.

Linde, A. D. (1982). A New Inflationary Universe Scenario: A Possible Solution of the Horizon, Flatness, Homogeneity, Isotropy and Primordial Monopole Problems. *Phys.Lett.*, B108:389–393.

Lovell, M. R., Eke, V., Frenk, C. S., Gao, L., Jenkins, A., et al. (2012). The Haloes of Bright Satellite Galaxies in a Warm Dark Matter Universe. *Mon.Not.Roy.Astron.Soc.*, 420:2318–2324, 1104.2929.

Lovell, M. R., Frenk, C. S., Eke, V. R., Jenkins, A., Gao, L., et al. (2014). The properties of warm dark matter haloes. *Mon.Not.Roy.Astron.Soc.*, 439:300–317, 1308.1399.

Lyth, D. H. and Riotto, A. (1999). Particle physics models of inflation and the cosmological density perturbation. *Phys.Rept.*, 314:1–146, hep-ph/9807278.

Ma, C.-P. and Bertschinger, E. (1995). Cosmological perturbation theory in the synchronous and conformal Newtonian gauges. *Astrophys.J.*, 455:7–25, astro-ph/9506072.

Maggiore, M. and Riotto, A. (2010a). The Halo Mass Function from Excursion Set Theory. I. Gaussian fluctuations with non-Markovian dependence on the smoothing scale. *Astrophys.J.*, 711:907–927, 0903.1249.

Maggiore, M. and Riotto, A. (2010b). The Halo mass function from excursion set theory. II. The diffusing barrier. *Astrophys.J.*, 717:515–525, 0903.1250.

Maggiore, M. and Riotto, A. (2010c). The Halo mass function from excursion set theory. III. Non-Gaussian fluctuations. *Astrophys.J.*, 717:526–541, 0903.1251.

Majerotto, E., Valiviita, J., and Maartens, R. (2009). Instability in interacting dark energy and dark matter fluids. *Nucl.Phys.Proc.Suppl.*, 194:260–265.

Majerotto, E., Valiviita, J., and Maartens, R. (2010). Adiabatic initial conditions for perturbations in interacting dark energy models. *Mon.Not.Roy.Astron.Soc.*, 402:2344–2354, 0907.4981.

Maki, Z., Nakagawa, M., and Sakata, S. (1962). Remarks on the Unified Model of Elementary Particles. *Progress of Theoretical Physics*, 28:870–880.

Malik, K. A. (2001). Cosmological perturbations in an inflationary universe. astro-ph/0101563.

Malik, K. A. and Wands, D. (2005). Adiabatic and entropy perturbations with interacting fluids and fields. *JCAP*, 0502:007, astro-ph/0411703.

Malik, K. A. and Wands, D. (2009). Cosmological perturbations. *Phys.Rept.*, 475:1–51, 0809.4944.

Malik, K. A., Wands, D., and Ungarelli, C. (2003). Large scale curvature and entropy perturbations for multiple interacting fluids. *Phys.Rev.*, D67:063516, astro-ph/0211602.

Malquarti, M. and Liddle, A. R. (2002a). Evolution of large scale perturbations in quintessence models. *Phys.Rev.*, D66:123506, astro-ph/0208562.

Malquarti, M. and Liddle, A. R. (2002b). Initial conditions for quintessence after inflation. *Phys.Rev.*, D66:023524, astro-ph/0203232.

Marsh, D. J. (2011). The Axiverse Extended: Vacuum Destabilisation, Early Dark Energy and Cosmological Collapse. *Phys.Rev.*, D83:123526, 1102.4851.

Marsh, D. J. and Ferreira, P. G. (2010). Ultra-Light Scalar Fields and the Growth of Structure in the Universe. *Phys.Rev.*, D82:103528, 1009.3501.

Marsh, D. J. E. and Silk, J. (2013). A Model For Halo Formation With Axion Mixed Dark Matter. 1307.1705.

Martin, J. (2012). Everything you always wanted to know about the cosmological constant problem (but were afraid to ask). *Comptes Rendus Physique*, 13:566–665, 1205.3365.

Mather, J. C., Cheng, E., Cottingham, D., Eplee, R., Fixsen, D., et al. (1994). Measurement of the Cosmic Microwave Background spectrum by the COBE FIRAS instrument. *Astrophys.J.*, 420:439–444.

Matos, T. and Guzman, F. S. (2000). Scalar fields as dark matter in spiral galaxies. *Class.Quant.Grav.*, 17:L9–L16, gr-qc/9810028.

Matos, T., Guzman, F. S., and Nunez, D. (2000a). Spherical scalar field halo in galaxies. *Phys.Rev.*, D62:061301, astro-ph/0003398.

Matos, T., Guzman, F. S., and Urena-Lopez, L. A. (2000b). Scalar field as dark matter in the universe. *Class.Quant.Grav.*, 17:1707–1712, astro-ph/9908152.

Matos, T., Guzman, F. S., Urena-Lopez, L. A., and Nunez, D. (2001). Scalar field dark matter. pages 165–184, astro-ph/0102419.

Matos, T. and Urena-Lopez, L. A. (2000). Quintessence and scalar dark matter in the universe. *Class.Quant.Grav.*, 17:L75–L81, astro-ph/0004332.

Matos, T. and Urena-Lopez, L. A. (2001). A Further analysis of a cosmological model of quintessence and scalar dark matter. *Phys.Rev.*, D63:063506, astro-ph/0006024.

Meekins, J. F., Fritz, G., Chubb, T. A., and Friedman, H. (1971). Physical Sciences: X-rays from the Coma Cluster of Galaxies. *Nature*, 231:107–108.

Mellier, Y. (1999). Cosmological applications of gravitational lensing. astro-ph/9901116.

Menci, N., Fiore, F., and Lamastra, A. (2013). The Evolution of Active Galactic Nuclei in Warm Dark Matter Cosmology. *Astrophys.J.*, 766:110, 1302.2000.

Milton, K. A. (2004). Casimir energies and pressures for delta function potentials. *J.Phys.*, A37:6391–6406, hep-th/0401090.

Milton, K. A. (2011). Local and Global Casimir Energies: Divergences, Renormalization, and the Coupling to Gravity. *Lect.Notes Phys.*, 834:39–95, 1005.0031.

Moore, B. (1994). Evidence against dissipation-less dark matter from observations of galaxy haloes. *Nature*, 370:629–631.

Moore, B., Ghigna, S., Governato, F., Lake, G., Quinn, T. R., et al. (1999). Dark matter substructure within galactic halos. *Astrophys.J.*, 524:L19–L22, astro-ph/9907411.

Moore, B., Governato, F., Quinn, T., Stadel, J., and Lake, G. (1998). Resolving the Structure of Cold Dark Matter Halos. *Astrophys. J. Lett.*, 499:L5–L8, astro-ph/9709051.

Mota, D., Pettorino, V., Robbers, G., and Wetterich, C. (2008). Neutrino clustering in growing neutrino quintessence. *Phys.Lett.*, B663:160–164, 0802.1515.

Mukhanov, V. F., Feldman, H., and Brandenberger, R. H. (1992). Theory of cosmological perturbations. Part 1. Classical perturbations. Part 2. Quantum theory of perturbations. Part 3. Extensions. *Phys.Rept.*, 215:203–333.

Musso, M. and Sheth, R. K. (2014). The importance of stepping up in the excursion set approach. *Mon.Not.Roy.Astron.Soc.*, 1306.0551.

Navarro, J. F., Frenk, C. S., and White, S. D. (1997). A Universal density profile from hierarchical clustering. *Astrophys.J.*, 490:493–508, astro-ph/9611107.

Olive, K. A. and Skillman, E. D. (2004). A Realistic determination of the error on the primordial helium abundance: Steps toward non-parametric nebular helium abundances. *Astrophys.J.*, 617:29, astro-ph/0405588.

O'Meara, J. M., Tytler, D., Kirkman, D., Suzuki, N., Prochaska, J. X., Lubin, D., and Wolfe, A. M. (2001). The Deuterium to Hydrogen Abundance Ratio toward a Fourth QSO: HS 0105+1619. *Astrophys. J.*, 552:718–730, astro-ph/0011179.

Pace, F., Moscardini, L., Crittenden, R., Bartelmann, M., and Pettorino, V. (2013). A comparison of structure formation in minimally and non-minimally coupled quintessence models. 1307.7026.

Pace, F., Waizmann, J.-C., and Bartelmann, M. (2010). Spherical collapse model in dark energy cosmologies. 1005.0233.

Papastergis, E., Martin, A. M., Giovanelli, R., and Haynes, M. P. (2011). The velocity width function of galaxies from the 40shedding light on the cold dark matter overabundance problem. *Astrophys.J.*, 739:38, 1106.0710.

Peccei, R. and Quinn, H. R. (1977a). Constraints Imposed by CP Conservation in the Presence of Instantons. *Phys.Rev.*, D16:1791–1797.

Peccei, R. and Quinn, H. R. (1977b). CP Conservation in the Presence of Instantons. *Phys.Rev.Lett.*, 38:1440–1443.

Peebles, P. (1982). Large scale background temperature and mass fluctuations due to scale invariant primeval perturbations. *Astrophys. J. Lett.*, 263:L1–L5.

Peebles, P. and Ratra, B. (1988). Cosmology with a Time Variable Cosmological Constant. *Astrophys.J.*, 325:L17.

Peebles, P. and Ratra, B. (2003). The Cosmological constant and dark energy. *Rev.Mod.Phys.*, 75:559–606, astro-ph/0207347.

Peebles, P. J. E. (1967). The Gravitational Instability of the Universe. *Astrophys. J.*, 147:859.

Penzias, A. A. and Wilson, R. W. (1965a). A Measurement of Excess Antenna Temperature at 4080 Mc/s. *Astrophys. J.*, 142:419–421.

Penzias, A. A. and Wilson, R. W. (1965b). Measurement of the Flux Density of CAS a at 4080 Mc/s. *Astrophys. J.*, 142:1149.

Penzo, C., Macciò, A. V., Casarini, L., Stinson, G. S., and Wadsley, J. (2014). Dark MaGICC: the effect of Dark Energy on galaxy formation. Cosmology does matter. 1401.3338.

Perlmutter, S., Aldering, G., Goldhaber, G., Knop, R. A., Nugent, P., Castro, P. G., Deustua, S., Fabbro, S., Goobar, A., Groom, D. E., Hook, I. M., Kim, A. G., Kim, M. Y., Lee, J. C., Nunes, N. J., Pain, R., Pennypacker, C. R., Quimby, R., Lidman, C., Ellis, R. S., Irwin, M., McMahon, R. G., Ruiz-Lapuente, P., Walton, N., Schaefer, B., Boyle, B. J., Filippenko, A. V., Matheson, T., Fruchter, A. S., Panagia, N., Newberg, H. J. M., Couch, W. J., and Project, T. S. C. (1999).

Measurements of Ω and Λ from 42 High-Redshift Supernovae. *Astrophys. J.*, 517:565–586, astro-ph/9812133.

Peter, A. H., Rocha, M., Bullock, J. S., and Kaplinghat, M. (2012). Cosmological Simulations with Self-Interacting Dark Matter II: Halo Shapes vs. Observations. 1208.3026.

Pettorino, V. (2013). Testing modified gravity with Planck: the case of coupled dark energy. *Phys. Rev. D 88,*, 063519, 1305.7457.

Pettorino, V., Amendola, L., Baccigalupi, C., and Quercellini, C. (2012). Constraints on coupled dark energy using CMB data from WMAP and SPT. *Phys.Rev.*, D86:103507, 1207.3293.

Pettorino, V., Amendola, L., and Wetterich, C. (2013). How early is early dark energy? *Phys.Rev.*, D87:083009, 1301.5279.

Pitrou, C. (2011). The tight-coupling approximation for baryon acoustic oscillations. *Phys.Lett.*, B698:1–5, 1012.0546.

Plunien, G., Muller, B., and Greiner, W. (1986). The Casimir Effect. *Phys.Rept.*, 134:87–193.

Polarski, D. and Starobinsky, A. A. (1996). Semiclassicality and decoherence of cosmological perturbations. *Class.Quant.Grav.*, 13:377–392, gr-qc/9504030.

Polisensky, E. and Ricotti, M. (2011). Constraints on the Dark Matter Particle Mass from the Number of Milky Way Satellites. *Phys.Rev.*, D83:043506, 1004.1459.

Polisensky, E. and Ricotti, M. (2014). Massive Milky Way Satellites in Cold and Warm Dark Matter: Dependence on Cosmology. *Mon.Not.Roy.Astron.Soc.*, 437:2922, 1310.0430.

Pontecorvo, B. (1968). Neutrino Experiments and the Problem of Conservation of Leptonic Charge. *Soviet Journal of Experimental and Theoretical Physics*, 26:984.

Pourtsidou, A., Skordis, C., and Copeland, E. (2013). Models of coupled dark matter to dark energy. *Phys.Rev.*, D88:083505, 1307.0458.

Press, W. H. and Schechter, P. (1974). Formation of galaxies and clusters of galaxies by selfsimilar gravitational condensation. *Astrophys.J.*, 187:425–438.

Primack, J. R. (2009a). Cosmology: small scale issues. *AIP Conf.Proc.*, 1166:3–9, 0902.2506.

Primack, J. R. (2009b). Cosmology: small scale issues revisited. *New J.Phys.*, 11:105029, 0909.2247.

Ratra, B. and Peebles, P. (1988). Cosmological Consequences of a Rolling Homogeneous Scalar Field. *Phys.Rev.*, D37:3406.

Readhead, A., Myers, S., Pearson, T. J., Sievers, J., Mason, B., et al. (2004). Polarization observations with the Cosmic Background Imager. astro-ph/0409569.

Refregier, A. (2003). Weak gravitational lensing by large scale structure. *Ann.Rev.Astron.Astrophys.*, 41:645–668, astro-ph/0307212.

Reichardt, C. L., de Putter, R., Zahn, O., and Hou, Z. (2012). New limits on Early Dark Energy from the South Pole Telescope. *Astrophys.J.*, 749:L9, 1110.5328.

Riess, A. G., Filippenko, A. V., Challis, P., Clocchiatti, A., Diercks, A., Garnavich, P. M., Gilliland, R. L., Hogan, C. J., Jha, S., Kirshner, R. P., Leibundgut, B., Phillips, M. M., Reiss, D., Schmidt, B. P., Schommer, R. A., Smith, R. C., Spyromilio, J., Stubbs, C., Suntzeff, N. B., and Tonry, J. (1998). Observational Evidence from Supernovae for an Accelerating Universe and a Cosmological Constant. *Astronom. J.*, 116:1009–1038, astro-ph/9805201.

Rindler, W. (1956). Visual horizons in world models. *MNRAS*, 116:662.

Robertson, H. P. (1935). Kinematics and World-Structure. *Astrophys. J.*, 82:284.

Robertson, H. P. (1936a). Kinematics and World-Structure II. *Astrophys. J.*, 83:187.

Robertson, H. P. (1936b). Kinematics and World-Structure III. *Astrophys. J.*, 83:257.

Rocha, M., Peter, A. H., Bullock, J. S., Kaplinghat, M., Garrison-Kimmel, S., et al. (2013). Cosmological Simulations with Self-Interacting Dark Matter I: Constant Density Cores and Substructure. *Mon.Not.Roy.Astron.Soc.*, 430:81–104, 1208.3025.

Rodriguez-Montoya, I., Magana, J., Matos, T., and Perez-Lorenzana, A. (2010). Ultra light bosonic dark matter and cosmic microwave background. *Astrophys.J.*, 721:1509–1514, 0908.0054.

Rubakov, V. A. and Shaposhnikov, M. E. (1983). Do we live inside a domain wall? *Physics Letters B*, 125:136–138.

Sachs, R. K. and Wolfe, A. M. (1967). Perturbations of a Cosmological Model and Angular Variations of the Microwave Background. *Astrophys. J.*, 147:73.

Sahni, V. (2002). The Cosmological constant problem and quintessence. *Class.Quant.Grav.*, 19:3435–3448, astro-ph/0202076.

Said, N., Baccigalupi, C., Martinelli, M., Melchiorri, A., and Silvestri, A. (2013). New Constraints On The Dark Energy Equation of State. *Phys.Rev.*, D88:043515, 1303.4353.

Sarkar, P., Yadav, J., Pandey, B., and Bharadwaj, S. (2009). The scale of homogeneity of the galaxy distribution in SDSS DR6. 0906.3431.

Sato, K. (1981). Cosmological Baryon Number Domain Structure and the First Order Phase Transition of a Vacuum. *Phys.Lett.*, B99:66–70.

Schive, H.-Y., Chiueh, T., and Broadhurst, T. (2014). Cosmic Structure as the Quantum Interference of a Coherent Dark Wave. 1406.6586.

Schneider, A., Anderhalden, D., Maccio, A., and Diemand, J. (2013). Warm dark matter does not do better than cold dark matter in solving small-scale inconsistencies. 1309.5960.

Schwarz, D. J. (2010). Cosmological backreaction. pages 563–577, 1003.3026.

Scott, D. and Moss, A. (2009). Matter temperature after cosmological recombination. 0902.3438.

Seager, S., Sasselov, D. D., and Scott, D. (1999). A new calculation of the recombination epoch. *Astrophys.J.*, 523:L1–L5, astro-ph/9909275.

Seager, S., Sasselov, D. D., and Scott, D. (2000). How exactly did the universe become neutral? *Astrophys.J.Suppl.*, 128:407–430, astro-ph/9912182.

Seljak, U., Slosar, A., and McDonald, P. (2006). Cosmological parameters from combining the Lyman-alpha forest with CMB, galaxy clustering and SN constraints. *JCAP*, 0610:014, astro-ph/0604335.

Sheth, R. K., Mo, H., and Tormen, G. (2001). Ellipsoidal collapse and an improved model for the number and spatial distribution of dark matter haloes. *Mon.Not.Roy.Astron.Soc.*, 323:1, astro-ph/9907024.

Sheth, R. K. and Tormen, G. (2002). An Excursion set model of hierarchical clustering : Ellipsoidal collapse and the moving barrier. *Mon.Not.Roy.Astron.Soc.*, 329:61, astro-ph/0105113.

Silk, J. (1968). Cosmic black body radiation and galaxy formation. *Astrophys.J.*, 151:459–471.

Smith, S. (1936). The Mass of the Virgo Cluster. *Astrophys. J.*, 83:23.

Sofue, Y. and Rubin, V. (2001). Rotation curves of spiral galaxies. *Ann.Rev.Astron.Astrophys.*, 39:137–174, astro-ph/0010594.

Sollom, I., Challinor, A., and Hobson, M. P. (2009). Cold Dark Matter Isocurvature Perturbations: Constraints and Model Selection. *Phys.Rev.*, D79:123521, 0903.5257.

Sotiriou, T. P. and Faraoni, V. (2010). f(R) Theories Of Gravity. *Rev.Mod.Phys.*, 82:451–497, 0805.1726.

Spergel, D. N. and Steinhardt, P. J. (2000). Observational evidence for selfinteracting cold dark matter. *Phys.Rev.Lett.*, 84:3760–3763, astro-ph/9909386.

Springel, V., Wang, J., Vogelsberger, M., Ludlow, A., Jenkins, A., et al. (2008). The Aquarius Project: the subhalos of galactic halos. *Mon.Not.Roy.Astron.Soc.*, 391:1685–1711, 0809.0898.

Starobinskiĭ, A. A. (1979). Spectrum of relict gravitational radiation and the early state of the universe. *Soviet Journal of Experimental and Theoretical Physics Letters*, 30:682.

Steffen, F. D. (2009). Dark Matter Candidates - Axions, Neutralinos, Gravitinos, and Axinos. *Eur.Phys.J.*, C59:557–588, 0811.3347.

Steigman, G. (2007). Primordial Nucleosynthesis in the Precision Cosmology Era. *Ann.Rev.Nucl.Part.Sci.*, 57:463–491, 0712.1100.

Steigman, G. and Turner, M. S. (1985). Cosmological Constraints on the Properties of Weakly Interacting Massive Particles. *Nucl.Phys.*, B253:375.

Steinhardt, P. J. (1982). NATURAL INFLATION.

Steinhardt, P. J., Wang, L.-M., and Zlatev, I. (1999). Cosmological tracking solutions. *Phys.Rev.*, D59:123504, astro-ph/9812313.

Strigari, L. E., Bullock, J. S., Kaplinghat, M., Simon, J. D., Geha, M., et al. (2008). A common mass scale for satellite galaxies of the Milky Way. *Nature*, 454:1096–1097, 0808.3772.

Suarez, A., Robles, V. H., and Matos, T. (2013). A Review on the Scalar Field/ Bose-Einstein Condensate Dark Matter Model. 1302.0903.

Sunyaev, R. A. and Zeldovich, Y. B. (1972). The Observations of Relic Radiation as a Test of the Nature of X-Ray Radiation from the Clusters of Galaxies. *Comments on Astrophysics and Space Physics*, 4:173.

Tegmark, M. (2007). The Multiverse Hierarchy. 0905.1283.

Tegmark, M., Aguirre, A., Rees, M., and Wilczek, F. (2006). Dimensionless constants, cosmology and other dark matters. *Phys.Rev.*, D73:023505, astro-ph/0511774.

Tocchini-Valentini, D. and Amendola, L. (2002). Stationary dark energy with a baryon dominated era: Solving the coincidence problem with a linear coupling. *Phys.Rev.*, D65:063508, astro-ph/0108143.

Tollerud, E. J., Bullock, J. S., Strigari, L. E., and Willman, B. (2008). Hundreds of Milky Way Satellites? Luminosity Bias in the Satellite Luminosity Function. *Astrophys.J.*, 688:277–289, 0806.4381.

Trotta, R. (2007). The isocurvature fraction after WMAP 3-year data. *Mon.Not.Roy.Astron.Soc.*, 375:L26–L30, astro-ph/0608116.

Tsujikawa, S. and Sami, M. (2004). A Unified approach to scaling solutions in a general cosmological background. *Phys.Lett.*, B603:113–123, hep-th/0409212.

Turner, M. S. (1983). Coherent Scalar Field Oscillations in an Expanding Universe. *Phys.Rev.*, D28:1243.

Urena-Lopez, L. A. (2002). Oscillatons revisited. *Class.Quant.Grav.*, 19:2617–2632, gr-qc/0104093.

Urena-Lopez, L. A. and Matos, T. (2000). A New cosmological tracker solution for quintessence. *Phys.Rev.*, D62:081302, astro-ph/0003364.

Uzan, J.-P. (1999). Cosmological scaling solutions of nonminimally coupled scalar fields. *Phys.Rev.*, D59:123510, gr-qc/9903004.

Valiviita, J. and Giannantonio, T. (2009). Constraints on primordial isocurvature perturbations and spatial curvature by Bayesian model selection. *Phys.Rev.*, D80:123516, 0909.5190.

Valiviita, J., Maartens, R., and Majerotto, E. (2010). Observational constraints on an interacting dark energy model. *Mon.Not.Roy.Astron.Soc.*, 402:2355–2368, 0907.4987.

Valiviita, J., Majerotto, E., and Maartens, R. (2008). Instability in interacting dark energy and dark matter fluids. *JCAP*, 0807:020, 0804.0232.

van den Bosch, F. C., Tormen, G., and Giocoli, C. (2005). The Mass function and average mass loss rate of dark matter subhaloes. *Mon.Not.Roy.Astron.Soc.*, 359:1029–1040, astro-ph/0409201.

Viel, M., Becker, G. D., Bolton, J. S., and Haehnelt, M. G. (2013). Warm Dark Matter as a solution to the small scale crisis: new constraints from high redshift Lyman-alpha forest data. *Physical Review*, D88(4):043502, 1306.2314.

Vilenkin, A. (1983). The Birth of Inflationary Universes. *Phys.Rev.*, D27:2848.

Vilenkin, A. (1995). Predictions from quantum cosmology. *Phys.Rev.Lett.*, 74:846–849, gr-qc/9406010.

Vogelsberger, M., Genel, S., Springel, V., Torrey, P., Sijacki, D., et al. (2014a). Introducing the Illustris Project: Simulating the coevolution of dark and visible matter in the Universe. 1405.2921.

Vogelsberger, M., Genel, S., Springel, V., Torrey, P., Sijacki, D., et al. (2014b). Properties of galaxies reproduced by a hydrodynamic simulation. *Nature*, 509:177–182, 1405.1418.

Walker, A. G. (1935). On Riemanntan spaces with spherical symmetry about a line, and the conditions for isotropy in genj relativity. *The Quarterly Journal of Mathematics*, 6:81–93.

Weinberg, D. H., Bullock, J. S., Governato, F., de Naray, R. K., and Peter, A. H. G. (2013a). Cold dark matter: controversies on small scales. 1306.0913.

Weinberg, D. H., Dave, R., Katz, N., and Kollmeier, J. A. (2003). The Lyman - alpha forest as a cosmological tool. *AIP Conf.Proc.*, 666:157–169, astro-ph/0301186.

Weinberg, D. H., Mortonson, M. J., Eisenstein, D. J., Hirata, C., Riess, A. G., et al. (2013b). Observational Probes of Cosmic Acceleration. *Phys.Rept.*, 530:87–255, 1201.2434.

Weinberg, S. (1972). *Gravitation and Cosmology: Principles and Applications of the General Theory of Relativity*. Wiley, New York, NY.

Weinberg, S. (1987). Anthropic Bound on the Cosmological Constant. *Phys.Rev.Lett.*, 59:2607.

Weinberg, S. (2003). Adiabatic modes in cosmology. *Phys.Rev.*, D67:123504, astro-ph/0302326.

Weinberg, S. (2004). Damping of tensor modes in cosmology. *Phys.Rev.*, D69:023503, astro-ph/0306304.

Weinberg, S. (2008). *Cosmology*. Oxford University Press.

Welton, T. A. (1948). Some Observable Effects of the Quantum-Mechanical Fluctuations of the Electromagnetic Field. *Physical Review*, 74:1157–1167.

Wetterich, C. (1988a). Cosmologies With Variable Newton's 'Constant'. *Nucl.Phys.*, B302:645.

Wetterich, C. (1988b). Cosmology and the Fate of Dilatation Symmetry. *Nucl.Phys.*, B302:668.

Wetterich, C. (1995). The Cosmon model for an asymptotically vanishing time dependent cosmological 'constant'. *Astron.Astrophys.*, 301:321–328, hep-th/9408025.

Wetterich, C. (2007). Growing neutrinos and cosmological selection. *Phys.Lett.*, B655:201–208, 0706.4427.

Wetterich, C. (2008). Naturalness of exponential cosmon potentials and the cosmological constant problem. *Phys.Rev.*, D77:103505, 0801.3208.

Wetterich, C. (2009). Dilatation symmetry in higher dimensions and the vanishing of the cosmological constant. *Phys.Rev.Lett.*, 102:141303, 0806.0741.

Wetterich, C. (2010a). The Cosmological constant and higher dimensional dilatation symmetry. *Phys.Rev.*, D81:103507, 0911.1063.

Wetterich, C. (2010b). Warping with dilatation symmetry and self-tuning of the cosmological constant. *Phys.Rev.*, D81:103508, 1003.3809.

Wetterich, C. (2014a). Eternal Universe. 1404.0535.

Wetterich, C. (2014b). Modified gravity and coupled quintessence. 1402.5031.

Winitzki, S. (2008). Predictions in eternal inflation. *Lect.Notes Phys.*, 738:157–191, gr-qc/0612164.

Wintergerst, N. and Pettorino, V. (2010). Clarifying spherical collapse in coupled dark energy cosmologies. *Phys.Rev.*, D82:103516, 1005.1278.

Wong, W. Y., Moss, A., and Scott, D. (2008). How well do we understand cosmological recombination? *Mon.Not.Roy.Astron.Soc.*, 386:1023–1028, 0711.1357.

Woo, T.-P. and Chiueh, T. (2009). High-Resolution Simulation on Structure Formation with Extremely Light Bosonic Dark Matter. *Astrophys.J.*, 697:850–861, 0806.0232.

Xia, J.-Q., Li, H., and Zhang, X. (2013). Dark Energy Constraints after Planck. *Phys.Rev.*, D88:063501, 1308.0188.

Zlatev, I., Wang, L.-M., and Steinhardt, P. J. (1999). Quintessence, cosmic coincidence, and the cosmological constant. *Phys.Rev.Lett.*, 82:896–899, astro-ph/9807002.

Zwicky, F. (1933). Die Rotverschiebung von extragalaktischen Nebeln. *Helvetica Physica Acta*, 6:110–127.

Zwicky, F. (1937). On the Masses of Nebulae and of Clusters of Nebulae. *Astrophys. J.*, 86:217.